Hydro-Mechanical Properties of Partially Saturated Sand

Dissertation

as a requirement of the degree of

Doktor - Ingenieur

at the Faculty of Civil Egineering
University Bochum

submitted by

Yvonne Lins
Weißenfels, Germany

Reviewers:

Prof. Dr.-Ing. habil. Tom Schanz
Prof. Dr. Maria Datcheva
Prof. Delwyn Fredlund, MSc, PhD
Prof. Dr.-Ing. habil. Rainer Helmig

May 12th, 2009

Preface by the publisher

I am very glad to open a new chapter of publications from the chair for Foundation Engineering, Soil and Rock Mechanics at Ruhr-Universität Bochum (Germany) with the PhD-thesis by Dr.-Ing. Yvonne Lins. The thesis is outcome of a six years research work in the frame of the research group "Mechanics of Unsaturated Soils" funded by the German Research Foundation (DFG). It was awarded best thesis of the Faculty of Civil & Environmental Engineering for the year 2009.

Yvonne Lins thesis focuses on the experimental and theoretical analysis of partially saturated granular materials. The complex and coupled physical phenomena include both mechanical and hydraulic processes. Element tests to quantify the capillary pressure versus water content relationship, the relative permeability, the collapse potential and the stiffness depending on the capillary pressure were performed. Beside these tests also two benchmark tests were performed and documented in a way the measurements are accessible to the international scientific community. Most of the experiments under capillary pressure controlled conditions were only possible because Dr. Lins developed, constructed and validated several new and unique testing cells. Parallel to the experimental work a new SWCC-model is suggested and validated based on micro structural considerations.

Main parts of the thesis were executed during the stay of our research group at Bauhaus-Universität Weimar (Germany) up to 2009. This thesis was the starting point for our group in the sense bringing our lab to be well recognized by the international scientific community. In this period also two major international conferences were realized on unsaturated soil mechanics. The internationally recognized success of both conferences would have been impossible without the excellent organization by Yvonne Lins. For this reason I am most thankful to her on this matter.

Finally I like to express my gratitude towards DFG for continuous financial support of our research without this success is not to be achieved.

Bochum, April 2010

Tom Schanz

Acknowledgement

The present dissertation was carried out in the frame of the DFG research unit "Mechanics of Unsaturated Soils" (FOR-444), where my main part was the processing of the subproject "Experimental and Theoretical Investigation of Granular Frictional Material". I would like to acknowledge the financial support provided by the DFG through the project. The work on the project enabled me not only to write on my PhD-thesis but also to be introduced to the scientific community working in the field of unsaturated soil mechanics. The attendance at several international conferences allowed me to come into contact with internationally accepted scientists and to discuss with them my experimental results and theoretical approaches. The outcome is among others an idea for ongoing research project.

My gratitude is also extended to all of my colleagues form the DFG group and to all of my "former" colleagues from Bauhaus-Universität Weimar for the active cooperation during the last years as well as the good communication. I appreciate to be well received from my "new" colleagues at Ruhr-Universität Bochum last year in 2009.

Special thank goes to my reviewers Prof. Maria Datcheva for providing me support in the modeling of SWCC's and Prof. Rainer Helmig for providing me support in the numerical simulation of experimental results. And special thanks also goes to my reviewer Prof. Delwyn G. Fredlund for the interesting discussions during his short stays at Bauhaus-Universität Weimar and my stay at SoilVision in Saskatoon (Canada) on unsaturated soil behavior.

Last but not least I want to thank my supervisor Prof. Tom Schanz. I am especially grateful, that he gave me the great opportunity to work with him after finishing my study in civil engineering on the topic of unsaturated soil mechanics. The years under his supervision are characterized by a great support and a fruitful collaboration.

Contents

List of Figures

List of Tables

List of Symbols

$\hat{m}$	Parameter used in Schanz's stress dependent stiffness modulus equation (-)
a	Parameter in Fredlund and Xing's SWCC model (kPa^{-1})
b	Parameter in Feng and Fredlund's SWCC model (-)
c	Parameter in Feng and Fredlund's SWCC model (-)
c'	Cohesion (kPa)
C_c	Compression index (-)
C_s	Swelling index (-)
C_u	Coefficient of uniformity (-)
CP	Collapse potential (%)
d	Parameter in Feng and Fredlund's SWCC model (-)
D_{10}	Grain size diameter corresponding to 10% passing on the grain-size distribution curve (mm)
D_{30}	Grain size diameter corresponding to 30% passing on the grain-size distribution curve (mm)
D_{50}	Grain size diameter corresponding to 50% passing on the grain-size distribution curve (mm)
D_{60}	Grain size diameter corresponding to 60% passing on the grain-size distribution curve (mm)
e	Void ratio (-)
E_{oed}	Oedometer stress dependent stiffness modulus, initial loading path (kPa)
E_{oed}^{ref}	Oedometer reference stiffness modulus, initial loading path (kPa)
E_{ur}	Oedoemeter stress dependent stiffness modulus, un-/ reloading path (kPa)

E_{ur}^{ref}	Oedometer reference stiffness modulus, un-/ reloading path (kPa)
k	Hydraulic conductivity (m/s)
k_a	Dielectric constant (-)
k_r	Relative conductivity (-)
k_s	Saturated conductivity (m/s)
m	Parameter in van Genuchten's and Fredlund and Xing's SWCC model (-)
n	Parameter in van Genuchten's and Fredlund and Xing's SWCC model (-)
N_c	Bearing capacity factor due to cohesion in bearing capacity equations (-)
N_q	Bearing capacity factor due to overburden pressure in bearing capacity equations (-)
N_γ	Bearing capacity factor due to weight of the soil in bearing capacity equations (-)
n_c	Contact number in Zou's SWCC model (-)
n_{f0}	Frustum number in Zou's SWCC model (-)
q_u	Bearing capacity (kPa)
R	Radius of curvature (mm)
r	Radius (mm)
R^2	Coefficient of regression determination (-)
RH	Relative humidity (%)
S	Saturation (i.e. degree of saturation) (-)
S_e	Effective saturation (-)
T	Absolute temperature (K)
T_s	Surface tension (kN/m)
u_a	Air pressure (kPa)
u_w	Pore water pressure (kPa)
u_{v0}	Saturated vapor pressure (kPa)
u_{v1}	Prevailing vapor pressure (kPa)
v_{w0}	Specific volume of water (m^3/kg)

w	Water content (%)
α	Contact angle in Zou's SWCC model (°)
α	Parameter in Brooks and Corey's and van Genuchten's SWCC model (kPa)
α_{max}	Maximum contact angle in Zou's SWCC model (°)
β_0	Parameter in the new SWCC model (-)
β_1	Parameter in the new SWCC model (-)
β_2	Parameter in the new SWCC model (-)
β_3	Parameter in the new SWCC model (-)
β_{31}	Parameter in the new SWCC model (-)
β_{32}	Parameter in the new SWCC model (-)
χ	Material parameter in Bishop's effective stress equation (-)
δ	Parameter in macroscopic model for determination of unsaturated hydraulic conductivity (-)
ϵ	Strain (-)
γ	Weight (kN/m^3)
κ	Parameter in Vanapalli's equation for prediction of unsaturated shear strength (-)
λ	Parameter in Brooks and Corey's SWCC model (-)
μ	Parameter in Zou's SWCC model (-)
ω_v	Molecular mass of the water vapor (kg/kmol)
ϕ	Friction angle (°)
ψ	Total suction (kPa)
ψ_m	Matric suction or capillary pressure (kPa)
ψ_o	Osmotic suction (kPa)
ψ_r	Suction at residual volumetric water content (kPa)
ψ_{aev}	Air-entry value (kPa)
ψ_{wev}	Water-entry value (kPa)

ρ	Density (g/cm^3)
ρ_d	Dry density (g/cm^3)
ρ_s	Density of the soil particles (g/cm^3)
σ	Total stress (kPa)
σ'	Effective stress (kPa)
σ_0	Preconsolidation pressure (kPa)
σ_{ref}	Reference stress (kPa)
τ	Shear strength (kPa)
Θ	Normalized volumetric water content (-)
θ	Volumetric water content (%)
θ'	Apparent saturated volumetric water content (%)
θ_r	Residual volumetric water content (%)
θ_s	Saturated volumetric water content (%)
$\tilde{\sigma}_0$	Yield stress (kPa)
ε	Random error (-)
ξ	Form parameter in Zou's SWCC model (-)
ξ_c	Shape factor due to cohesion in bearing capacity equations (-)
ξ_γ	Shape factor due to unit weight in bearing capacity equations (-)
ζ	Material parameter in Zou's SWCC model (-)

Chapter 1

Introduction

1.1 Background

During the last decades it was realized that the conventional principles and concepts of soil mechanics are often not suitable for solving requirements of geotechnical engineering practice. The theories of the conventional soil mechanics are based on the principles and concepts of saturated materials (either fluid saturated or gas saturated). As can be seen in case of the humidity index of the earth, in reality an unsaturated soil is present (see Fig. 1.1) and its behavior is different from saturated soil. With decreasing and increasing water content, which is related to an increasing and decreasing soil suction, the constitutive behavior of unsaturated soils is significantly changing. For this reason the influence of water content in a soil on the hydro-mechancial behavior becomes of major interest when solving geotechnical engineering problems. The changes are related to the hydraulic conductivity, the shear strength, the stiffness as well as the volume change behavior (e.g. shrinkage, swelling, collapse). Following examples summarize typical engineering problems involving predominantly unsaturated soils:

- Problems related to flow phenomenon
  - Seepage through unsaturated soils
  - Construction of dams and dikes
  - Modeling of environmental problems (e.g. waste disposals, landfills, contaminant transports, leaching processes)
- Problems related to stress phenomenon
  - Slope stabilities, bearing capacities
  - Construction of tunnels
- Problems related to deformation phenomenon
  - Heave or subsidence of the ground surface

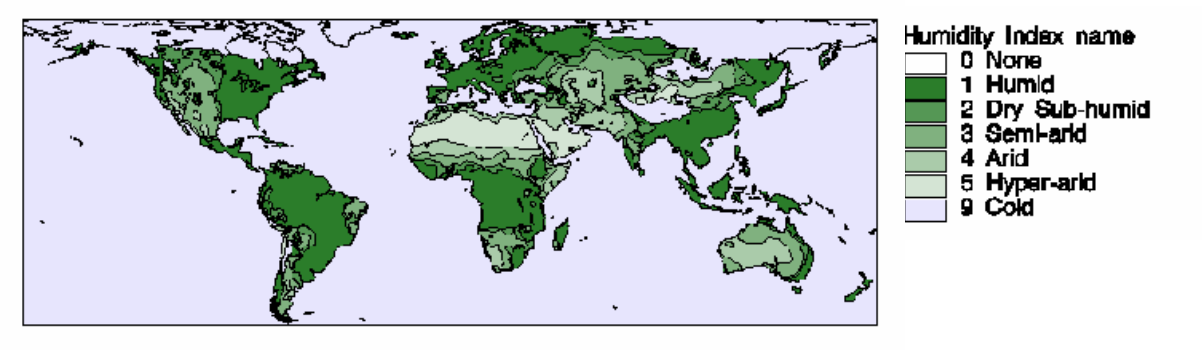

Figure 1.1: Global Humidity Index (from UNEP/GRID and UEA/CRU)

- Collapsing soil
- Shrinkage and swelling soil
- Compaction of soil

Depending on the type of soil, for instance clay, silt or sand, the above given phenomena have to be taken into account, when designing constructions such as dams, embankments, foundations or slopes.

1.2 Scope and Objectives

The scope of the present work is the investigation of an unsaturated granular material and its hydro-mechancial behavior. Furthermore, the phenomena (e.g. collapse, hysteresis) that belong to it, which is important for reliable prediction of settlements of buildings, failure mechanisms as base failure of strip footing or square footing, slope stability as well as the flow of fluid through dams in geotechnical engineering practice. Low suction values, for instance are able to maintain the stability of slopes or to improve the stiffness of a soil. Therefore experimental and theoretical analysis were conducted on Hostun sand. The contribution of capillary stresses (i.e. matric suction), which is the main force affecting the hydro-mechancial behavior of an unsaturated granular material, is usually ignored in conventional analysis of civil engineering constructions, for instance when predicting the bearing capacity of shallow foundations or settlements and deformations of buildings. Based on these concepts and models, constructions and buildings are designed and dimensioned.

To predict reliable unsaturated soil properties deep understanding of its coupled hydro-mechancial behavior is required. Compared to clayey soils the sand is not undergoing shrinkage and swelling. Experiments for prediction of the hydro-mechancial unsaturated soil behavior are commonly focused on cohesive soils as silts and/or clays. The complete hydro-mechancial behavior of sand has been poorly investigated to date. This behavior is quite different compared to silty or clayey soils. There is limited laboratory data available in liter-

ature with respect to the influence of suction on the hydro-mechancial behavior of a granular material.

To understand the complex behavior of unsaturated granular soil the following hydraulic and mechanical properties have to be determined:

- Soil-water characteristic curve
- Unsaturated hydraulic conductivity
- Stiffness
- Shear strength

In the present research work the hydraulic behavior is extensively investigated by determining the soil-water characteristic curve under several initial conditions (influence of void ratio), loading path directions (initial drainage, main drainage and main imbibition, scanning drainage and scanning imbibition process) and flow conditions (i.e. steady state flow, transient state flow) using testing devices, which measure water content and/ or water pressure and/ or cumulative water outflow and inflow. The influence of net stress on the soil-water characteristic curves is investigated additionally. The investigations of the hydraulic behavior lead to two constitutive relationships, namely the soil-water characteristic curve and the unsaturated hydraulic conductivity function, which are needed to describe the flow in unsaturated soils. Nevertheless, when dealing with unsaturated soils the key relationship is the soil-water characteristic curve, because based on this curve shear strength, stiffness and also hydraulic conductivity of an unsaturated soil can be derived. In general flow experiments (i.e. drainage and imbibition flow experiments) were carried out in small scale test (element test) and large scale column test (boundary value problem).

The mechanical behavior is estimated by determining stress-strain relation under one dimensional condition, where the influence of the suction on the stiffness of loose as well as dense packed Hostun sand specimens is considered. The collapse potential is estimated during one-dimensional compression tests on loose specimen. In large scale foundation experiments the influence of suction on the shear strength of the sand is obtained.

Due to large particles of granular materials and thus larger pores, the soil-water characteristic curve takes place in a narrow range of suction. This requires a high resolution and accuracy to the testing equipment. Because of this reason the present work involves modification of equipment as well as development of new equipment that fulfills these requirements and make it possible to investigate unsaturated granular materials. The main objectives of the investigations are:

- To provide appropriate equipment for investigation of unsaturated granular materials with focus on both, hydraulic and mechanical behavior.

- Model building and development of a simple suction-water content model, including scanning process.
- Determination of soil-water characteristic curve, $\theta(\psi)$ and determination of the influence of suction on the hydraulic conductivity, $k(\psi)$ and on the oedometer stiffness modulus, $E_{oed}(\psi)$.
- Derivation of reliable experimental data for validation of constitutive equations.
- Determination of reliable model parameters for numerical simulations of geotechnical problems. Only realistic soil parameters lead to realistic simulations and conclusions.
- Numerical simulations of experiments for parameter identification as well as improvement and/ or development of underlying constitutive equations.

An example is used to underline the importance of investigation as well as implementation of unsaturated soils to engineering practice. The change of mechanical behavior due to suction in a soil is carried out using the classical problem of shallow foundation (i.e. the influence of suction on bearing capacity, $q(\psi)$ is investigated), that is a typical civil engineering problem. Furthermore, the importance of the soil-water characteristic curve is given, which is used as an important tool when dealing with unsaturated soils in combination with the saturated shear strength for prediction of bearing capacity of unsaturated soils.

1.3 Organization of the Dissertation

The thesis contains eleven chapters. The first chapter (i.e. this chapter) outlines the background, the scope and objectives of the investigation as well as the organization of the dissertation. The second chapter summarizes basic literature on unsaturated soils related to the objectives of this study. Important hydraulic and mechanical functions as well as methods to determine them are introduced. Sets of equations and models used in unsaturated soil mechanics are presented and discussed. Background, theory and the main variables of process modeling are presented in the third chapter. Process modeling is used in this study for developing a model, that relates the suction to volumetric water content. Extended overview of the developed and modified testing devices and the equipment used to study the hydro-mechancial behavior of unsaturated sand are introduced in the fourth chapter. The material used and the experimental program carried out are discussed in the fifth chapter. The experimental program includes the investigation of hydraulic and mechanical unsaturated sand properties under consideration of for instance several initial and loading conditions, or different boundary conditions. This chapter also includes detailed explanations regarding to specimen preparation (preparation of homogenous, reproducible specimens) and the testing procedure. The experimental results derived from the extensive laboratory program are presented in the sixth chapter. The experimental results are analyzed and interpreted in the seventh chapter. The

eight chapter shows the results of numerical simulation of transient state tests by means of FE method and numerical models. In this simulations as input two sets of parameters are used, namely the parameter set derived from transient state tests and the parameter set derived from conventional tests. The introduced method of process modeling (see third chapter) is applied in chapter nine using experimental results, that were measured in the study. As a result a new soil-water characteristic curve model was developed. Unsaturated soil mechanics is applied in the tenth chapter on a typical engineering problem, i.e. bearing capacity of footing. The influence of suction to the bearing capacity behavior is revealed. The final chapter summarizes the results of the present investigation on the developed equipment for investigating unsaturated sand properties, the influence of suction on the hydro-mechancial behavior of sand, the introduced new soil-water characteristic curve model and the numerical simulations of the experimental data carried out. An outlook and perspectives for further studies on unsaturated sand are given.

Chapter 2

State of the Art

2.1 General

In the chapter the basics of unsaturated soil mechanics relevant to this study are briefly presented. Concepts of stress state variables in saturated and unsaturated soils are discussed. A survey on hydraulic functions in unsaturated soils, namely the soil-water characteristic curve and the hydraulic conductivity function, is given. Techniques for measurement of suction and water content, laboratory as well as field methods for determination of hydraulic functions and several approaches to model these relationships are critically discussed. A review on modeling of unsaturated soils is presented. Studies on volumetric mechanical behavior (stress-strain behavior, collapse and preconsolidation pressure) of soil are also presented. This literature review is focused on work performed on frictional granular materials.

2.2 Unsaturated Soils

Depending on the soil type a variety of methods for the characterization of soils and their properties are available. According to the principles of civil engineering, soils are classified into the following main soil groups:

- gravel, sand (non-cohesive soils)
- silt (cohesive soil)
- clay (cohesive soil)

The classification is based on the grain-size distribution, the coefficient of gradation and the coefficient of uniformity for non-cohesive soils and the plasticity index as well as the liquid limit for cohesive soils. Each type of soil is characterized by its mechanical and hydraulic behavior, that is also dependent on the water content or suction in the soil. The saturated conductivity for sand is about $k_s \approx 1 \cdot 10^{-3}$ to $1 \cdot 10^{-5}$ m/s, where a large cross sectional area of pore space for conduction of water flow is available. The typical value of saturated

conductivity for clays is about $k_s \approx 1 \cdot 10^{-7}$ to $1 \cdot 10^{-12}$ m/s (von Soos 2001). In this case the flow path of the water around the clay platelets is more tortuous, the water is partially bonded to the clay particles and thus becomes less. The oedometric stiffness modulus at $\sigma = 100$ kPa for sand is approximately $E_{oed} \approx 15.000$ to 70.000 kN/m^2. The oedometric stiffness modulus of a clay is approximately $E_{oed} \approx 600$ to 5.000 kN/m^2 (von Soos 2001). The incompressible grains of the sand cause the higher stiffness. Depending on the soil type, its behavior is governed by different mechanisms. The behavior of a soil is strongly influenced by its structure, mineralogy, fabric and the soil-water interaction.

Coarse grained materials (sand and gravel) consist of particles larger than 0.002 mm, that are commonly minerals as silicates, oxides, carbonates and sulphates. On the other hand the structure of fine grained materials consists of hydrated aluminium silicates and hydrous oxides in a crystalline structure (Mitchell 1993). Fine grained soils (i.e. clay and silt) encompasses a wide range of particle sizes varying between 10 to 1000 Å. The specific surface area of silt and clay is large and a large portion of the total molecules belong to the surface molecules. Thus the physico-chemical interactions between the soil particles and the pore fluid are significant. Therefor the main factors controlling fine grained soils properties are the surface area and the cation exchange capacity. Pore water is retained by molecular bonding, electrical field polarization caused by negative charge on the surface of the minerals, van der Waals attraction arising from the interaction between the molecules comprising the surface of the soil particles and the molecules comprising the pore fluid as well as the exchangeable cation hydration (osmotic effects). In coarse grained soils, since the surface area is relatively small, surface molecules constitute only a fraction of the total molecules. Hence surface area and the cation exchange capacity are not affecting the properties of coarse materials. Their characteristic behavior is mainly driven by contact forces between the grains as well as the matric suction, which is also called capillary force or negative pore-water pressure.

The soils fabric consists of the arrangement of soil particles, groups of particles and pores (Mitchell 1993). Gens & Alonso (1992) suggested 3 basic fabric types as shown in Fig. 2.1. In Fig 2.1 a) the fabric consists of elementary particle arrangements of clay platelets (also called matrix) and coarse grains, that could be sand or silt particles. The pore space between the elementary particle arrangements are intra-matrix pores. Several elementary particle arrangements joined together form aggregates as can be seen in Fig. 2.1 b). In the aggregates intra-aggregate pores and between the aggregates inter-aggregate pores can be distinguish. Coarse grains and the aggregates lead to a structure of a granular type material and to a multi modal pore-size distribution. In both fabrics a further type of pore exists, that are the intra-element pores (see Fig. 2.1 c). The fabric in Fig. 2.1 b) is known to be typical in natural and compacted clays. Due to different pore sizes (i.e. multi modal pore-size distribution) the material may become sensitive to, e.g. changes in loading condition, changes in suction or chemical changes. In coarse grained materials the main features are grains and pores.

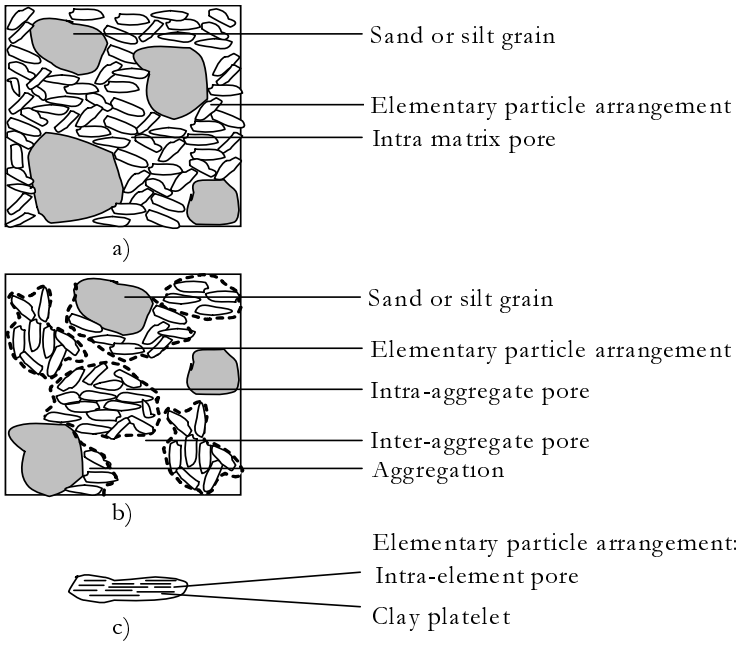

Figure 2.1: Fabric types of a soil: a) fabric consisting of elementary particle arrangements of clay platelets and coarse grains including intra-matrix pores, b) fabric consisting of elementary particle arrangements of clay platelets and coarse grains joined together to aggregates including inter -and intra-aggregate pores, c) fabric consisting of elementary particle arrangements including intra-element pores between clay platelets

Several grain particles in a loose packed granular soil joined together also can form aggregates including intra-aggregate pores and inter-aggregate pores between them (see Fig. 2.2).

However, the hydraulic behavior (i.e. hydraulic conductivity) and mechanical behavior (i.e. shear strength, stiffness, bearing capacity) of any soil is strongly influenced by its water content, saturation (i.e. degree of saturation) and respectively its suction. The suction in a

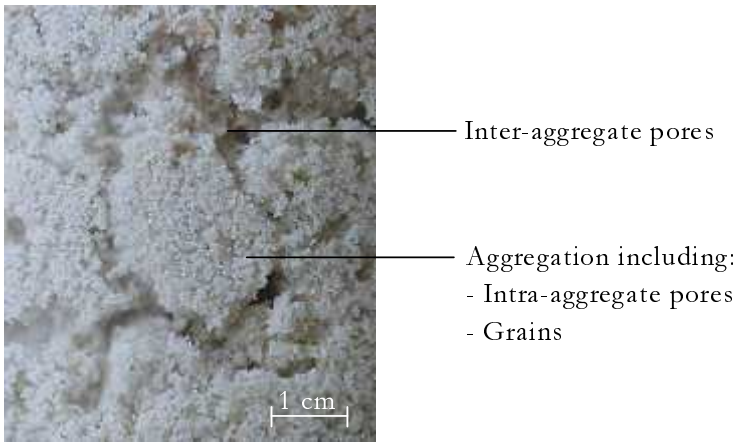

Figure 2.2: Fabric of a granular material

soil is governed mainly by the soils pore size distribution, grain-size distribution, density, the surface area and cation exchange capacity. Different phenomena are caused in a soil due to the presence of suction. Considering a fine grained soil, it undergoes collapse and is subjected to shrinkage as well as swelling phenomenon when changing water content in the soil. The soil-water characteristic curve occurs in a wide range of suction. Coarse grained soils undergo collapse and the soil-water characteristic curve occurs in a narrow range of suction.

The two important relationships describing the hydraulic behavior are the soil-water characteristic curve and the unsaturated hydraulic conductivity function. The influence of water content on the mechanical behavior of soils is reflected in their stress-strain behavior, e.g. volume change and shear strength.

2.2.1 Stress State in Unsaturated Soils

The mechanical behavior of a soil, e.g. volume change or shear strength, are described using the state of stress in the soil. Several combinations of the state of stress in a soil exists and are referred to stress state variables. Stress state variables have to be independent of the soil properties.

Soil mechanic is historically focused on the study of saturated soils. Effective stress is considered to be a fundamental variable for describing the mechanical effects due to a change in stress in the soil. The effective stress is applicable to all types of soil (e.g. sand, silt, clay), because it is independent of the soil properties. Fundamental principles and the concept of effective stress are suggested by Terzaghi (1943). In saturated soils the effective stress σ' is defined as difference between the total stress σ and the pore pressure u_w. The effective stress sits exclusively in the solid skeleton of the soil and is given by:

$$\sigma' = \sigma - u_w \tag{2.1}$$

The effective stress can be defined at any point in a soil if total stress and pore pressure are known. The validity of Terzaghi's effective stress equation for saturated soils is well accepted (Rendulic 1936, Skempton 1961).

In unsaturated soils it has to be considered that stress is acting in the air phase as pore air pressure as well as matric suction, which is defined as difference between air pressure and water pressure $(u_a - u_w)$, where u_a is the pore-air pressure and u_w is the pore-water pressure. Thus the state of stress in unsaturated soils is fundamentally different from the state of stress in saturated soils. Saturated soils are two phase systems composed of either solids and liquid (e.g. water saturated soil) or solids and gas (e.g. dry soil). Unsaturated soils are three phase systems comprised of solids (soil particles), liquid (pore water), and gas (pore air) (Lambe & Whitman 1969). As fourth phase Fredlund & Morgenstern (1977) introduced the contractile skin. Changes in pore water phase and pore-air phase directly influence the state of stress acting on the soil skeleton. Thus Bishop (1959) expanded Terzaghi's classical effective stress equation and suggested an effective stress equation, later named after him, for unsaturated

soils. Bishop's effective stress equation contains a single parameter χ, which was been found to depend on the type of soil:

$$\sigma' = (\sigma - u_a) + \chi(u_a - u_w) \tag{2.2}$$

where: σ is the total stress, u_a the pore-air pressure and u_w the pore-water pressure. χ is an effective stress parameter varying between 0 for dry soil and 1 for fluid saturated soil. It is captured by its strong dependency on the degree of saturation in the soil. Assuming a fluid saturated soil, Bishop's equation reduces to Terzaghi's equation. Various other expressions defining effective stress were proposed by Croney et al. (1958), Aitchison (1961), Jennings (1961). Jennings & Burland (1962) explored the limitations in the use of the effective stress concept and found that it may not be adequate for description of collapse behavior in soils. Also the single valued effective stress equation includes the material parameter χ, which leads to difficulties both in theory and its measurement. The material parameter χ depends on the type of soil and/or stress path (Jennings & Burland 1962, Coleman 1962, Bishop & Blight 1963, Burland 1965, Blight 1965). To describe the consolidation in unsaturated soils Biot (1941) already suggested the use of two independent stress state variables, namely the excess of total applied stress over the pore-water pressure $(\sigma - u_w)$ and the pore water pressure, u_w. Coleman (1962) suggested the use of net normal stress $(\sigma - u_a)$ and matric suction $(u_a - u_w)$ as stress variables to describe stress strain relations in unsaturated soils.

Variables used for description of a stress state should be independent of the soil properties (Fung 1977). The approach of independent stress state variables was continued from experimental and theoretical point of view by Fredlund & Morgenstern (1977). They proposed the use of net stress $(\sigma - u_a)$ and matric suction $(u_a - u_w)$ as independent stress state variables in unsaturated soils. They argued this approach is consistent with the principles of continuum mechanics. Three independent possible normal stress variables were defined: 1. $(\sigma - u_a)$, 2. $(u_a - u_w)$ and 3. $(\sigma - u_w)$. Their theory yields to three possible combinations of stress state variables for describing the deformation of unsaturated soils:

1. $(\sigma - u_a)$ and $(u_a - u_w)$ with reference pressure u_a
2. $(\sigma - u_w)$ and $(u_a - u_w)$ with reference pressure u_w
3. $(\sigma - u_a)$ and $(\sigma - u_w)$ with reference pressure σ

This approach was supported by null-type triaxial tests conducted earlier by Fredlund (1973), which showed that the volume of unsaturated soil specimen remains constant while decreasing and increasing the stress state variables by an equal amount. Very small changes in the specimen volume under null-type test condition prove the applicability of stress state variables in unsaturated soils. The stress state variables are related to equilibrium conditions in the unsaturated soil. The combination of the net normal stress $(\sigma - u_a)$ and matric suction $(u_a - u_w)$ is commonly used in engineering practice. Datcheva & Schanz (2003) for instance used

the net stress and suction stress variables for development of a constitutive model describing the behavior of unsaturated cohesionless soils under complex loading conditions and loading history.

The stress state variable must be measurable or predictable. Thus total stress state, pore-water pressure and/or pore-air pressure are determined and measured in the laboratory, when testing unsaturated soils. Using high-air entry disk enables to measure both pore-water pressure and pore-air pressure independently in unsaturated soils. Measurement devices as for instance tensiometer sensors enable to obtain pore-water pressure. The total stress is controlled by applying load to the specimen.

2.2.2 Phases in Unsaturated Soils

An unsaturated soil is a multi-phase system comprising of more than two phases (as in saturated soils), namely the solid phase, the liquid phase including the contractile skin and the gas phase. The solid phase consists of the soil grains. Depending on the grain sizes the soils may range from fine grained soils as silts and clays to coarse grained soils as sands and gravels. The liquid phase consists of any liquid or a miscible or immiscible combination of two or more liquids (e.g. water, oil, light non-aqueous-phase-liquid LNAPL, dense non-aqueous-phase-liquid DNAPL). Additionally the liquid phase may include the contractile skin, which may act as a tensile force on the liquids surface. In this work the solid phase, the liquid phase and the gas phase of the unsaturated soil are assumed to be the soil solids, water (with the contractile skin) as well as air, that leads to a 3-phase system. The phases of unsaturated soil are schematically given in Fig. 2.3.

2.2.3 Soil Suction

The total soil suction is referred to the free energy state of the soil pore water (Edlefsen & Anderson 1943, Fredlund & Rahardjo 1993*a*). The thermodynamic relation between the total suction or free energy of the soil water and the relative humidity of the soil air is given in the following equation:

$$\psi = -\frac{RT}{v_{w0} \cdot \omega_v} \cdot ln\frac{RH}{100} \tag{2.3}$$

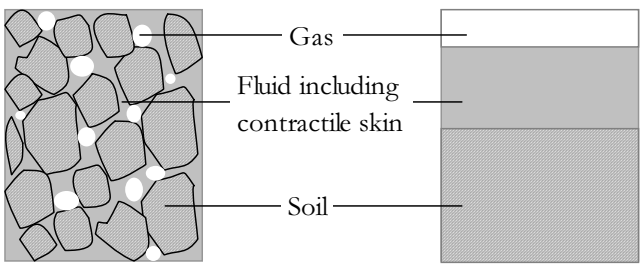

Figure 2.3: 3 Phase system representing unsaturated soils

where: ψ is the total suction or free energy, R is the universal gas constant, T is the absolute temperature, v_{w0} is the specific volume of water, ω_v is the molecular mass of the water vapor and RH is the relative humidity. The relative humidity is defined as the amount of water vapor that is in a gaseous mixture of air and water and is given as $RH = u_{v1}/u_{v0} \cdot 100$, where u_{v1} is the partial pressure of water vapor in the mixture and u_{v0} is the saturated vapor pressure of water of the mixture at the temperature T in equilibrium with the free water.

The concept of capillary potential in unsaturated soils was defined by Buckingham (1907). Richards (1928) defined the soil water potential as the sum of the capillary potential and a gravitational term. Neglecting temperature effects, the main mechanism influencing the pore water potential in a soil are capillary effects and osmotic effects. Thus the total suction consists of two components, namely the matric suction or capillary suction and the osmotic suction:

$$\psi = \psi_m + \psi_o \tag{2.4}$$

where: ψ_o is the osmotic suction. The difference across the air-water interface is the matric or capillary suction $\psi_m = u_a - u_w$ with the pore-air pressure u_a and the pore-water pressure u_w. This leads to Eq. 2.5:

$$\psi = (u_a - u_w) + \psi_o \tag{2.5}$$

Matric suction is associated with the capillary phenomenon. The capillary phenomenon is arising from the surface tension of the water and involves the air-water interface. Effects of the osmotic suction have to be considered when dissolved solutes are present in the pore-water. With increasing concentration of dissolved solutes in the pore-water the relative humidity decreases and the osmotic suction increases respectively. When dealing with sand the osmotic suction is assumed to be negligible small because dissolved solutes are not present. Therefore the term suction is equal to the term capillary pressure or matric suction in this thesis.

The main matric suction component is the capillarity (i.e. the force caused from surface tension) and it is assumed the pores in the soil act as capillary tubes. The surface tension is the tangential force between a liquid and a gas caused by the difference in attraction between the molecules of the liquid and the gas. The well known Young-Laplace equation provides a general relationship between the matric suction and the interface geometry:

$$u_a - u_w = T_s \cdot (\frac{1}{R_1} + \frac{1}{R_2}) \tag{2.6}$$

where: T_s is the surface tension of the liquid phase, and R_1 and R_2 are the radii of curvature of the membrane in two orthogonal directions.

Since the pores in a soil are different in sizes the capillary tubes are different in diameter, causing different surface tension values. As smaller the tube as smaller the radii and as larger the surface tension. The influence of the radius on the surface tension is shown in Fig. 2.4 based on the capillary tube model, where the pores in a soil are assumed to act like capillary tubes.

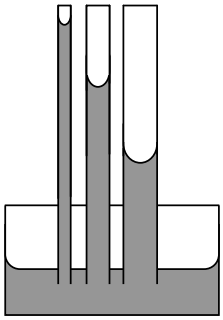

Figure 2.4: Rise of water in capillary tubes of different diameter (Lu & Likos 2004)

Equilibrium between two interconnected drops of water is additionally presented in Fig. 2.5. Two water drops with different radii ($R_1 > R_2$) are connected through a pipe filled with water. The valve of the pipe is closed at first. Both drops have an internal pressure u_{w1} and u_{w2}. The water pressure in drop 1 is smaller than in drop 2 ($u_{w1} < u_{w2}$), because the radius of curvature for drop 1 is larger. When opening the valve the system will equilibrate. The water will flow from higher pressure to smaller pressure. Thus the water will flow from drop 2 to drop 1, drop 1 becomes larger and drop 2 becomes smaller. Equilibrium state is reached, when the fluid of drop 2 enters the pipe and a convex meniscus with a radius equal to R_1 is formed (Lu & Likos 2004).

In Fig. 2.6 a capillary tube and a wide closed container are given. The interaction between air, water and solid is shown. Two pressure points $(1, 2)$ are observed in the tube and in the container. The tube and the container are connected with a water filled pipe, where the valve is at first closed. The air pressure in both systems is the same. Point 1 is located in the middle and point 2 is located at the border of the container. The pressure in both points is equal in the tube, because both points have the same spherical meniscus with the radius R. The pressure difference can be calculated by using the meniscus geometry as $u_a - u_{w1/2} = 2T_s/R$

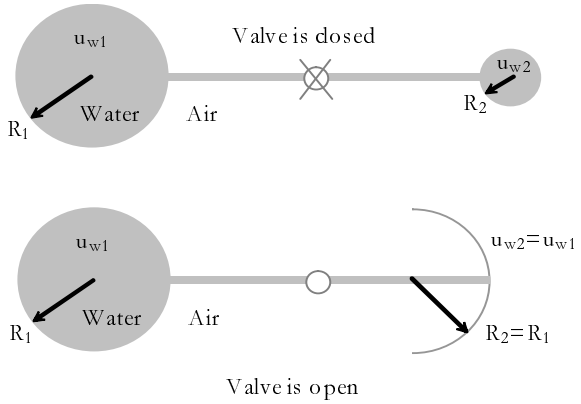

Figure 2.5: Equilibrium between two interconnected drops of water - the effect of drop's radius (Lu & Likos 2004)

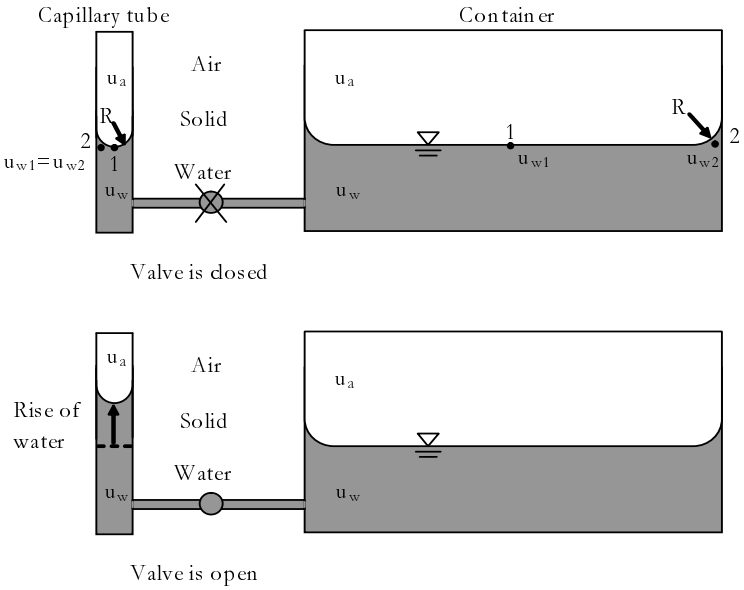

Figure 2.6: The interaction between air and water (Lu & Likos 2004)

with T_s the surface tension and R the radii of curvature. Because the air-water interface in the middle of the container is flat, the pressure in point 1 is equal to the air-pressure $u_{w1} = u_a$. The curvature of the air-water interface in point 2 leads to a water pressure less then the air pressure. Here the pressure difference can be calculated using also the meniscus geometry $u_a - u_{w2} = 2T_s/R$. Thus in the container the pressure in point 1 is larger than in point 2 indicating larger water pressure in the container. When opening the valve the total head in the water phase in both the container and the tube will tend towards equilibrium. Since the pressure in the tube is less than in the container the water table in the tube will rise above the water table in the container (Lu & Likos 2004).

2.3 Hydraulic Functions

Important hydraulic functions when dealing with unsaturated soils are the soil-water characteristic curve as well as the hydraulic conductivity functions that are explained in detail in the following.

2.3.1 Soil-Water Characteristic Curve

Definition and General Information

The fundamental constitutive relationship in unsaturated soils relates the gravimetric water content w, the volumetric water content θ or the saturation S to the suction in the soil. Several names are proposed for this relation, namely:

- *Suction-water content relationship (SWCR)*

  The suction-water content relationship relates the suction to the water content in the soil. The suction-water content relationship is estimated at any initial state in the soil for any loading path (i.e. drainage or imbibition process). The curve starts in between the main drainage and imbibition loop.

- *Soil-water characteristic curve (SWCC)*

  The soil-water characteristic curve is the relationship between suction and water content during drainage test from fully saturated state ($S = 1$) up to dry soil condition and consequent imbibition test from dry state to zero suction in the soil

- *Capillary pressure-saturation relationship (pcS-curve)*

  Capillary pressure-saturation relationship is often used in soil science and relates the saturation to the capillary pressure in the soil. This expression may be used when granular medias are considered, because in case of granular materials osmotic suction is negligible small.

In the present study initially water saturated sand specimens are investigated and thus the term soil-water characteristic curve is used. The soil-water characteristic curve of a soil is the key function when dealing with unsaturated soils (Fredlund 2002). The importance of the soil-water characteristic curve is not only in giving insight of soil-water interaction but it is also used to estimate the hydraulic conductivity and the shear strength, which are subsequently needed to estimate the unsaturated soils behavior (Fredlund et al. 2000). The soil-water characteristic curve is required for modeling and predicting water as well as solute transport in unsaturated porous media.

Soil-water characteristic curves for different type of soils differ from each other and depend upon the structure or arrangement of the soil particles, the grain-size distribution, pore-size distribution as well as the density (Richards & Weaver 1944, Croney & Coleman 1954, Salter & Williams 1965, Reeve et al. 1973). Fig. 2.7 shows typical drainage soil-water characteristic curves for sand, silt and clay. From Fig. 2.7 it can be seen that the soil-water characteristic curve of the sand is located in a narrow range of suction while the soil-water characteristic of clay is located in a large range of suction. With increasing soil suction the water content and the degree of saturation are decreasing. At high water content the corresponding suction is low. At low water content the corresponding suction is high. After the drainage process the soil-water characteristic curve may be determined also for imbibition process. Other well known terms for the drainage process are drying process as well as desorption process and for the imbibition process are wetting as well as adsorption process.

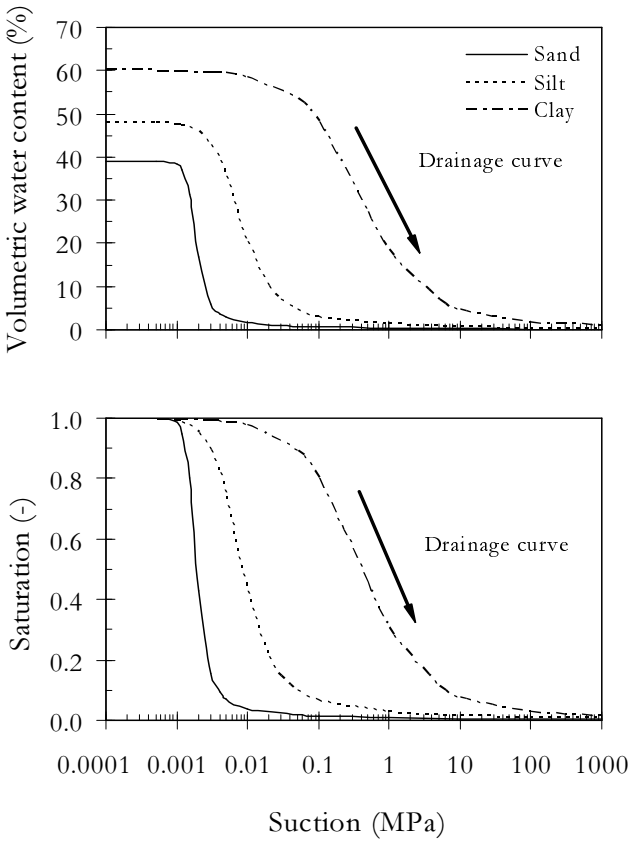

Figure 2.7: Soil-water characteristic curves for different types of soils

Zones and Parameters of the Soil-water characteristic curve

Soil-water characteristic curves can be divided into the following 3 zones for drainage process:

- *Saturated zone*

  The saturated zone is the zone between soil suction $\psi = 0$ and the air-entry value ψ_{aev}, where nearly all pores are filled with liquid. In the saturated zone the liquid phase is continuous and the gas phase is non-continuous.

- *Transition zone*

  After reaching the air-entry value ψ_{aev} larger pores of the soil begin to drain followed by smaller pores. The volumetric water content is decreasing till reaching the residual water content θ_r. The air-entry value ψ_{aev} and the residual volumetric water content θ_r enclose the transition zone. The amount of water in the pores in the saturated zone and the transition zone mainly depends on the grain-size distribution and pore-size distribution. There the capillary force may be the main driving force. Both, the liquid and the gas phases are continuous.

- *Residual zone*

  The transition zone is followed by the residual zone. Whereas in the transition zone the pore water is retained mainly by capillary forces, in the residual zone the pore water is retained in form of thins films on the soils grains. This is caused by the surface area and the surface charge density of the soil. The gas phase is the continuous phase and the liquid phase is the non-continuous phase. Water is transported only by water vapor diffusion.

Following Fredlund & Xing (1994) typical parameters of the soil-water characteristic curve can be estimated. These parameters are:

- *Air-entry value* ψ_{aev}

  The air-entry value ψ_{aev} is the value of soil suction, where air starts to enter the largest pores of the soil during drainage process.

- *Saturated volumetric water content* θ_s

  The saturated volumetric water content is the water content in a soil, where all pores are filled with liquid $S = 1$.

- *Residual soil suction* ψ_r *and corresponding residual volumetric water content* θ_r

  The residual soil suction ψ_r and corresponding residual volumetric water content θ_r is the point, where the water starts to be held in the soil by adsorption forces (Sillers 1997).

- *Water-entry value* ψ_{wev}

  The water-entry value is the soil suction where water starts to displace air in the soil and enters the pores in the soil during imbibition process (Wang et al. 2000, Yang, Rahardjo, Leong & Fredlund 2004*a*). When reaching the water-entry in a soil the water content starts to increase significantly.

For sand the residual zone is generally very limited, because both the surface area of the soil particles and the surface charge density are negligibly small. The pore-size distribution mainly influences the shape and the slope of the soil-water characteristic curve. Uniform soils have steep soil-water characteristic curves, because the majority of pores are drained at a narrow range of soil suction. Well-graded soils have flatter soil-water characteristic curves, because the pores are different in size and drained over larger range of soil suction. Controlled by relatively large pores the air-entry pressure as well as the water-entry pressure are low, when working with sand. The soil-water characteristic curve of a silt is characterized by a larger range of soil suctions. Silts absorb a greater amount of pore water due to smaller pores and a significant surface area as well as surface charge density. The smaller pores retain

the water up to a higher matric suction resulting in a larger air-entry value and water-entry value. As already mentioned clays have a very high surface area and a high surface charge density is typical for this type of soils. Thus the capacity of water absorption is the highest for clay and the soil-water characteristic curve takes place over a wide range of soil suctions. Capillary forces are responsible for relatively low suction values and the corresponding high water contents governed by the pore-size distribution and grain-size distribution. At low values of water content and corresponding high soil suction values, where water is only available as a thin film on the grain surfaces, the dominant mechanism influencing the shape of the soil-water characteristic curve are the surface properties of the grains. The exemplary drainage curve is shown in Fig 2.8 for a sand with typical soil-water characteristic curve parameters and zones.

Hysteresis and Scanning Curves

Since the soil-water characteristic curve depends on the soil suction history it is required to distinguish between drainage characteristic and imbibition characteristic of the soil. During drainage process more water is retained by a soil than during imbibition process for the same suction value. Thus the relation between water content and suction is hysteretic and is presented by the existence of a initial drainage curve, main drainage and imbibition curves as well as an infinite number of scanning curves in between the main drainage-imbibition loop (see Fig. 2.9). The drainage process of an initially fluid saturated ($S_0 = 1$) soil specimen results in the initial drainage curve. The wetting (up to $\psi = 0$) of an initially dry soil specimen gives the main imbibition curve. Due to occluded air bubbles, redistribution of the pore system or

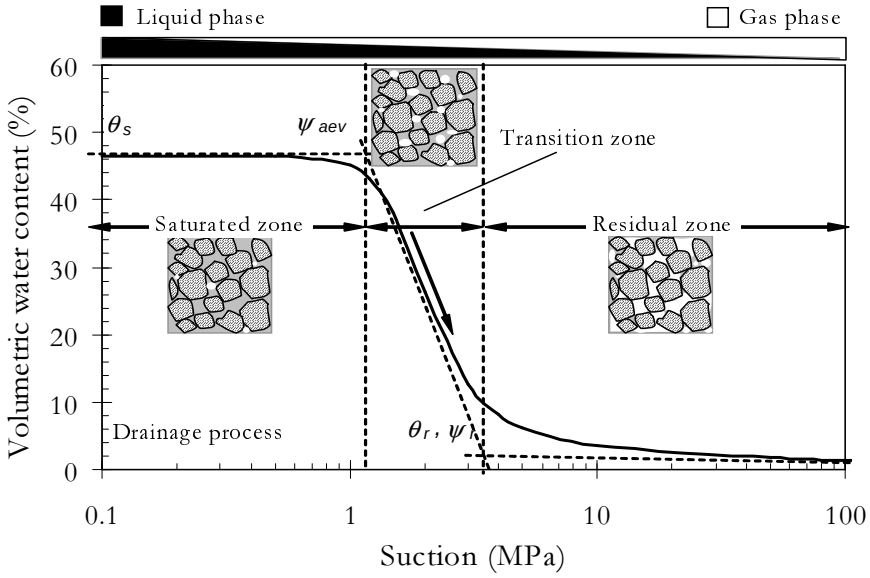

Figure 2.8: Typical soil-water characteristic curve parameters and zones

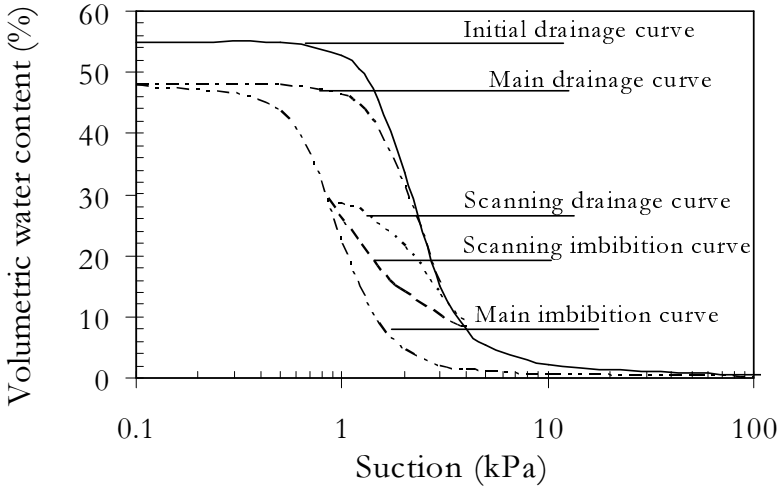

Figure 2.9: Soil-water characteristic curve showing the initial drainage curve, main imbibition curve, main drainage curve and scanning curves

closed pores for most soils it is not possible to achieve fully saturated state by imbibition after drainage. The following drainage of the soil specimen is called main drainage curve. Whereas the initial drainage curve is irreversible, the main loop consisting of both the main drainage curve and main imbibition curve can occur in numerous cycles. Drainage scanning curves as well as imbibition scanning curves are located within the main soil-water characteristic loop. The names commonly used for the several drainage and imbibition branches are summarized in the following:

- Initial drainage curve (irreversible curve)
- Main drainage curve and main imbibition curve (reversible curves)
- Scanning drainage curve and scanning imbibition curve (infinite number of scanning curves available between main drainage and imbibition curve)

The phenomenon of hysteresis can be found in several natural sciences such as magnetism and in chemistry. A independent domain theory for modeling hysteresis as physical phenomenon in soil science was presented by Everett & Whitton (1952), Everett & Smith (1954). The phenomenon of hysteresis has been gained from experimental and theoretical experiences (Haines 1930, Topp 1969, Poulovassilis 1970, Pavlakis & Barden 1972, Mualem 1984*b*, Nimmo 1992, Iwata et al. 1995, Pham et al. 2003) and there is broad agreement in the research literature regarding the relevance and phenomenological background of hysteresis in the soil-water characteristic curve. The phenomenon of hysteresis was first detected and reported by Haines (1930) and is attributed to several factors as the rain drop effect (Bear

1972), the ink-bottle effect (Haines 1930, Miller & Miller 1988), the snap-off effect and the effect of by-passing (Chatzis & Dullien 1983). Above given reasons for the phenomenon of hysteresis suggested from multi-scale considerations are explained below:

- *Rain drop effect* (Bear 1972)

  There are different angles of contact during drainage (θ_1) and imbibition (θ_2) cycles that give rise to the rain drop effect. Comparing the angle between the tangent of the air-water interface and the tangent between the water-solid interface (the contact angle) then the angle of contact is large during the wetting phase and the angle of contact is small during the drying phase ($\theta_1 < \theta_2$). In Fig. 2.10 the raindrop effect is visualized by a drop running down a surface and tubes at drainage and imbibition process.

- *Ink-bottle effect* (Haines 1930, Miller & Miller 1988)

  According to the geometry of the pores at equal matric suctions, the volume of fluid in the pores depends on the hydraulic loading path. Therefore, the volume of the fluid in the pores during drying is larger than during wetting. This effect is known as ink-bottle effect and is sketched in Fig. 2.11. In Fig. 2.11 the two tubes *a*) and *b*) show different heights in capillary rise due to different diameters. In *c*) the drainage of a tube with non-uniform diameters is shown, where the water is kept at the pore neck. In *d*) the imbibition of a tube with non-uniform diameters is shown, where the water is kept at the pore body. When draining the tube *c*) the capillary rise corresponds to that of the smaller tube *a*) and when wetting the tube *d*) the capillary rise corresponds to that of the larger tube. Although the same pressure is applied to the tubes, the drained tube *c*) contains more water than the wetted tube *d*). Thus the saturation history is influencing the capillary rise.

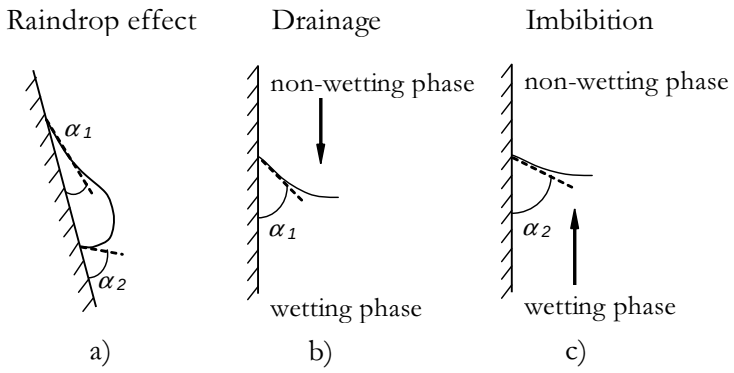

Figure 2.10: Raindrop effect visualized by a drop running down a homogeneous surface and in tubes during drainage and imbibition process (Bear 1972)

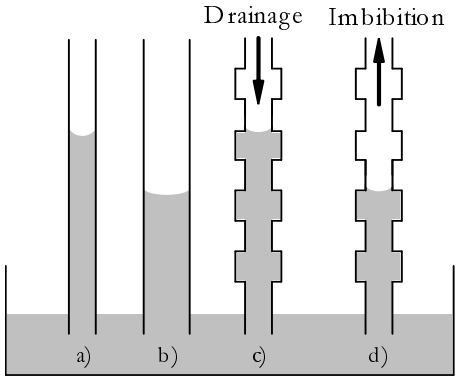

Figure 2.11: Capillary rise in tubes different in diameter and drainage as well as imbibition process in tubes with varying diameters (Haines 1930, Miller & Miller 1988)

- *Snap-off effect* (Chatzis & Dullien 1983)

  The inclusion of the non-wetting phase (i.e. gas) during the wetting cycle is known as snap-off effect. In Fig. 2.12 can be seen that it depends on the diameter of the pore bodies and the pore necks.

- *Effect of by-passing* (Chatzis & Dullien 1983)

  Consider the combining of two capillary tubes different in diameter. The system is fluid saturated and starts to drain. Then the non-wetting phase (gas) is replacing the wetting phase (fluid). Due to less capillarity the larger tube is first filled with gas. In the smaller tube fluid is still retained and separated from the fluid continuum causing entrapped fluid (see Fig. 2.13). Vice versa during imbibition process entrapment of gas occurs.

Yang, Rahardjo, Leong & Fredlund (2004*b*) discussed the hysteretic behavior and correlated it to grain size parameters (e.g. grain size parameter d_{10}).

The relevance of the hysteresis mechanism is still a topic of discussion. However, in the context of coarse-grained granular material, such as sand used in this study, hysteresis is most

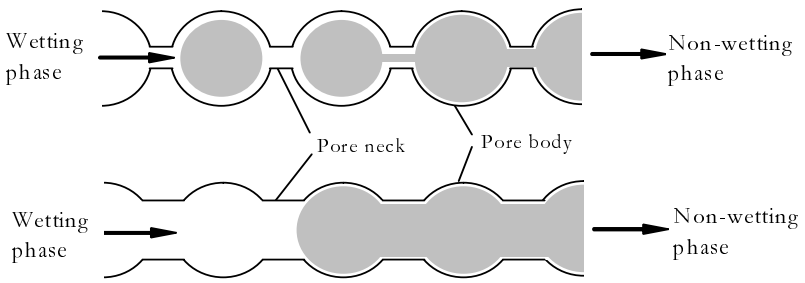

Figure 2.12: Influence of the pore geometry on the inclusion of a fluid caused by snap-off effect (Chatzis and Dullien 1983)

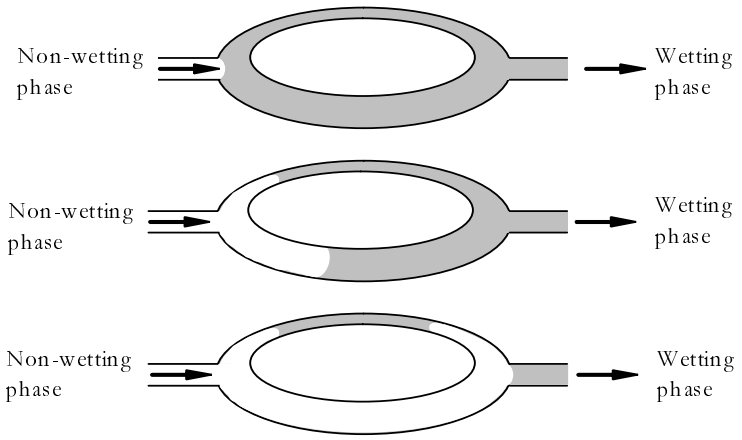

Figure 2.13: Influence of the pore geometry on the fluid placement caused by by-passing effect (Chatzis and Dullien 1983)

likely attributable to a combination of the ink bottle effect (*intra* particle arrangement) and the contact angle hysteresis (*inter* particle scale).

2.3.2 Hydraulic Conductivity Function

Definition and General Information

The unsaturated hydraulic conductivity describes the ability of the soil fluid to flow through the soil pores under a specified hydraulic gradient and is essential for dealing with pollutant transport or the modeling of flow through earth structures. Whereas the saturated hydraulic conductivity of granular materials is a function of void ratio and the type of pore fluid, the unsaturated hydraulic conductivity is also a function of water content or degree of saturation or volumetric water content (Leong & Rahardjo 1997*a*). The shape of the hydraulic conductivity function is influenced by the void ratio, the amount of fluid (e.g. water content) and the type of fluid (e.g. viscosity) in the pores.

The hydraulic conductivity for one type of soil can vary several orders in magnitude depending on the water content, degree of saturation or suction in the soil. As qualitatively presented in Fig. 2.14 the magnitude of the conductivity for different soil types also vary from high values as for gravel and very low values as for clay. Several exemplary hydraulic functions of a sand, a silt and a clay are presented in Fig. 2.14. The suction-water content drainage curve, that is directly related to the unsaturated hydraulic conductivity, the unsaturated hydraulic conductivity function and the relative conductivity function are given for each type of soil. The relative conductivity function relates the relative conductivity to the effective saturation. The effective saturation S_e (the normalized water content) is defined as:

$$S_e = \frac{S(\psi) - S_r}{1 - S_r} \tag{2.7}$$

where: S is the saturation and S_r is the residual saturation. In case of silt, the shape of the unsaturated hydraulic conductivity function is explained. It is assumed the initial condition is a water saturated specimen, where the suction is equal to zero and the volumetric water content is $\theta_s = 48$ %. The soil matrix is saturated with water and the saturated conductivity, that is the maximum conductivity (maximum cross sectional area for water to flow is available), is equal to $k_s = 1 \cdot 10^{-7}$ m/s. Consequently the conductivity of air is equal to zero at this state. Until reaching the air-entry value the soil retains nearly all amount of water (see also suction water content relationship) that causes only a slight decrease in unsaturated hydraulic conductivity. Desaturation commences when passing the air-entry value, where air starts to enter the soil largest pores. With increasing suction the pore

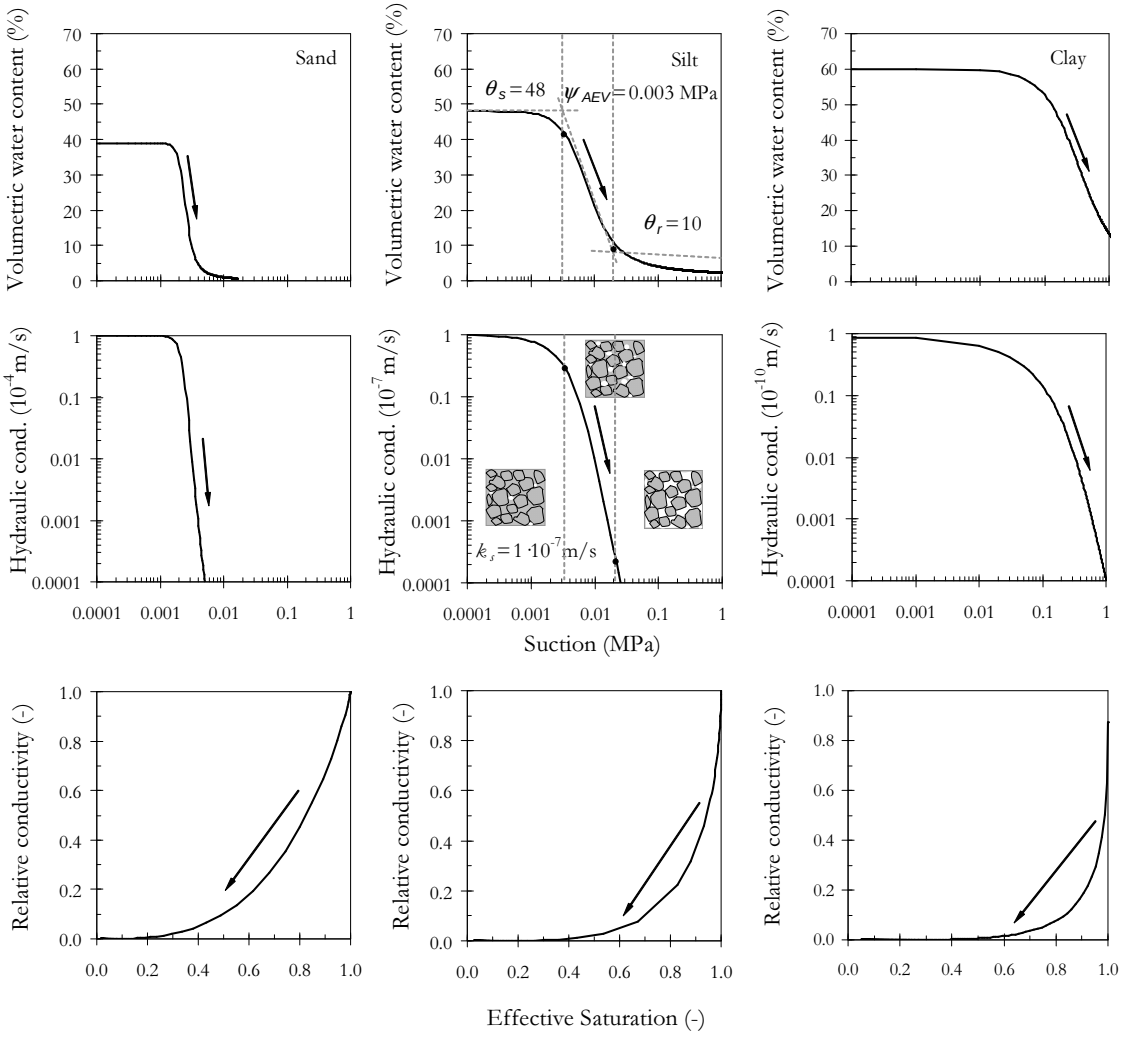

Figure 2.14: Exemplary hydraulic functions (soil-water characteristic curve - top, hydraulic conductivity function - middle, relative hydraulic conductivity function - bottom) for sand, silt and clay

system is drained continuously and the water content as well as the unsaturated hydraulic conductivity is drastically decreasing. The flow of air is increasing. Passing the residual water content the pore water exists mainly as a thin film around the grains or disconnected radii between the grains and the unsaturated hydraulic conductivity reduces to zero. Typically for soils the unsaturated hydraulic conductivity is changing between air-entry value and residual water content in a large range. It is also common to normalize the hydraulic conductivity $k(\psi)$ of unsaturated soil with respect to the saturated conductivity k_s (see also Fig. 2.14). This value is known as relative conductivity k_r:

$$k_r = \frac{k(\psi)}{k_s} \tag{2.8}$$

Whereas the water flow is governed by the total potential of the water phase the air flow is governed by the total potential of the air phase. Neglecting the existence of the vapor phase and its transport, in an unsaturated soil pore water is flowing only through the continuous liquid phase. And neglecting diffusive transport in the liquid phase of an unsaturated soil than air is flowing in the continuous gas phase. The flow of water and the flow of air occur under different conditions depending on the type of soil. The flow is differed into:

1. pore water flow (fluid saturated soil)
2. pore water flow and pore air flow (unsaturated soil)
3. pore air flow (air saturated soil)

At water content larger than the air-entry value water content, where remaining air is present only as isolated bubbles and a continuous water phase exits, the main mechanism is the water flow. In a condition, where the water content is larger than the residual water content but smaller than air-entry value, simultaneous the pore air and the pore water are flowing. Whereas the driving potential for the airflow is the gradient in air potential, the driving potential in water flow is the gradient in pore water potential. At a water content equal or less to residual condition the pore water exists only in isolated pores or thin films around the soil grains and the continuous paths for water flow are essentially cut off. The primarily mechanism for liquid flow, is through vapor phase transport only. No continuous liquid phase is available and no liquid flow occurs. But on the other hand the flow of pore air occurs, that is caused by gradients in air potential.

Hysteresis and Scanning Curves

In the previous section the phenomenon of hysteresis in soil-water characteristic curve was introduced. Because the unsaturated hydraulic conductivity function is directly related to the soil-water content relationship, the phenomena of hysteresis becomes evident in unsaturated hydraulic conductivity curve $k(\psi)$. This means the hydraulic conductivity is larger along the

drainage process, where following the soil-water characteristic curve the amount of water filled pores is greater, than during imbibition process.

The effect of hysteresis in the relationship between unsaturated hydraulic conductivity and volumetric water content or saturation is supposed to be minor. Experimental results of drainage and imbibition hydraulic conductivity versus water content $k(\theta)$ or hydraulic conductivity versus saturation $k(S)$ can be grouped in two converse categories:

- *Hysteresis:*

  Youngs (1964), Staple (1965) found differences between imbibition path and drainage path for slate dust and silt loam. Poulovassilis (1969) studied sand giving significant hysteresis in the intermediate range of volumetric water content but vanishing for both low and high values of volumetric water content. For high degrees of saturation in a clay Pavlakis & Barden (1972) found differences up to a factor of 10. Dane & Wierenga (1975) found no hysteresis for a sand but significant hysteresis for intermediate and low ranges of volumetric water content for a clay loam. Based on the independent domain theory it is assumed, that the pore water is contained in pores not common during drainage and imbibition process. While during drainage process the water volume is contained in pores with larger radii, the radii of the pores containing the water volume at imbibition path are smaller (Poulovassilis 1969).

- *No significant hysteresis:*

  Most of the studies which concluded no significant effect of hysteresis on hydraulic conductivity function are related to uniform granular materials such as sand (Klute et al. 1964, Collis-George & Rosenthal 1966, Talsma 1970, Poulovassilis 1970, Topp 1969) and glass beads (Topp & Miller 1966). Little evidence is available for clay and silt loam (Nielsen & Biggar 1961, Topp 1971*a*). Under the assumption that no volume changes occur in the tested specimen the effect of hysteresis is supposed to be negligible. Differences only can be found between initial drainage and main drainage curve due to consolidation associated with the applied suction (Nielsen & Biggar 1961, Enderby 1955).

When analyzing the results from the research literature, the following aspects are noteworthy. Most of the studies are missing precise information on volume change behavior during drying and wetting cycles. Derivation of suction-hydraulic conductivity functions is performed using different methodologies, including both direct and indirect procedures. Experimental devices include different scales ranging from oedometer type cells up to soil column devices. Applied sensors show different precision depending on the installation procedure and sample geometry. Hysteresis in the suction-hydraulic conductivity function seems to be dependent on the type of soil and the range of volumetric water content: Clay soils seem to have a tendency for hysteresis, particularly in the intermediate range of volumetric water contents. Most of the

referenced studies date back almost 20 to 30 years. Precision of measurements related to water content and suction must be carefully considered when deriving the final conclusions.

2.3.3 Methods for Determination of Hydraulic Functions

As already mentioned the important hydraulic functions in unsaturated soil mechanics are both the soil-water characteristic curve $\theta(\psi)$ and the unsaturated hydraulic conductivity function $k(\psi)$. Several methods are available to measure these two constitutive functions, e.g.:

- Determination of $\theta(\psi)$ from experiments conventionally performed in tempe cells or pressure cells and deriving $k(\psi)$ by combining $\theta(\psi)$ with different model assumptions.
- Determination of $\theta(\psi)$ and $k(\psi)$ independently from experiments.
- Determination of one-step flow, multistep flow or continuous flow experiments and estimating both functions simultaneously using inverse modeling (see Section 2.6).

A literature review on flow experiments, that are used for predicting hydraulic functions of unsaturated soils is given in Tab. 2.1. The table gives an extensive overview of flow experiments carried out by several researchers. It gives the testing devices and the equipment used (PT-Pressure transducer, T-Tensiometer, GRA-Gamma Ray Attenuation, TDR-Time Domain Reflectometry sensor), the method applied (OM-One step Method, MM-Multistep Method), the loading applied to the specimen (D-Drainage, I-Imbibition) and the material, that was used for the investigation. Only few researches used tensiometer and TDR sensor measurements in their investigation to study unsaturated flow.

Table 2.1: Literature review on flow experiments

Author	Cell	Equipment	Method	Loading	Material
Liakopoulos (1964)	Column device	PT	Gravitation	D	Sand
Vachaud and Thony (1971)	Column device	3T, GRA	Infiltration	D, I	Sand
Kool et al. (1985)	Tempe pressure cell	-	OM	D	Sandy loam, silt loam, sandy clay loam, clay
van Dam et al. (1992)	Tempe pressure cell	-	OM	D	Loamy sand, clay loam
Toormann et al. (1992)	Outflow apparatus	3T, 3TDR	OM	D	Synthetic soil
Eching and Hopmanns (1993)	Modified pressure cell	1T	OM, MM	D	Silt loam, loam, sandy loam, fine sand
van Dam et al. (1994)	Tempe pressure cell	-	OM, MM	D	Loam
Wildenschild et al. (1997)	Modified pressure cell	PT	OM, TM	D	6 different sands
Lehmann et al. (1998)	Column device	3T, 7TDR	TM	D, I, SC	Sand
Ruan and Illangasekare (1999)	Column device	6T	TM	I	Sand
Rassam and Williams (2000)	Column device	2T, 1TDR	TM	D	Tailing samples, sand
Stauffer and Kinzelbach (2000)	Column device	4T, GRA	MM	D, I	Sand
Wildenschild et al. (2001)	Modified pressure cell	2T	OM, MM, TM	D	Sand, fine sandy loam
Fujimaki and Inoue (2003)	Modified pressure cell	2T	MM	D	Loamy sand, sandy loam, loam
Chen et al. (2007)	Pressure cell	PT	MM	D, I, SC	Fine sand, ultra fine sand, silt

Determination of Soil-Water Characteristic Curve

Commonly the soil-water characteristic curve is determined by relating the suction to the water content that are measured in cells under equilibrium condition and fitting a parametric suction-water content function to these data pairs. To achieve equilibrium condition in a soil is extremely time consuming and laborious. Thus flow experiments were developed and in combination with inverse modeling of experimental data the soil-water characteristic curve was estimated among others. Several flow experiments are available for determining hydraulic properties of an unsaturated soil. As proposed by Schultze et al. (1997) in this work flow experiments are classified into: multistep flow experiments, one-step flow experiments and continuous flow experiments. These experiments are performed either under steady-state condition (equilibrium) or transient state condition (non-equilibrium) (Topp et al. 1967). State of the art in inverse modeling of one-step, multistep and continuous flow experiments is given in Durner et al. (1999). An overview of several equipments used for determination of soil-water characteristic curve is given in Tab. 2.2. Some of the listed equipment is explained in detail in Chapter 2.4.

- *Multistep Method:*

  The multistep method (Gardner 1956, Klute 1986, van Dam et al. 1990) is used to perform steady-state experiments, where several suction steps are imposed to the specimen and the next suction increment is not applied before reaching equilibrium condition in the soil, i.e. no inflow (during imbibition process) or outflow (during drainage process) of water is measured or observed. Multistep outflow experiments were performed for instance by Eching & Hopmans (1993), Dam et al. (1994), Schultze et al. (1997), Wildenschild et al. (2001), Fujimaki & Inoue (2003). Different equipment devices are available to determine the suction-water content drainage/ imbibition relationship under steady-state conditions. The relationship can be directly determined using a suction cell apparatus (Haines 1930) or pressure cell apparatus (Richards 1941, 1947). Tempe cell for application of matric suctions up to 100 kPa (Reginato & van Bavel 1962), volumetric pressure plate for application of matric suctions up to 200 kPa and large pressure plate for application of 500 and 1500 kPa (Fredlund & Rahardjo 1993*b*) were developed. Pressure plate apparatus was developed also by Pham et al. (2004). The change of water volume or mass of water in the specimens is measured during testing procedure carried out in these cells. After finishing the test, the specimen is dismantled and the gravimetric water content is measured by oven drying method. Using back-calculation method the water content is related to each imposed suction step. By using the axis-translation technique (Hilf 1956) suctions are applied to the specimen. The approximate measurement range for the axis-translation technique is 0 kPa to 1500 kPa depending on the air-entry value of the ceramic disk used. Additionally some modified cells are equipped with tensiometers or pressure transducers for measuring the pressure

Table 2.2: Overview of equipment for determination of the soil-water characteristic curve

Equipment	Technique	Type	Range (10^3 kPa)
Tempe pressure cell	Axis-translation	Matric suction	0...1.5
Pressure Plate Apparatus	Axis-translation	Matric suction	0...1.5
Thermal Conductivity Sensor	-	Matric suction	0.01...1
Thermocouple Psychrometer	Humidity measurement	Total suction	0.01...8
Chilled Mirror Hygrometer	Humidity measurement	Total suction	1...450
Filter Paper	-	Total or Matric suction	0...1000

in the soil specimen (Eching & Hopmans 1993, Eching et al. 1994, Wildenschild et al. 2001, Fujimaki & Inoue 2003). Consequently the hydraulic properties of the porous medium can be determined based on the applied/ measured pressure and water mass data.

- *One-step Method:*

  The one-step flow method is a transient state test and was first proposed by Gardner (1956). During the testing procedure a specimen is placed in a cell with a porous plate at the bottom. After the saturation process pressure is applied from the upper compartment of the cell. The resulting outflow of the fluid is measured as a function of time. One-step flow experiments were performed by Topp et al. (1967), Kool et al. (1985*b*), Dam et al. (1992), Toorman & Wierenga (1992), Wildenschild et al. (1997, 2001), Schultze et al. (1997). The authors carried out the one-step method experiments either in tempe cells, pressure cell apparatus (Kool et al. 1985*b*, Dam et al. 1992, 1994) or modified pressure cells (Toorman & Wierenga 1992, Eching & Hopmans 1993, Wildenschild et al. 1997, 2001). Wildenschild et al. (1997, 2001) used their modified pressure cell also to induce a continuous outflow scenario at a constant flow rate using an attached syringe pump.

- *Continuous Flow Experiments:*

  Continuous flow experiments, that are for instance evaporations tests, gravity drainage tests or test where a flow rate is applied to the soil, are performed in large column apparatuses. Conventional column apparatuses are equipped with sensors (e.g. tensiometer sensors, TDR sensors) for measuring the soil-water characteristic curve while draining and wetting the soil and usually the soil is placed on a porous stone (Schultze et al. 1997). In many studies only pore water pressure measurements (Chapius et al. 2007) are performed and therefore inverse procedure has to be used to determine unsaturated soil parameters. Nützmann et al. (1998) used a column apparatus for determining hy-

draulic properties of porous media, where water content and pressure were measured. The pressure and water content measurements were obtained in different depths and thus the suction-water content curve could be not obtained directly. Experiments in a column apparatus were also performed by Yang, Rahardjo, Leong & Fredlund (2004*b*) and Yang, Rahardjo, Wibawa & Leong (2004), where the pore water pressure and also the water content was measured pairwise in several depths. Their study considered infiltration tests on coarse materials. However, the effect of hysteresis was not investigated by applying several drainage and imbibition cycles to the soil. If water content and suction can be measured as a function of time, soil-water characteristic curve can be determined by pairing the water content value with the suction value at a given time under transient state condition. Measurements of this type of experiment were conducted by Watson (1965), Topp et al. (1967), Wana-Etyem (1982), Perroux et al. (1982). Infiltration tests were performed by Ahuja & El-Swaify (1976) and instantaneous profile method by Watson (1965), Rogers & Klute (1971), Vachaud et al. (1972).

As already mentioned, it is traditionally assumed that the soil-water characteristic curve could be measured either under steady state condition (equilibrium condition) or transient state condition (non-equilibrium condition). Comparison of suction-water content measurements obtained under conventional method (steady state condition) and using transient state method indicates the presence of the so called dynamic effect for some type of soils. Investigation of several authors showed that the hydraulic properties could also depend on the dynamic of water flow (e.g. rate of suction changes).

Davidson et al. (1966) performed drainage as well as imbibition experiments. They found, that more water was removed from the sample when one large suction increment was applied rather than many small suction increments during drainage process. In contrast more water was absorbed when many small suction increments were applied during imbibition process. Topp et al. (1967) conducted tests on a sand column under static state condition and transient state condition. At a given potential the water content measured under transient state condition was significantly higher than the water content measured under static state condition during drainage process. Topp et al. (1967) found that the difference between static soil-water characteristic curve and transient soil-water characteristic curve depends on the size of the imposed pressure step and on the time, which is required to reach equilibrium condition in the tested soil. The dynamic flow in a sand column was investigated by Stauffer (1977), who also measured higher water content at a given suction during drainage process compared to static state tests. One-step and multi-step outflow experiments were performed by Wildenschild & Hopmans (1997). The soil-water characteristic curve was determined from tensiometer measurements and the average water content. For large suction increments the water content was higher at given suction value. Dependence of flow rate on unsaturated hydraulic properties has been investigated by few authors. Experiments were carried out

by Wildenschild et al. (1997), Plagge et al. (1997), Schultze et al. (1997), Wildenschild et al. (2001). Plagge et al. (1997) investigated both the influence of flow rate and the influence of boundary condition on the hydraulic conductivity function. They found an increase in unsaturated hydraulic conductivity with increasing water potential gradients. Wildenschild et al. (2001) analyzed the flow rate dependency of unsaturated hydraulic characteristics using steady-state and transient flow. One-step and multistep experiments were performed on a sandy soil and a loamy soil. Several processes causing the observed phenomenon were suggested and discussed on the basis of their experimental and theoretical results.

Theoretically the dynamic effect was investigated first by Stauffer (1977), who analyzed the rate of change of saturation and the rate of change of suction for both transient state and steady state experiments. Hassanizadeh & Gray (1990, 1993), Hassanizadeh et al. (2002) developed and applied successfully an approach including macroscopic balance laws, constitutive relationships for interfacial as well as phase properties of the porous medium. They extended the relationship between suction and saturation as proposed by e.g. Bear & Verruijt (1987). As a result a model describing two-phase flow in a porous medium based on thermodynamic theory has been proposed. Detailed investigation on dynamic effects in porous media is given by Manthey (2006).

Determination of Hydraulic Conductivity Function

The unsaturated hydraulic conductivity can be measured directly and several indirect methods are also available to determine this relationship. The hydraulic conductivity of an unsaturated soil can vary with respect to soil suction by several orders of magnitude and is time-consuming to measure. Direct methods for measuring the unsaturated hydraulic conductivity can be generally classified as either laboratory techniques or field techniques and can be performed under steady state condition or transient state condition. Outflow methods are not only used to measure the soil-water characteristic curve of a soil but also to measure its unsaturated hydraulic conductivity. These methods are already explained above. Detailed review of outflow methods used for measuring hydraulic conductivity was given by Benson & Gribb (1997).

- *Direct Method performed under Steady State Condition:*

  Under steady state conditions, a constant hydraulic head or a constant flow rate is imposed to the specimen under predetermined matric suction. The most commonly used laboratory technique is the constant head method, where a constant head is maintained across a soil specimen and the corresponding flow rate through the specimen is measured. Numerous authors described the constant head method (Corey 1957, Klute 1972, Klute & Dirksen 1986*a*, Barden & Pavlakis 1971, Huang, Fredlund & Barbour 1998). The constant flow method is a laboratory technique, where a flow rate (hydraulic gradient)

is applied to the specimen. Klute (1986) provides description of steady-state methods for measuring unsaturated hydraulic conductivity.

The steady state centrifugation method is a laboratory method. It uses a spinning centrifuge, which establishes fast steady-state fluid flow trough a soil. The unsaturated hydraulic conductivity is calculated by measuring the steady-state flow under the elevated gravitational gradient (Nimmo et al. 1987, Nimmo & Akstin 1988).

The crust method is a steady state test to measure the unsaturated hydraulic conductivity in the field (Hillel & Gardner 1970). Tension infiltrometer, which measures the infiltration rate under carefully controlled suctions also can be used in the field. Different methods for calculating the unsaturated hydraulic conductivity based on these data were proposed by Elrick et al. (1987), Ankeny et al. (1991), Reynolds & Elrick (1991), Logsdon & Jaynes (1993).

- *Direct Method performed under Transient State Condition:*

Under transient state conditions, the specimen is subjected to continuous unsaturated flow conditions and measurements are carried out while the specimen comes to equilibrium. Transient state methods are for instance the horizontal infiltration method, the outflow methods and the instantaneous profile method. Transient state test was performed by Klute (1965) in a horizontal column. The column consisted of several segments. The saturation of the dry soil in the column was stepwise increased from $S = 0$ to $S = 1$, by introducing water from one end of the column. Thus a hydraulic gradient is imposed to the soil. After some time the inflow of water is stopped, the column is disassembled into its segments and the water content is determined. Horizontal infiltration tests have been also explored by Jackson (1964), Rose (1968), Clothier et al. (1983).

The instantaneous profile method is applicable in the laboratory and in the field and was first proposed by Richards & Weeks (1953). This method uses transient profiles of water content and suction to calculate the unsaturated hydraulic conductivity. Drainage process was induced by gravity (Watson 1966), by withdrawing fluid from the specimen via applied suction (Richards & Weeks 1953), by applying flow rate to the specimen (Overman & West 1972) or by evaporation (Wind 1966, van Grinsven et al. 1985, Wendroth et al. 1993, Meerdink et al. 1996). Imbibition was performed by adding water to the soil specimen (Hamilton et al. 1981, Daniel 1982, Meerdink et al. 1996). Most recent approaches include both measurement of suction and water content (Malicki et al. 1992, Meerdink et al. 1996). Example of permeameter for conducting instantaneous profile method is suggested in Meerdink et al. (1996). When suction as well as water content measurements are available then the unsaturated hydraulic conductivity and also the soil-water characteristic curve can be determined. Laboratory instantaneous profile method is performed in a horizontal or vertical column. During the testing

procedure (drainage and imbibition) sensors along the column measure the water content and/or the suction. The measurements are used to calculate the unsaturated hydraulic conductivity function. Instantaneous profile method was described by Watson (1966), Daniel (1983), Meerdink et al. (1996). Similar to the laboratory instantaneous profile method the field instantaneous profile method is performed. Usually the soil is wetted ($S = 1.0$) and than drained under gravity gradient (Watson 1966, Hillel et al. 1972).

- *Indirect Method:*

  A variety of indirect methods (Fredlund et al. 1994, Leong & Rahardjo 1997*a*, Agus et al. 2003) can be used to describe the unsaturated hydraulic conductivity function. Mualem (1986) classified three approaches for determination of hydraulic conductivity function, namely, Empirical models, Macroscopic models as well as Statistical models. These models are introduced and described in detail in Chapter 2.5.

A review of methods for measuring unsaturated hydraulic conductivity has been given by Klute (1972). Benson & Gribb (1997) provided an overview of about fourteen field methods and laboratory methods for measuring the unsaturated hydraulic conductivity.

2.4 Equipment and Measurement Techniques for Testing Unsaturated Soils

The properties of an unsaturated soil are functions of the stress state variables. Therefore it is necessary to develop suitable equipment, which enables the control, application and measurement of stress state variables as total stress as well as matric suction. An essential part of such kind of equipment is the high air-entry ceramic disk. The high air-entry ceramic disk separates the air and water phase and thus allows the control and/or measurement of the pore-water pressure. Several sensors for measuring water content or suction are available. Amongst others, measurement techniques for testing unsaturated soils have been described by Bishop et al. (1960), Bishop (1960), Blight (1961), Fredlund & Rahardjo (1993*b*), Lu & Likos (2004), Tarantino et al. (2008).

2.4.1 Measurement of Water Content

Measurement of water content plays an important role when dealing with unsaturated soil problems. The measurement of water content in unsaturated soil has undergone an excellent development in the last years. Numerous options are available for water content measurements, e.g. thermogravimetric method, time-domain reflectometry (TDR), ground penetrating radar (GPR), capacitance and impedance devices (Gardner et al. 2001, Ferré & Topp 2002). TDR, GPR as well as capacitance and impedance devices are based on electromagnetic measurements in the soil. Information on electromagnetic properties of soils and their

relation to soil water content are described in Topp et al. (1980), Topp & Reynolds (1998), Ferré & Topp (2002). The electromagnetic method makes use of the difference between the high dielectric constant of water ($k_a = 80$) and the low dielectric constant of the other soil components as air ($k_a = 1$) and the solids ($k_a = 2 - 4$). The large difference allows to draw conclusions to the volumetric water content (Selig & Mansukhani 1975, Topp et al. 1980, Look & Reeves 1992).

- *Time Domain Reflectometry (TDR):*

  In the measurement of water content the technology of time domain reflectometry (TDR) received the most attention (Topp 1987) and the overview is focused on this method. The first who applied TDR to measurements in soil were Davis & Chudobiak (1975). From that time on TDR method has been used frequently to measure water content at several scales and under several conditions (Topp & Reynolds 1998, Robinson et al. 2003) and has become a standard method for measurement of water content in unsaturated soil in the field and in the laboratory. Topp et al. (1980) tested 4 mineral soils and found insignificant influence of properties such as salinity, temperature, texture and dry density on the dielectric constant. A calibration function was obtained by Topp et al. (1980), which originally was believed to apply universally to all soil types. Similar equation was proposed by Ledieu et al. (1986). Later numerous authors (Herkelrath et al. 1991, Malicki et al. 1996, Suwansawat 1997) showed that the composition of solids of the soil, surface electrical conductivity and density of a soil can significantly effect the relationship between dielectric constant and volumetric water content. Thus although the universal equation by Topp works well for soils composed of quartz, a unique relationship between the dielectric constant and the volumetric water content does not exists for all type of soils (Roth et al. 1992, Dasberg & Hopmans 1992, Suwansawat 1997). A soil specific calibration is recommended (Benson & Bosscher 1999, Suwansawat & Benson 1999). Recommendations regarding calibration procedure and experimental setup are given in Suwansawat & Benson (1999). Siddiqui & Drnevich (1995) extended the TDR measurements to geotechnical application and related the TDR measurements to water content and dry density. A method for determination of soil water content as well as dry density using TDR measurements is described in detail in Yu & Drnevich (2004).

- *Ground Penetrating Radar (GPR):*

  The physics of the GPR method is identical to the physics of the TDR method (Weiler et al. 1998). GPR method is widely applied in geosciences and was recently developed to measure water contents in soils (Davis & Annan 2002, Huisman et al. 2003). Compared to TDR method, GPR method provides data from larger spatial region.

- *Impedance and Capacitance Devices:*

  Impedance and capacitance devices are electromagnetic instruments operating at frequencies within the range of TDR and GPR. Impedance or capacitance values are influenced by the amount of water in the soil. Capacitance devices determine the apparent capacity in a soil (Dean et al. 1987, Robinson et al. 1998, Gardner et al. 2001, Kelleners et al. 2004).

2.4.2 Measurement of Soil Suction

Various methods are available to measure suction in an unsaturated soil (Ridley & Wray 1996). Soil suction consists of two components, namely, matric suction and osmotic suction. Therefore it has to differentiate between measurement of total suction (sum of osmotic suction and matric suction), matric suction as well as osmotic suction. Krahn & Fredlund (1972) presented data on the independent measurement of total, matric as well as osmotic suction. Techniques for measuring suction are divided in direct (i.e. determination of negative pore water pressure, that requires the separation of the gas phase and the fluid phase usually realized by a ceramic disk or ceramic cup) and indirect methods for measuring matric suction. Indirect methods (e.g. the suction is determined by measuring the relative humidity, that is related to the suction) only are available for measurement of total as well as osmotic suction (Agus 2005).

Measurement of Total Suction

Total suction in a soil is measured when using for instance, the psychrometer, the chilled mirror hygrometer, the non-contact filter paper method, the humidity control technique or the resistance capacitance sensor. Agus (2005) compared 4 methods for measuring total suction in a soil. Leong et al. (2003), Tripathy & Schanz (2003) presented two new devices for measuring relative humidity and temperature in a soil and thus the total suction. The relative humidity and temperature transmitter for in situ total suction measurements as well as chilled-mirror technique with a selectable temperature environment for measurement of total suction in the laboratory were developed. These methods are described below.

- *Psychrometer:*

  In geotechnical engineering practice the Peltier psychrometer (Spanner 1951) is most commonly used. It utilizes the Seebeck effect (1821) as well as the Peltier effect (1834) to measure the total suction. The Peltier effect as well as Seebeck effect, setup, mode of operation and calibration procedure of psychrometers are described in detail in Fredlund & Rahardjo (1993*b*). Psychrometers have been used by many researchers for measuring total suction (Krahn & Fredlund 1972, Hamilton et al. 1979, Ridley & Burland 1993).

- *Hygrometer:*

  The use of chilled mirror hygrometer for total suction application was described by Gee et al. (1992). The hygrometer consists of a metallic mirror, a photodetector, and a light. When the mirror is cooled down condensation occurs from the ambient water vapor in the closed chamber. Due to condensed water on the mirror the light reflected from the mirror is scattered and the intensity of the light is reduced. The intensity is detected by the photodetector. The dew point temperature is related to the ambient relative humidity and the total suction in the soil using Kelvin's law. Leong et al. (2003) used the chilled mirror hygrometer for measuring total suction in 2 residual soils. The authors independently measured also the matric as well as osmotic suction of the soils and found that the device can be used for rapid determination of total suction.

- *Filter Paper Method:*

  Filter paper method is an indirect method, which can be used to measure either total suction or matric suction. It is assumed that the filter paper comes after sufficient time into equilibrium with the specific suction of an unsaturated soil. When placing the filter paper not in contact to the specimen total suction is measured. The water content of the paper is measured gravimetrically at equilibrium condition. A predetermined calibration curve relates the water content to the total suction (Fawcett & Collis-George 1967, Houston et al. 1994, Leong et al. 2002).

- *Humidity Control Techniques:*

  Humidity control techniques imply the measurement of water content for specimens of controlled total suction. The suction is controlled by adjusting the relative humidity in a closed chamber and the application of Kelvin's equation. The specimen is placed in the controlled humidity environment, where water is adsorbed or desorbed until reaching equilibrium condition in the soil. Lu & Likos (2004) describe two humidity control techniques in more detail, namely the isopiestic control technique and the two-pressure humidity control technique.

Measurement of Matric Suction

Matric suction can be measured using direct or indirect methods. Techniques for measuring matric suction are amongst others, the tensiometer sensor, the thermal conductivity sensor as well as the electrical conductivity sensor and the contact filter paper method. Whereas the tensiometer sensor measures the matric suction directly the other techniques measure the matric suction indirectly.

- *Tensiometer:*

  In the laboratory and in situ tensiometers enable to measure matric suction directly. A review of theory and the behavior of tensiometers was given by Stannard (1992). The

author differs between 3 types of tensiometers, namely, manometer type of tensiometer, gauge type of tensiometer and transducer type of tensiometer. The author discusses in detail the advantages and disadvantages of each type of tensiometer and found that vacuum gauge type tensiometers are not recommended for measuring unsaturated hydraulic gradients. Mercury manometer type tensiometers are probably the most accurate and robust sensors. Hysteresis in a manometer tensiometer is much less than in a gauge type tensiometer or pressure type tensiometer. Transducer type tensiometers are well suited to collect a large quantity of data. Measurements can be performed in predetermined time intervals and are recorded automatically. The accuracy is excellent but there is a need for frequently calibration procedure. Working range of standard tensiometers is limited by the cavitation process, which occurs approximately at $80 - 100$ kPa. Details on the preparation, installation and usage of tensiometers are also discussed in the former work of Cassel & Klute (1986). Ridley & Burland (1993) designed a stainless steel miniature pore-water pressure transducer with a working range up to 3500 kPa. The suction probe uses a 15 bar ceramic disc, an electronic pressure transducer and an electrical connection for measuring the matric suction. The very thin water reservoir ($\sim 250\mu m$) between ceramic disc and transducer avoids the formation of air bubbles and thus increases the measuring range of the instrument. Evaluation of the suction probe yields to reliable measurement of matric suctions up to $\sim$ 1500 kPa. Guan & Fredlund (1997) developed a suction probe measuring pore-water pressure up to 1250 kPa for both saturated and unsaturated conditions and tested a glacial till and Regina clay. They found reasonable agreement between measured values in the suction probe and those measured by the filter-paper method as well as thermal conductivity sensor. With decreasing saturation differences in the measurements appeared. Problems in usage of suction probes arise for the calibration procedure. The calibration is carried out in the positive range of pore-water pressure (hydraulic pressure) and extrapolated to the negative range of pore-water pressure (matric suction). A tensiometer similar in conception was designed by Tarantino & Mongiovi (2002). Additionally their design was modified to perform calibration also at negative-pore water pressures. Further suction probes were developed by several researchers, e.g. Mahler & Diene (2007).

- *Thermal and Electrical Conductivity Sensor:*

Indirect measurements are performed using either thermal conductivity sensors or heat dissipation suction sensors. Because water is a better thermal conducter than air, thermal properties and electrical properties of an unsaturated soil can be related to the water content in the soil. Such kind of sensor consists of a temperature sensor and a heater as developed by Shaw & Baver (1939). Different soils required different calibration curves to relate the thermal conductivity to the water content. Therefore several researchers suggested to enclose the thermal conductivity sensor in a porous medium,

which is calibrated (Johnston 1942, Phene et al. 1971). Dane & Topp (2002) give an overview of sensors and devices related to the measurement of soil suction. Electrical conductivity sensors measure the electrical conductivity using two embedded electrodes. Main disadvantage of electrical conductivity sensor measurements is their inherent sensitivity to changes in electrical conductivity which is not related to the water content of the porous medium but to dissolved solutes. Thus thermal conductivity sensors have found a greater amount of use in geotechnical engineering practice.

- *Contact Filter Paper Method:*

  Following the contact filter paper method a filter paper is placed in direct contact to the specimen and matric suction is measured indirectly, by measuring the amount of water transferred to the dry paper. Both non-contact and contact filter paper method are discussed and analyzed in Fawcett & Collis-George (1967), Al-Khafaf & Hanks (1974), Houston et al. (1994).

Measurement of Osmotic Suction

The osmotic suction can be determined by measuring the electrical conductivity of the pore-water in the soil, which is related to the osmotic suction. With increasing dissolved salts in the pore-water the electrical conductivity is increasing and thus the osmotic suction. The pore-water, that is used for the measurement of the electrical conductivity can be extracted using several methods, e.g. the saturation extract method, the centrifuging method, leaching method or the squeezing method (Iyer 1990, Leong et al. 2003). The pore fluid squeezing method has shown to be the most reliable measurement technique of osmotic suction (Krahn & Fredlund 1972, Wan 1996, Peroni & Tarantino 2005). This technique consists of squeezing a soil specimen to extract the fluid from the macropores, that is used for measuring the electrical conductivity. The authors showed, that the method appears to be influenced by the magnitude of applied extraction pressure.

2.5 Constitutive Models for Hydraulic Functions

As already mentioned in the previous chapter the soil-water characteristic curve and hydraulic conductivity function must be known in order to model flow through unsaturated soils. Originating from classical studies in soil science, a large number of related models can be found. As mentioned before the soil-water characteristic curve describes the relation between water content or saturation and soil suction ($\theta(\psi)$, $S(\psi)$) and the unsaturated hydraulic conductivity function describes the relation between suction and hydraulic conductivity ($k(\psi)$) as well as water content or saturation and hydraulic conductivity ($k(S)$, $k(\theta)$). These unsaturated soil functions are subsequently used when modeling hydro-mechancial behavior of unsaturated soils (Donald 1956, Bishop & Donald 1961, Fredlund et al. 1996*a*, Vanapalli et al. 1996).

2.5.1 Models for Soil-Water Characteristic Curve

The soil-water characteristic curve is the key function for estimation of unsaturated soil properties. Based on this relationship several other relations describing unsaturated soil behavior are derived. Therefore it is important to establish a function, which relates the suction to the water content. Numerous approaches, namely, empirical and physical models, have been suggested for mathematical representation of the soil-water characteristic curve. Literature regarding to this topic is presented in the next section.

Empirical Models

Empirical models (Brooks & Corey 1964, Gardner 1958, van Genuchten 1980, Fredlund & Xing 1994) use statistical analysis to best fit experimental data to the selected equation. However, the parameters have no physical meaning. A large number of empirical equations have been proposed by different researchers to best fit experimental data of the soil-water characteristic curve. Empirical models can be classified into models that do not consider hysteretic behavior and into models that do consider hysteretic behavior in the soil-water characteristic curve.

Equations including 2 parameters or 3 parameters were proposed for instance by Gardner (1958), Brooks & Corey (1964), Campbell (1974), van Genuchten (1980), Fredlund & Xing (1994). The parameters in the empirical equations are usually related to the air-entry value and the rate of desaturation of the investigated soil. Equations proposed by Brooks & Corey (1964), Farrell & Larson (1972), Williams (1982) are non-sigmoidal functions and equations proposed by Gardner (1958), van Genuchten (1980), Fredlund & Xing (1994) are sigmoidal functions. All these empirical equations can be used for the fit of either drainage curves or imbibition curves. Hysteretic behavior is not taken into account. Detailed reviews and analysis of empirical equations were summarized by several authors (Leong & Rahardjo 1997*b*, Singh 1997, Sillers & Fredlund 2001). Leong & Rahardjo (1997*a*) analyzed the effect of parameters on the shape of the soil-water characteristic curve for several equations. Only few researchers as for instance Hanks (1969), Dane & Wierenga (1975), Jaynes (1984), Pham et al. (2003) presented empirical equations, which consider the hysteresis in soil-water characteristic curve.

Frequently used models are that by Brooks and Corey (1964), van Genuchten (1980) and Fredlund & Xing (1994). The models are not capable to predict hysteresis or scanning curves in the suction water content relationship. However, for each drainage or imbibition cycle different set of parameters has to be provided. The above mentioned equations are explained in the following and are used in the present investigation for analysis of the experimental results of the soil-water characteristic curves.

- *Brooks and Corey (1964)*

  One of the earliest equation was proposed by Brooks and Corey (1964). Brooks and Corey (1964) suggested an power-law relationship for relating volumetric water content

to matric suction:

$$\Theta = \left(\frac{1}{\alpha\psi}\right)^{\lambda} \tag{2.9}$$

where: $\Theta = (\theta - \theta_r)/(\theta_s - \theta_r)$ is the normalized volumetric water content, θ_s is the saturated volumetric water content and θ_r is the residual volumetric water content, α defines the air-entry value and λ is called a pore size distribution index. This equation only applies for suction values greater than the air-entry value. This equation is not valid in the saturated zone.

- *Van Genuchten (1980)*

  A well known and frequently used sigmoidal type equation is that given by van Genuchten (1980) :

$$\Theta = \frac{1}{[1 + (\alpha\psi)^n]^m} \tag{2.10}$$

  where: a, n, and m are curve fitting soil parameters. Burdine (1953) suggested that m be calculated as $m = 1 - \frac{2}{n}$ and Mualem (1976) suggested that m be calculated as $m = 1 - \frac{1}{n}$. These assumptions reduce the accuracy of the suction-water content curve fit but allow the relative hydraulic conductivity function to be represented as closed-form equations.

- *Fredlund and Xing (1994)*

  Fredlund and Xing (1994) proposed an equation for the soil-water characteristic curve that is similar in form to the van Genuchten (1980) equation :

$$\Theta = C(\psi) \cdot \frac{1}{\left\{ ln\left[e + \left(\frac{\psi}{a}\right)^n \right] \right\}^m} \tag{2.11}$$

  where: a, n as well as m are curve-fitting parameters related to the air-entry value and the shape of the curve and $C(\psi)$ is a correction function. The correction function enables the best-fit to reach a suction equal to 10^6 kPa at a water content equal to zero and is defined as:

$$C(\psi) = \frac{-ln\left(1 + \frac{\psi}{\psi_r}\right)}{ln\left[1 + \left(\frac{10^6}{\psi_r}\right)\right]} + 1 \tag{2.12}$$

  where: ψ is the suction and ψ_r is the residual suction and ln is the natural logarithm.

Brooks and Corey (1964) applied their model on sand, silt, and glas beads, van Genuchten (1980) tested his model on sandstone, loam and clay, Fredlund and Xing (1994) tested their model on sand, silt as well as clay.

To show the shape of the curves (residual analysis performed as well as parameters are given in detail for Hostun sand in Chapter 7) in Fig. 2.15 experimental results for sand

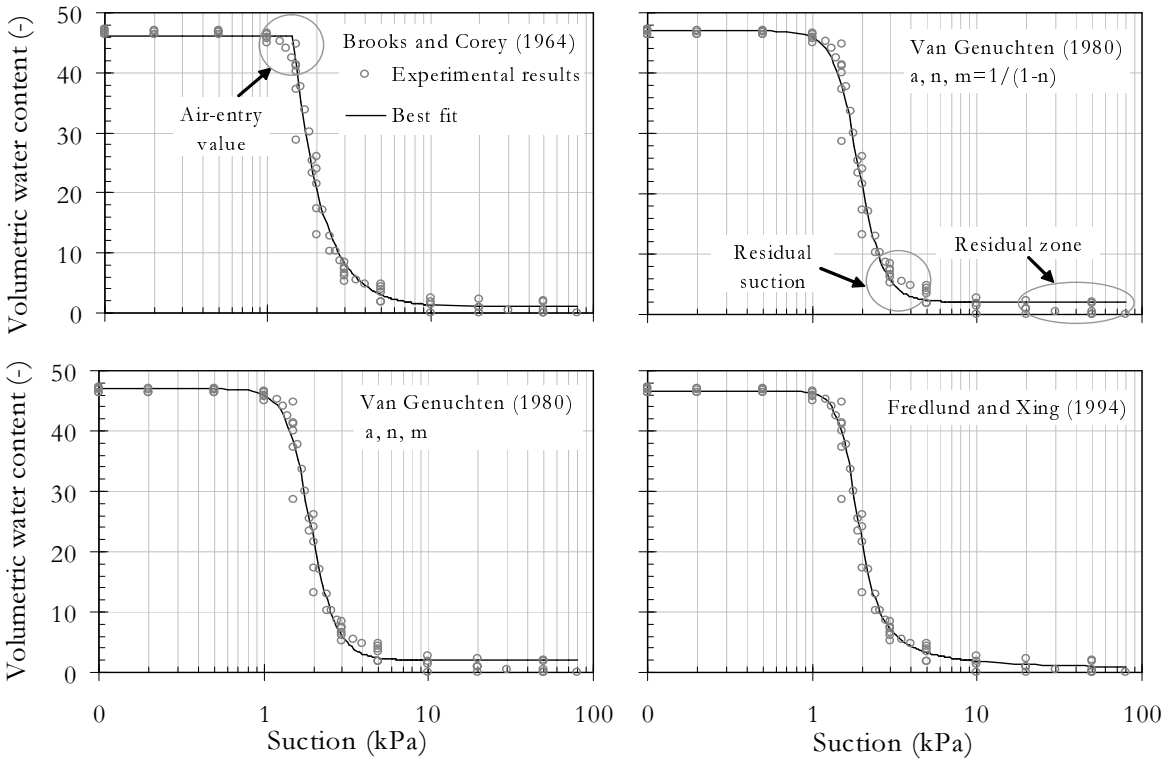

Figure 2.15: Experimental results for Hostun sand from drainage: soil-water characteristic curve and fitted results using empirical models

(see Chapter 6) are fitted using the above mentioned equations. In general good agreement between observed and calculated values was found for all used models. An disadvantage of the equation proposed by Brooks and Corey is, that the calculated results in the region of the air-entry value are not proper conform to the experimental results. The calculated results fit well to the experimental results in the saturated zone, transition zone and residual zone. Comparing the experimental and calculated results using van Genuchten's equations it can be observed that the calculated results in the region of the residual suction as well as the residual zone are in better agreement to the experimental results when using the flexible parameter m. Good fit was found when using Fredlund and Xing's equation. Whereas van Genuchten's equation does not tend to 0 in the residual zone, Fredlund and Xing's equation even considers the water content to be 0 at a suction of 10^6 kPa.

The influence of the parameters α and λ on the shape of the curve is given in Fig. 2.16 for Brooks and Corey's equation. The parameter α is changing while the parameter λ is kept constant in Fig. 2.16 on the left hand side. With decreasing α the curve is shifting to larger values of suction and the air-entry value is increasing. When λ is decreasing the slope of the curve is decreasing.

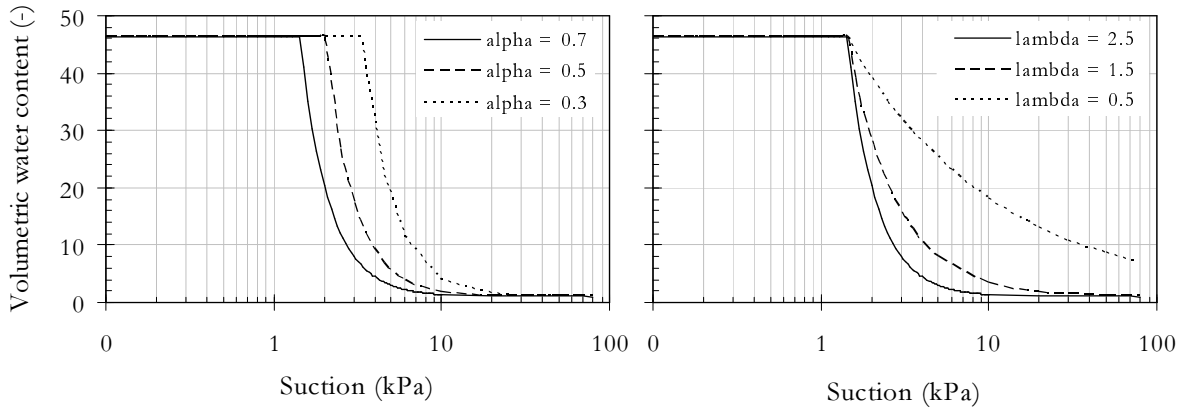

Figure 2.16: Influence of Brooks and Corey parameters α and λ on the shape of the soil-water characteristic curve

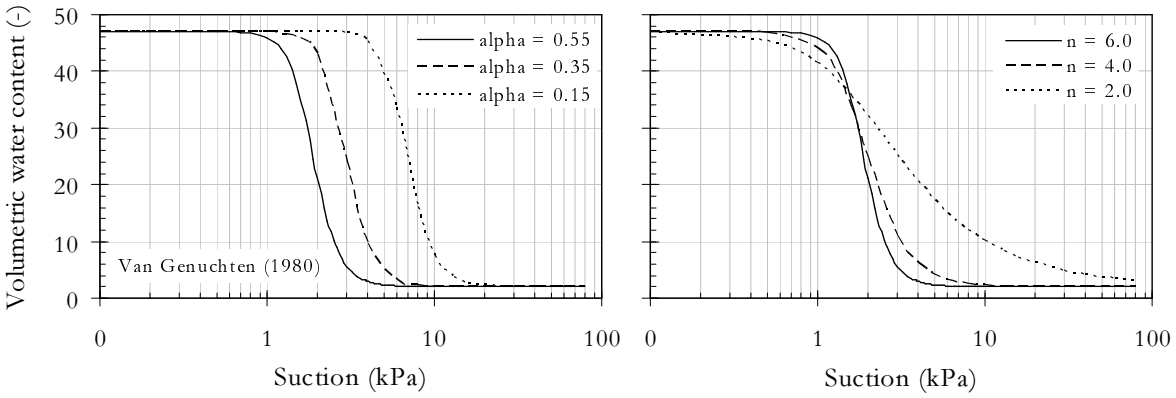

Figure 2.17: Influence of van Genuchten parameters α and n on the shape of the soil-water characteristic curve (in case m is a function of n)

The influence of the parameters α and n on the shape of the curve is presented in Fig. 2.17 using van Genuchten's equation. In this case the parameter m is fixed to $m = 1-1/n$. Similar to Brooks and Corey with decreasing α the curve is moving to larger values of suction. A change of α influences the air-entry value. When n is changing while α is kept constant the curve is rotating around its inflection point. With decreasing n the transition zone is increasing and the value of the residual suction is also increasing. The slope of the curve becomes lower when the parameter m is decreasing as shown in Fig. 2.18. Here m is a flexible parameter.

The influence of the parameters α, n and m on the shape of the curve for Fredlund and Xing's equation shows Fig. 2.19. An increase in the parameter α causes a shift of the curve to

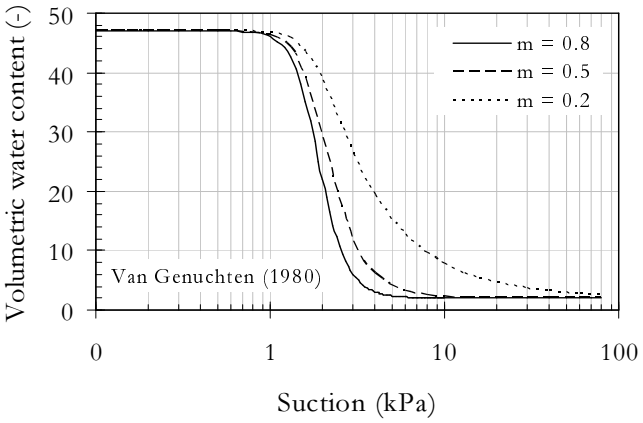

Figure 2.18: Influence of van Genuchten parameter m on the shape of the soil-water characteristic curve

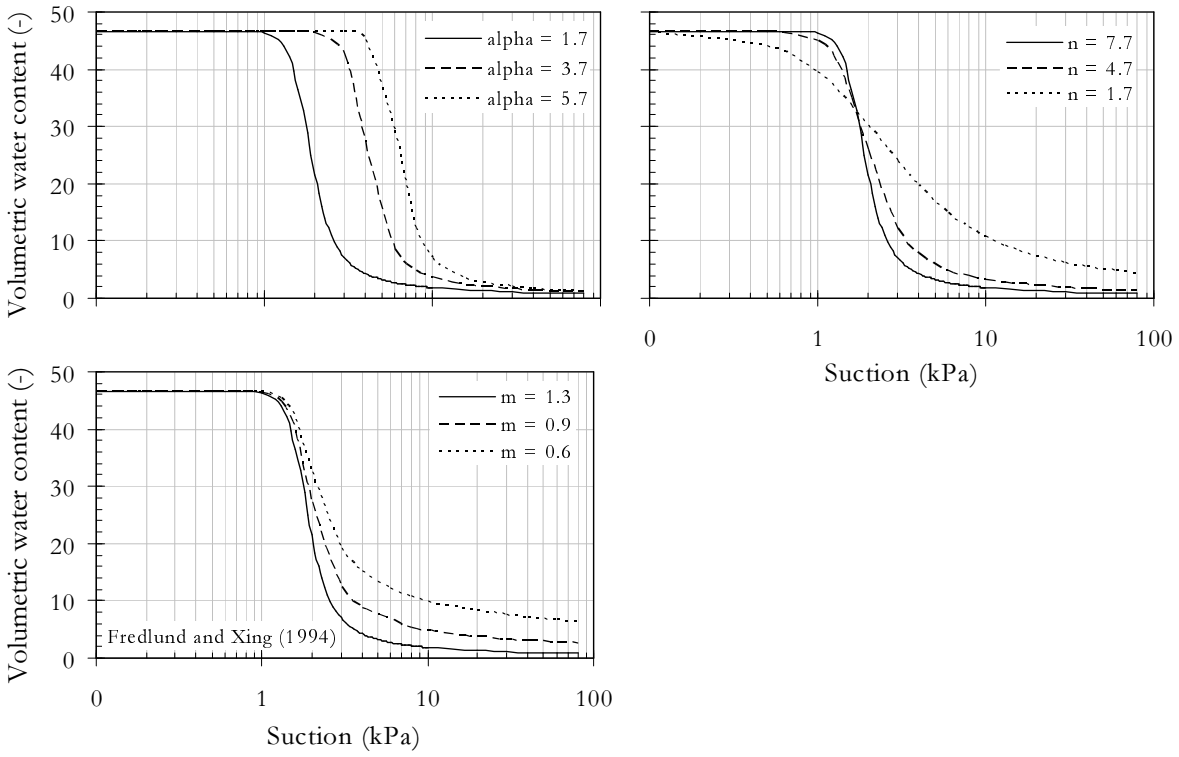

Figure 2.19: Influence of Fredlund and Xing parameters α, n and m on the shape of the soil-water characteristic curve

larger suction values and an increase in the air-entry value. The curve is rotating around the inflection point when the parameter n is changing. As larger n as steeper the curve and as

smaller the transition zone and the residual suction. The parameter m influences the plateau of the curve. With increasing m the lower plateau moves up in the residual zone.

- *Feng & Fredlund (1999), Pham (2003)*

  An empirical model that takes hysteresis into account is that proposed by Feng & Fredlund (1999). The relation utilizes the main drainage curve and two experimental data on the main imbibition curve to predict the entire relation between water content w and suction during imbibition (see Fig. 2.20):

$$w(\psi) = \frac{w_u b_d + c\psi^{d_d}}{b + \psi^{d_d}} \tag{2.13}$$

  where: w is the water content, w_u is the water content on the main drainage curve at zero soil suction, c presents the water content at high soil suction and b_d and d_d are curve-fitting parameters for the drainage curve. Pham et al. (2003) enhanced the above written model and suggested the following equations to define two suction values along the main drainage curve by using parameters derived from main imbibition curve fit:

$$\psi_{1i} \approx \left(\frac{b_d}{10}\right)^{1/d_d}, \quad \psi_{2i} = \psi_{1i} - 2\left\{\left[\frac{b_d(w_u - w_{1i})}{w_{1i} - c}\right]^{1/d_d} - b^{1/d_d}\right\} \tag{2.14}$$

  where: b_d and d_d are best-fit parameters from the main drainage curve using Eq. 2.13 and ψ_{1i}, ψ_{2i} and w_{1i}, w_{2i} are the water content and the suction values in the two points. Knowing ψ_1 and ψ_2 and the measured water contents w_{1i} and w_{2i} the unknown curve

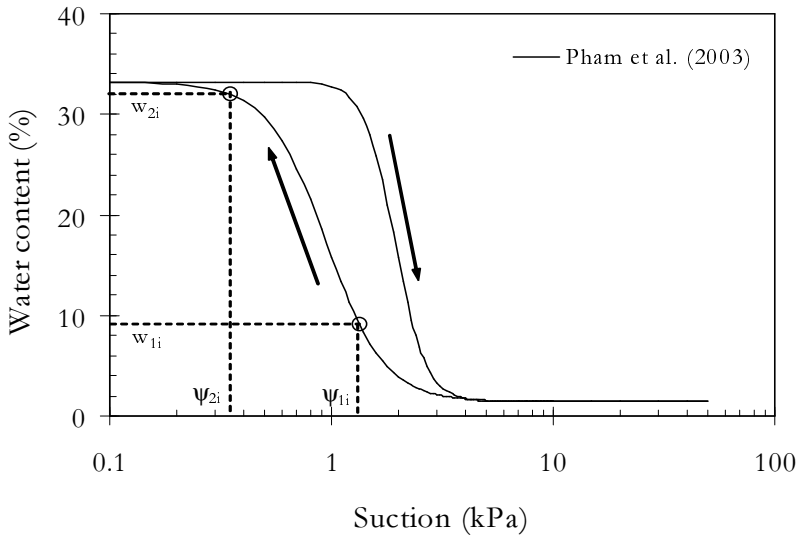

Figure 2.20: Soil-water characteristic curve including the two points used for estimation of imbibition curve

fitting parameters b_i and d_i for imbibition curve can be calculated using:

$$d_i = \frac{\log\left[\frac{(w_{1i}-c)(w_u-w_{2i})}{(w_u-w_{1i})(w_{2i}-c)}\right]}{\log(\psi_{2i}/\psi_{1i})}, \quad b_i = \frac{(w_{1i}-c)\psi_{1i}^{d_i}}{w_u-w_{1i}} \tag{2.15}$$

The parameters b_d and d_d in Eq. 2.13 are replaced by the determined parameters b_i and d_i used for estimation of the main imbibition curve. Exemplary main drainage and imbibition curve are given in Fig 2.20 for Hostun sand, where the additional two points for deriving the main imbibition curve from the main drainage curve are included.

Physical Models

Domain models are based on physical properties of the soil. Domain models are divided into independent domain models and dependent domain models. Based on Néel´s diagram (Néel 1942, 1943) or Mualem´s diagram (Mualem 1974), where the distribution of water in a soil is defined during drainage and imbibition processes, the hysteresis was described by Everett & Smith (1954), Everett (1955), Poulovassilis (1962), Philip (1964), Mualem (1974, 1984*a*), Hogarth et al. (1988) (independent domain models) and Mualem & Dagan (1975), Mualem (1984*b*), Topp (1971*b*), Poulovassilis & El-Gharmy (1978) (dependent domain models). Dependent models were derived from independent models and additionally consider the effect of pore water blockage against the air-entry value and the water-entry value in a soil during drainage and imbibition. Poulovassilis (1962) performed drainage-imbibition tests on glass bead porous medium and was one of the first who applied the domain theory to hysteresis. He obtained good agreement between predicted values and observed values. Further models were suggested by Everett (1967), Topp (1971*b*). For these models a set of measured suction-water content data at the scanning curves is required. To reduce the amount of required experimental data Philip (1964), Mualem (1974) proposed similarity hypothesis. Based on similarity hypothesis Mualem proposed several models (Mualem 1977, 1984*b*). These models require boundary drainage curve for prediction.

The measurement of suction water content relationship in the field and also in the laboratory is a time consuming procedure. Sometimes it is useful to estimate the suction water content before. Physical models are capable to estimate the relation between saturation and suction based on typical soil parameters as grain-size distribution or porosity. Physical models based on soil parameters (e.g. grain-size distribution, void ratio) and/or pore geometry were suggested amongst others by Arya & Paris (1981), Haverkamp & Parlange (1986), Fredlund et al. (1997), Zapata et al. (2000), Aubertin et al. (2003), Zou (2003, 2004). These models utilize soil properties as well as geometric properties to estimate the suction water content relationship. Rojas & Rojas (2005) suggested a probabilistic model that is based on the physical description of a porous system. Therefore two different elements, the sites (cavities) and bonds (throats) are considered each with a proper size distribution. Whereas most models

developed do not consider hysteresis the models by Zou (2003, 2004), Rojas & Rojas (2005) take hysteresis into account.

Following are physical models that have been adopted in the present investigation. The models by Aubertin et al. (2003) and Zou (2003, 2004) were chosen to predict the soil-water characteristic curve of Hostun sand.

- *Kovacs (1981), Aubertin (2003)*

  Kovacs (1981) proposed a model, that was extended by Aubertin et al. (2003) for a general application to porous media. The model makes use of a reference parameter defined as the equivalent capillary rise of water in a porous medium to define the relationship between saturation and matric suction. The equivalent capillary rise is derived from the expression for the rise of water in a capillarity with certain diameter. Two components of saturation are considered: i) the saturation held by capillary forces, the component that is obtained from cumulative pore-size distribution function and ii) the saturation held by adhesive forces at higher suction values, that is the van der Waals attraction between grain surface and water dipoles. Following Aubertin et al. (2003), where the coefficient of uniformity C_u, the diameter corresponding to 10% passing the grain-size distribution curve D_{10}, the void ratio e and a shape factor α are used, the drainage suction-saturation relationship was preliminary estimated for loose as well as dense Hostun sand specimens as given in Fig. 2.21. Estimated results are compared to experimental results carried out for Hostun sand specimens (see Chapter 6). Parameters used for the prediction are given in Tab. 2.3. The soil classification parameter D_{10} is estimated from the grain-size distribution curve (see Fig. 5.1) and C_u is calculated using the following relation:

$$C_u = \frac{D_{60}}{D_{10}} \tag{2.16}$$

  where: D_{60} and D_{10} are the diameters corresponding to 10% as well as 60% passing the grain-size distribution curve. According to loose and dense packed specimen the void ratio is taken. The shape factor α is chosen following Kovacs (1981), who suggested $\alpha = 10$.

- *Zou (2003, 2004)*

Table 2.3: Parameters used for prediction of soil-water characteristic curve (Aubertin et al. (2003)

	D_{10}	C_u	e	α
Loose specimen	0.21	1.72	0.89	10
Dense specimen	0.21	1.72	0.66	10

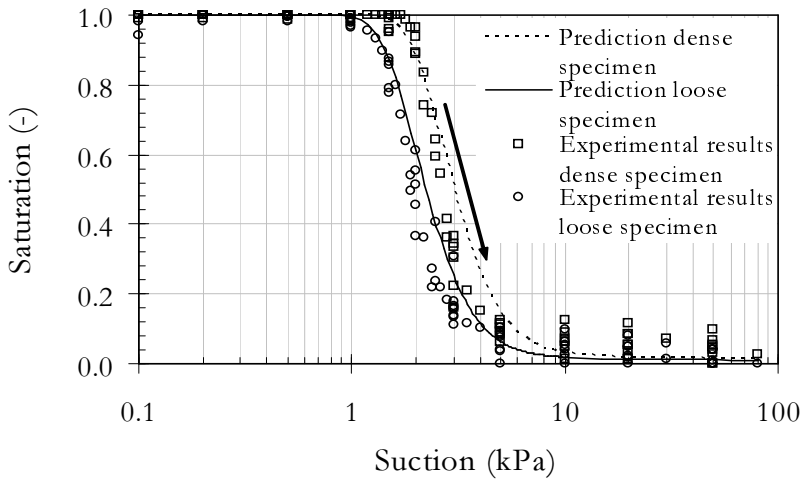

Figure 2.21: Estimated drainage soil-water characteristic curve for Hostun sand using the model by Aubertin et al. (2003) in comparison with experimental results (loose and dense specimen)

To predict the boundary hysteresis curves and the scanning curves of unsaturated soils a physical model was proposed by Zou (2003, 2004) and tested on Hostun sand (Lins et al. 2007). Because the equations are not trivial it is explained in more detail in Appendix A. In this model, pores in an unsaturated soil are considered to be composed of the contact regions between two tangent soil particles and the irregular frustum-shaped pores among several adjacent particles (Fig. 2.22 a)). It is also assumed that all particles in the soil are sphere-shaped and have the same sphere radius r_s and that all frustum-shaped pores are regular symmetrical frustum-shaped pores which have the same height r_s, the same lower radius r_1 and the same upper radius $r_1 + \xi \cdot r_s$ (Fig. 2.22 b)). The average number of the contact points of a particle with its neighbors is termed as contact number n_c. The average number of the frustum-shaped pores per particle is called as frustum number n_{f0}.

The model includes 7 parameters. To determine the influence of the parameters on the shape of the curves an analysis was performed. While the influence of the parameter n_c is negligible the parameters α_{max}, n_{f0}, ξ, ζ, μ and S_{r0} are influencing the shape of the soil-water characteristic curve. To clarify the influence of the parameters on the shape of the soil-water characteristic curve, it is classified into three sections, namely the saturated zone, the unsaturated zone as well as the residual zone. Additionally typical parameters for the air-entry value ψ_{aev}, the saturated volumetric water content θ_s, and the residual volumetric water content θ_r, with the corresponding residual suction ψ_r, and the water-entry value ψ_{wev} are used (see also Fig 2.8). The parameter ξ is

responsible for the geometry of the frustums, the parameter n_{f0} describes the number of the frustums, and the parameter μ describes the drainage process of some residual frustums, thus they are responsible for the volume of water in the frustum-shaped pores, and influence mainly the saturated and the unsaturated zone.

Maximum contact angle α_{max}: The maximum contact angle α_{max} is reached, when adjoining contractile skins are in contact and the frustum-shaped pores are filled with water. As smaller the contact angle α_{max} as higher the suction, which has to be applied for draining the contact regions. With decreasing contact angle α_{max} the unsaturated zone is increasing and the residual zone is decreasing during drainage process (see Fig. 2.23).

Frustum number n_{f0} per sphere: When α_{max} is reached, the frustum-shaped pore between the grains is filled with water. The remaining pore volume is taken into account by a function, describing the volume of a frustum. The largest volume of water is located in these pores. Thus the number of frustums n_{f0} is influencing the shape of the curve significantly in the saturated zone as well as unsaturated zone. With increasing n_{f0} the saturated zone and unsaturated zone is shifting to higher suction values during drainage process. Same behavior can be observed for the imbibition process. As larger n_{f0} as larger the air-entry value ψ_{aev} and the water-entry value ψ_{wev} (see Fig. 2.24).

Form parameter ξ: The form parameter ξ defines the geometry of the frustum and estimates the upper diameter of the frustum. With increasing ξ the curve becomes flatter for drainage and imbibition process. As smaller ξ as more distinct the air-entry value ψ_{aev}. The saturated zone is shifting to higher suction values for decreasing ξ while wetting the specimen (see Fig. 2.25).

Material parameter ζ: The material parameter ζ is responsible for the form of the meniscus in the frustum-shaped pores and thus it influences the suction $(u_a - u_w)$

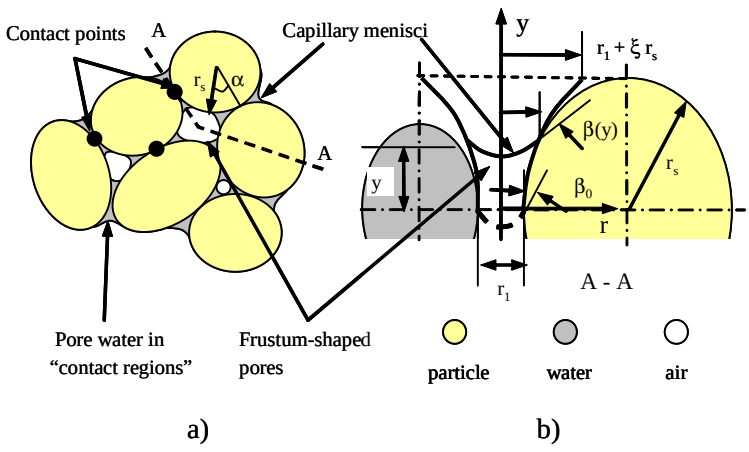

Figure 2.22: Pore spaces and pore water (Zou 2003)

when the frustum-shaped pores are wetting or draining. Furthermore, it influences the saturated and unsaturated zone. The larger ζ is, the larger the air-entry value ψ_{aev}.

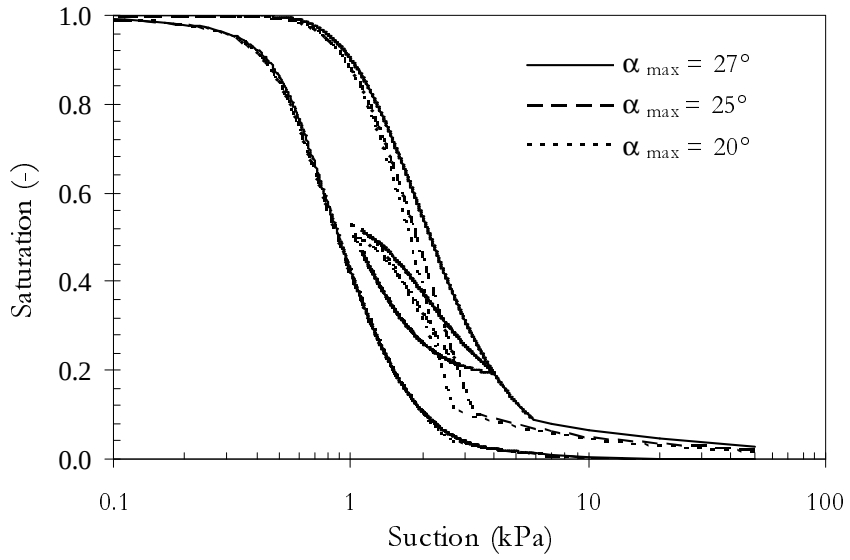

Figure 2.23: Influence of the parameter α_{max} on the shape of the soil-water characteristic curve

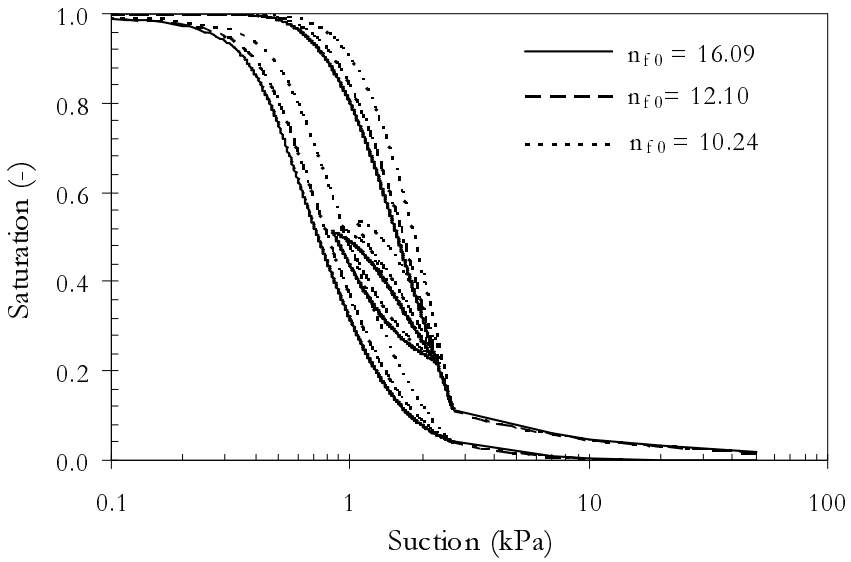

Figure 2.24: Influence of the parameter n_{f0} on the shape of the soil-water characteristic curve

Fraction of frustums μ: The fraction of frustums μ only influences the drainage process. During the drainage process the larger frustum-shaped pores are draining first while the smaller pores still remain water. With increasing μ the residual degree of saturation S_r is increasing for the corresponding residual suction ψ_r (see Fig. 2.26).

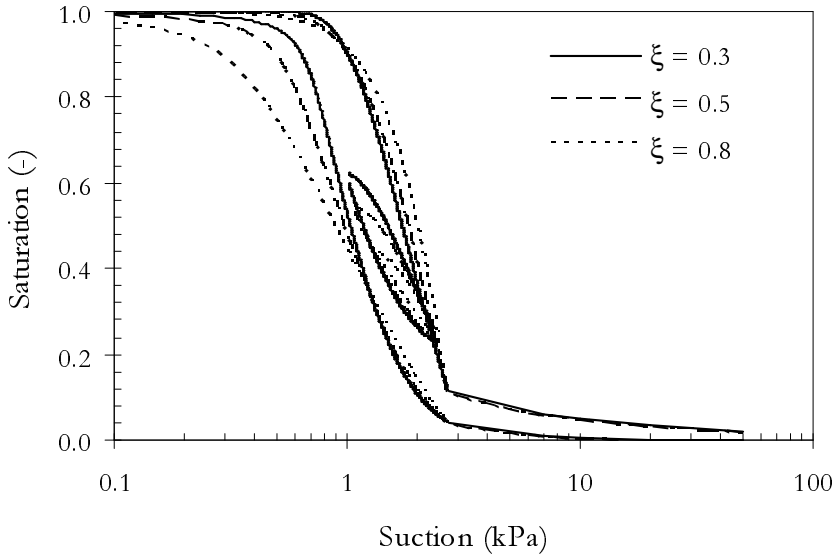

Figure 2.25: Influence of the parameter ξ on the shape of the soil-water characteristic curve

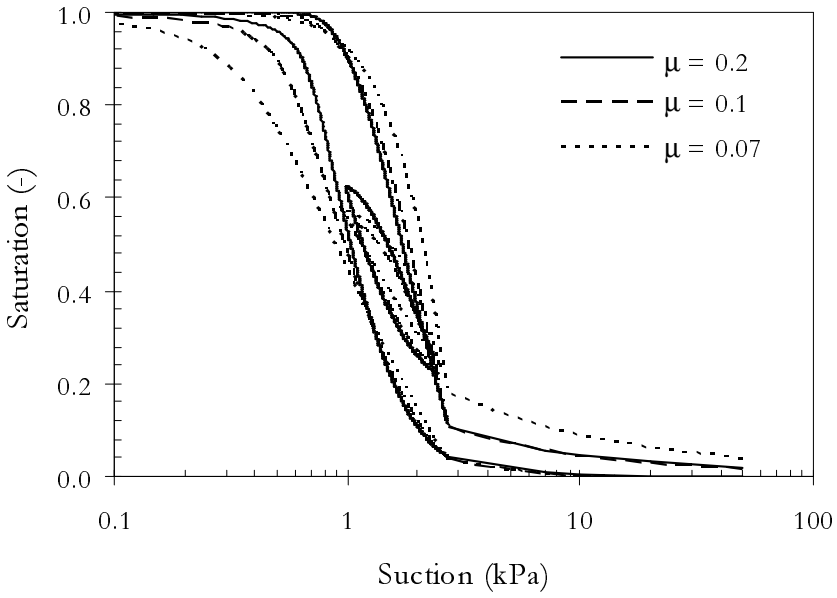

Figure 2.26: Influence of the parameter μ on the shape of the soil-water characteristic curve

Degree of saturation S_{r0} for $(u_a - u_w) \approx 0$: During the imbibition process of a soil some air bubbles can be occluded in the pore water. If the ratio of the net volume of pore water to the total volume of pore water (including the volume of the closed air bubbles) during the imbibition process is assumed to be constant, then the ratio is just the degree of saturation S_{r0} for $(u_a - u_w) \approx 0$. The parameter S_{r0} influences mainly the saturated zone and thus influences the air-entry value ψ_{aev}.

Various hysteresis models for calibrating the soil-water characteristic curve were compared to each other by several authors Jaynes (1984), Viaene et al. (1994), Pham et al. (2005). Jaynes (1984) compared the so called point method (Dane & Wierenga 1975), the slope method that is a modified point method, the linear method (Hanks 1969) and the domain model (Mualem 1974). While the last two models predicted the best shape, the linear method was suggested to use for numerical simulation of hysteretic flow because of its simplicity. A statistical analysis of 6 hysteresis soil-water characteristic curves was carried out by Viaene et al. (1994). The authors considered empirical models (Hanks 1969, Scott et al. 1983) as well as independent (Mualem 1974, Parlange 1976) and dependent (Mualem 1984*a*) domain models. Best agreement between observed and measured data was found when using both models of Mualem, which are not trivial to use. When applying the empirical model by Scott et al. (1983) good agreement was found. They confirmed that neglecting the hysteresis behavior when describing drainage and imbibition path results in significant errors. In a recent study Pham et al. (2005) compared 2 empirical models with 6 domain models on 34 soils different of type. For the prediction of drainage and imbibition curves the empirical model by Feng & Fredlund (1999) was suggested. For predicting scanning curves the domain model by Mualem (1974) seemed to be the most accurate.

Discussion on soil-water characteristic curve as expressed by linearized functions and essentially non-linear functions have been presented by Stoimenova et al. (2003*a*,*b*, 2005). The methodology to assess the quality of the curve fitting through statistical analysis is also addressed. Agus et al. (2003) assessed three statistical models (Childs and Collis-George model (1950), Burdine model (1950), Mualem model (1976)) with different soil-water characteristic curves (Gardner 1958, van Genuchten 1980, Fredlund & Xing 1994).

2.5.2 Models for Unsaturated Hydraulic Conductivity

Unsaturated hydraulic conductivity functions can be calculated using either an indirect method or a direct method. A variety of indirect methods can be used to determine the unsaturated hydraulic conductivity function, namely, empirical models, macroscopic models and statistical models (Leong & Rahardjo 1997*a*).

Empirical Models

Empirical models (Richards 1931, Gardner 1958, Brooks & Corey 1964) incorporate the saturated hydraulic conductivity and a sufficient set of experimental data of unsaturated hydraulic conductivity measurements, that are best fitted. One of the earliest equation, a linear function, was proposed by Richards (1931). The equations are either related to the suction (Richards 1931, Wind 1955, Gardner 1958) or to the volumetric water content (Gardner 1958, Campbell 1973, Dane & Klute 1977). Because water is only flowing through the water phase in soils unsaturated hydraulic conductivity and soil-water characteristic curve are similar in shape. Thus soil-water characteristic curve parameters of well established soils can also be used to determine unsaturated hydraulic conductivity function. Advantages and disadvantages of direct and indirect methods for obtaining the unsaturated hydraulic conductivity have been given by Leong & Rahardjo (1997*a*).

Macroscopic Models

Macroscopic models were developed on the assumption that laminar flow occurs on a microscopic scale that obeys Darcy´s law at the macroscopic level. Generally macroscopic models are based on the following general form:

$$k_r(\psi) = S_e(\psi)^\delta \tag{2.17}$$

where S_e is the effective degree of saturation, ψ is the suction and the exponent δ is a fitting parameter. Depending on the type of soil the parameter δ is varying between 2 and 4. Averjanov (1950) suggested $\delta = 3.5$, Irmay (1954) suggested $\delta = 3.0$ and Corey (1954) suggested $\delta = 4.0$. Brooks & Corey (1964) showed that the exponent $\delta = 3$ is valid for uniform soils only. To account for the effect of pore-size distribution Brooks & Corey (1964) expanded the exponent to $\delta = (2 + 3\lambda)/\lambda$, where λ is a pore-size distribution index. A knowledge of the soil-water characteristic curve and the saturated hydraulic conductivity is required when using macroscopic models. The main disadvantage of macroscopic models is, that the effect of pore-size distribution is neglected.

Statistical Models

Statistical models use the best-fitted suction-water content relation in connection with the saturated hydraulic conductivity to derive the relative hydraulic conductivity function. The unsaturated hydraulic conductivity function $k(\psi)$ can be calculated from the following relationship:

$$k_r(\psi) = k(\psi)/k_s; \;\; with \;\; k_r(\psi) = 1 \;\; for \;\; \psi \leq \psi_{aev} \tag{2.18}$$

where: k_r is the relative hydraulic conductivity and k_s is the saturated hydraulic conductivity. Statistical models are based on the following assumptions (Mualem 1986):

1. The porous medium is assumed to be an assembly of randomly interconnected pores with a certain statistical distribution.

2. The Hagen-Poiseuille equation is valid and used to determine the conductivity in a pore channel.

3. The soil-water characteristic curve is a representation of the pore-size distribution function based on Kelvins capillary law.

Mualem (1986) provided an extensive study of statistical models for estimating unsaturated hydraulic conductivity. The author reviewed the statistical models and found three general pore-size functions, namely the Childs and Collis-George model (1950), the Burdine model (1953) and the Mualem model (1976). Review of hydraulic conductivity functions utilizing empirical expressions can be found in the geotechnical literature (Fredlund et al. 1994, Leong & Rahardjo 1997*a*, Huang, Barbour & Fredlund 1998, Agus et al. 2003). Agus et al. (2003) assessed statistical methods with different suction-water content equations for sands, silts and clays. They found best agreement between experimental and measured results for sand when using the modified Childs & Collis-George (1950) model together with the Fredlund & Xing (1994) suction-water content model.

Numerous equations have been proposed by several researchers to predict the relative hydraulic conductivity function from the soil-water characteristic curve. Among them are the models by Marshall (1958), Millington & Quirk (1961), Kunze et al. (1968). An attractive closed-form equation for the unsaturated hydraulic conductivity function was given by van Genuchten (1980), who substituted the soil-water characteristic curve in the conductivity model of Mualem (1976). Disadvantage of the closed form equation is, that the van Genuchten soil-water characteristic curve parameter m is restricted to $m = 1 - 2/n$ and thus reduces the accuracy of the best fit. Therefore the closed form equation is not used in this thesis. Fredlund et al. (1994) combined Fredlund and Xing's model for soil-water characteristic curve with the statistical pore-size distribution model of Childs & Collis-George (1950) and derived a flexible relative hydraulic conductivity function. Three models, namely the Childs and Collis-George model (1950), the Mualem model (1976) and the Fredlund et al. model (1994) are used in this study. In the following the expressions are introduced.

- *Childs & Collis-George (1950)*

  Based on randomly interconnected pores with a statistical distribution Childs & Collis-George (1950) obtained the following expression:

$$k(\theta) = M\left(\int_{\varrho=R_{min}}^{\varrho=R(\theta)}\int_{r=\varrho}^{r=R(\theta)} \varrho^2 f(\rho) f(r) dr d\rho + \int_{\varrho=R_{min}}^{\rho=R(\theta)}\int_{r=R_{min}}^{r=\varrho} r^2 f(r) f(\varrho) d\varrho dr\right) \tag{2.19}$$

where: $f(r)$ represents the probability of the pores with a larger radius, r, and $f(\varrho)$ represents the probability of the pores with a smaller radius, ϱ and M is a geometry and fluid parameter. It is assumed that the resistance to flow is from the smaller pores ϱ and only one connection exists between the pores. Childs and Collis-George also suggested the summation form of the above integral. By dividing the integral into equal intervals of water content Marshall (1958) calculated the saturated conductivity. Kunze et al. (1968) provided further modifications and calculated the unsaturated hydraulic conductivity. The most general form of the Childs & Collis-George (1950) type of statistical model is given as:

$$k_r(\theta) = \Theta^n \frac{\int_0^{\theta} \frac{(\theta - \zeta)d\zeta}{\psi(\theta)^{2+m}}}{\int_0^{\theta_s} \frac{(\theta_s - \zeta)d\zeta}{\psi(\theta)^{2+m}}} \tag{2.20}$$

where: ζ is a dummy integration variable and n, m are parameters. In the modified Childs and Collis-George model the parameters are set to $n = m = 0$.

- *Mualem (1976)*

Mualem (1976) derived a similar model for establishing the relative conductivity function:

$$k_r = \Theta^q \left(\frac{\int_{\theta_r}^{\theta} \frac{d\theta}{\psi(\theta)}}{\int_{\theta_r}^{\theta_s} \frac{d\theta}{\psi(\theta)}} \right)^2 \tag{2.21}$$

where: q is a value depending on the properties of the specific type of soil fluid. Mualem (1976) tested 45 soils and suggested $q = 0.5$.

- *Fredlund et al. (1994)*

Fredlund et al. (1994) substituted Eq. 2.11 into the integral form of the Childs & Collis-George model and predicted the following relative conductivity function for unsaturated soils using the soil water characteristic curve:

$$k_r(\theta) = \frac{\int_{ln(\psi)}^{b} \frac{\theta(e^y) - \theta(\psi)}{e^y} \cdot \theta'(e^y)dy}{\int_{ln(\psi_{aev})}^{b} \frac{\theta(e^y) - \theta_s}{e^y} \cdot \theta'(e^y)dy} \tag{2.22}$$

where: b is equal to ln(1,000,000), y presents the logarithm of suction, θ' is the time derivative of Eq. 2.11 and e is the base of the natural logarithm. Whereas this equation requires the functional relation between suction and water content using Fredlund and Xings (1994) model, the other two are applicable with any soil-water characteristic curve model.

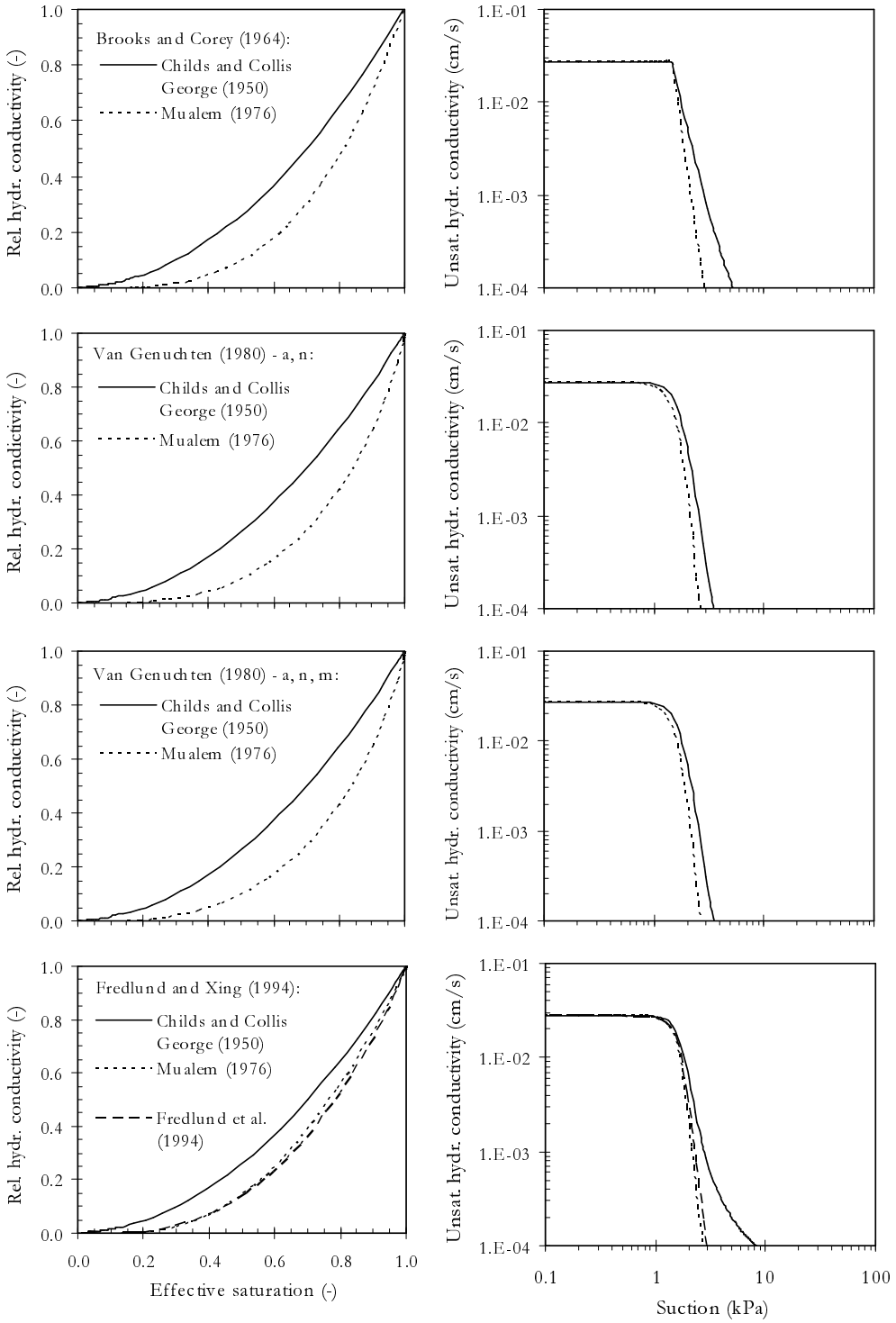

Figure 2.27: Unsaturated hydraulic conductivity of sand derived from several soil-water characteristic curve models using statistical models

Fig. 2.27 shows results of indirectly estimated hydraulic conductivity functions using the above introduced statistical models in correlation with the soil-water characteristic curves given in the previous section. The model by Fredlund et al. (1994) is restricted to use only in combination with their proposed soil-water characteristic curve. The relative hydraulic conductivity versus effective saturation as well as unsaturated hydraulic conductivity versus suction are shown.

2.6 Identification of Hydraulic Functions using Inverse Procedures

The use of inverse modeling techniques has increased in the past years. In comparison to the determination of hydraulic functions using conventional experiments performed under equilibrium condition inverse modeling is a fast method to estimate unsaturated hydraulic functions using measurements from outflow and inflow experiments. With increase in computer power inverse methods based on parameter optimization for soil hydraulic functions have been developed for estimation of unsaturated hydraulic properties. Traditionally experimental results from following inflow/ outflow tests were utilized for inverse procedures:

- one-step method including water outflow data
- one-step method including water outflow data plus pressure head measurements
- multistep method including water outflow data
- multistep method including water outflow data plus pressure head measurements
- continuous flow method including flow data and pressure head or water content measurements

The set up of the experiment as well as the boundary conditions have to be selected carefully to guarantee unique and robust identification of the unsaturated hydraulic parameter set. In the last years several researchers applied the inverse approach to one-step outflow experiments, but encountered problems with the non-uniqueness of the solution. Differences between inversely determined and independently measured data were found. Carrera & Neumann (1986) defined criteria of uniqueness, stability and identifiability for inverse problems. The use of inverse methods for the determination of unsaturated flow parameters using transient experimental data was first reported by Zachmann et al. (1981, 1982). State of the art report for inverse modeling of flow experiments is given in Durner et al. (1999).

- *Inverse procedure using experimental results derived from the One-step method*

  Kool et al. (1985a) investigated the feasibility of the determination of unsaturated hydraulic functions using cumulative outflow measurements from one-step pressure

method. The authors examined the parameter identification procedure on two hypothetical soils (parameters correspond approximately to those of a sandy loam and a clay loam) in combination with van Genuchten's model. Unique identifications only were performed when the applied suction increment was large enough to yield a low final water content under an adequate period of time and thus a broad range in water contents was examined. Initial parameter estimates close to their true values as well as precise experimental data are necessary for the approach. In a second paper Kool et al. (1985*b*) used data of cumulative outflow versus time from one-step outflow experiment for calculation of the van Genuchten parameters by inverse simulation of the flow problem. Experiments were carried out for drainage on 4 different soils (sand loam, silt loam, sandy clay loam, clay) by applying a pressure step of 100 kPa to the initially saturated specimens. 3 methods were compared: i) a method, where the cumulative outflow with time was used, ii) a method, that includes additionally measured data of the water content at a pressure head of 1500 kPa and iii) a method, which uses data from conventional equilibrium experiments. Predicted and measured cumulative outflow data, diffusivity as well as predicted and measured soil-water characteristic curves were compared. Using the 2^{nd} method yields the best fit in cumulative outflow data and hydraulic diffusivity. While the 3^{rd} method gave the best description of the soil-water characteristic curve. Although good results were achieved for all methods, pressure head data were required to get unique solutions.

Similar to the work of Kool et al. (1985*b*) the work by Toorman & Wierenga (1992) is concerned with the inverse approach for estimating unsaturated flow parameters from one-step method on a synthetic soil. Response surfaces of van Genuchten parameters (i.e. one of the three parameters was kept constant during optimization procedure, while the other two were changed) were plotted to show the non-uniqueness and ill-posedness of the solutions. Non-uniqueness was proven by wide valleys for instance in the $\alpha - n$ plane indicating that there are many solutions for providing reasonable good predictions of one outflow problem. To improve the inverse approach additionally water content as well as pressure head measurements were carried out during the one-step outflow test. However, measurements of water content did not improve the parameter estimates. The authors found, that combining outflow data and pressure head data appears most promising for estimating unsaturated flow parameters.

Dam et al. (1992) performed an extensive work on the reliability of inverse estimation using one-step outflow data on loess, silt loam, sand and loam. They used different parameter combinations and input data to estimate the unsaturated hydraulic conductivity functions of the investigated soils and compared the results with unsaturated hydraulic conductivity function measurements. The results showed, that it is insufficient to carry out inverse simulation only on cumulative outflow data. Independent data of

soil-water characteristic curve are necessary to estimate reliable unsaturated hydraulic conductivity functions.

- *Inverse procedure using experimental results derived from the Multistep method*

  Unsaturated hydraulic conductivity was directly estimated using tensiometer measurements during multistep outflow experiments and in a additionally performed steady-state downward flow experiment (Klute & Dirksen 1986*b*). Three different soils were investigated (loamy sand, sandy loam, loam). The direct estimation of the unsaturated hydraulic conductivity using tensiometer measurements only gave 2 results for each soil, that is not very meaningful. The comparison of the results showed that the unsaturated hydraulic conductivity calculated from steady-state downward flow experiment were underestimated by the inversely determined unsaturated hydraulic conductivity using multistep outflow data. The authors found the multistep method is superior to the one-step method and is more feasible for simulating unsaturated flow.

  A comparison of inverse solutions for determination of unsaturated hydraulic functions using both one-step and multistep experimental data was conducted by Eching & Hopmans (1993) on silt loam, loam, sandy loam and fine sand for one drainage cycle. To avoid the lack of uniqueness simulations were performed not only in combination with initial and final water content and pressure date, but also including soil water pressure head data. Therefore a pressure cell was additionally instrumented with a tensiometer sensor and pressure transducer. The authors found that the identification of soil-water characteristic curves by using one-step and multistep outflow data are improved when using simultaneously measured water content and corresponding suction data.

  Both one-step and multistep approaches for the estimation of unsaturated hydraulic functions using inverse modeling were also compared by Dam et al. (1994) on a loam. Using the outflow measurement data only the multistep outflow method resulted in unique estimates while the one-step outflow method often yielded in non-unique solutions. Major problem of the one-step pressure method is the fast change in pressure, that does not occur in nature and that may leads to non-equilibrium condition in the investigated soil (Dam et al. 1992, 1994).

  The multistep method was reevaluated by Fujimaki & Inoue (2003), who checked the reliability of the multistep method through comparisons with independently measured unsaturated hydraulic conductivity. Unsaturated hydraulic conductivity was determined using outflow data and i) an optimization method and tensiometer readings, ii) a direct method using tensiometer readings in one depth and iii) a direct method using tensiometer readings in two depth. Best agreement was found between the direct measured results. The observed results using optimization method were underestimated by the measured results.

When using van Genuchtens model for inverse simulation of hydraulic unsaturated soil properties (Eching et al. 1994, Dam et al. 1994, Zurmühl & Durner 1996) demonstrated that the multistep method is superior to the one-step method.

- *Inverse procedure using experimental results derived from the continuous flow method*

  Alternatively to the one step and multistep method Durner (1991) suggested the continuous flow method. A comparison of inverse modeling of one-step, multistep and continuous flow method experiments by Durner et al. (1999) showed that the multistep method and the continuous flow method are the preferred methods to identify unsaturated hydraulic parameters.

A free-form parameterization approach for estimation of soil hydraulic properties was suggested by Bitterlich et al. (2004) to avoid often experienced problems of ill-posedness of inverse problems. Mathematical and numerical modeling concepts for simulation of unsaturated/multiphase flow were discussed in detail by Helmig (1997).

2.7 Volumetric Behavior of Partially Saturated Soils

In the review below it is focused on one-dimensional behavior of sand that is derived from one dimensional compression and rebound tests performed in oedometer cell.

2.7.1 Stress-Strain Behavior

Several tests are available to measure the stress-strain behavior of a soil, e.g. the isotropic compression test, the one-dimensional compression test, the triaxial test or the direct shear test. In the present study the stress-strain behavior of unsaturated soil was investigated using one-dimensional compression and rebound tests. This type of experiments are performed in conventional oedometer cells. The test includes the application of stress to a soil specimen along the vertical axis, while the strain in the horizontal direction is restricted. Typical results are shown in Fig. 2.28. For determination of stress-strain behavior one-dimensional compression and rebound test is often used, because it is simple to perform and the strain condition in the soil specimen is approximately similar to the situation of the soil in civil engineering problems as settlements of an embankment. The loading of a soil specimen can be applied either under drained or undrained conditions. Under drained condition the pore-air and pore-water pressure are allowed to drain during testing procedure while under undrained condition the total stress is applied to the specimen resulting in an excess of pore-water and pore-air pressure (Rahardjo & Fredlund 2003). Major problem when dealing with oedometer is the friction between the soil sample and the oedometer ring, where shear forces develop. The presence of side friction disturbs the one-dimensional state of strain and prevents the applied axial force to reach to 100% the bottom part of the specimen. For minimizing this effect the

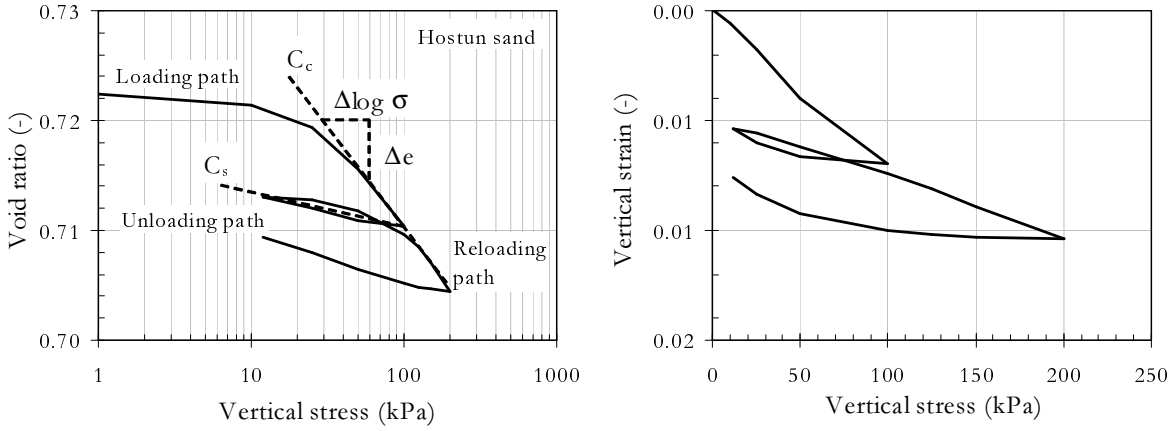

Figure 2.28: Vertical stress versus void ratio (left) as well as vertical stress versus vertical strain curves (right) including loading, unloading and reloading path for Hostun sand

ratio between thickness and diameter is kept as small as possible (e.g. 1:3 or 1:4) (Lambe & Whitman 1969).

Important parameters derived from one-dimensional compression tests are the stiffness modulus $E_{oed,ur}$, the compression index C_c as well as swelling index C_s. Following equations are used to calculate these parameters (DIN 18135):

$$C_c = -\frac{\Delta e}{\Delta \log \sigma} \qquad C_s = -\frac{\Delta e}{\Delta \log \sigma} \tag{2.23}$$

where: e is the void ratio and σ is the vertical net stress. According to Eqs. 2.24 the stress dependent stiffness moduli E_{oed} and E_{ur} can be calculated, where E_{oed}^{ref} is the reference stiffness modulus for initial loading and E_{ur}^{ref} is the reference stiffness modulus for un-/reloading path determined for a reference stress σ_{ref} and $\hat{m}$ is a parameter (Ohde 1939, Schanz 1998):

$$E_{oed} = E_{oed}^{ref} \cdot \left(\frac{\sigma}{\sigma_{ref}}\right)^{\hat{m}} \qquad E_{ur} = E_{ur}^{ref} \cdot \left(\frac{\sigma}{\sigma_{ref}}\right)^{\hat{m}} \tag{2.24}$$

The parameter $\hat{m}$ and the normalized stiffness modulus E_{oed}^{ref} and E_{ur}^{ref} respectively are derived by regression process, that is presented in the diagrams in Fig 2.29. To linearize the function between vertical net stress and strain $\varepsilon(\sigma)$ the logarithm of the strain $\ln(\varepsilon)$ and the logarithm of the normalized stiffness modulus $\ln(\sigma/\sigma_{ref})$ is used:

$$\ln(\varepsilon) = \alpha \cdot ln\left(\frac{\sigma}{\sigma_{ref}}\right) + \beta \qquad E_{oed,ur}^{ref} = \frac{1}{\alpha} \cdot \frac{\sigma_{ref}}{\exp^{\beta}} \qquad \hat{m} = 1 - \alpha \tag{2.25}$$

where: α and β are parameters.

The influence of suction on the stress-strain behavior of unsaturated soils has been examined experimentally based on the independent stress state variables, namely the net stress as

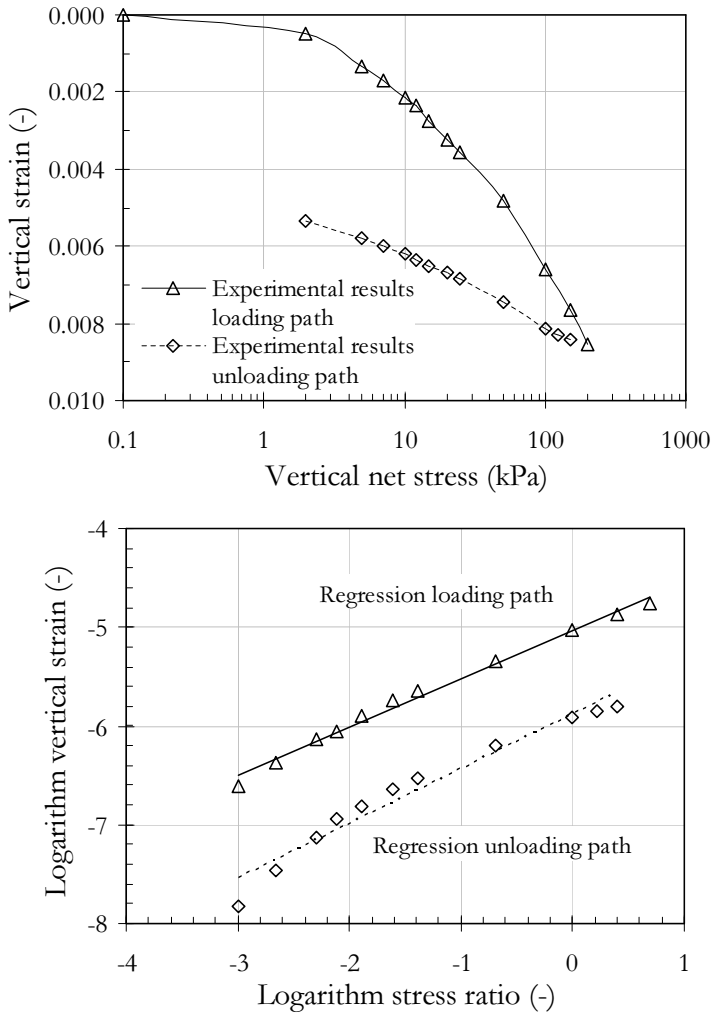

Figure 2.29: One dimensional compression and rebound results for Hostun sand and appropriate regression functions

well as matric suction (Alosnso et al. 1987, Delage 2002, Rahardjo & Fredlund 2003). When dealing with experiments on unsaturated soils special test features are required, e.g. ceramic disk for separation of air phase and water phase, equipment for application of pore-air pressure as well as pore-water pressure for application and control of matric suction. Among others, oedometer cells for investigation of unsaturated soils were developed by Kassiff & Shalom (1971), Escario & Saez (1973), Romero (1999), Rampino et al. (1999). Most of these cells were used to investigate the volume change behavior of unsaturated silts or clays. Several authors (Cui & Delage 1996, Rahardjo & Fredlund 2003) have been demonstrated that the suction has a significant influence on the mechanical unsaturated soil behavior of cohesive soils as volume change and stiffness. For instance Cui & Delage (1996), Rampino et al. (2000)

investigated the stress-strain behavior of a silt using dimensional compression and rebound tests and their results confirm that increasing suction has a beneficial effect on its mechanical behavior. That means with increasing suction the compressibility decreased and the stiffness increased.

Considering granular materials most experimental studies were performed on saturated ($S = 0, S = 1$) specimen as done by Oda et al. (1978) who performed plane strain and triaxial compression tests on samples of naturally deposited sands. Desrues et al. (1996) performed triaxial tests on sand. Gennaro et al. (2004) investigated the influence of different loading path on the undrained behavior of saturated sand (Hostun sand) carried out in several triaxial tests. Schanz & Vermeer (1996) derived elasticity moduli of dry sand specimen (Hostun sand) from one-dimensional compression and triaxial tests. The influence of void ratio was studied. Many researchers studied the influence of void ratio and loading path on the stress strain behavior of sand. The influence of suction or water content was not from interest even it is well known that the suction (in this case the matric suction) is the main force influencing the hydro-mechancial behavior of granular materials.

2.7.2 Collapse Behavior

An important feature of the volume change behavior of unsaturated soils is the collapse phenomenon. The oedometer apparatus usually is used to predict the collapse potential of a soil. The collapse phenomenon is defined as the decrease of total volume of a soil resulting from a induced wetting and the breakdown of the structure of the soil at unchanging vertical stress. The collapse potential CP conducted in a oedometer apparatus is the change in specimen height Δh resulting from wetting, divided by the initial height h_0 of the tested specimen, expressed in percent:

$$CP = \left(\frac{\Delta h}{h_0}\right) \cdot 100 \tag{2.26}$$

The collapse can be slow or fast and its magnitude can vary between less than 1% and up to 10% (Lawton, Fragaszy & Hardcastle 1991). The literature review by Lawton, Fragaszy & Hetherington (1991) showed, that nearly all types of compacted soils are subjected to collapse under certain conditions. But also naturally deposited soils, clean sands and pure clays and also soils containing gravel fractions can undergo collapse (Lawton et al. 1992). Whereas compacted soils generally collapse at high stress levels, naturally deposited soils can collapse at low stress levels. Among others the amount of collapse increases with the applied vertical stress, decreases with initial water content as well as decreases with dry density (Cox 1978, Lawton et al. 1989). Some conditions that are required for a soil to collapse are an open partially unstable, unsaturated fabric in the soil and vertical stress. A suction that is high enough to stabilize the unsaturated specimen or cementing agent between the grains are required for a soil to collapse.

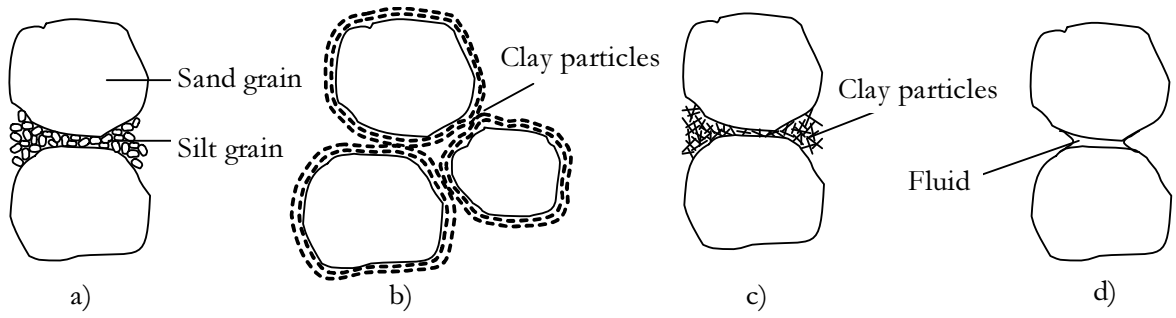

Figure 2.30: Several cases of bonding

Barden et al. (1973) suggested several cases of bonding. This cases are shown in Fig. 2.30. Four types of bond are presented: a fine silt bond (Fig. 2.30 a)), a clay bond (Fig. 2.30 b)) and flocculated clay buttress (Fig. 2.30 c)) and a bonding due to fluid (Fig. 2.30 d)). An Environmental Scanning Electron Microscope (ESEM) photo (Schanz et al. 2001) of bonding between sand grains due to capillary meniscus and cementing agent is given in Fig. 2.31. Metastable structure was investigated by Barden et al. (1973). The authors found that due to matric suction the decrease in strength will be immediate and due to clay bonding or cementing agent the collapse might be retarded. In general the collapse process in unsaturated soils is considered in terms of two separate components of stress, namely the applied vertical

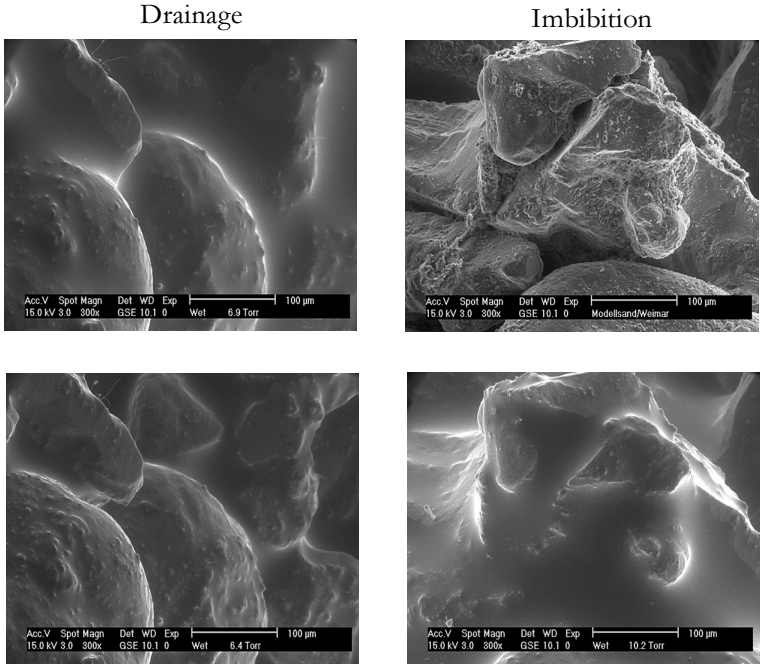

Figure 2.31: Capillary meniscus during drainage (left) and imbibition (right) as well as cementing in partially saturated sand

stress and the suction. The addition of water to the unsaturated specimen reduces the suction in the soil and weakens or destroys the bonding or cementing agent and thus causes shear failure at the interaggregate or intergranular contacts (Casagrande 1930, Barden et al. 1973, Mitchell 1993).

2.7.3 Influence of Stress History on Mechanical Behavior

The preconsolidation stress σ_0, is the maximum effective stress to which the soil has been exposed. Estimation of stress history characteristic are most often based on one-dimensional compression tests. The interpretation of the stress-strain curve during initial loading gives information, if the soil was already compressed by a greater overburden pressure. The preconsolidation pressure can be determined using several methods. Common used methods are that proposed by Casagrande (1936) and Janbu (1969). Both methods are briefly described below:

- *Casagrande's method (1936)*

  As presented in Fig. 2.32 Casagrande (1936) proposed a graphical method using the plot of void ratio versus effective vertical net stress ($e - \log \sigma'$). First the point of maximum curvature (point A) on the recompression part is determined. Then the straight-line part BC is produced. A Tangent is drawn to the curve at point A and the horizontal is drawn through A. The angle between the horizontal and tangent is bisected. The point of intersection of the bisector and BC gives the approximate value of the preconsolidation pressure σ_0.

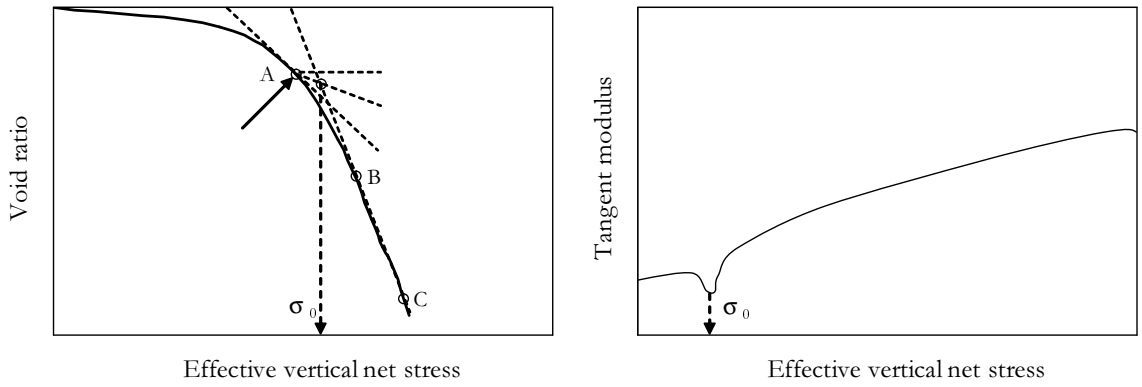

Figure 2.32: Casagrande's (1936) and Janbu's method (1969) for prediction of preconsolidation pressure

- *Janbu's method (1969)*

  Janbu (1969) proposed that the preconsolidation pressure can be determined from the plot of tangent modulus M versus effective vertical net stress ($M - \sigma'$):

$$M = \frac{\Delta\varepsilon}{\Delta\sigma'} \tag{2.27}$$

  where: ε is the strain and σ' is the effective vertical net stress (see Fig. 2.32). He found a drop in stiffness modulus near the preconsolidation pressure signifying a breakdown of the structural resistance. He defined the preconsolidation pressure as the point just before the stiffness modulus levels out.

A detailed review of evaluation of of the preconsolidation pressure and a investigation of these various methods is given by Grozic et al. (2003). Investigations on silt (Rahardjo & Fredlund 2003) showed, that soil has not only a memory with respect to effective stress, but also with respect to suction. In the present study the methods given by Casagrande (1936) and Janbu (1969) are used to estimate, if there is an influence of the applied matric suction on the stress history behavior of granular material. The maximum stress to which the soil has been exposed (i.e. due to suction) is determined equivalent to the preconsolidation pressure and called here yield stress $\tilde{\sigma}_0$.

2.8 Summary

This chapter summarizes important literature referring to unsaturated soils. In the beginning unsaturated soils are introduced and differences in hydro-mechanical behavior of several types of soils are given. Further stress state in saturated as well as unsaturated soils is explained. Several authors suggested single valued stress equations and other authors suggested the approach of independent stress state variable for describing unsaturated soils. In the present study the approach of independent stress state variables is preferred and used to perform experimental investigation on unsaturated sand. That is the application of suction and total net stress with reference to the air-pressure or water pressure.

Phases in unsaturated soils as well as soil suction and its components are discussed. In case of granular materials as sand the matric suction is the main component influencing its characteristics.

The definition and meaning of both hydraulic functions, namely the soil-water characteristic curve and unsaturated hydraulic conductivity function is given. Mainly the chapter is focused on the methods for determination of hydraulic functions. Most common methods are the one-step, multistep method and the continuous flow experiment that are used traditionally in combination with inverse methods to determine hydraulic functions. However, in the present work parallel measurements of water content and matric suction are carried out for the direct identification of hydraulic functions for drainage and imbibition cycles.

Typical equipment and measurement techniques needed when dealing with unsaturated soils are introduced. Special features in the equipment used in this study allow to investigate granular materials that includes for instance measurement of volume changes using dial gauge with high resolution, attached burettes for application of small matric suction as well as matric suction changes and the development of modified pressure plate apparatus.

An overview of several models for prediction of hydraulic functions is given. The review showed that there is a need for a simple equation that considers determination of scanning behavior of soil-water characteristic curve. Existent models are quite complex in use or their parameters are difficult to measure in the laboratory.

Common type of test for prediction of the stress-strain behavior of soils is presented, that is the one-dimensional compression and rebound test. Usually this type of test is performed on saturated soils. The present study is concerned with unsaturated sand (the equipment and measurements have to fulfill appropriate requirements as given above). Relevant equations are given.

Chapter 3

Introduction to Process Modeling - A Statistical Approach

3.1 General

Direct determination of the relation between suction and volumetric water content, saturation or gravimetric water content from experiments on sand are difficult to handle due to the narrow soil suction within which the drainage and vice versa imbibition process take place. That is the relevant range of suctions (e.g. between 0 to 20 kPa) to be measured is relatively small but the measurement error of the instrument (e.g. tensiometer) may be large. For this reason the assessment of the error and model validation are of critical importance in experimental building up the soil-water characteristic curve for sand.

Most models suggested in literature for prediction of the hysteretic nature of the soil-water characteristic curve are not trivial to use or do not fit the experimental data very well (see also comparison of experimental and predicted data of sand in Chapter 7). Therefore in the present chapter a method is proposed that can be used to develop suction-water content model based on statistical analysis for experimental suction (i.e. total suction, matric suction, osmotic) and water content (saturation, gravimetric water content) results.

3.2 Steps of Model Building

The main steps to be done for building an appropriate model are given in Fig. 3.1. Basic assumption for process modeling is the availability of experimental results. However, in the model selection step diagrams of the experimental data, knowledge of the process and assumptions about the process are collected to determine the form of the model, that will be used for curve fitting. Then the selected model and possible information about the experimental data, assumptions regarding to the process and a convenient curve fit method are used to estimate the unknown parameters in the model. Using the model parameter estimates and the experimental data, the model is assessed wether or not the model assumptions are valid.

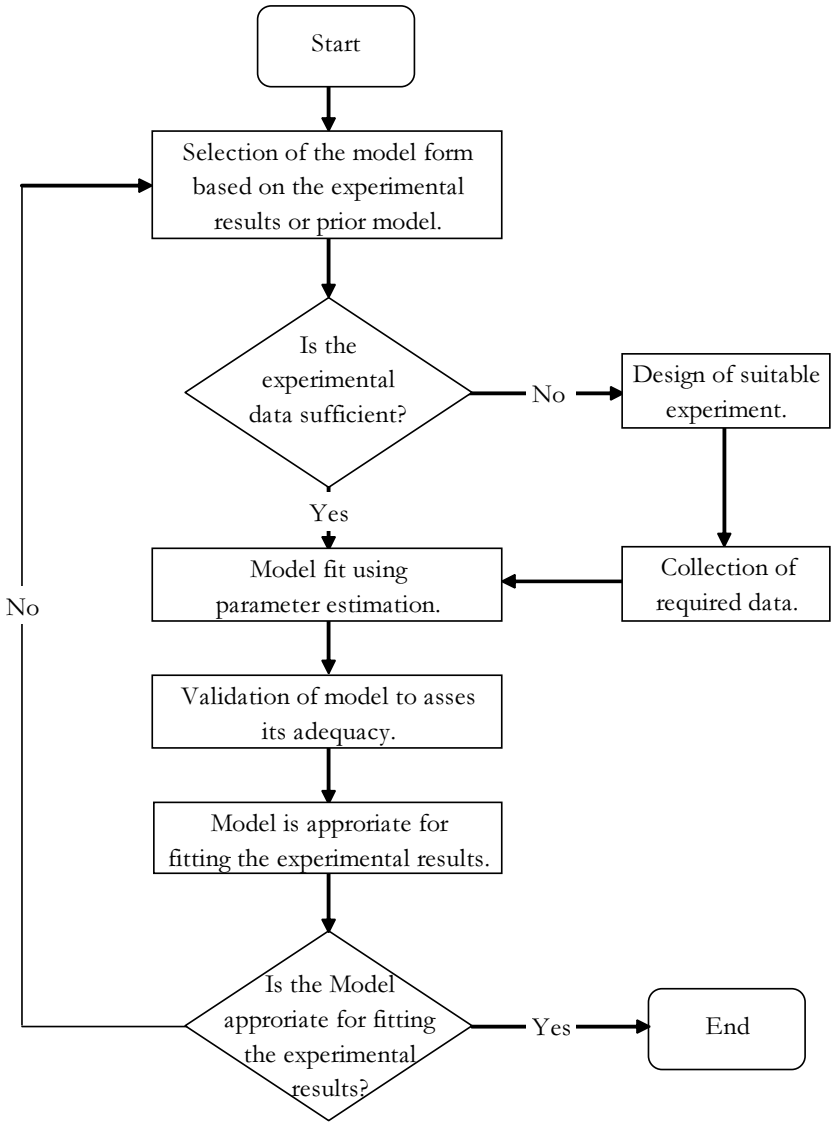

Figure 3.1: Flow chart giving the main steps for developing a process model

If the assumptions of the model seem to be valid the model can be used for the present problem. If the model validation identifies problems with the current model the modeling process should be improved using the information from the model validation or a new model should be developed. It also could be necessary to design new experimental setup to collect new data and start new parameter estimation and model validation procedure.

3.2.1 Collection of Data for Model Building

Model building of a certain process requires the design of an appropriate experiment as well as the data collection. Data also can be collected from literature.

3.2.2 Selection of the Model Form

Plots of the data, process knowledge and assumptions about the process are used to determine the form of the model to be fitted to the data. Process modeling is mainly used for estimation, prediction, calibration and optimization. In the present work the model is used for prediction of any combination of explanatory (suction ψ) and response variables (volumetric water content θ), including also values (within the interval of present data) for which no measurements are available. In the model it is assumed that the volumetric water content is subjected to a random error. Hence the model equation should contain at least a random element with a specified probability distribution. The following general form is supposed for the process model:

$$y = f(\vec{x}, \vec{\beta}) + \varepsilon \tag{3.1}$$

The model contains 3 main parts:

1. The response variable, that is denoted by y and represents the volumetric water content θ.

2. The mathematical function $f(\vec{x}, \vec{\beta})$, where x represents the explanatory variable (suction ψ) and the parameters β ($\beta_0, \beta_1 ... \beta_n$) in the model.

3. The random error ε.

Thus in our problem, where the function defines the relationship between the volumetric water content (water content, saturation) and suction the general form leads to:

$$\theta = f(\vec{\psi}, \vec{\beta}) + \varepsilon \tag{3.2}$$

The random error is the difference between the experimental data and the calculated data and is assumed to follow a particular probability distribution.

Because of its effectiveness and completeness linear least square regression method will be used for model building and for minimizing the error between observed and predicted results. Therefor the experimental data of suction and volumetric water content have to be transformed to linear relationship (see 3.2.3).

3.2.3 Appropriate Data Transformation and Selection of the New Model

As can be seen in Fig. 2.7 for several types of soils the soil-water characteristic curve is a non-linear relationship. In this study the construction of non-linear regression model for soil data following the methodology given in Stoimenova et al. (2003*b*, 2006) is illustrated. It demonstrates fitting a non-linear model and the use of transformations to deal with violation of the assumption of constant standard deviations for the residuals. For the construction of the non-linear model transformation of the data to linear function is used. The transformations are applied to the experimental data to achieve the following goals:

- To satisfy the assumption, that the variances of the residuals are homogeneous.

- To linearize the experimental results as much as possible.

First it is tried to transform the response variable, that is the volumetric-water content θ to get homogeneous variances. Often the square root $(\sqrt{\theta}, \sqrt{\psi})$, the power of 2 (ψ^2, θ^2), or logarithm $(\ln(\theta), \ln(\psi))$ and even double logarithm $(\ln\ln(\theta), \ln\ln(\psi))$ work well for such kind of purpose. After examining these plots the data giving the best linear form is chosen for model building. Based on the appropriate transformation found finally the corresponding non-linear model is proposed.

3.2.4 Model Fit

In the present study the Levenberg-Marquardt algorithm, which is an improvement of the Gauss-Newton method was used for solving non-linear least-squares regression problems. The Levenberg-Marquardt algorithm provides a numerical solution to the problem by minimizing a generally non-linear function over a range of parameters of the function. The parameters β of a model curve are optimized so that the sum of the squares of the deviations becomes minimum value:

$$g(\beta) = \sum(\theta_i - f(\beta, \psi_i))^2 \tag{3.3}$$

where: ψ_i and θ_i are sets of measured suction and volumetric water content and β represents the parameters of the model $f(x, \beta) + \varepsilon$.

3.2.5 Model Assumption and Model Calibration

Model validation is possibly the most important step in model building sequence. The validation of the fit from a selected model does not only include the quoting of the coefficient of regression determination R^2. A high value of R^2 does not guarantee that the model sufficiently fits the experimental data. Also the residual analysis is available, that is the primary tool for model validation. Whereas the coefficient of regression determination R^2 for model validation is focused on a particular aspect of the relation between the model fit and the experimental data and the information is compressed in a single value, the residual analysis illustrates a broad range of complex aspects between the model fit and the experimental data. The residual is the difference between the responses observed or measured (experimental results of volumetric water content) and the corresponding responses computed using the model (calculated results of volumetric water content):

$$e_i = \theta_i - f(\overrightarrow{\psi}_i, \overrightarrow{\beta}) \tag{3.4}$$

where: e_i is the residual, θ_i represents the $i-th$ response in the experimental data set and ψ_i the corresponding variable in the $i-th$ observation in the data set. If the plots of the residuals are conform to the assumptions described below the model fitting succeeded:

- A basic assumption to statistical methods for process modeling is that the described process is a statistical process. Thus the model process should include random variation.

- The most methods of process modeling rely on the availability of observed responses (here volumetric water content measurements) that are on average directly equal to the regression function value. This means the random standard error at each combination of explanatory variable values is zero.

- Due to the presence of random variation it is difficult to determine if the data are from equal quality. The most process modeling procedures treat all data equally when estimating the unknown parameters in the model. Therefore it is assumed that the random errors have a constant standard deviation.

- Process modeling involves the assumption of random variation. But not all intervals of the regression function include the true process parameters. To check these intervals the form of the distribution and the probability of the random errors must be known. It is assumed the random errors follow a normal distribution.

Several plots are used to appreciate wether or not the model fits the experimental data well:

- *Plots of residual versus predicted variables and observed versus predicted variables:*

  The random variation is checked using scatterplot of residuals versus predicted variables (volumetric water content θ) and observed versus predicted values are used for checking the sufficiency of the functional form of the proposed model and the assumption of constant standard deviation of random error. The plots allow the comparison of the amount of random variation of the entire range of data. If the plot of residuals versus predicted variables (volumetric water content θ) is randomly distributed the model fits the experimental data well. The scatter of the residuals should be constant across the whole range of the predictors. Any systematic structure in the plot is an indiction for the need to improve the model. A comparison of the amount of random variation is also possible when plotting observed values versus predicted values. This relation should be non-random in structure and linearly related.

- *Normal probability plot:*

  Normal probability plots are used to check wether or not the errors are distributed normally. The normal probability plot gives the sorted values of the residuals versus the associated theoretical values from the standard normal distribution. Unlike the residual scatter plots (i.e. residual versus predicted variables and observed versus predicted values) a random scatter of points does not indicate a normal distribution. Instead if the plotted points lie close to the straight line the errors are normally distributed. Another curvature indicates that the errors are not normally distributed. Significant deviations

of few points far from the line could be outliers. Compared to the histogram the normal probability plot is conveniently used to discern deviations from normality.

- *Histogram:*

  Similar to the normal probability plot the histogram is used to check the normal distribution of the analyzed data set. Histograms summarize the distribution of a data set and shows the location (i.e. center), the scale (i.e. spread), the skewness of the data and the presence of outliers. Compared to the normal probability plot a histogram of the residuals of the fit provides a detailed picture of the shape of the distribution. More or less bell shaped histograms confirm conclusions of a normally distributed data set.

3.3 Summary

A method for model building for determination of soil-water characteristic curve using data transformation was introduced in the present chapter, that is based on statistical analysis. The data transformation is used to find linear relation, that gives the possibility to use linear regression. In detail the steps for model building are given and described. The method presented above will be used later for developing soil-water characteristic curve model for Hostun sand, that includes prediction of drainage as well as imbibition process.

Chapter 4

Experimental Setups

4.1 General

The investigation of unsaturated soils demands for particular requirements of the testing equipment. Depending on the type of soil, if it is a clay, silt or sand, equipment has to be carefully chosen to be able to study the entire range of suction (where the soil-water characteristic curve takes place), to measure either suction, matric suction or osmotic suction (i.e. unsaturated soil behavior of clay is influenced by osmotic as well as matric suction and unsaturated soil behavior of sand is influenced by the matric suction) or to be able to carry out proper measurements with suitable accuracy (i.e. volume changes during vertical loading of a clay are larger than the volume changes of a sand). Among others the investigation of unsaturated soils requires the measurement of either the suction and/ or the water content.

During the present work several devices for testing unsaturated sand are developed and modified. The aim of the newly developed equipments is to design testing devices and to propose special experimental setups for investigation of hydraulic and mechanical behavior of sand. For application of suction, that is for sand experiments varying between $\psi = 0.1$ and 50 kPa, hanging water column and axis-translation technique are used. Other cells (column testing device I and II) are equipped with tensiometers and TDR sensors.

For determination of hydraulic functions of unsaturated Hostun sand different testing devices are developed in the present investigation:

- *Modified pressure plate apparatus*

  The main feature of the modified pressure plate apparatus is a ceramic disk, which enables to use hanging water column technique and axis-translation technique for determination of soil-water characteristic curve under equilibrium condition (multistep flow method). Thus suction is controlled in the cell. Precise cumulative water outflow and inflow measurements are carried out by means of the attached burette, that has a high accuracy. The apparatus additionally allows to investigate the influence of net

stress on the shape of the soil-water characteristic curve. Volume measurements are performed by the attached dial gauge.

- *Column testing device I*

  In the column testing device I large scale (boundary condition problem) sand specimen are examined. Special feature of the cell are pairs of tensiometer and TDR sensors in several depth, that directly measure suction and water content while withdrawing and injecting water from the specimen. The measurements of volumetric water content and matric suction enable to apply steady state flow (multistep method) and also transient state flow (continuous flow method) to the specimens. Therefore the relation between suction and water content obtained under equilibrium and dynamic condition can be compared. The unsaturated hydraulic conductivity can be either directly (e.g. via instantaneous profile method) or indirectly determined (e.g. by use of statistical models).

- *Column testing device II*

  Further drainage transient state tests (boundary condition problem) are conducted in column testing device II, where suction is applied to the specimen using axis-translation technique. Pairs of tensiometer and TDR sensors in several depths directly measure soil-water characteristic curve. Due to the ceramic disc on the bottom of the column the cell allows to apply certain suction to the specimen (hanging water column technique, axis translation technique). Also the cell has a piston for application of mechanical stress at top of the specimen. Volume measurements are performed by the attached dial gauge. The influence of the net stress on the hydro-mechancial behavior of Hostun sand specimens using column testing device II is not discussed in this work.

Hydraulic functions are measured and/ or estimated under different flow conditions (steady state and transient state flow condition) and loading path directions (initial drainage, main drainage and main imbibition, scanning drainage and scanning imbibition processes) using hanging water column as well as axis-translation technique and/ or tensiometer and TDR sensor measurements and/ or measurements of cumulative water flow.

For determination of mechanical behavior of unsaturated Hostun sand suction-controlled oedometer cell is used. The suction-controlled oedometer cell developed by Romero (1999) for the purpose of testing clay samples is upgraded with a burette for applying and controlling small suctions in the cell using hanging water column technique. The mechanical behavior of unsaturated sand was investigated by performing one dimensional compression and rebound tests at different constant suctions as well as collapse tests.

4.2 Modified Pressure Plate Apparatus

The modified pressure plate apparatus (Fig. 4.1) enables the determination of the soil-water characteristic curve for both drainage and imbibition cycles as well as scanning drainage and scanning imbibition cycles and thus to asses the phenomena of hysteresis. Tests performed in the modified pressure plate apparatus are element tests. Due to the small size of the specimen, it is supposed to be homogeneous in void ratio and in the distribution of water content respectively volumetric water content and saturation. The influence of net stress on the behavior of the soil-water characteristic curve can be determined by applying mechanical load via loading piston.

The experimental set up consists of a burette, a scale, an air-pressure system and the cell itself. A detailed scheme of the cross section of the modified pressure plate apparatus is given in Fig. 4.2. The apparatus has a specimen ring with a diameter of 70 mm and a height of 20 mm. A coarse porous stone is placed on the top of the soil specimen and a ceramic disk is placed at the bottom of the specimen. The ceramic disk used below the soil specimen in this study has an air-entry value of 100 kPa. There is the possibility to replace this ceramic disk by a ceramic disk with an air-entry pressure of 500 kPa when investigating the behavior of silty or clayey soils or a porous stone for performing conventional tests. Below the ceramic disc a water reservoir is located. A burette with a capacity of 25 cc and a least count of 0.05 cc is connected to this water reservoir. Water inflow and outflow is measured in the burette following several drainage and imbibition paths. Air pressure is applied to the top of the specimen through a coarse porous stone. Net stress can be applied to the specimen by placing the modified pressure plate apparatus in an oedometer loading frame. Volume changes of the specimens are measured by an attached dial gauge. Contrary to conventional

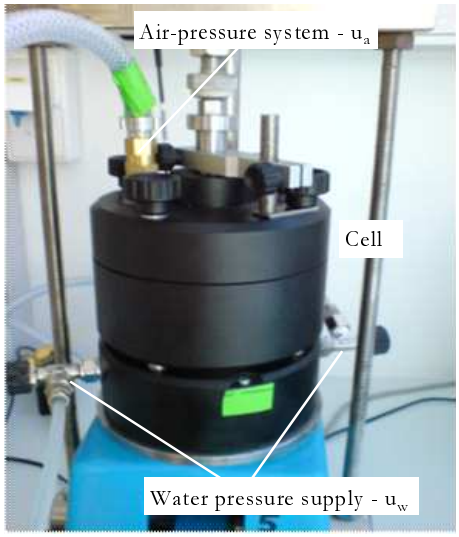

Figure 4.1: Modified pressure plate apparatus

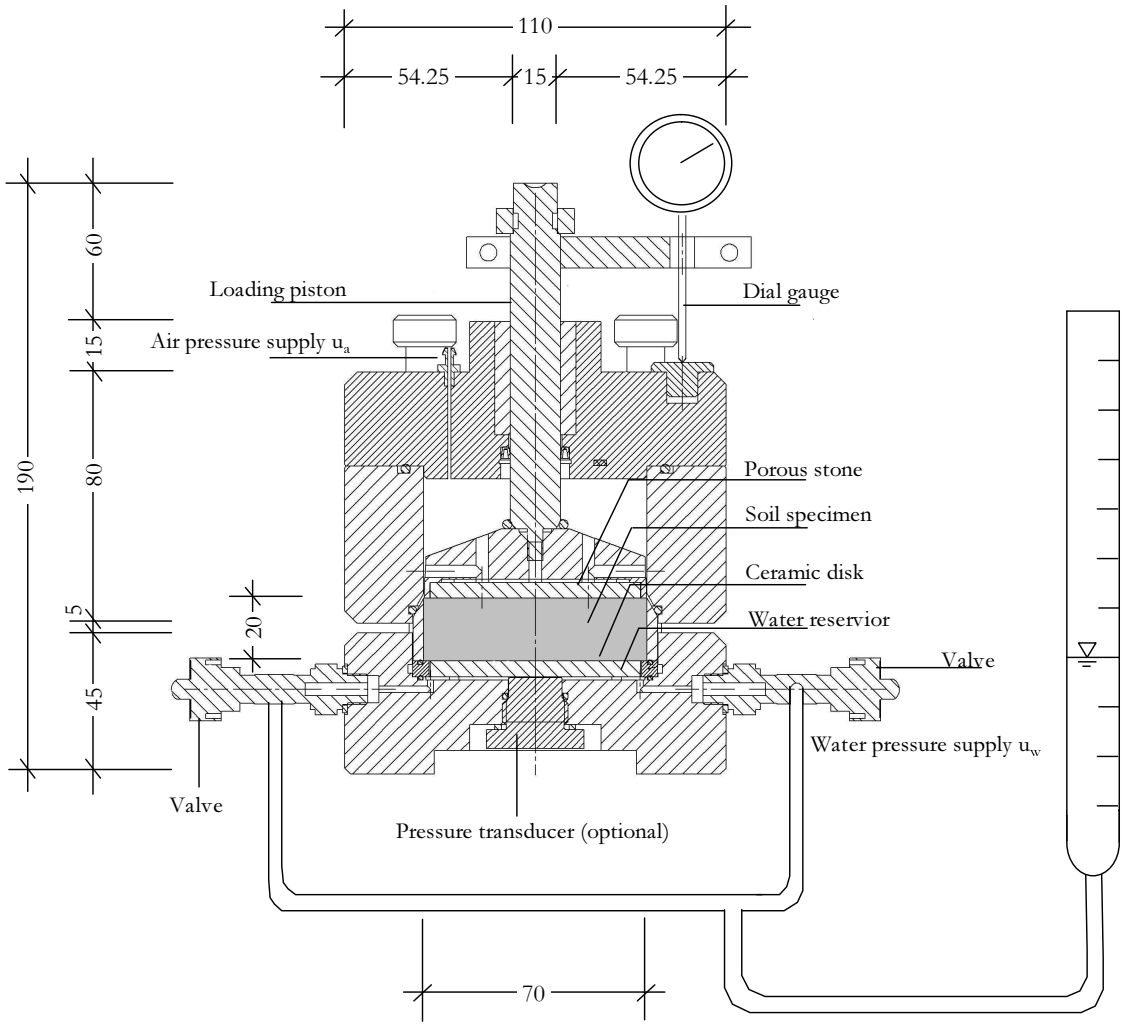

Figure 4.2: Cross sectional area of the modified pressure plate apparatus (all dimensions in mm)

oedometer cells the modified pressure plate apparatus permits to investigate one dimensional compression and rebound behavior of soils under controlled suction.

Granular materials show a relatively small range of suctions over which the soil becomes unsaturated. A low air-entry value is characteristic for this type of materials. To be able to apply low suction the cell allows for the use of the hanging water column technique (Haines 1930). By lowering the attached burette with respect to the top of the ceramic disk and using the scale with a resolution of 1 mm, suctions up to 4.0 kPa in steps of 0.1 kPa may be applied to the specimen. The burette has a resolution of 0.05 cc enabling precise readings of water inflow and outflow. Suctions up to 100 kPa may be applied to obtain test results along the soil-water characteristic curve. The air pressure is applied to the top of the cell using the axis-translation technique (Hilf 1956). Detailed literature review regarding hanging water column and axis-translation technique for control of suction in a soil was presented

by Vanapalli et al. (2008). There in detail the limitations of these techniques with respect to air diffusion, water volume change and evaporation are discussed.

4.3 Sand Column I

The sand column device I (Fig. 4.3) enables to determine drainage and imbibition soil-water characteristic curves of the tested material. Steady state flow tests and transient state flow tests can be performed on the specimen.

A schematic sketch of the experimental setup of the sand column testing device I is shown in Fig. 4.4. The setup consists of a Trase System including Multiplexer and 5 TDR sensors (Time Domain Reflectometry), 5 Tensiometers connected to a datalogger, computers for computing and saving experimental results, an electronic pump and a cylinder and the column. In detail the column device is given in Fig. 4.5. Totally the column is 780 mm high and 305 mm in diameter. The soil specimen has a height of maximal 630 mm. The bottom part of the column consists of a water reservoir made of steel that is sufficiently rigid. It consists of a 10 mm thick base plate, a cast iron pipe 100 mm high and 323 mm in diameter and a muff. The base plate, the pipe and the muff are welded. A connection in the pipe enables to inject or withdraw water to the reservoir. The top part consists of a PVC tube that has also a muff on the bottom. The water reservoir and the PVC tube are departed by a perforated plexiglas plate with 10 mm thickness. The plexiglas plate has 82 boreholes 3 mm in diameter that are uniformly distributed over the entire plate. This enables a uniform inflow and outflow of water from and into the specimen. The water reservoir, the plexiglas plate and the PVC tube are connected by 6 bolts to the muff. Between the PVC tube and

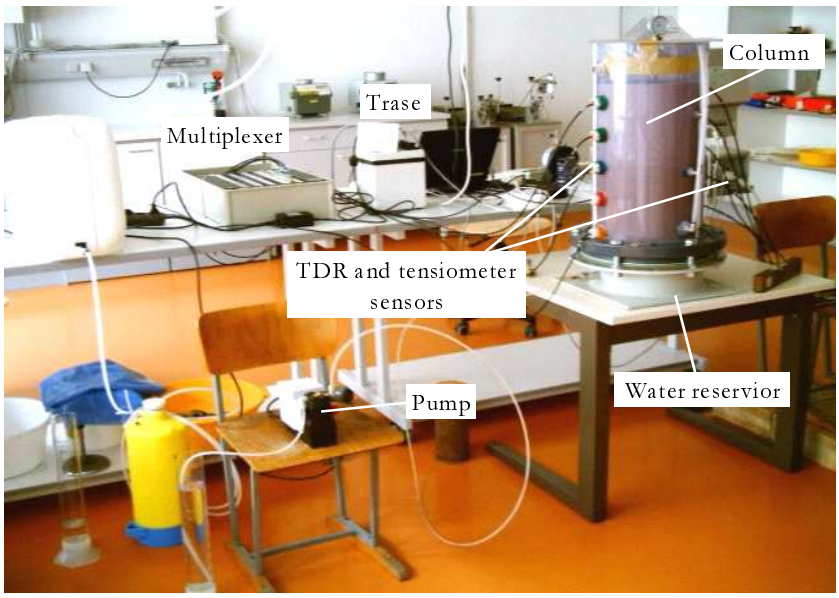

Figure 4.3: Column testing device I

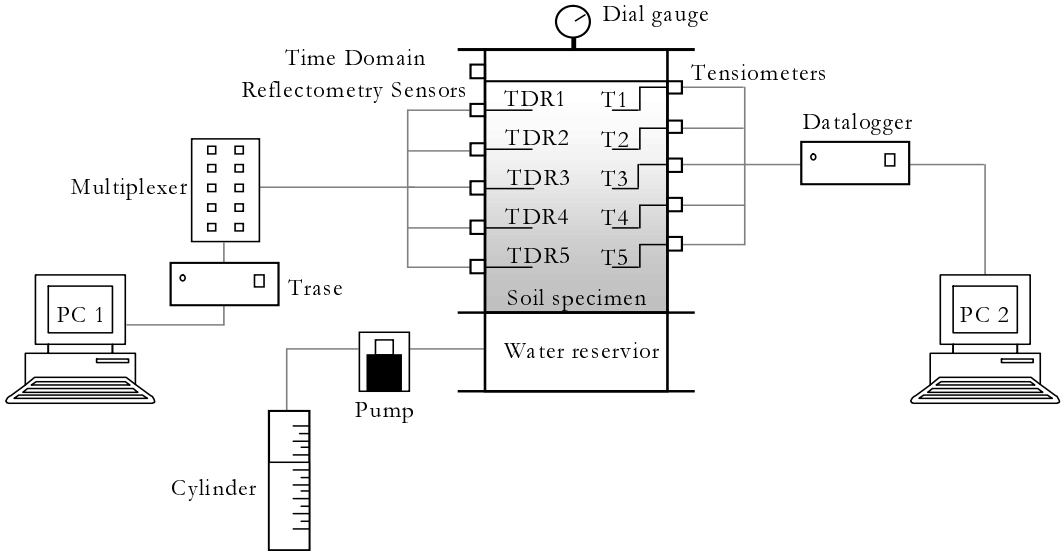

Figure 4.4: Set up of column testing device I

the plexiglas plate as well as between the plexiglas plate and the water reservoir sealing rings are placed to ensure leakproof connection. A highly permeable geotextile is placed between the soil specimen and the perforated plexiglas plate to avoid flushing soil grains to the water reservoir. Several openings (6 openings on one side and 5 openings on the opposite side) along the column enable to connect sensors to the column.

Five miniature tensiometers (UMS Umweltanalytische Mess-Systeme GmbH) and 5 miniature Time Domain Reflectometry probes (Soil Moisture Equipment Corp.) are placed in a row along the height of the column in a distance of about 100 mm between measurement points. The tensiometers are pressure transducer tensiometers which are horizontally installed into the soil specimen. The TDRs are three rode sensors, which are also horizontally installed into the soil specimen. One couple of TDR sensor and tensiometer sensor is installed at the same height. This procedure allows directly to link suction to the volumetric water content in the soil in different layers during drainage and imbibition of the specimen.

An electronic pump is connected to the reservoir at the bottom of the column to facilitate the injection and withdrawing of water at a constant rate. In this study a membrane pump of type KNF FM 15KT18 (LAT Labor- und Analysentechnik GmbH) was used. By changing the stroke of the membrane, the flow rate can be changed from 10 to 150 ml/min. The motor of the pump has a constant speed of 75 revolutions per minute. Thus the pump is able to withstand 6 bar back-pressure and the flow rate is not depending on a hydraulic head up to 6 bar back-pressure. Because in the transient state test a constant flow rate is applied to the soil specimen, it was carefully checked that the flow rate is constant (see Fig. 4.6). The diagram shows that there is no influence of the hydraulic head on the flow rate. The flow rate is constant. Atmospheric pressure was acting at the top of the column. Volume changes

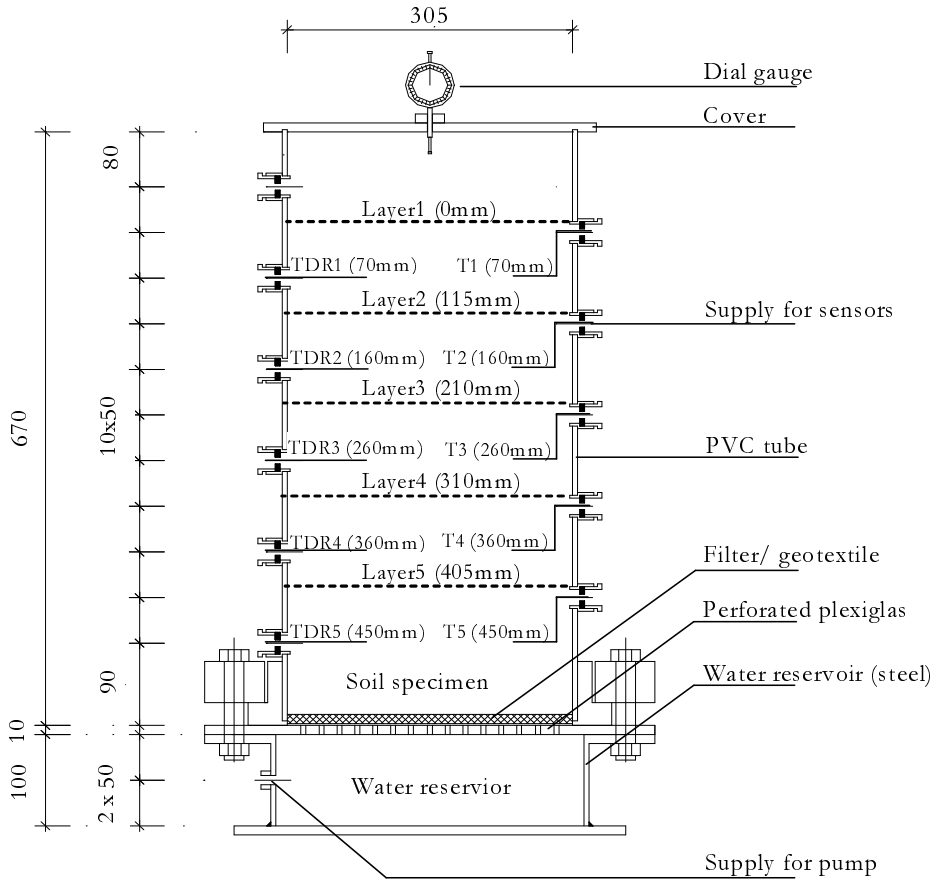

Figure 4.5: Cross sectional area of column testing device I (all dimensions in mm)

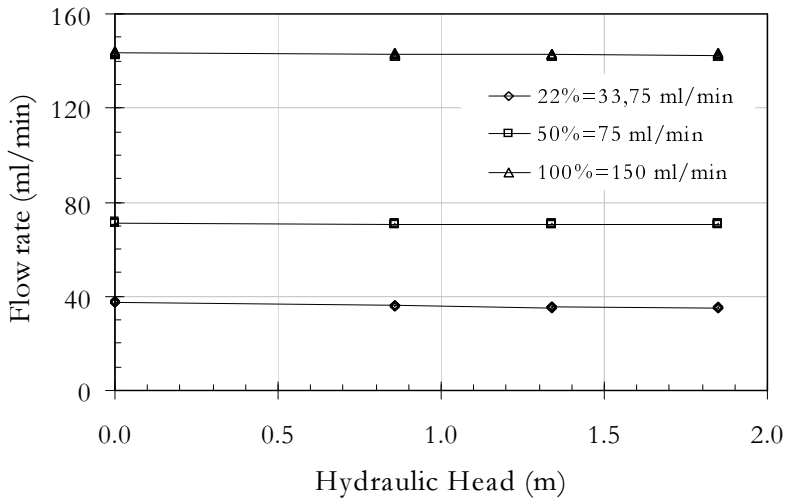

Figure 4.6: Calibration of the electronic pump

during the experiment were measured using a dial gauge fixed to the top of the specimen. To ensure no expansions of the column due to stress the strain at loading condition cell filled with Hostun sand and water up to top edge was calculated. A strain of $\varepsilon = 0.0002$ was derived that is negligible small and not influencing the testing procedure and experimental results.

4.4 Sand Column II

The sand column testing device II (see Fig. 4.7) is additionally used to determine the soil-water characteristic curve of Hostun sand specimen. Due to the ceramic disk on the bottom of the cell in contrast to the sand column testing device I, the sand column testing device II allows to induce a predefined suction to the specimen using axis-translation technique. By applying air pressure on top of the cell to the specimen, a suction is induced and thus the influence of transient state condition on the shape of the soil-water characteristic curve is investigated. During the tests the attached dial gauge at the top of the cell was measuring the volume changes in the specimen. Even there is the possibility to perform drainage as well imbibition cycles in the testing device II, in this study the cell was used only for performing drainage procedure.

As shown in Fig. 4.8 the experimental set up consists of a Trase System including Multiplexer and 3 TDR sensors (Time Domain Reflectometry), 3 tensiometers connected to a datalogger, 2 computers for computing and saving experimental results and the cell. The schematic cross sectional area of the column testing device is given in Fig. 4.9. It contains a bottom part with a 100 kPa ceramic disk and a water reservoir below the disk, a plexiglas tube 282 mm in height and 240 mm in diameter and a top part with a loading piston. The loading piston consists of a plate made of plastic. To the loading piston a dial gauge is at-

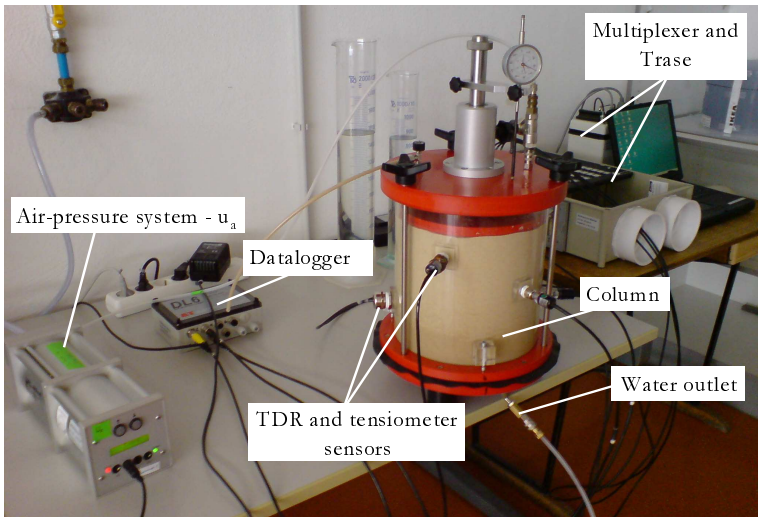

Figure 4.7: Column testing device II

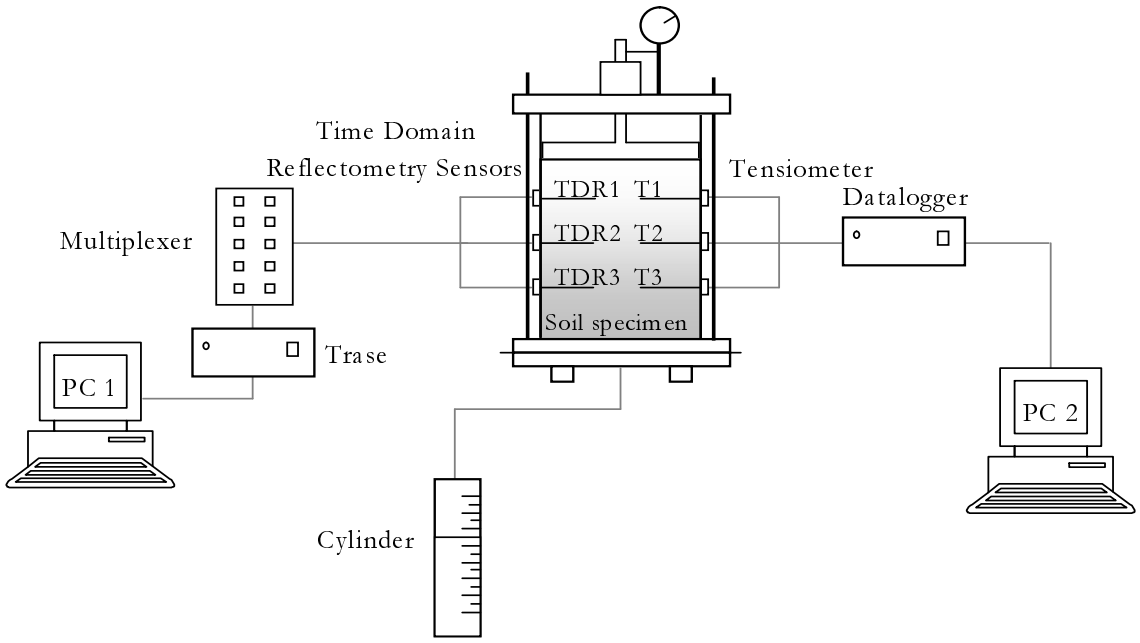

Figure 4.8: Set up of the column testing device II

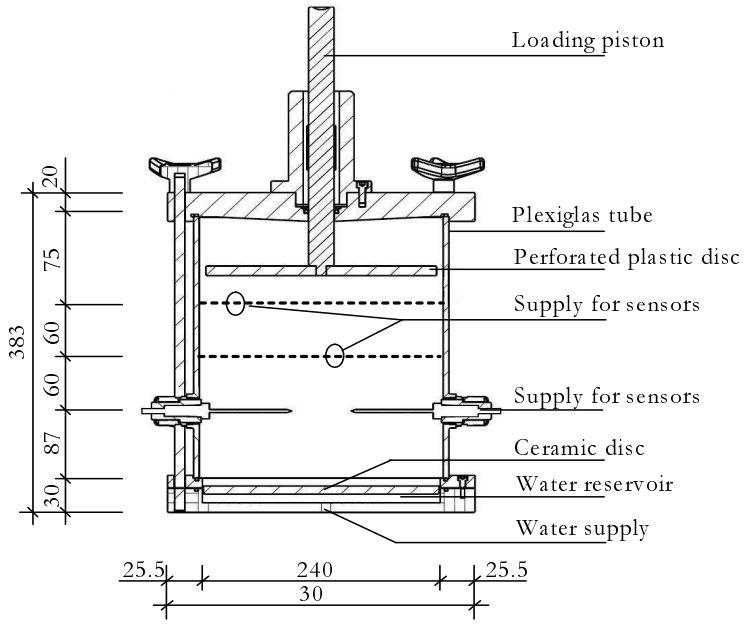

Figure 4.9: Cross sectional area of the column testing device II

tached for measuring volume changes of the specimen during testing procedure. For further investigations the piston on top of the cell will enable to apply vertical stress to the specimen. An air-pressure system is connected at the top of the cell to the air compartment for inducing matric suction to the soil specimen. The top part and the bottom part are screwed by 3 bolts. One o-ring between the top plate and the plexiglas tube as well as one o-ring

between the bottom plate and the plexiglas tube prevent from leakage. A tube with a valve is connected to the water reservoir below the ceramic disk. By using a cylinder attached to this tube the water outflow is measured. At all 6 openings (3 openings for tensiometer sensors, 3 openings for TDR sensors) enable to equip the specimen with tensiometer sensors as well as TDR sensors. In 3 depths along the column 2 openings are installed opposite to each other. The openings are installed equally spaced (see Fig. 4.9). In three layers with a distance of 60 mm pairs of tensiometer and TDR sensors are placed to measure simultaneously pore-water pressure and volumetric water content in the specimen during the experiment. The same tensiometer sensors and TDR sensors used for column testing device I were used for column testing device II.

4.5 UPC Controlled-Suction Oedometer Cell

One dimensional compression and rebound tests and collapse tests were performed by using the controlled-suction oedometer cell (Fig. 4.10). Similar to the modified pressure plate apparatus the cell allows to apply suction to the specimen and to keep the suction constant during the testing procedure.

The controlled-suction oedometer cell is also equipped with a burette and a scale with the same accuracy as the equipment for the modified pressure plate apparatus, one air-pressure system for application of matric suction as well as one air-pressure system for application of vertical net stress. The application of matric suction to the specimen is equal to the procedure used in the modified pressure plate apparatus (i.e. hanging water column technique, axis

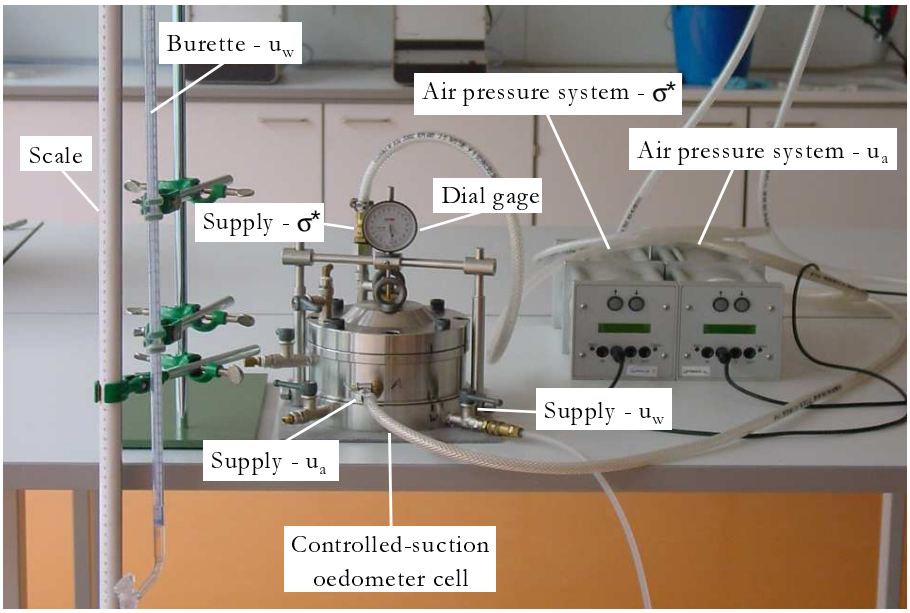

Figure 4.10: Controlled-suction oedometer cell

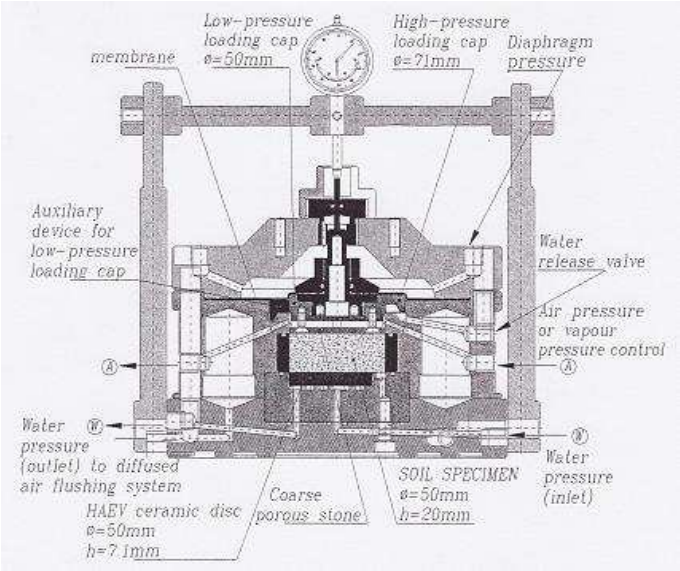

Figure 4.11: Cross sectional area of the controlled suction oedometer cell UPC

translation technique). The cell is equipped (see Fig 4.11) with a specimen ring 50 mm in diameter and 20 mm high. Like the specimen in the modified pressure plate apparatus the specimen here is assumed to be homogeneous in void ratio and in the distribution of water content (volumetric water content, saturation).

The controlled-suction oedometer cell consists of 5 parts (top part, middle part, bottom part, membrane including porous stone and ceramic disk) and is made of steel to prevent any deformations of the cell itself. The bottom part is a steel plate including the ceramic disk. The ceramic disk used in this investigation has an air-entry value of 100 kPa and may be replaced by another one, e.g. by a ceramic disk with 500 kPa air-entry value for testing silty and clayey soil or a porous stone for performing conventional tests (i.e. tests on saturated soil specimen). Directly to the specimen ring the bottom disk is placed. The steel plate also provides a water reservoir below the disk, that is connected to a burette. By using the burette with a capacity of 25 cc (resolution of 0.05 cc) as well as the scale (resolution of 1 mm) suctions up to $\psi = 4.0$ kPa in steps of $\Delta\psi = 0.1$ kPa can be applied to the specimen. The water inflow and the water outflow is measured in the burette during testing procedure. By adjusting the burette a constant suction is maintained in the specimen when performing the experiments. The middle part acts as a strengthening of the specimen ring and offers a connection to an air pressure system, that acts on top of the specimen below the porous stone. The air pressure system is used to apply suctions up to $\psi = 50$ kPa to the sand specimen. The top part and the middle part are separated by a membrane, that includes the porous stone. Whereas the modified pressure plate is set into a oedometer frame for application of vertical net stress in the controlled-suction oedometer an air pressure system applies stress to the membrane from the top and thus vertical stress to the specimen. The bottom part,

the middle part and the top part are screwed by 8 bolts. A frame attached with a dial gauge enables the measurement of volume changes during the loading paths.

4.6 Equipment used

Equipment used in this study are tensiometer sensors, TDR sensors and a pump. The equipment is introduced in detail and accuracy of the sensors is given.

4.6.1 Tensiometer Sensors

The type of tensiometer used in the present study is shown in Fig. 4.12 and the corresponding calibration functions are given in Fig. 4.13. The tensiometer is a Miniature Pressure Transducer Tensiometer (UMS-UmweltUmweltanalytische Mess-Systeme). Typical applications for this type of tensiometer are:

- Determination of soil-water characteristic curve of a soil
- Determination of movement of water in the soil
- Punctual measurement of pore-water pressure in the soil
- Measurement of pore-water pressure of the soil in the laboratory
- Measurement of pore-water pressure of the soil in the field

As shown in Fig. 4.12 the tensiometer consists of a body and a tensiometer cup including a ceramic cup and a water filled shaft. The tensiomter has an overall length of 81 mm and the body is 20 mm wide. The body consists of the pressure transducer, the acrylic plastic body and the lead.

Based on the piezoresistive effect of the silicon semiconductor the sensor measures the change of the specific electric resistance due to deformations. These deformations are caused on the sensitive silicon chip by changes in pore-water pressure. By using a Wheatstone Bridge the change of the specific electrical resistance is processed to a signal, which corresponds to

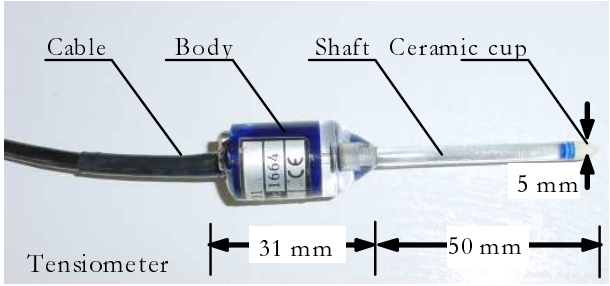

Figure 4.12: Tensiometer sensor

a certain pore-water pressure value. The ceramic cup has an active surface of 0.5 cm^2 and is 5 mm in diameter. Thus the soil disturbance of the tested soil is small. The response time of the sensor is fast. The shaft is transparent and thus air bubbles are easily detectable. Due to its small dimension the sensor is suitable for experiments performed in the laboratory. The electronic pressure transducer in the tensiometer has a high resolution measuring device. This is advantageous when measuring continuously changes in pore-water pressure in the soil.

The tensiometers have a measuring range from 100 kPa positive pore-water pressure (hydrostatic pressure) to 85 kPa negative pore-water pressure (matric suction, capillary pressure) and an accuracy of ± 0.5 kPa. In this study a data-logger system is used for assessing the voltage measurements. The data-logger system is specially used for readout of these tensiometer results.

For calibration of tensiometer sensors predefined negative pore-water pressures (-1 kPa, -2 kPa, -5 kPa, -10 kPa), viz matric suctions (capillary pressures), were applied to each sensor by using hanging water column. Results are given in Fig. 4.13, where the measurements of the tensiometers are related to the applied pore-water pressures. For each tensiometer indirect linear relationship as calibration function was determined. Before performing the experiments it is necessary to check the zero offset of each tensiometer. Therefore the tensiometers are placed into a water filled cylinder until the ceramic cup is 3 mm below the water level. The data-logger system should readout a constant value between ± 0.5 kPa. Otherwise this has to be corrected.

To asses wether or not the sensor measurements are reasonable and not delayed in response of time, tensiometer sensor and TDR sensor measurements were performed in an extra experiment. Detailed description and the results of this test are given in later subsection.

4.6.2 Time Domain Reflectometry Sensors

Fig. 4.14 shows a photo of the TDR sensor used in this investigation. It is a Mini Buriable Waveguide (Soilmoisture Equipment Corp.) that is used in the following applications:

- Determination of soil-water characteristic curve of a soil
- Determination of movement of water in the soil
- Punctual measurement of water content in the soil
- Measurement of water content of the soil in the laboratory
- Measurement of water content of the soil in the field

The TDR sensor consists of 3 parallel rods and a cable. It is designed to be installed permanently in the soil and allows the measurement of the dielectric constant of the tested soil. The rods of the mini TDR sensor are 80 mm long with a 25 mm spacing between the outer rods. The wire spacing is 12.5 mm. For computing, analyzing and saving the test results the TDR

sensors are connected to a Multiplexer and then to a Trase System. The Multiplexer allows measurements to be made automatically of several TDR sensors. A switching board with 16 channels for connecting up to 16 TDR sensors was used. Measurements, computations and analysis of the data is done by the Trase system. A computer connected to the Trase system is used to display the results.

The TDR probe measures the dielectric constant, which is related to the volumetric water content. Therefore the speed, an electromagnetic pulse of energy needs to travel down a par-

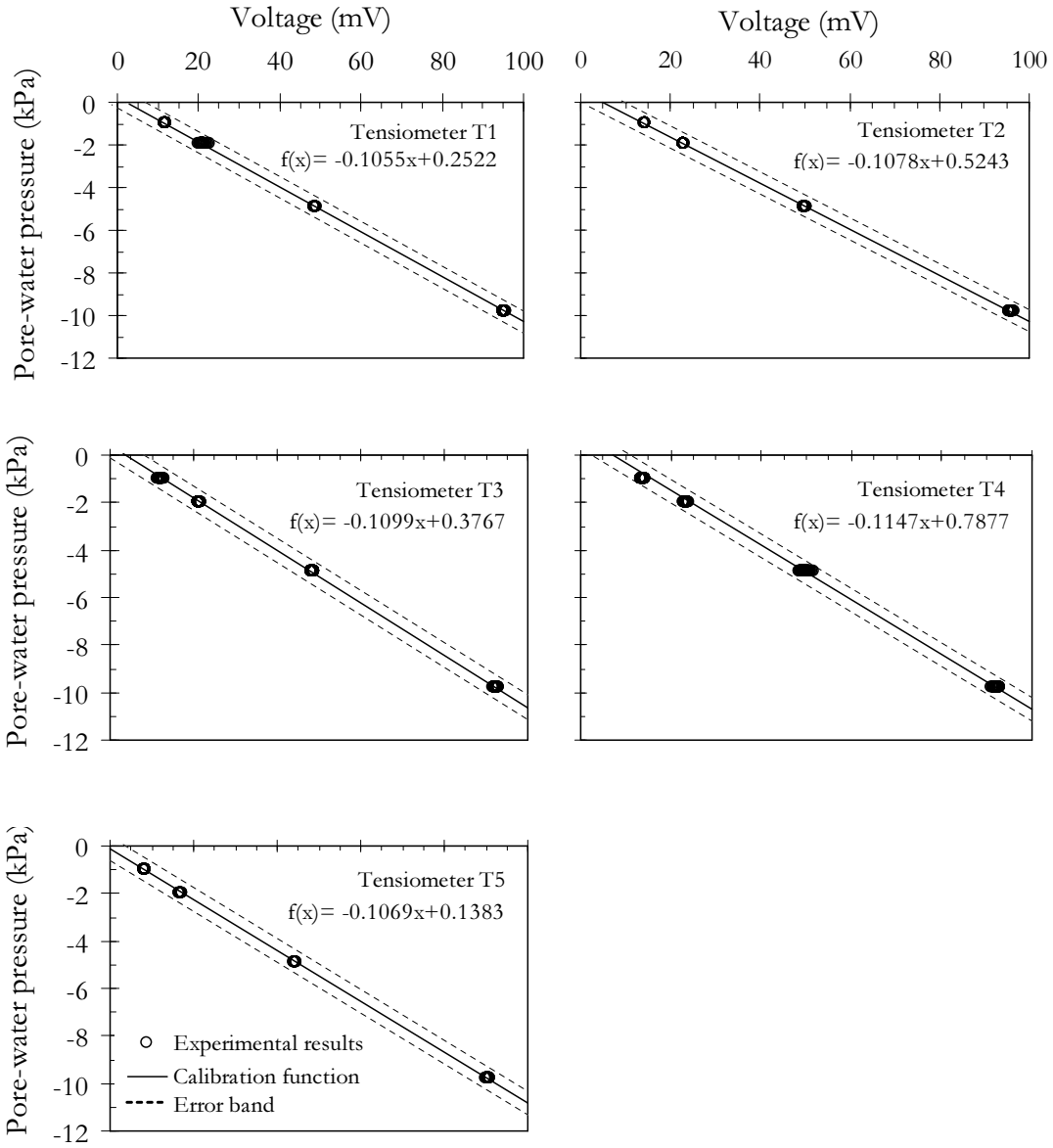

Figure 4.13: Calibration of the tensiometers

allel transmission line, is measured. The speed depends on the dielectric constant surrounding the transmission line. The higher the dielectric constant, the slower the speed. Because of the significant difference between the dielectric constant of air ($k_a = 1$), water ($k_a = 2...4$) and solids ($k_a = 81$) the traveling speed of an electromagnetic pules of energy along parallel transmission line in a soil is dependent on the volumetric water content in the soil. Thus the time required for a electromagnetic pulse to travel down a known length (in this case 80 mm) of transmission line is measured and then used for calculation of the dielectric constant. Fig. 4.15 shows a typical measurement of a TDR sensor. The dielectric constant is corresponding to a certain volumetric water content in the soil. Using TDRs, volumetric water content in a range of 0 to 100% is measured. The TDRs have an accuracy of ±2% full scale.

The dielectric constant-volumetric water content relationship has been established by careful measurements of k_a in a test cell with known volume. Before it was checked that all TDR sensors measure the accordant dielectric constant for air as well as water. The results are presented in Fig. 4.16 where the top diagram shows the results of the measurements in the

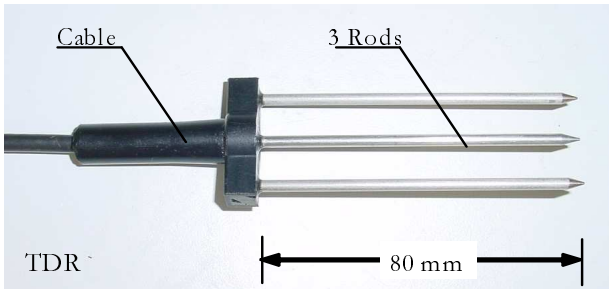

Figure 4.14: Time Domain Reflectometry Sensor (TDR)

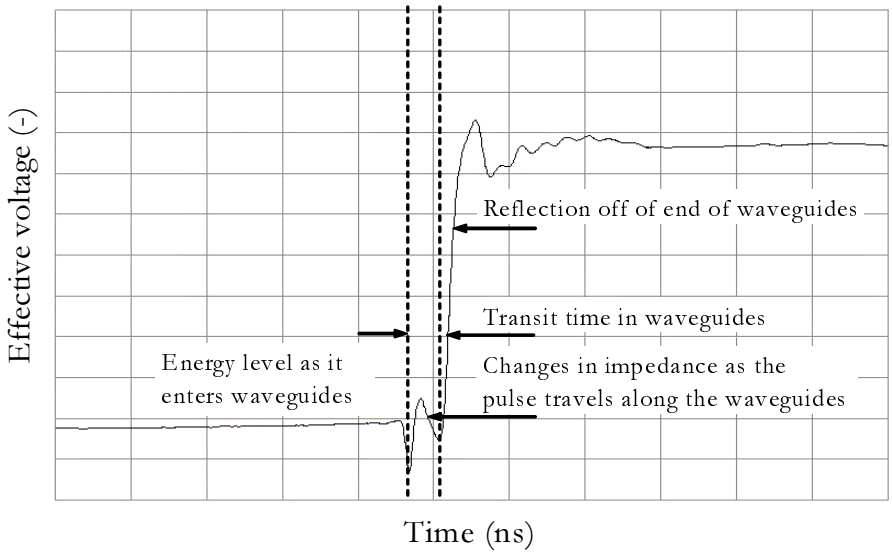

Figure 4.15: Typical output of TDR sensor

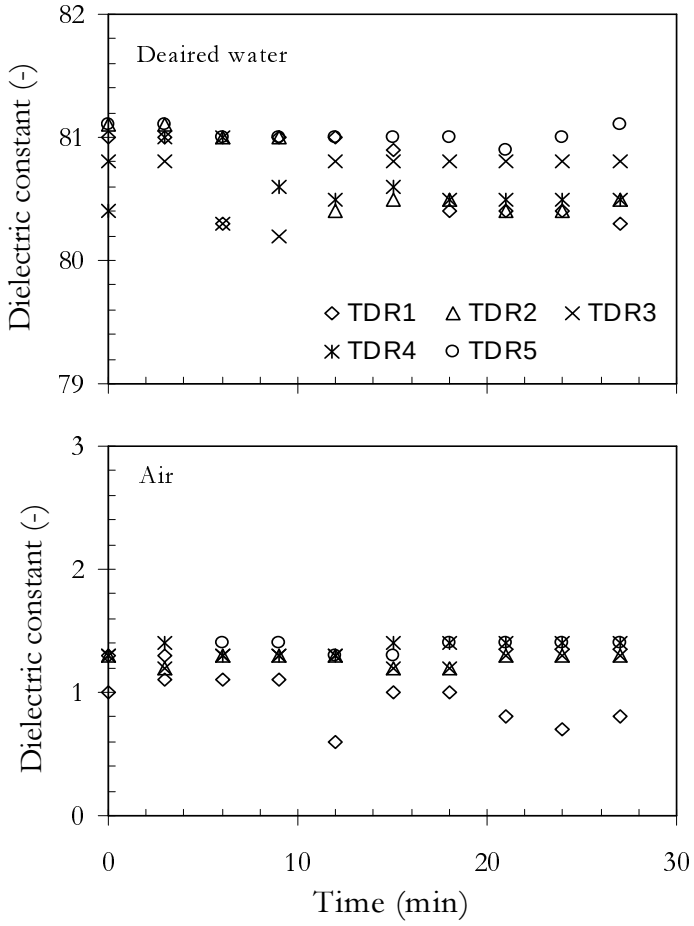

Figure 4.16: Measurement of the dielectric constant of water (top) and air (bottom)

deaired water and the bottom diagram the measurements in the air. As expected the dielectric constant for the deaired water was $k_a = 1$ and for air $k_a = 80$. The measurements also differ not so much.

Cabral et al. (1999) examined the influence zone around TDR probes and found an influence zone for the Mini Buribale Waveguides (TDR probes used for this investigation) that is 90 mm in length, 15 mm in height and 35 mm in depth. Sizing of a calibration cell, that can be used for the determination of the relationship between dielectric constant and volumetric water content $\theta(k_a)$ was studied by Suwansawat & Benson (1999). The authors found that a distance of 36 mm between the cell and the probe as well as a distance of 30 mm between the probes is required for determination of the calibration function. The calibration cylinder used in this study is considering the influence zone given by Cabral et al. (1999) and the distances given by Suwansawat & Benson (1999). For calibration of the TDR probes Hostun sand samples with predefined volumetric water content and void ratio, were prepared in a

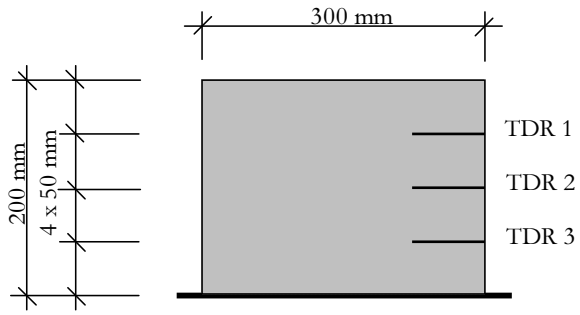

Figure 4.17: Container for TDR sensor calibration

plastic container of 200 mm height and 300 mm diameter (see Fig. 4.17). 3 TDR probes with a distance of 50 mm were horizontally placed in a cylindrical plastic container and measured the dielectric constant of the wet sand specimen. After receiving constant values in electrical conductivity the measurement was stopped and the water content was calculated by oven drying the sand specimen. Knowing the water content the dry density and thus the volumetric water content the dielectric constant was related to the volumetric water content. The calibration results of the TDR sensors are given in Fig. 4.18, where the output signal (dielectric constant) corresponds to the predefined volumetric water content. Calibration functions for the experimental results derived for loose, dense as well as loose and dense specimens are given in Eq. 4.1 to 4.3. Calibration curves (Eq. 4.1 to 4.3) were determined for loose specimen and dense specimen separately as well as loose and dense specimen combined. But

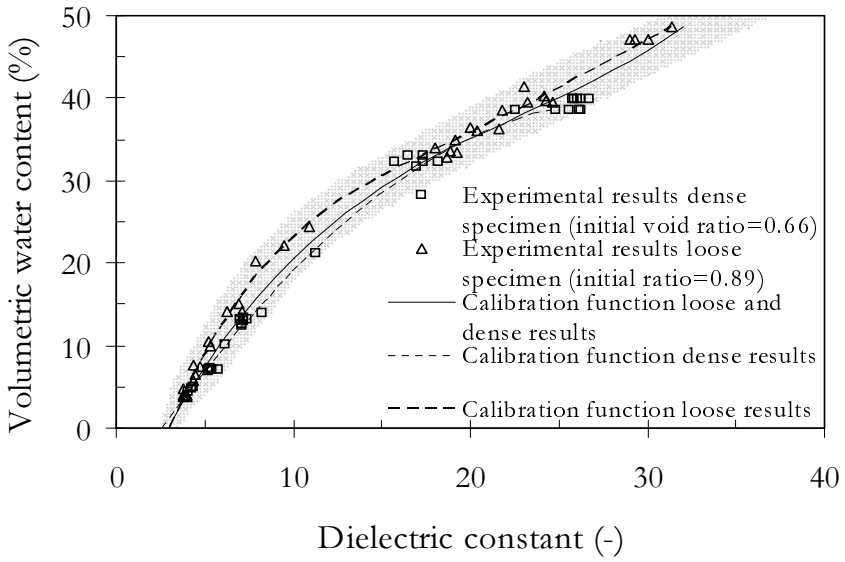

Figure 4.18: Calibration of TDR sensors for different initial void ratios

since the electrical conductivity of sand is negligible small, the density of the specimen is not influencing this relationship and Eq. 4.3 is used for analysis of the experimental results. According to Topp et al. (1980) a polynomial function of third order was suggested for relating the dielectric constant to the volumetric water content:

$$\theta(k_a)_{loose} = -18.888 + 7.481 \cdot k_a - 0.448 \cdot k_a^2 + 0.013 \cdot k_a^3 \tag{4.1}$$

$$\theta(k_a)_{dense} = -7.989 + 3.232 \cdot k_a - 0.052 \cdot k_a^2 + 0.0001 \cdot k_a^3 \tag{4.2}$$

$$\theta(k_a)_{loose/dense} = -12.085 + 4.638 \cdot k_a - 0.161 \cdot k_a^2 + 0.003 \cdot k_a^3 \tag{4.3}$$

To asses wether the sensor measurements are reasonable and not delayed in response of time, a saturated sand specimen was prepared in the column testing device. During removing stepwise 1000 ml from the saturated specimen measurements of the TDR sensors as well as tensiometer sensors were performed. Experimental results are given in Fig. 4.19. On the left hand side TDR sensor measurements and on the right hand side corresponding tensiometer sensor measurements are shown.

The specimen is 550 mm in height and has an initial void ratio of $e_0 = 0.68$. Layer 1 (TDR 1, Tensiometer 1) is located in a depth of 70 mm, Layer 2 (TDR 2, tensiometer 2) in a depth of 160 mm and Layer 3 (TDR 3, tensiometer 3) in a depth of 260 mm. Layer 1 is the top layer and layer 3 is the bottom layer. Initially the specimen is a water saturated specimen and thus each TDR sensor measurement refers to a volumetric water content $\theta_s = 41\%$. The tensiometer sensor measurements refer to positive pore-water pressure. The pore-water pressure in the bottom layer is greater than in the top layer. Tensiometer sensor measurements were taken every minute and TDR sensor measurements were taken every third minute due to limitations in equipment. After a time period of 6 minutes 1000 ml of water were withdrawn from the specimen. Tensiometer measurements are decreasing immediately from positive pore-water pressure to negative pore-water pressure (matric suction) when removing the first 1000 ml of water. Even though the water level is falling from 550 mm to 260 mm and is passing all three layers no changes in TDR measurements occur. Water still remains in the pores because the air-entry value is not reached till now. TDR measurements in layer 1 are decreasing to $\theta = 26\%$ after removing the $2nd$ 1000 ml of water from the soil. Here the pores start to drain, whereas the volumetric water content in layers 2 and 3 remain constant. From the tensiometer measurements an air-entry value of approximately $\psi_{aev} = 2.0$ kPa can be derived. Volumetric water content is further decreasing when removing the next 1000 ml. Tensiometer measurements are decreasing continuously with decreasing water table. Removing the fourth 1000 ml of water, also sensor T2 is reaching the air-entry value and thus the volumetric water content in sensor TDR2 is decreasing. The measurements in T1 as well as in TDR1 are only slightly changing, because small pores retain the water in the soil.

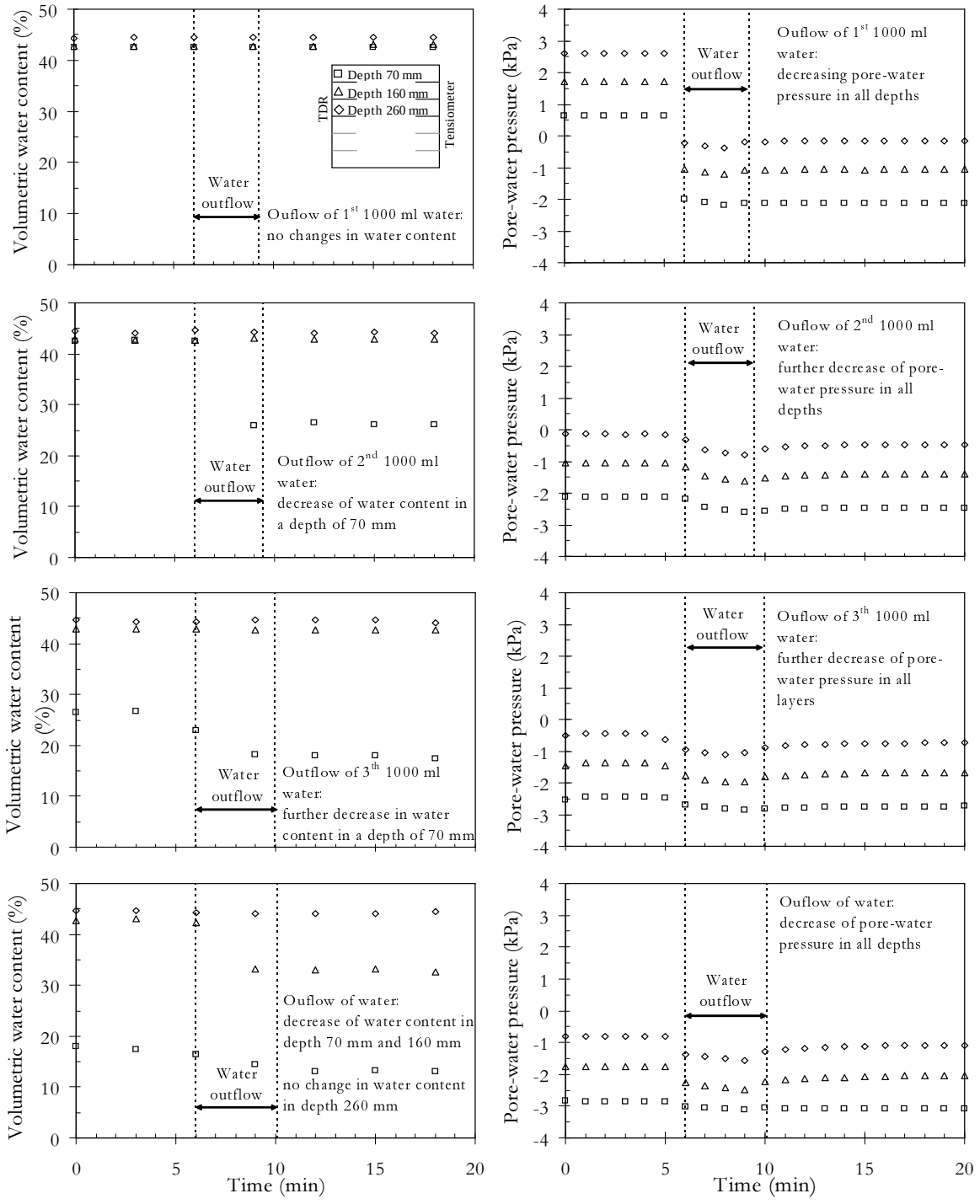

Figure 4.19: Verification of response time and suitability of TDR sensor and tensiometer measurements in column testing device - experimental results

The measurements in Fig. 4.19 prove that both sensors, the TDR sensors and tensiometer sensors, are suitable for investigation of unsaturated sand in a column device. The sensors react immediately and the measurements are reasonable. As soon as water is removed from the specimen the tensiometers are responding to changes in water pressure. The difference in change of water-pressure is decreasing when reaching negative pore-water pressure (matric suction), due to the fact that the pores are retaining water. As soon as the air-entry value is reached, the water starts to enter the largest pores in the soil and thus the volumetric water content is decreasing.

4.7 Summary

Testing unsaturated sand is a challenge for testing cells and equipment. When testing sand it has to be taken into account that the suction-water content takes place in a narrow range of suction, where suction as well as water content have to be precisely measured and controlled. Hanging water column technique and axis-translation technique fulfill these requirement. Moreover in the present study burettes with high resolution as well as TDR and tensiometer sensors with high accuracy are used to perform measurements. For observation of volume changes in the specimen during loading and unloading path the controlled-suction oedomater cell is equipped with a dial gauge with a high accuracy. The testing devices and equipments introduced in this chapter are appropriate to perform experiments on sand that investigate hydraulic (modified pressure plate apparatus, sand column testing device I and II) as well as mechanical behavior (controlled-suction oedometer cell) of unsaturated sand.

Chapter 5

Material used and Experimental Program

5.1 General

In this chapter the investigated material is introduced and classified. For the present investigations Hostun sand (Flavigny et al. 1990, Mokni & Desrue 1999, Desrues & Viggiani 2004) was chosen, that is a well known reference sand in the literature. The main classification properties are presented. To ensure the investigation on reproducible, homogenous sand specimens a study on preparation of Hostun sand specimen is carried out, that includes computer tomography (CT) on saturated (S=0) and unsaturated sand specimens and an electron microscopy study.

It follows a detailed description of the experimental program including initial conditions, loading history, the specimen preparation and also the testing procedure in the different testing devices. In the tests the hydro-mechancial behavior of unsaturated Hostun sand was investigated. Therefore flow experiments in different columns are performed (modified pressure plate apparatus, sand column testing device I and II). The influence of initial condition (i.e. void ratio), the hydraulic loading path (i.e. drainage or imbibition paths) and the test boundary condition (i.e. steady state and transient state tests) were considered in the derivation of the soil-water characteristic curve and the unsaturated hydraulic conductivity function. Special attention was paid to the significance of hysteresis with regard to both the hydraulic relations. Additionally the effect of suction rate on the flow process was quantified in the sand column device I and II under different boundary conditions.

The volumetric mechanical behavior of unsaturated sand is investigated. Therefore the stiffness behavior as well as the collapse potential is determined by conducting one-dimensional compression and rebound tests in a controlled suction oedometer cell. The influence of initial conditions (i.e. void ratio, suction), the mechanical loading path (i.e. loading or unloading paths) and the hydraulic loading path (i.e. saturation procedure) were considered in the derivation of the stiffness behavior.

5.2 Hostun Sand

The experimental program for this study was conducted on Hostun Sand, a reference sand well studied in the research literature (Biarez et al. 1989, Flavigny et al. 1990, Hammad 1991, Schanz & Vermeer 1996, Schanz 1998, Gennaro et al. 2004). Hostun Sand is a quartz sand with grain sizes ranging from 0.1 mm to 1.0 mm in diameter. According to the USCS classification the material is a poorly-graded medium sand SP (Fig. 5.1). The main classification properties as the density of the soil particles ϱ_s, the coefficient of uniformity C_u, the coefficient of curvature C_c, the values of maximum and minimum void ratio $e_{max/min}$, as well as the corresponding values of maximum and minimum specific weight $\gamma_{max/min}$ are summarized in Table 5.1. The saturated hydraulic conductivity of the sand is required when computing the unsaturated hydraulic conductivity from the soil-water characteristic curve using the indirect method. The saturated hydraulic conductivity of the sand for several initial void ratios was measured using constant head permeability test (Lins et al. 2002, Lins & Schanz 2005). The results are given in Table 5.1. Experimental results of the saturated hydraulic conductivity are presented in Fig. 5.2. In further calculations and predictions for loose Hostun sand specimen ($e = 0.89$) saturated hydraulic conductivity of $k_s = 2.75 \cdot 10^{-4}$ m/s and for dense Hostun sand specimen ($e = 0.66$) $k_s = 2.03 \cdot 10^{-4}$ m/s were used. Shear strength parameters obtained by Hammad (1991) and Schanz & Vermeer (1996) under plain strain and triaxial condition on saturated sample tests are given in Table 5.2. These parameters are necessary for prediction of unsaturated shear strength using indirect method and also for prediction of unsaturated bearing capacity.

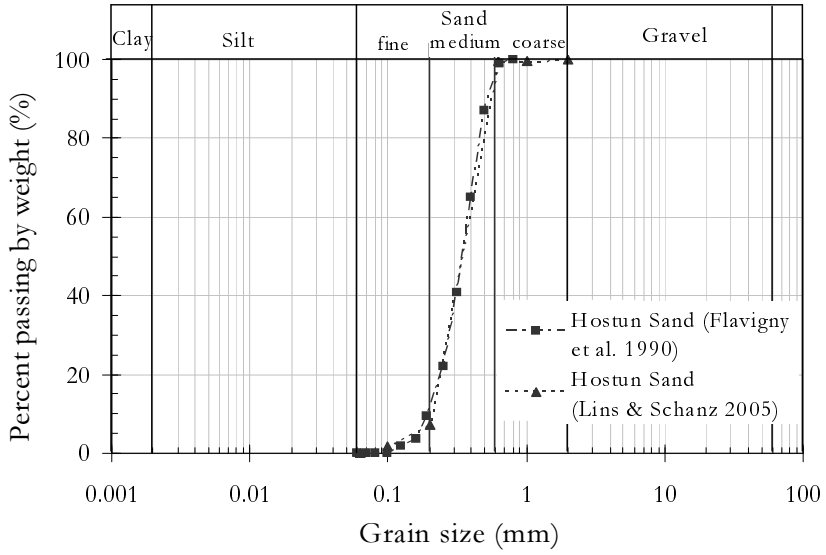

Figure 5.1: Grain-size distribution of Hostun Sand

Table 5.1: Properties of Hostun sand

Parameter	Biarez et al. (1989)	Schanz and Vermeer (1996)	Desrues et al. (1996)	De Gennaro et al. (2004)	BUW
$\rho_s(g/cm^3)$	-	2.65	2.65	2.65	2.65
D_{50}	0.3	-	0.32	0.34	0.36
D_{30}	-	-	-	-	0.29
D_{10}	-	-	-	-	0.21
C_u	-	-	1.70	-	1.72
C_c	-	-	-	-	1.05
e_{max}	1.000	1.041	1.000	1.000	1.000
e_{min}	0.630	0.648	0.660	0.656	0.650
$\gamma_{max}(kN/m^3)$	16.30	16.08	15.99	16.00	16.06
$\gamma_{min}(kN/m^3)$	13.20	12.98	13.24	13.25	13.25
$k_{s,loose}(10^{-4}m/s)$	-	-	-	-	2.75
$k_{s,dense}(10^{-4}m/s)$	-	-	-	-	2.03

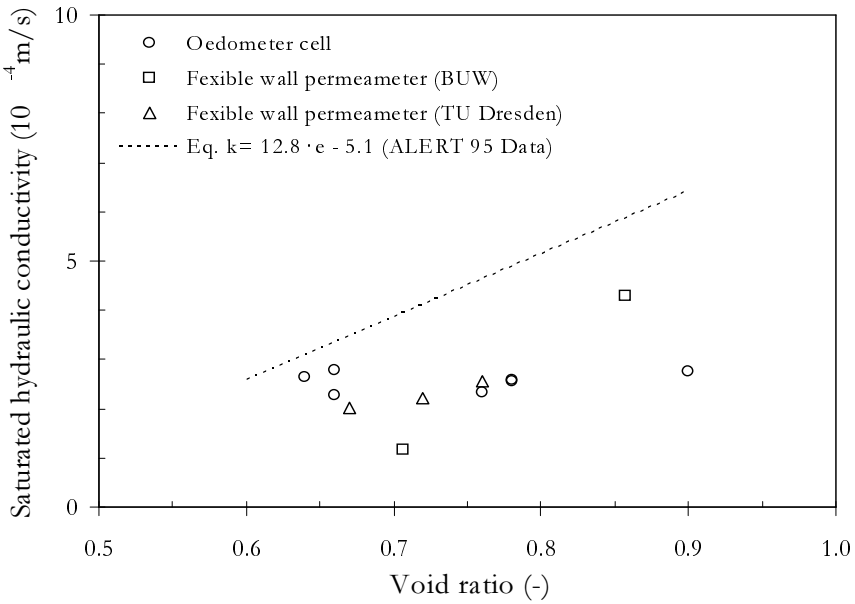

Figure 5.2: Saturated hydraulic conductivity of Hostun Sand

5.3 Specimen Preparation and Testing Procedure

For fundamental studies of the behavior of soils and their characterization it is required to test homogeneous and reproducible specimen. The specimen preparation has to be a reliable and robust procedure to test several specimen under same initial conditions. The majority of experiments performed on granular materials as for instance sand are carried out on re-

Table 5.2: Angles of friction of Hostun sand derived from biaxial test (Hammad 1991) and triaxial test (Schanz 1996)

Biaxial test, σ_3	ϕ_p^{ps}, $e = 0.71$	ϕ_p^{ps}, $e = 0.91$
100	$46.7 - 47.5$	35.5
200	$46.4 - 47.0$	$32.5 - 34.5$
400	$45.1 - 45.3$	$33.0 - 33.3$
Triaxial test, σ_3	ϕ_p^{ps}, $e = 0.64$	ϕ_p^{ps}, $e = 0.91$
300	41.9	34.4

constituted specimens. The investigation of undisturbed specimens under natural condition is difficult, because granular materials are cohesionless. Consequently a variety of procedures have been developed and assessed for reconstitution of granular specimens (Ladd 1974, Mulilis et al. 1975, 1977, Ladd 1978, Miura & Toki 1982, Gilbert & Marcuson 1988, Vaid & Negussy 1988, Frost & Park 2003). For instance the moist tamping technique, undercompaction technique, water-pluviation technique or air-pluviation technique are available to produce dense or loose sand specimen:

- *Moist tamping technique*

  The moist tamping technique includes the preparation of a wet specimen using a number of layers of equal dry weight and volume. Each layer is compacted to the same target density. As a result the lower portion of the sand specimen becomes higher density (Mulilis et al. 1977, Gilbert & Marcuson 1988).

- *Under compaction technique*

  An improvement of the moist tamping procedure was suggested by Ladd (1978) and is known as undercompaction technique. The undercompaction method takes into account that the compaction of each succeeding layer further densify the layers below. In this case each layer is compacted to a lower density than the predetermined final value.

- *Air pluviation technique*

  Pluvial deposition is a widely used technique to reconstitute cohesionless soil specimens for laboratory testing. The air pluviation technique allows the preparation of specimens over a broad range of densities to a high level of global repeatability, when carefully controlling the height of the sand particles (Miura & Toki 1982, Gilbert & Marcuson 1988). Implementation of the air pluviation technique is described in Jang (1997).

- *Water pluviation technique*

  Water pluviation technique, where the soil is pluviated into water, is commonly used to provide an initially saturated specimen. Similarly to the air pluviation technique specimens prepared by water pluviation tend to be uniform (Vaid & Negussy 1988).

Frost & Park (2003) performed image analysis on moist tamped sand specimen and air-pluviated as well as water-pluviated sand specimen. The sand specimens were preserved using epoxy resin (Jang et al. 1999) and vertically cut for R-ray analysis. Their results show significant discontinuities in density in the moist tamped specimen. Discontinuities in density were especially observed between the contact area of the layers. The X-ray images of the air-pluviated and also the water-pluviated sand specimens show uniform density along the specimens. Variations in density were only found on the bottom and on the top of the specimen. Thus specimens prepared by pluviating the sand into water or air tend to be uniform, whereas specimens prepared using compaction methods are less uniform. Finn et al. (1971), Vaid & Negussy (1988) used water-pluviation method for reconstituting initially saturated sand specimen. Schanz & Vermeer (1996), Desrues et al. (1996), Gennaro et al. (2004) used pluviation technique for preparation of sand samples to ensure homogeneity and reproducibility.

Because the air-pluviated and water-pluviated specimens show homogeneous distribution of density the pluviation method was selected for preparation technique. To provide a fully saturated specimen, sand was directly pluviated into the equipment, that was filled with deaired water. The sand used in this study is an poorly graded medium sand with insignificant amount of finer particles, where segregation is not influencing homogeneity. Thus water pluviation technique is used to produce homogeneous initially saturated sand specimen. Preferably in this investigation the water-pluviation method was used because nearly all experiments were conducted on initially saturated sand specimen (column testing device I, column testing device II). Due to limitations of equipment, specimens in the modified pressure plate apparatus and in the controlled-suction oedometer cell were prepared using the air-pluviated method, which includes the pluviation of dry sand into the equipment. The specimens were saturated in an additional step. Special care was taken to produce homogeneous and reproducible specimen. For instance during large scale experiments in the sand column device I (SC I) in each layer the mass of dry sand filled into the cell and thus the void ratio was checked. The mass of dry sand filled into the bearing capacity box (BCB) was controlled every fifth centimeter. Some results of dry density and void ratio for each layer are given for these tests in Tab. 5.3.

To analyze the homogeneity (distribution of density, distribution of water) in the pluviated sand specimen computer tomography (CT) was used additionally (Dewitz 1996). Computer tomography is an adequate non-destructive method for the investigation of the internal structure of samples. This method has been successfully used not only in medical science but also in soil science, rock mechanics or hydrology (Duliu 1999). Based on the attenuation of

Table 5.3: Results of dry density and void ratio with depth from specimen preparation in the sand column device I and the bearing capacity box

Cell	Height layer (cm)	ρ_d (g/cm^3)	e (-)	Height layer (cm)	ρ_d (g/cm^3)	e (-)
	Loose specimen			Dense specimen		
SCI	7.5	1.403	0.889	8.3	1.596	0.660
	17.5	1.405	0.886	17.5	1.594	0.663
	26.8	1.404	0.888	27.9	1.596	0.660
	37.0	1.406	0.885	37.7	1.600	0.656
	46.0	1.402	0.890	46.6	1.605	0.651
	54.0	1.401	0.891	52.7	1.596	0.660
BCB	-	-	-	5.20	1.503	0.760
	-	-	-	10.25	1.548	0.712
	-	-	-	15.35	1.533	0.709
	-	-	-	20.40	1.548	0.712
	-	-	-	25.40	1.563	0.695
	-	-	-	30.40	1.563	0.695
	-	-	-	35.57	1.550	0.710

gamma-ray, the distribution of the attenuation coefficient of the sample over an entire section is measured. The main common components of CT scanners are a gamma-ray source and a series of detectors, which measure the attenuation of the gamma-ray signal. The gamma-ray signal is attenuated by the investigated object that is placed between the source and the detectors. As illustrated in Fig. 5.3 the source and the detectors are moving around the stationary object, which is in this study the sand specimen. The result of a complete gamma-ray CT scan is a two-dimensional matrix of attenuation values that are graphically displayed and

Figure 5.3: Experimental set up for the Computer Tomography (CT)

analyzed. The tests were performed using a mobile computer tomograph from the Institute of Material Testing, Eberswalde (Fig. 5.3). The distribution of density and water was analyzed for several sand specimens, which were prepared in the modified pressure plate apparatus. The distribution of density was investigated on a dry sand specimen (S=0). For investigation of distribution of density and water, specimen with a suction value $\psi = 1.5$ kPa (located in the transition zone of the soil-water characteristic curve) and specimen with a suction value $\psi = 20.0$ kPa (located in the residual zone of the soil-water characteristic curve) were prepared (following the preparation procedure in chapter 7.4.3) and scanned by computer tomography.

Figure 5.4 shows the results of computer tomography on the sand specimens. The dry specimen shows a uniformly distributed density and also the specimen with a suction $\psi =$ 20.0 kPa shows a homogeneous cross section. Some inhomogeneities can be observed in the specimen with a suction $\psi = 1.5$ kPa, where the small pores are still retaining water while the large pores are already drained due to applied suction. The relation between the density of the investigated material and the measured attenuation coefficient is linear (Dewitz 1996). An attenuation of 84 refers to a density $\rho = 1.0\ g/cm^3$ that is water. The densities of the Hostun sand specimens (please see also Fig. 5.4 for clarification) are $\rho = 1.59\ g/cm^3$ ($S = 0.0$), $\rho = 1.78\ g/cm^3$ ($\psi = 1.5$ kPa) and $\rho = 1.61\ g/cm^3$ ($\psi = 20.0$ kPa). As expected the largest density was found for the unsaturated specimen with induced suction $\psi = 1.5$ kPa, where most pores are still filled with water. All specimen were scanned in a fixed oedometer ring made of plastic (see also Fig. 5.3).

A study was also performed on Hostun sand specimen (20 mm in height, 70 mm in diameter) prepared with epoxy resin. The hardened specimen were horizontally cut at a height of 10 mm. In several steps the surface of the specimens was carefully polished using grinding machine:

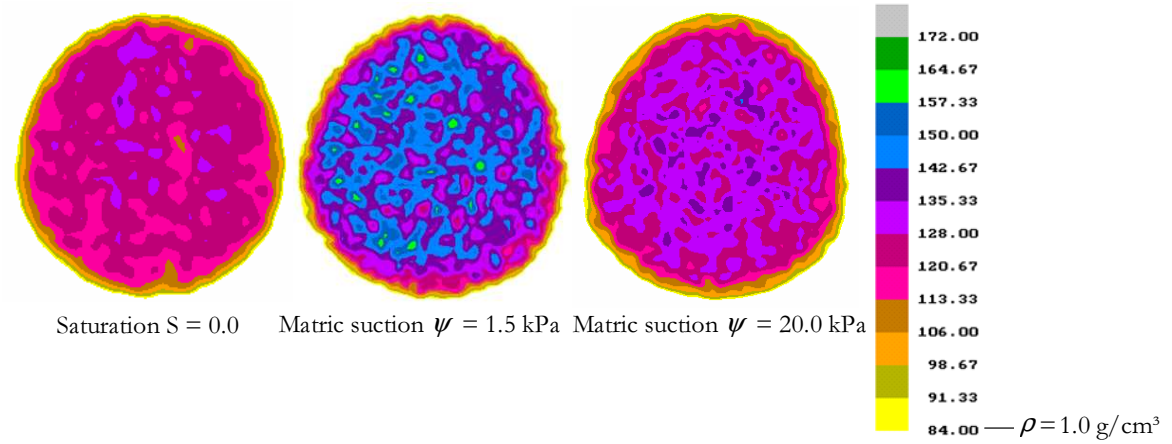

Figure 5.4: Results from Computer Tomography (CT) study of a dry sand specimen $S = 0$ (left) and sand specimens with a suction of 1.5 kPa (middle) and 20.0 kPa (right)

- Polishing at 20 μm for 15 min with adding water.
- Polishing at 15 μm for 15 min with adding oil.
- Polishing at 3 μm for 10 min with adding diamond paste .
- Cleaning of specimen in ultrasonic bath.

The distribution of void ratio of the horizontal area was observed using electron microscopy (see Fig. 5.5). A digital camera attached to the microscopy took photos of the specimen, that are further analyzed using image processing and analysis program. Binary filtered images were used for determination of the void ratio (Fig. 5.5 right). The void ratio was determined for 11%, 33%, 44% and 66% (see Fig. 5.6) of the total area ($A = 2651$ mm^2) as well as for the total area. The determined void ratios of the areas varied from $e = 0.71$ to $e = 0.76$, that leads to the results the void ratio is uniformly distributed over the investigated range.

Specimen preparation and testing procedure - modified pressure plate apparatus

Before each test the ceramic disk was saturated in a first step. To ensure full saturation of the ceramic disk, deaired, deionized water was passed through the ceramic disk using an air pressure of 70 kPa in the upper air compartment. The system was closed and opened in a step-wise manner using the valves. The water outflow was collected in the attached burette and the ceramic disk was assumed to be fully saturated when no air bubbles were collected in the burette. All experiments conducted in the modified pressure plate apparatus were long time tests (approximately 2 month for determination of one drainage or imbibition curve).

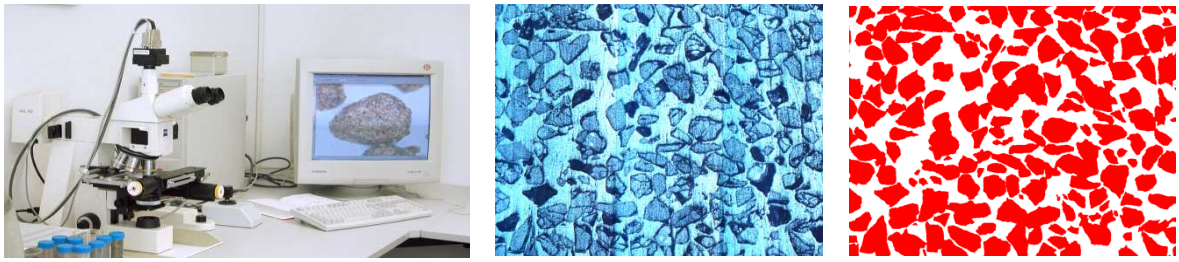

Figure 5.5: Electron microscopy (left), Hostun sand specimen hardened with epoxy resin (middle) and picture of Hostun sand specimen after image analysis (right)

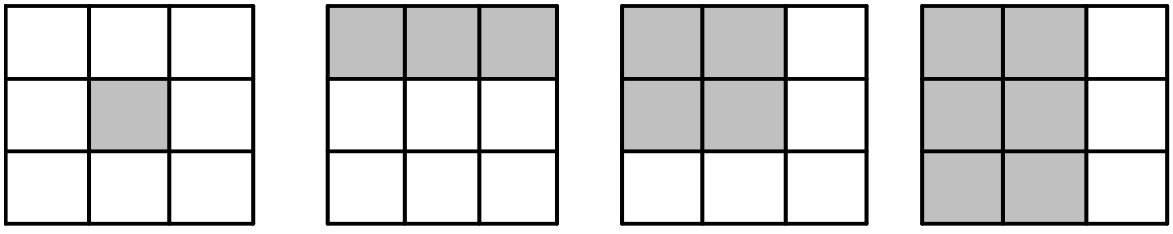

Figure 5.6: Investigated areas for determination of void ratio

To prevent air bubbles from accumulating in the water reservoir below the ceramic disk, the system was periodically flushed with deaired water.

The testing procedure consisted of preparing an oven dry specimen with a predetermined void ratio, as a fixed ring specimen. The specimens are 20 mm high, 70 mm in diameter and where produced using a funnel with a capacity of 100 ml. When preparing loose specimens the falling height was 0 mm and when preparing dense specimens the falling height was 100 mm (see Fig. 5.7). To achieve a plane surface the top of the sand specimens were planed by using a metal sheet. The specimen was saturated by supplying water from the burette through the bottom ceramic disk. Saturation process of the sand specimen means, that the required amount of water was injected through the water reservoir and the ceramic disk by using the attached burette. The saturation process was finished when the water level in the burette reaches the top of the specimen and is left there for 10 hours equilibrium time.

The specimens were subjected to a predetermined matric suction using either a suction mode test or a pressure mode test (i.e. axis-translation technique). All tests were started at fluid saturated conditions. The experiments performed in the modified pressure plate apparatus were steady state type tests. After the specimen had reached equilibrium (i.e. no water inflow or outflow), it was subjected to the next suction increment. Suctions up to 4 kPa were induced by suction mode test. This means that a hanging water column was subjected to the sand specimen by using the attached burette and the attached scale. The bottom of the specimen was used as a reference value, where the suction is equal to zero ($h_0 = 0$ cm, $\psi = 0$ kPa). Following steps for application of suction using hanging water column technique were carried out:

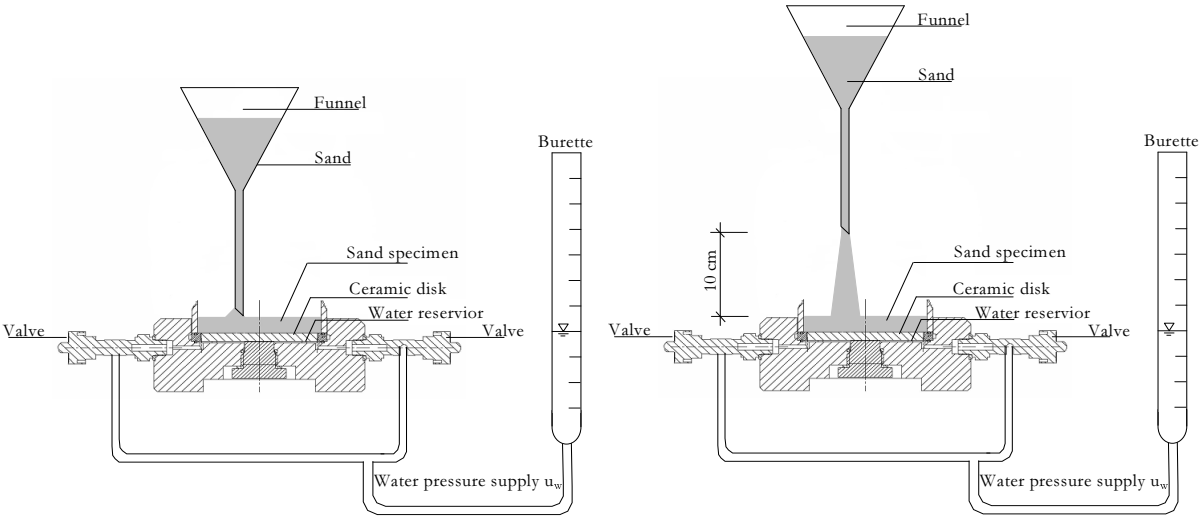

Figure 5.7: Preparation of loose (left) and dense (right) sand specimen in modified pressure plate apparatus

1. Placing the water table in the burette to the height of the bottom of the sand specimen ($h_0 = 0$ cm).
2. Open all valves (i.e. u_a = atmospheric pressure).
3. Lowering the water table down (e.g. $h_1 = -30$ cm that is equal to $\psi = 3$ kPa) by using the burette with reference to the bottom of the specimen (h_0) and using the attached fixed scale.
4. Due to applied suction water is flowing out of the specimen. Hence the water table has to be adjusted continuously by lowering the water table back to h_1.
5. Repetition of the procedure 4. until equilibrium state is reached (no water flow observed).

The pressure mode test realized the application of suctions larger than 4 kPa. The application of suction using pressure mode test includes the following steps:

1. Connection of the upper valve to an air-pressure system.
2. Placing the water table in the burette to the height of the bottom of the sand specimen ($h_0 = 0$ cm).
3. Application of air-pressure (e.g. $u_a = 10$ kPa that is equal to $\psi = 10$ kPa).
4. Open all valves.
5. Due to applied suction water is flowing out of the specimen. Therefore the water table has to be adjusted continuously by lowering the water table back to h_0.
6. Repetition of the procedure 5. until equilibrium state is reached (no water flow observed).

Generally during drainage process water is flowing from the specimen into the burette. When wetting the specimen water is flowing from the burette to the sand specimen. The change of water table in the burette during all induced suction steps was carefully obtained. The final gravimetric water content was calculated by oven-drying the specimen at the end of the test. Volumetric water contents, degree of saturations and gravimetric water contents corresponding to each suction step were back-calculated from these final values using incremental amounts of water flow from each applied step.

Specimen preparation and testing procedure - column device I

Loose and dense specimens with a height of about 540 mm and 300 mm in diameter were prepared by uniformly pluviating oven dry sand with a funnel (500 ml capacity) into the column filled with deaired water, thus ensuring almost 100% saturation. The deaired water was continuously injected into the cell by using the pump attached to the water reservoir at

the bottom of the column. During the preparation procedure the water level was always kept above the sand specimen. When preparing loose specimen the falling height of the sand was approximately 50 mm, when preparing the dense specimen the falling height of the sand was approximately 300 mm (see Fig. 5.8). Every tenth centimeters the void ratio in the column was checked using the mass of dry sand in the column. With a distance of about 100 mm five TDR sensors where placed in a row along the column to measure water content during the testing procedure. Opposite to the TDR sensors tensiometer sensors where placed to measure the corresponding water pressure during the testing procedure (see Fig. 5.9).

After the preparation procedure the dial gauge was attached to the top of the specimen. The initially saturated specimen was left for $\approx$ 12 hours to reach equilibrium conditions before starting the testing procedure. Following the laboratory program for steady state tests as well as transient state tests the loose and dense specimens were drained and wetted using the attached pump. Throughout the drainage process the water table was kept above the bottom water reservoir. The imbibition process was not stopped until the water table reached the top of the sand specimen. Between each cycle the specimen was left for $\approx$ 12 hours to reach equilibrium state.

During the whole testing procedure TDR and tensiometer sensors computed the measurements every third minute. The flow rate was measured and settlements were obtained continuously.

Specimen preparation and testing procedure - column device II

The high air-entry ceramic disk was saturated before performing the experiment equal to the saturation process in the modified pressure plate apparatus.

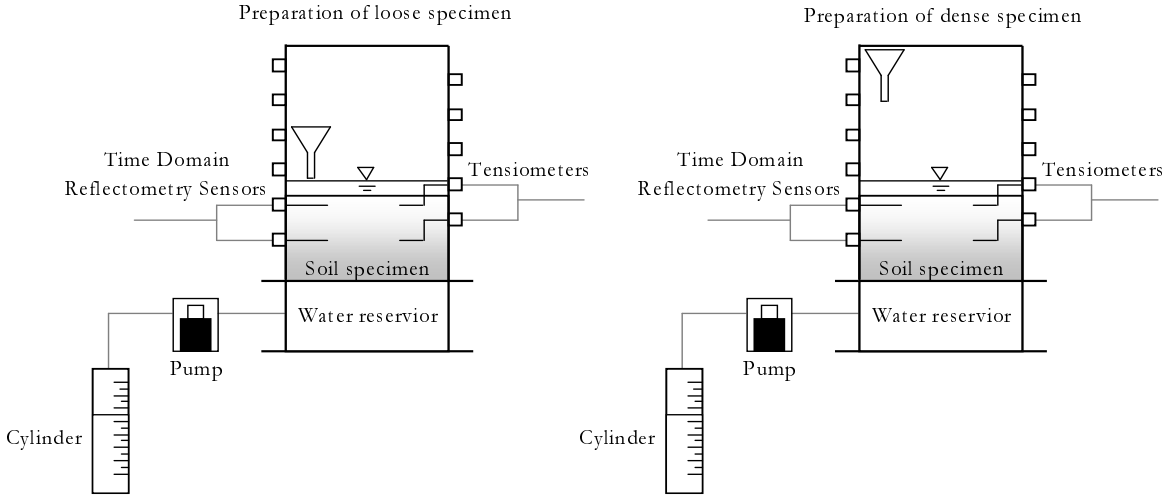

Figure 5.8: Preparation of loose and dense sand specimen in column testing device I

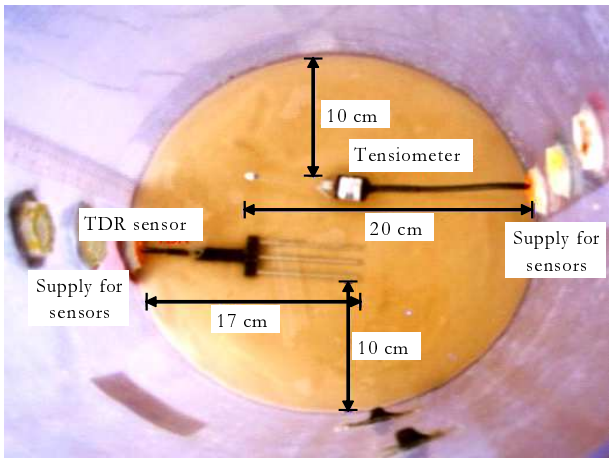

Figure 5.9: Placement of TDR sensor and tensiometer in column testing device I

Similarly to the preparation procedure in the column testing device I specimens were pluviated using a funnel (500 ml capacity) into the column filled with water. Whereas the water in the column testing device I is injected from the bottom water reservoir into the cell, in the column testing device II the water is carefully filled from the top into the cell. For both the loose and dense specimen the mass of water required for saturated condition was poured into the column before pluviating oven dry sand into the cell. When preparing loose specimen the falling height of the sand was approximately 50 mm, when preparing the dense specimen the falling height of the sand was approximately 300 mm. Every fifth centimeters the void ratio in the column was checked using the mass of dry sand in the column. With a distance of 60 mm pairs of TDR sensor and tensiometer sensor were inserted into the specimen. Specimens approximately 230 mm high and with a diameter of 240 mm were produced.

While the system was closed (all valves closed) an air-pressure of approximately 3.5 kPa was applied from the top of the cell to the initially water saturated specimen. After 30 min the valve of the water reservoir was opened and the drainage procedure started. The tests were finished when the top tensiometer sensor reached a matric suction of 3.5 kPa.

During the whole testing procedure TDR and tensiometer sensors computed the measurements every minute. The flow rate was measured and settlements were obtained continuously.

Specimen preparation and testing procedure - controlled-suction oedometer cell

As explained for the modified pressure plate apparatus the ceramic disk was saturated before each experiment and the system below the ceramic disk was thoroughly flushed with deaired water.

The specimen preparation in the controlled-suction oedometer cell is similar to the preparation procedure in the modified pressure plate apparatus. All specimen were prepared directly into the fixed oedometer ring 20 mm high and 50 mm in diameter. Loose and dense

oven dry specimens were prepared directly in the fixed oedoemter ring for the one dimensional compression and rebound tests using a funnel. When preparing loose specimens the falling height was 0 mm and when preparing dense specimens the falling height was 100 mm, followed by the saturation process. After planing the top of the specimen the sand was saturated from the bottom through the water reservoir and the ceramic disk. The attached burette was used for this procedure. According to the experimental program suctions were induced either by suction mode test for $\psi = 1.5$ kPa and $\psi = 3$ kPa or pressure mode test for $\psi = 20$ kPa and $\psi = 50$ kPa. Here the same procedure for suction mode and pressure mode test as described for the modified pressure plate apparatus was adopted. When no water outflow was observed in the attached burette the specimen were loaded and unloaded. During the loading and unloading procedure the suction was kept constant by adjusting the attached burette.

Loose wet specimens were prepared in the oedometer cell for performance of collapse tests. Therefore oven dry sand was mixed with a predetermined amount of water. Two methods were used for preparation of unsaturated Hostun sand specimen with a suction of $\psi = 2.0$ kPa:

- *Method 1:*

  This method includes the preparation of wet sand specimens with a water content of $w = 5\%$. From the soil-water characteristic curve for loose specimen one can find out that a water content of $w = 5\%$ corresponds to a suction less than $\psi = 5$ kPa. The specimens were prepared in 3 layers and slightly tamped after each layer. By applying 5 kPa air pressure (pressure mode test) from the top of the specimen suction was applied. When no change in water table in the burette was observed the predetermined suction of 5 kPa was achieved. It followed the loading procedure, where the suction was kept constant by adjusting the attached burette. Samples were saturated at vertical net stress $\sigma = 5$ kPa, 12 kPa and 25 kPa, further loaded and then unloaded as described in the experimental program.

- *Method 2:*

  Specimens with a water content of $w = 3\%$ were prepared in 3 layers. After each layer the specimen was tamped. The specimen with a water content of $w = 3\%$, which correlates to a suction of $\psi = 5$ kPa, were loaded for undrained test conditions up to $\sigma = 5$ kPa, 12 kPa and 25 kPa, saturated by the attached burette, further loaded up to 100 kPa and unloaded (see experimental programm). In difference to the first method the ceramic disc on the bottom was replaced by a porous stone.

5.4 Experimental Program

The laboratory program consists of the determination of the soil-water characteristic curve as well as unsaturated hydraulic conductivity function under various loading conditions (inves-

tigation of hydraulic behavior) and the determination of stiffness behavior as well as collapse potential (investigation of mechanical behavior). Element tests (in the modified pressure plate apparatus and in the controlled-suction oedometer cell) and benchmark tests (in the sand column testing device I and II) were performed and compared.

Steady state tests were performed in a modified pressure plate apparatus. The influence of loading path history (drainage process, imbibition process, scanning process) and void ratio (loose specimen $e_0 = 0.89$, dense specimen $e_0 = 0.66$) on the soil-water characteristic curve was examined. Additionally the influence of net stress on the shape of the soil-water characteristic curve of loose specimen was investigated. Based on axis-translation technique measurements of the soil-water characteristic curve were directly obtained. The results were used to predict indirectly the unsaturated hydraulic conductivity (statistical models).

Steady state as well as transient state tests were performed using a large scale column testing device (column device I). Several drainage and imbibition curves were measured to investigate the influence of the loading path history (drainage process, imbibition process, scanning process), void ratio (loose specimen $e_0 = 0.89$, dense specimen $e_0 = 0.66$) and water flow condition on the shape of the soil-water characteristic curves. Results derived from the transient state test were used for direct determination of the unsaturated hydraulic conductivity by instantaneous profile method. However, the unsaturated hydraulic conductivity also was estimated indirectly from the steady state and transient state test results using indirect models.

Transient state tests were performed also using a small scale column testing device (column device II). Drainage tests were performed to investigate the influence of the void ratio (loose specimen $e_0 = 0.89$, dense specimen $e_0 = 0.66$) and the water flow condition on the shape of the soil-water characteristic curve. Similar to the steady state tests the unsaturated hydraulic conductivity was indirectly estimated. In both experiments, the column device I and column device II experiments, TDR sensors as well as tensiometer sensors measurements were conducted. These measurements gave information about the water content versus time relationship and the pore-water pressure versus time relationship during testing procedure. Negative pore-water pressure measurements (matric suction) linked to the appropriate water content measurements yield directly to the soil-water characteristic curve.

One dimensional compression and rebound tests investigated the mechanical behavior of unsaturated loose ($e_0 = 0.89$) and dense ($e_0 = 0.66$) sand specimen. Tests were performed under constant suction condition in a controlled-suction oedometer cell (Romero 1999). For different initial conditions the collapse behavior of Hostun sand was studied. These specimens were prepared for loose conditions.

Experiments performed for the investigation of the hydro-mechancial behavior of unsaturated Hostun sand are briefly summarized in Tab. 5.4 and 5.5, where the conditions of the flow experiments and the performed measurements are summarized. Tab. 5.6 gives an

Table 5.4: General overview of flow experiments for investigation of hydraulic properties of unsaturated Hostun sand

Cell	e_0	ψ_0	S_0	Test method	σ	Loading
$MPPA$	0.89/0.66	0	1	Steady state	-	Drainage, Imbibition
$MPPA$	0.89	0	1	Steady state	10.0/20.0	Drainage, Imbibition
SCI	0.89/0.66	0	1	Steady, transient state	-	Drainage, Imbibition
$SCII$	0.89/0.66	0	1	Transient state	-	Drainage

Table 5.5: Performed measurements during flow experiments

Cell	Test method	TDR	Tensiometer	Cumulative water
$MPPA$	Steady state	No	No	Yes
SCI	Steady state	Yes	Yes	Yes
SCI	Transient state	Yes	Yes	Yes
$SCII$	Transient state	Yes	Yes	Yes

overview of the conditions of the mechanical experiments. All the tests were performed in a climate-controlled room ($21°C \pm 1°C$).

5.4.1 Tests Performed using Modified Pressure Plate Apparatus

Water outflow and inflow experiments performed in the modified pressure plate apparatus are element tests conducted on small and thus homogenous, reproducible sand specimens. The experiments performed are steady state type tests.

All tests were started at water saturated conditions. The specimens were subjected to a protocol of several predetermined suction steps using either a suction mode test or a pressure mode test (i.e. axis-translation technique). The final gravimetric water content was calculated by oven-drying (ASTM D2216) the specimen at the end of the test. Volumetric water contents, degree of saturations and gravimetric water contents corresponding to each suction step were back-calculated from these final values using incremental amounts of water flow from each step

Table 5.6: General overview of experiments for investigation of mechanical properties of unsaturated Hostun sand

Cell	e_0	ψ_0	S_0	Loading	Unloading	Collapse
Oedometer	0.89/0.66	1.5/3.0/20.0/50.0		×	×	
Oedometer	0.89	5.0		×	×	×
Oedometer	0.89		1.0	×	×	×

(see Fig. 6.1). To investigate the hydraulic behavior of unsaturated sand initially saturated loose and dense specimens were drained in several predetermined suction steps up to 50 kPa and wetted up to 0.1 kPa. Scanning curves were determined by further drainage up to:

- 1.7 kPa, imbibition up to 0.6 kPa and drainage to 1.7 kPa (loose specimen)
- 2.2 kPa, imbibition up to 0.8 kPa and drainage to 2.2 kPa (loose specimen)
- 2.4 kPa, imbibition up to 1.0 kPa and drainage to 2.4 kPa (loose specimen)
- 1.9 kPa, imbibition up to 0.2 kPa and drainage to 1.9 kPa (dense specimen)
- 2.4 kPa, imbibition up to 0.7 kPa and drainage to 2.4 kPa (dense specimen)
- 2.6 kPa, imbibition up to 1.3 kPa and drainage to 2.6 kPa (dense specimen)

For each loose and dense packed Hostun sand 3 saturated specimen were prepared to determine the scanning imbibition and drainage curves.

To investigate the influence of net stress on the hydro-mechancial behavior of unsaturated sand loose specimens were loaded with 10 kPa and 20 kPa before saturating the specimen. Then suction values up to 50 kPa (drainage process) were applied and suction values up to 0.1 kPa (imbibition process) were applied.

5.4.2 Tests Performed using Sand Column I

Steady state experiments as well as transient state experiments were carried out using the large scale column testing device I. Saturated loose and dense specimens with a height of about 540 mm were prepared. Starting with an initially water saturated specimen, the sand was dried and wetted following different paths. The outflow and inflow of water from the sand sample was induced by increasing and decreasing the water content or saturation using the electronic pump attached to the lower water reservoir.

In the steady state test successive 1000 ml were removed (drainage process) from the initially saturated specimen and injected to the specimen (imbibition process). When no changes in measurements of the TDR sensors and tensiometer sensors were observed equilibrium conditions in the sand specimen was achieved. Next 1000 ml were withdrawn from the sand specimen, viz versa injected to the specimen. From the loose specimen with initially 18000 ml in the pores 10 times 1000 ml were removed and 8 times 1000 ml were injected. From the dense specimen with initially 17000 ml in the pores 8 times 1000 ml were removed and 8 times 1000 ml were injected. During drainage process water was pumped out successive until the water level reached the bottom of the specimen. During imbibition process water was pumped into the specimen until the water level reached the top of the specimen. The loading history of the steady state experiment is given in Fig. 5.10.

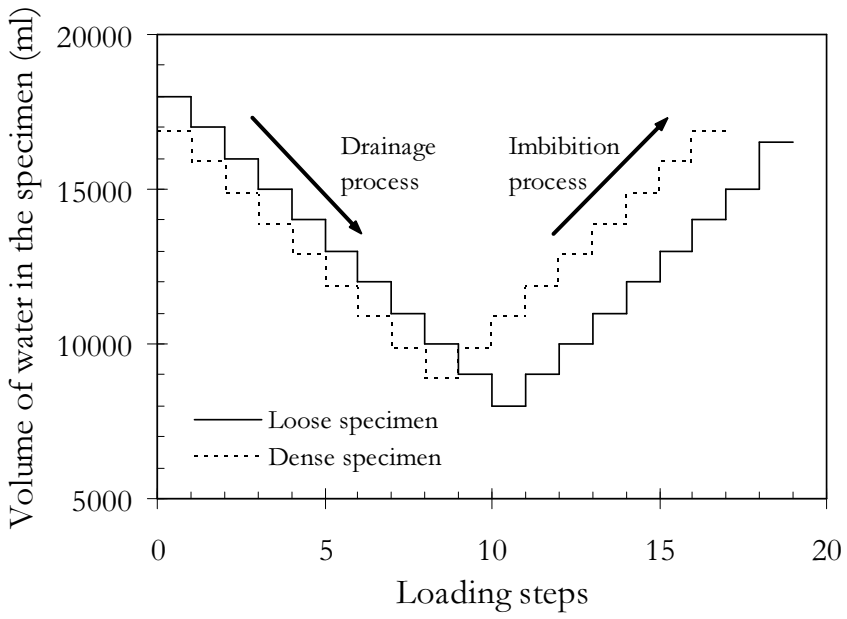

Figure 5.10: Loading history of steady state experiment in column testing device I for loose and dense specimen

Transient state test was performed to study the influence of water flow condition on the soil-water characteristic curve. Therefor water was withdrawn or injected to the sand sample with a flow rate of 30ml/min and with a flow rate of 100ml/min through the reservoir at the bottom (Tab. 5.7, Fig. 5.11). Water was pumped out of the specimen until the water level reached the bottom of the specimen (drainage process) and then water was pumped into the specimen until the water level reached the top of the specimen (imbibition process). The applied flow rate caused a continuous change in suctions throughout the specimen.

Table 5.7: Experimental programm for transient state sand column tests

Loading path	Flow rate [ml/min]
Initial drainage process	30
1^{st} Imbibition process	30
1^{st} Drainage process	30
2^{nd} Imbibition process	100
2^{nd} Drainage process	100

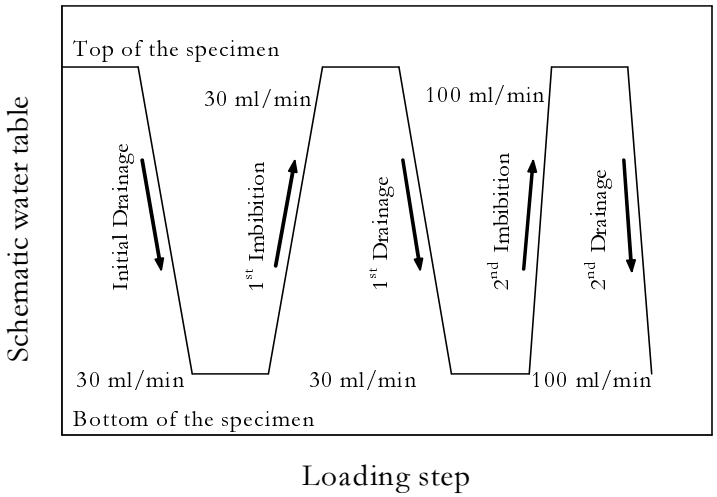

Figure 5.11: Loading history of transient state experiment in column testing device I for loose and dense specimen

5.4.3 Tests Performed using Sand Column II

The column testing device II was used to conduct transient state tests on loose and dense specimen. Drainage tests were performed by applying an air-pressure of approximately 3.5 kPa from the top of the cell to the initially water saturated specimen.

5.4.4 One Dimensional Compression and Rebound Tests

One dimensional compression and rebound test were performed in a controlled-suction oedometer cell. Tests were carried out for loose specimen with an initial void ratio of $e_0 = 0.89 \pm 0.005$ and dense specimen with an initial void ratio of $e_0 = 0.66 \pm 0.005$. The precision for measured deformation is 0.001 mm and 0.6% of the absolute value for stresses (both vertical stress and air pressure).

Special attention was given to the error estimation related to the vertical net load. Correction was applied to the measured vertical net stresses due to shear stresses between the oedometer ring and the soil sample. Both frictional (fixed ring, triangular distribution of horizontal stress: $\sigma_h^{max} = (1 - \sin\phi_p)\sigma_v$, loose: $\phi_p = 34^o$, dense: $\phi_p = 42^o$ (Schanz 1998)) and cohesional effects (derivation of capillary cohesion from soil-water characteristic curve) were taken into account following (Fredlund et al. 1996*b*). Loose and dense specimens with a predetermined suction value were prepared. Suctions were applied using suction mode test ($\psi = 1.5$ kPa and $\psi = 3$ kPa) and pressure mode test ($\psi = 20$ kPa and $\psi = 50$ kPa) to the sand samples and kept constant during the loading and unloading path. Specimens were loaded up to 200 kPa and then unloaded to 2 kPa. Loading history and loading steps of the one dimensional compression and rebound tests are given in Fig. 5.12 as well as Tab. 5.8.

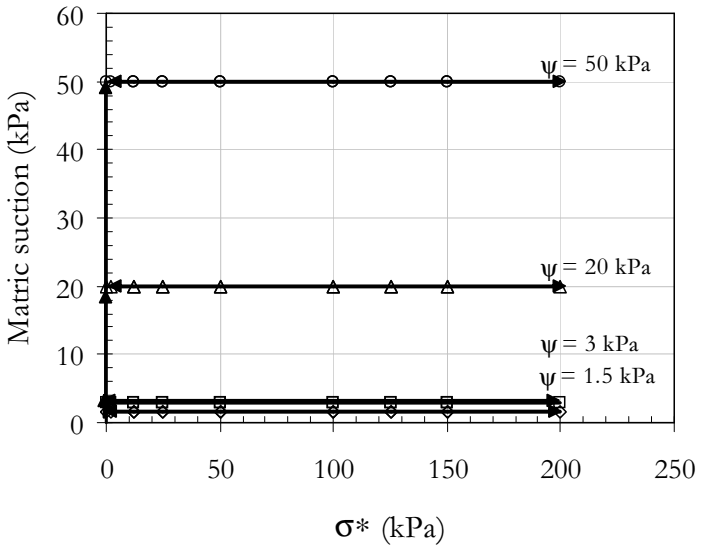

Figure 5.12: Loading history of one dimensional compression and rebound tests

Unsaturated Hostun sand specimen with a suction value $\psi = 5$ kPa were wetted to study the collapse potential. All specimen were prepared for loose conditions. During loading the specimens with constant suction or water content were saturated from the bottom of the cell by the attached burette at certain vertical net stress. The saturated specimen was loaded up to 100 kPa and unloaded in fixed steps. Saturation process was carried out at vertical net stresses of 5 kPa, 12 kPa and 25 kPa. The loading steps for loading and unloading path are summarized in Tab. 5.9.

Table 5.8: Experimental programm for one dimensional compression and rebound tests

$\psi = const$	Net	stress	σ					
$\psi = 1.5$ kPa	0	12	25	50	100	125	150	200
$\psi = 3.0$ kPa	0	12	25	50	100	125	150	200
$\psi = 20.0$ kPa	0	12	25	50	100	125	150	200
$\psi = 50.0$ kPa	0	12	25	50	100	125	150	200
$\psi = const$	Net	stress	σ					
$\psi = 1.5$ kPa	200	150	125	100	50	25	12	2
$\psi = 3.0$ kPa	200	150	125	100	50	25	12	2
$\psi = 20.0$ kPa	200	150	125	100	50	25	12	2
$\psi = 50.0$ kPa	200	150	125	100	50	25	12	2

Table 5.9: Experimental programm for collapse tests

initial suction ψ_0	Net	stress	σ							
5.0 kPa	2	5	S=1	7	10	12	20	25	50	100
5.0 kPa	2	5	7	10	12	S=1	20	25	50	100
5.0 kPa	2	5	7	10	12	20	25	S=1	50	100
$S = const$	Net	stress	σ							
S=1	100	50	25	20	15	12	7	5	2	
S=1	100	50	25	20	15	12	7	5	2	
S=1	100	50	25	20	15	12	7	5	2	

5.5 Summary

In this chapter the investigated material is classified. It was found, that homogeneous specimen were produced when pluviating the testing material directly into the oedometer ring of the modified pressure plate apparatus. Investigations using computer tomography as well as electron microscopy supported this. Saturated specimen, the initial condition for the tests performed in column testing device I and II, are produced by pluviating sand directly into the column filled with deaired water. Air-pluviated specimens were prepared in the modified pressure plate apparatus and in the controlled suction oedometer and saturated in an additional step.

Overall the experimental programm consists of the investigation of the hydro-mechancial behavior of unsaturated Hostun sand. Testing devices as the modified pressure plate apparatus, the sand column testing device I and II as well as the controlled-suction oedometer are used to determine the hydraulic functions of Hostun sand, the influence of suction on the compression and swelling index as well as the stiffness modulus. Initial conditions (initial void ratio, initial suction), applied loading paths (drainage, imbibition, loading, unloading with vertical net stress) and flow conditions (steady state test, transient state test) are considered in the experimental programm to estimate hydro-mechancial behavior of unsaturated sand and to account for the phenomena (phenomenon of hysteresis, collapse, occluded air, dynamic effect) associated with it.

Chapter 6

Experimental Results

6.1 General

The following chapter gives an extensive overview of the experimental data derived from the laboratory program.

Results of the steady state experiments performed in the modified pressure plate apparatus are cumulative water outflow and cumulative water inflow versus time measurements. These cumulative water flow measurements and the applied suction values lead to soil-water characteristic curves of the investigated sand, which are also given in the section below. Experimental results performed in the column testing device I under transient state as well as steady state flow condition and column testing device II under transient state flow condition are pore-water pressure measurements and volumetric water content measurements observed in several depth along the columns during draining and wetting the sand specimens. Further these measurements are directly linked to the soil-water characteristic curve. Typical results of the column testing device I experiments performed under transient state condition are also pore-water pressure as well as volumetric water content profiles.

Experimental results from the one dimensional compression and rebound as well as collapse tests are given that include strain versus vertical net stress as well as void ratio versus vertical net stress data.

6.2 Soil-Water Characteristic Curve

For determination of the soil-water characteristic curve of Hostun sand, that includes the initial drainage curve, the main drainage and imbibition curve as well as scanning drainage and imbibition curve the following measurements from steady state or transient state experiments were used:

- Cumulative water outflow and inflow measurements

- Pore-water pressure measurements

- Volumetric water content measurements

The measurements and the resultant soil-water characteristic curves are given in the section below. In case of steady state tests it was also focused on the volumetric mechanical behavior, by applying net stress to the specimen. The influence of net stress on the shape of the soil-water characteristic was observed.

6.2.1 Steady State Test Results

Cumulative water outflow as well as inflow measurement results were derived from the tests performed in the modified pressure plate apparatus. Experimental results of cumulative water outflow and inflow during drainage process as well as imbibition process are plotted in Fig. 6.1. Depending on the suction step it took a period up to 12000 min till reaching equilibrium condition in the specimen. Before reaching the air-entry value (suction steps between 0

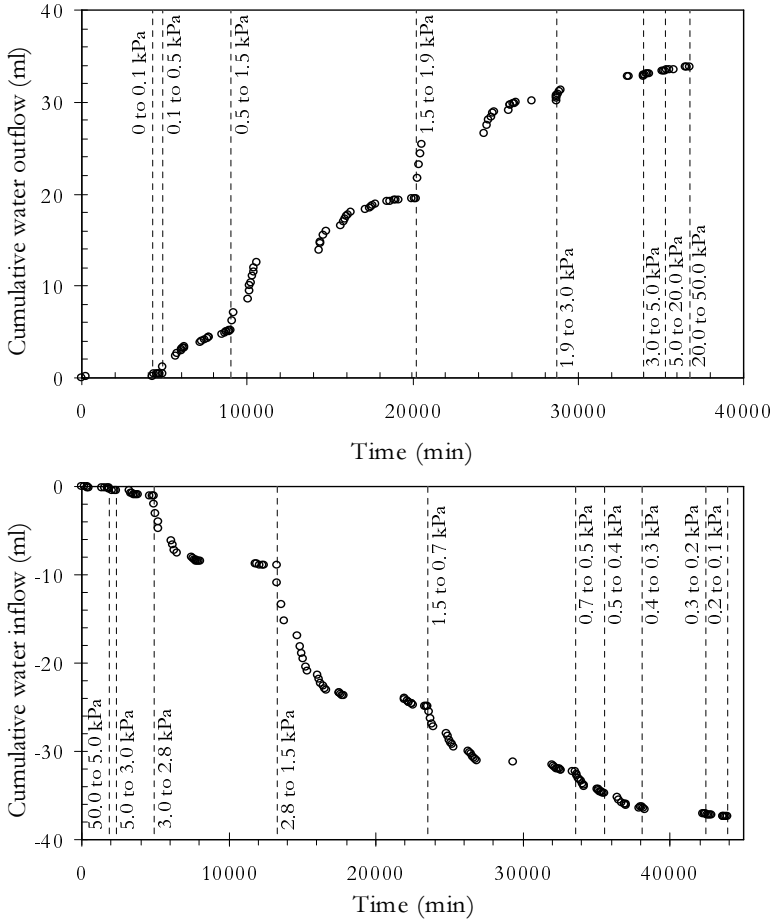

Figure 6.1: Experimental results of cumulative water outflow (top) and inflow (bottom) from drainage and imbibition process in modified pressure plate apparatus (loose specimen)

to 1.5 kPa) most amount of water is retained in the specimen. After passing the air-entry value, that is between a suction of 1.5 and 1.9 kPa, air starts to enter the water filled pores. Thus water is leaving the soil and the time period to reach equilibrium significantly increases for drainage path. The uniform grain-size distribution of the investigated material leads to uniform pores and therefore most water is flowing out when passing the air-entry value. With further increase in suction the volume of water that is leaving the specimen is decreasing. Viz versa the time period for reaching equilibrium condition increases when passing the residual suction (between 2.8 and 1.5 kPa) along the imbibition path, where the specimen starts to absorb water. Fig. 6.2 presents the experimental results of the soil-water characteristic curves derived from back calculation using the final water contents and the amount of water outflow (drainage curve) and inflow (imbibition curve). Both the suction versus volumetric water content $\theta(\psi)$ and suction versus saturation $S(\psi)$ drainage and imbibition relations are given for loose and dense specimens. The results for specimens prepared in both a loose and dense state show significant hysteresis behavior. Thus during drainage cycle a certain suction corresponds to a lower volumetric water content (or saturation) then during the imbibition cycle.

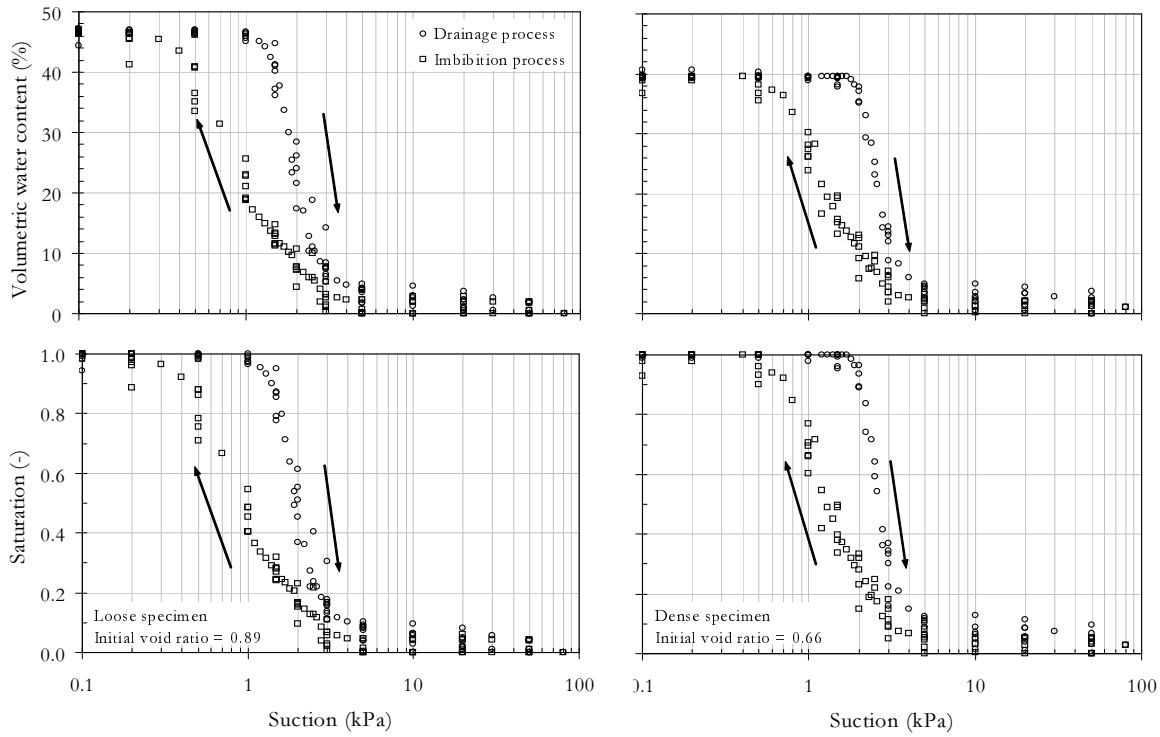

Figure 6.2: Experimental results of soil-water characteristic curves from steady state tests performed in the modified pressure plate apparatus (loose specimen-left, dense specimen-right)

Scanning drainage cycles and imbibition cycles were also performed during the experimental procedure in the modified pressure plate apparatus on 3 loose and 3 dense Hostun sand specimen. The derived soil-water characteristic curves including scanning imbibition and drainage curves are presented in Fig. 6.3 for loose and for dense specimen. The volumetric water content versus suction and saturation versus suction plots are shown, where also the volumetric water content was back calculated using the final water content measurements and the amount of water outflow (drainage curve) and inflow (imbibition curve). Comparison of the scanning cycles of both specimen, the loose and the dense one, clearly show that the dense specimen is retaining larger quantity of water for a certain applied soil suction value. Due to smaller voids in the dense specimen, that retain water up to higher suction value, scanning cycles are located in the top part of the hysteresis loop.

During steady state tests performed in the modified pressure plate apparatus it was also focused on the volumetric mechanical behavior by applying net stress to the specimen and thus the influence of net stress on the shape of the soil-water characteristic curve. Volumetric water content, saturation and void ratio versus suction relationships for different applied net

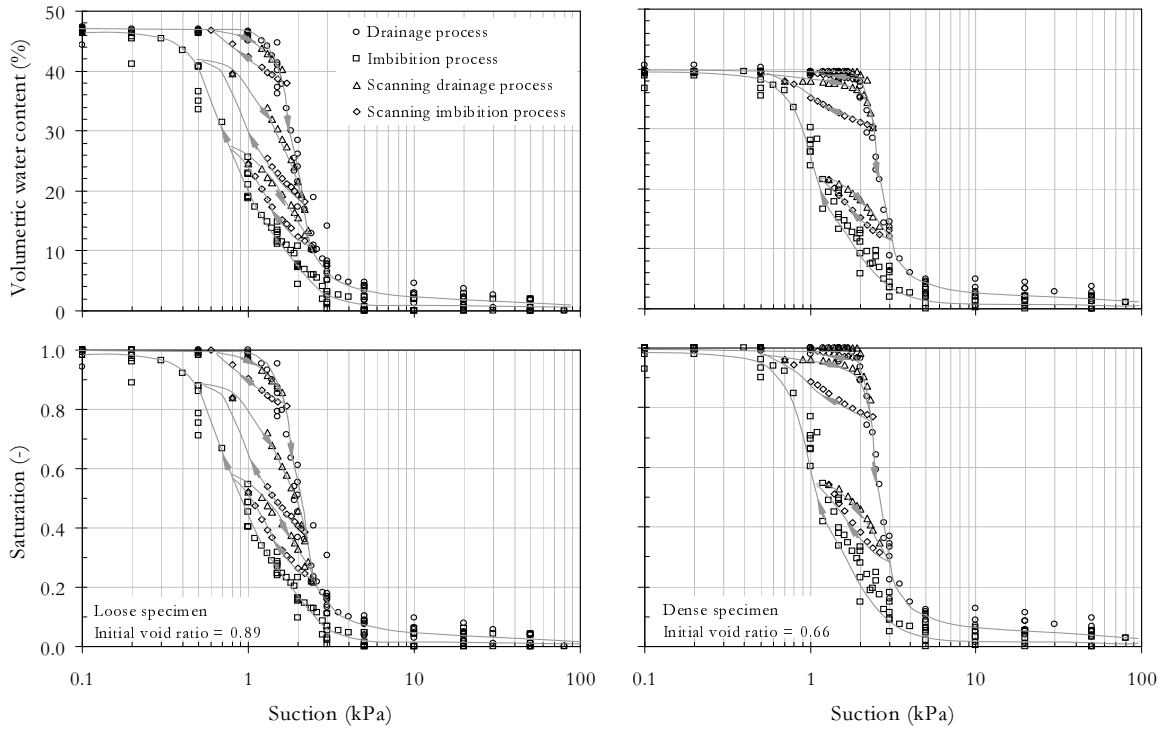

Figure 6.3: Experimental results of soil-water characteristic curves including scanning drainage and imbibition curves from steady state tests performed in the modified pressure plate apparatus (loose specimen-left, dense specimen-right)

stresses are presented in Fig. 6.4 for loose specimen. Drainage results as well as imbibition results are given.

Soil-water characteristic curve results derived from measurements performed during steady state test in the column testing device I shows Fig. 6.5. After removing or inducting water equilibrium conditions were achieved. The measured water contents and pore water pressures at equilibrium condition were measured and linked to the soil-water characteristic curve as given in Fig. 6.5 for loose and dense specimen. The diagrams show initial drainage curves and imbibition scanning curves derived from the 3 upper depths in the column. The soil-water characteristic curve takes place in a narrow range of matric suction. After the first drainage procedure the occluded air could not be replaced by the following imbibition process.

In general experimental results from steady state tests derived in modified pressure plate apparatus and sand column testing device I show an influence of void ratio on the shape of the

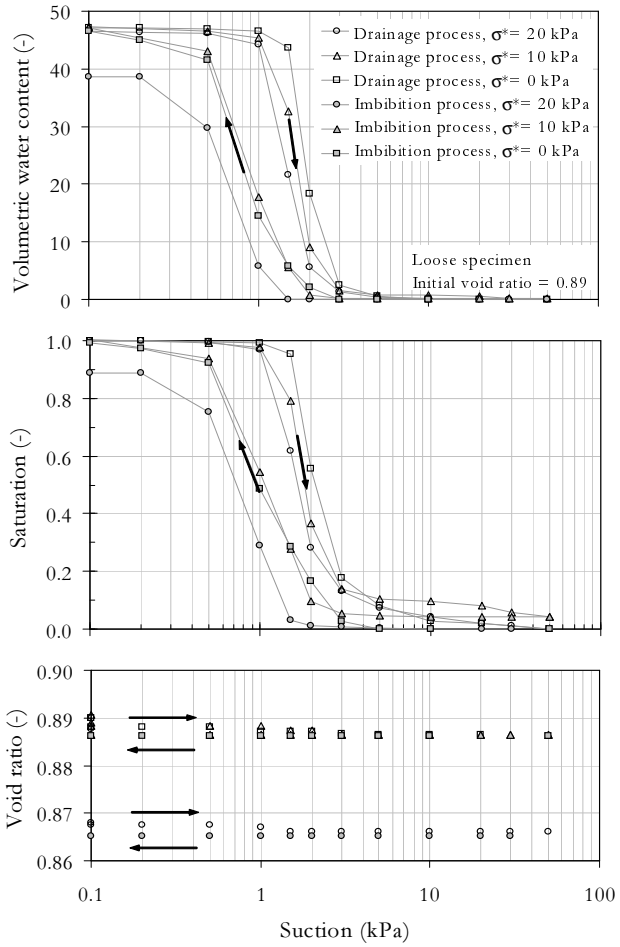

Figure 6.4: Experimental results of soil-water characteristic curve applied with net stress from steady state test in modified pressure plate apparatus (loose specimen-left, dense specimen-right)

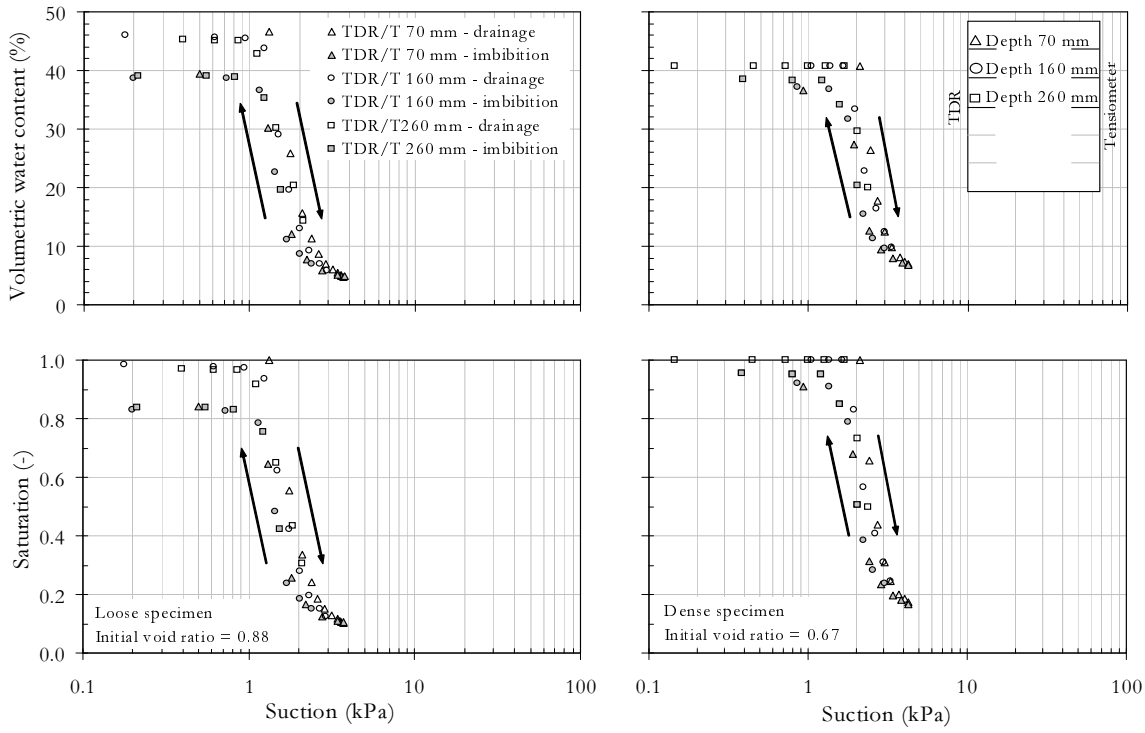

Figure 6.5: Readings from tensiometers and TDR sensors linked to drainage and imbibition soil-water characteristic curves from steady state column test I (loose and dense specimen)

soil-water characteristic curve. Similar to the measurements observed in the modified pressure plate apparatus, the experimental results measured in the sand column testing device I show the effect of hysteresis. Between main drainage and imbibition loop several scanning drainage and imbibition curves were found in the modified pressure plate test results. Comparing the hysteresis of the volumetric water content-suction curves the loose specimen enclose a larger area than the dense specimen. The effect of occluded air bubbles was found to be significant for the results derived from the sand column I tests, particularly for the loose specimen.

6.2.2 Transient State Test Results

Suction measurements were performed in several depth during experiments carried out in sand column device I under transient state condition using tensiometer sensors (Fig. 6.6). These measurements were carried out parallel to volumetric water content measurements using TDR sensors that are also presented below (Fig. 6.7). The results are pairs of tensiometer and TDR readings, which are linked to the soil-water characteristic curve (Fig. 6.8).

Typical tensiometer results measured in transient state column test I are given in Fig. 6.6. These figures respectively show the measurements derived from the drainage and imbibition processes observed from both the loose and dense specimen. As described in the laboratory

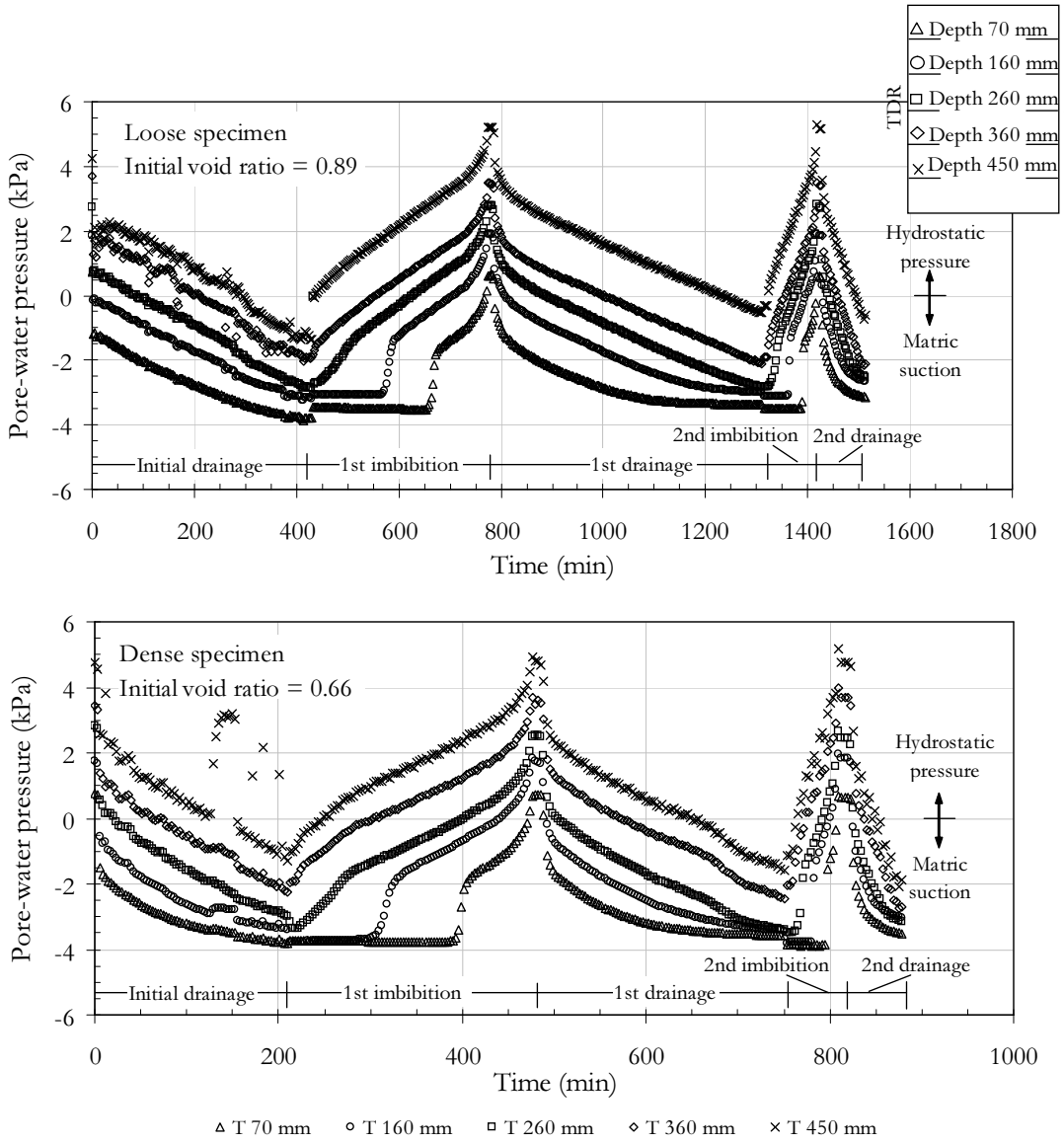

Figure 6.6: Suction measurements for drainage and imbibition processes from transient state column test I (loose specimen-top, dense specimen-bottom)

program to an initially saturated specimen several flow rates were induced for several flow processes:

1. Initial drainage process with an applied flow rate of approximately 30 ml/min.

2. First imbibition/ drainage process with an applied flow rate of approximately 30 ml/min.

3. Second imbibition/ drainage process with an applied flow rate of approximately 100 ml/min.

Measurements of the sensors were performed in 5 depth. Tensiometer T (450 mm) and the TDR probe TDR (450 mm) are located at the bottom of the column in a depth of 450mm and T (70 mm) and TDR (70 mm) are located at the top of the column in a depth of 70 mm (TDR measurements see Fig. 6.7 given below). The initial condition for the initial drainage process is a water saturated specimen with the water table located at the top of the specimen. Under saturated condition the tensiometers measure positive pore-water pressure (hydrostatic pressure). The pore water pressure is increasing with depth. The original state for each imbibition cycle corresponds to an unsaturated sand specimen, where the water table is located at the bottom of the specimen. Under unsaturated condition the tensiometers measure initially negative pore-water pressure (matric suction, capillary pressure). With increasing depth the pore-water pressure is increasing. Thus the matric suction is decreasing with

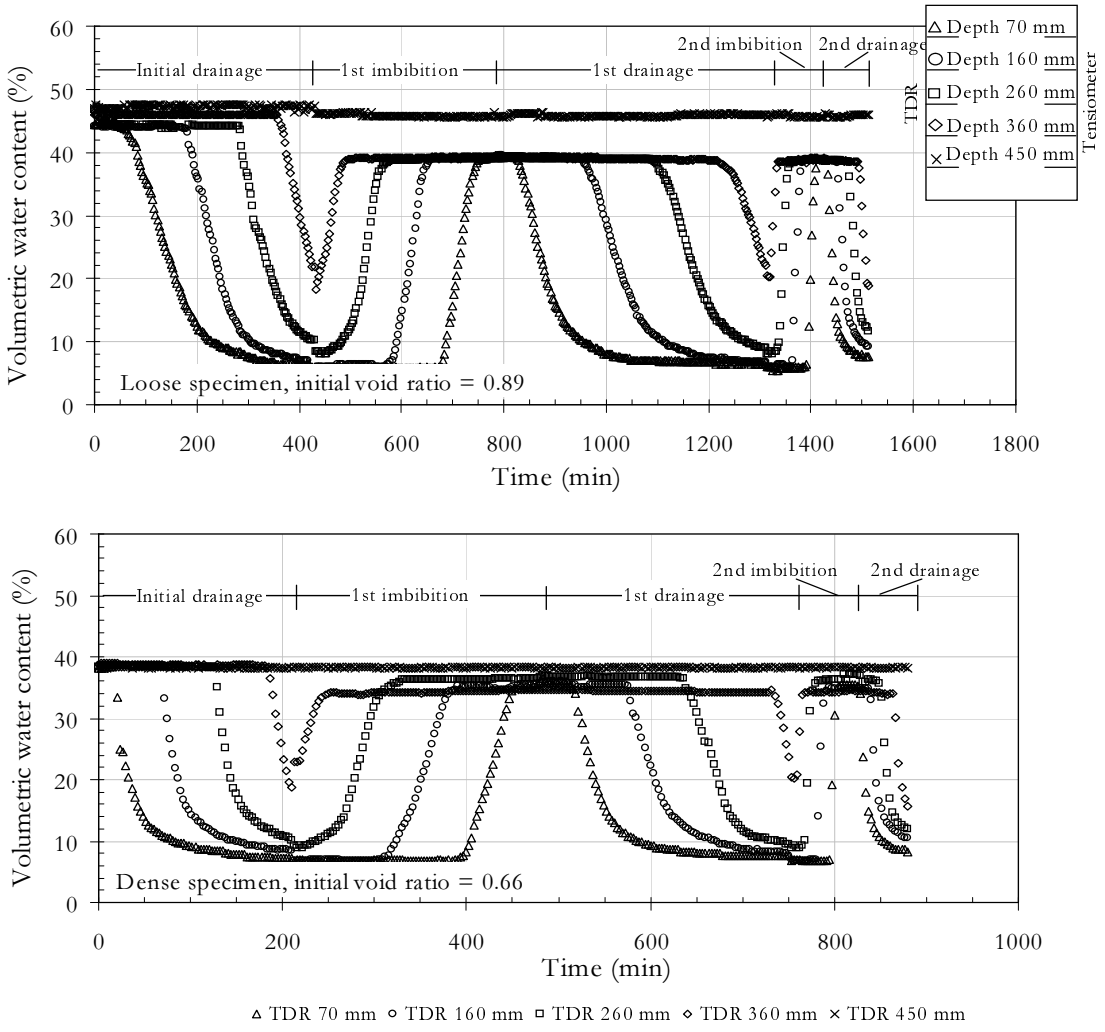

Figure 6.7: Example of volumetric water content measurements for drainage and imbibition processes from transient state column test (loose specimen-top, dense specimen-bottom)

depth. Following for instance the 1^{st} imbibition process in Fig. 6.6 the tensiometer T (70 mm) measures a lower negative pore-water pressure than tensiometer T (450 mm), referring to a higher suction at the top of the sand specimen. With increase in water table due to water inflow the suction is increasing. Saturated conditions are reached in the specimen when the tensiometers measure positive pore-water pressures. The imbibition process is stopped when the water table reaches the top of the specimen.

Following the experimental results derived from the 1^{st} drainage process in Fig. 6.6 tensiometer T (450 mm) measures a lower positive pore-water pressure than tensiometer T (70 mm), indicating a higher hydrostatic pressure at the bottom of the specimen. During drainage of the sand specimen the positive pore-water pressures are decreasing until reaching negative pore-water pressures. The measured negative pore-water pressures at the end of the draining process is lower at the top of the specimen than at the bottom of the specimen. Consequently, the suction is higher at the top of the specimen than at the bottom of the specimen.

Volumetric water content measurements are given in Fig. 6.7. As mentioned before the initial condition for the initial drainage process is a water saturated specimen with the water table located at the top of the specimen. For the initially saturated specimen the TDR sensors measure the saturated volumetric water content (corresponding to $S = 1$), which is equal in each depth.

It was also mentioned before, that the original state for the imbibition cycles correspond to an unsaturated sand specimen, where the water table is located at the bottom of the specimen. Thus TDR sensors measure the volumetric water content in the specimen, that differs with depth. On the bottom a larger volumetric water content is measured than on the top.

Following for instance the 1^{st} imbibition process in Fig. 6.7 the measured volumetric water content at the top of the specimen is lower than the volumetric water content at the bottom of the specimen. During imbibition process the volumetric water content is increasing corresponding to a decreasing suction. During the imbibition process the volumetric water content increases first at the bottom of the specimen and then at the top of the specimen. The imbibition process is stopped when the water table reaches the top of the specimen. Even when the water table is at the top of the specimen, measurements in sensors TDR (70 mm) to TDR (450 mm) refer to a degree of saturation less than 1 (apparent saturation S'). Thus the measured volumetric water contents are influenced by occluded air bubbles (also called apparent volumetric water content θ'). The TDR (450 mm) sensor at the bottom of the specimen measures the volumetric water content referring to water saturated conditions, $S = 1$. This portion of the specimen remains saturated during the entire testing procedure and occluded air bubble cannot occur. The experimental results derived from the 1^{st} drainage process in Fig. 6.7 show that the sand specimen is saturated and the measurements from the TDR sensors, TDR (450 mm) to TDR (70 mm), correspond to a degree of saturation close to 1. During drainage the volumetric water contents are decreasing, first at top of the specimen

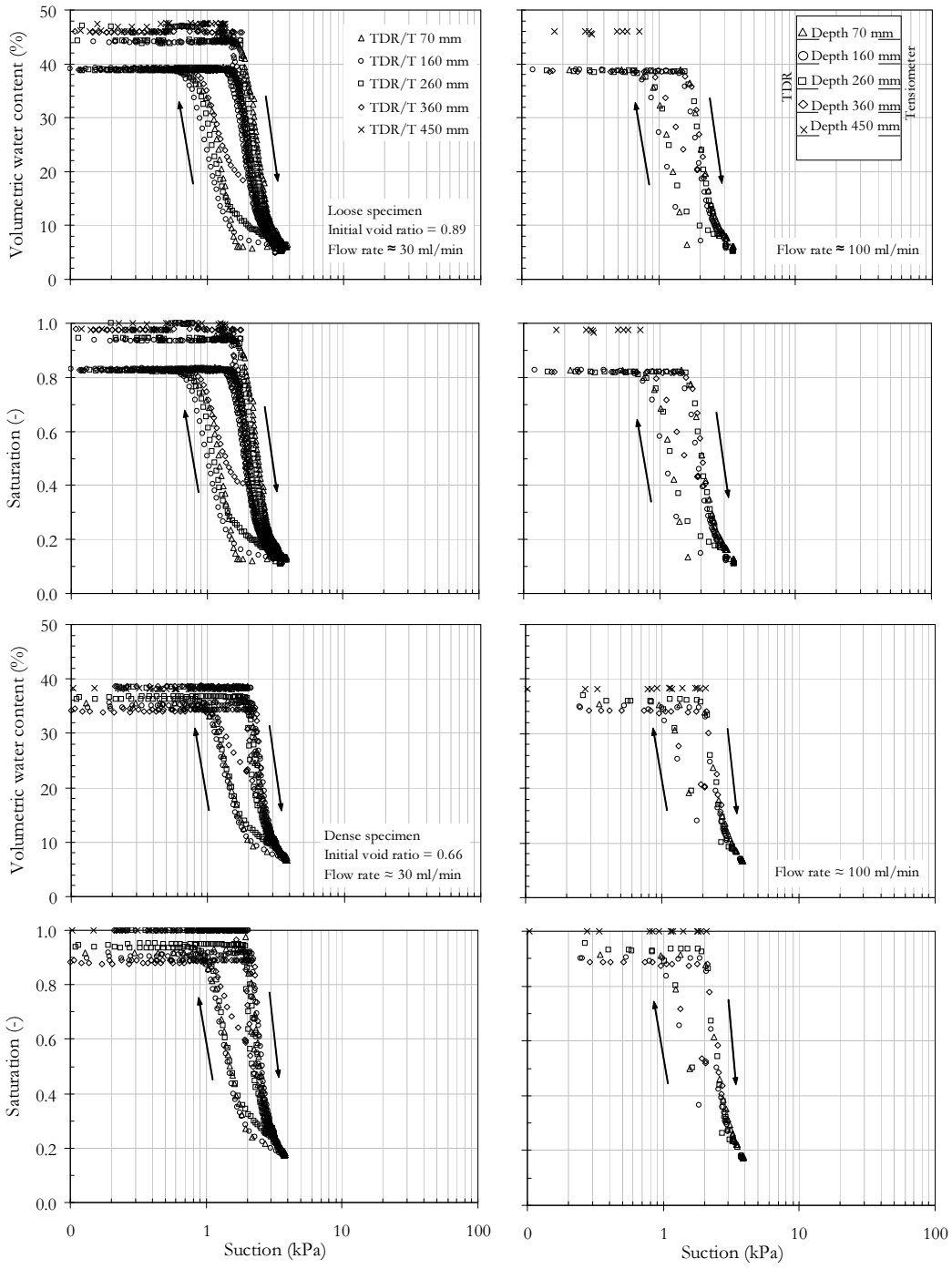

Figure 6.8: Readings from tensiometers and TDR sensors linked to drainage and imbibition soil-water characteristic curves from transient state column test I (loose specimen-left, dense specimen-right)

and than at the bottom of the specimen. The sensors on the bottom of the cell (TDR/T 450 mm) are located in the saturated zone through the complete testing procedures. Therefore the volumetric water content is constant through the complete testing procedure (TDR 450 mm: $\theta_{s,loose} = 46\%$, $\theta_{s,dense} = 39\%$). The other sensors give results for saturated as well as unsaturated conditions.

As shown in Fig. 6.8 the tensiometer as well as the TDR probe measurements enable a direct measurement between negative pore water pressure (matric suction, capillary pressure) and volumetric water content that finally lead to the observation of the soil-water characteristic curve. For loose as well as dense specimen the measurements are presented as volumetric water content versus matric suction and saturation versus matric suction. The main drainage path, $1st$ imbibition and drainage paths (flow rate $\approx$ 30 ml/min) as well as $2nd$ imbibition and drainage paths (flow rate $\approx$ 100 ml/min) obtained in the different depths are shown. It was observed that after the first wetting, complete saturation ($S = 1$) was not again recovered. The occluded air could not be displaced during subsequent imbibition paths. Different placement depths of the sensors resulted in different initial suctions and volumetric water contents, respectively, in the unsaturated zone during further imbibition cycles. Subsequent curves are located within the main drainage and imbibition loop and are known as scanning curves.

Similar to the flow experiments in the sand column test I, the tests performed in the column testing device II were carried out under transient state condition. Therefore measurements of pore-water pressure by using tensiometer sensors and volumetric water content by using TDR sensor were carried out in several depth. Pore-water pressure versus time measurements are given in Fig. 6.9 for the loose specimen and for the dense specimen. Corresponding TDR sensor measurements are given in Fig. 6.10 as volumetric water content versus time measurement results. After application of air-pressure $u_a = 3.5$ kPa that is conform to a suction $\psi = 3.5$ kPa to the specimens from the upper part of the apparatus the specimen starts to drain. At the beginning of the test tensiometers measure positive pore-water pressure, which is higher at the bottom than at top of the cell (see Fig. 6.9). When applying air-pressure the pore-water pressure is decreasing first in the top layer than in the bottom layer until reaching negative-pore water pressure. Initially the specimens are water saturated and a saturated volumetric water content of $\theta_{s,loose} = 47\%$ and $\theta_{s,dense} = 41\%$ was measured (see Fig. 6.10). After application of air-pressure to the specimens from the upper part of the apparatus the specimen starts to drain. First the volumetric water content in the top layer is increasing and than the volumetric water content in the bottom layer is increasing. Cumulative water outflow measurement results derived during column testing device II for loose and dense specimen are given in Fig. 6.11. Larger amount of water flow out from the loose specimen than from the dense specimen. Measurements stopped when water was flowing out no longer.

Similar to the tests performed in the column testing device I the TDR and tensiometer measurements are directly linked to the soil-water characteristic curve, that is given in

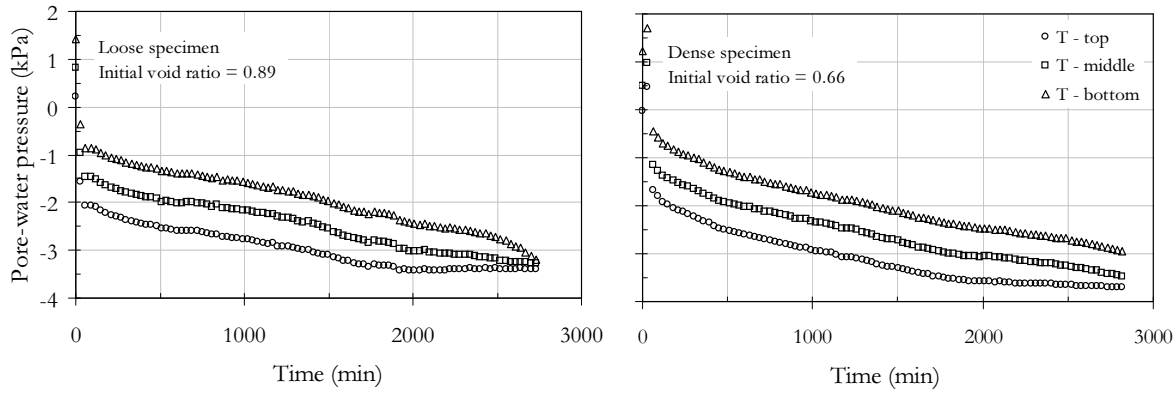

Figure 6.9: Suction measurements for drainage process from transient state column test II (loose specimen-left, dense specimen-right)

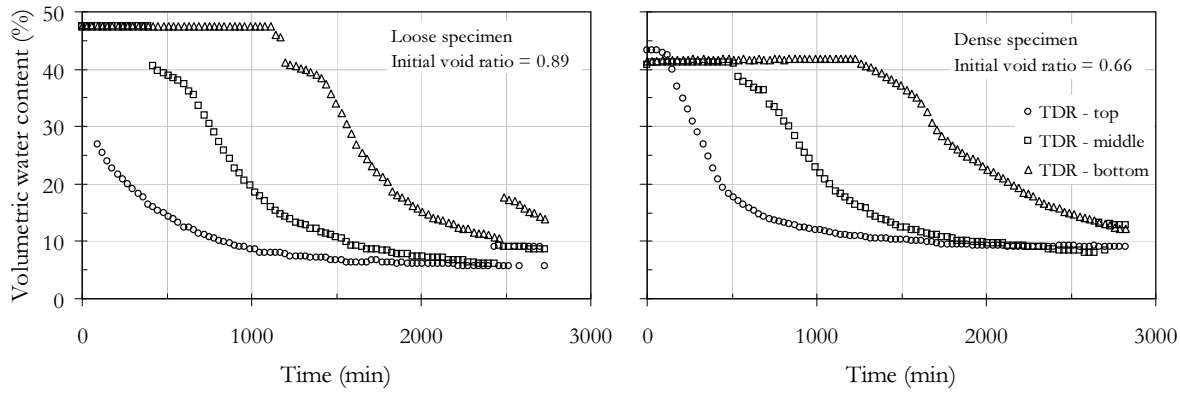

Figure 6.10: Volumetric water content measurements for drainage process from transient state column test II (loose specimen-left, dense specimen-right)

Figs. 6.12 for both loose and dense specimen. Since the initial condition is equal in each measurement depth (initially saturated specimen), the shape of the measured soil-water characteristic curve is similar.

As the steady state test results, the transient state results show an influence of void ratio on the shape of the soil-water characteristic curve, that will result in different soil-water characteristic curve parameters as for instance air-entry value, residual suction and water-entry value for loose and dense specimen. The measurements derived during drainage and imbibition process are not unique that leads to the phenomena of hysteresis. In sand column test I experiments several scanning imbibition curves were found. Even after several performed imbibition processes in sand column I tests a fully saturated specimen was not achieved again. Here also the effect of occluded air bubbles was found to be significant for both the loose and

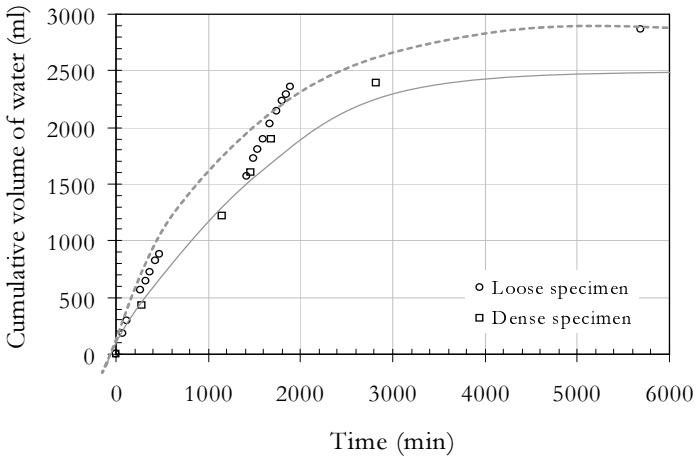

Figure 6.11: Measurements of cumulative water outflow from transient state column test II (loose and dense specimens)

dense specimen. Independent from the experimental procedure (specimen were drained and wetted with a flow rate of 30 ml/min as well as 100 ml/min and a suction of 3.5 kPa was

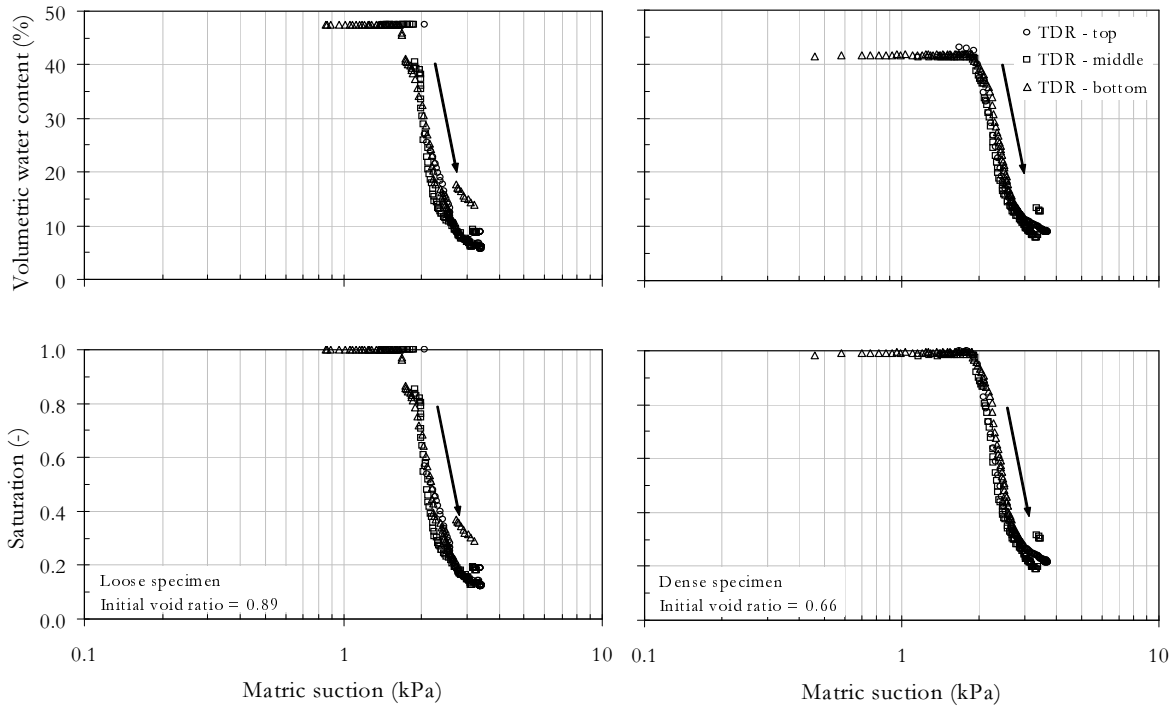

Figure 6.12: Readings from tensiometers and TDR sensors linked to drainage soil-water characteristic curves from transient state column test II (loose specimen)

suddenly applied to an initially saturated specimen) it seems, that the parameters as air-entry value, residual suction, residual water content and water-entry value are similar for the loose specimens and respectively for the dense specimens.

6.3 Unsaturated Hydraulic Conductivity

The unsaturated hydraulic conductivity was directly determined using suction and also volumetric water content measurements from the transient state sand column test I. Exemplary pore-water pressure (hydrostatic pressure has positive sign and matric suction has negative sign) and also exemplary volumetric water content profiles are presented in Fig. 6.13 for initial drainage process and in Fig. 6.14 for 1^{st} drainage process of loose specimen. Measurements every 20 th minutes are presented for several depths. Fig. 6.13 presents the initial condition which is a fully saturated specimen. The tensiometer sensors measure the hydrostatic pressure (positive pore water pressure) of water that shows a linear distribution in the specimen. The TDR sensors measure the volumetric water content that is constant along the column. Fig. 6.14 also presents a saturated specimen with a linear distributed positive pore water pressure. But after 1^{st} imbibition process air remains in the pores and therefore full saturation of the specimen is not reached ($\theta_s' = 39\%$) as given in the volumetric water content profile. Only the bottom TDR sensor is located in the saturated zone through the experiment ($\theta_s = 46\%$). Both Figures show with outflow of water decreasing pore water pressure and decreasing volumetric water content first in the top part and then in the bottom part of the specimen.

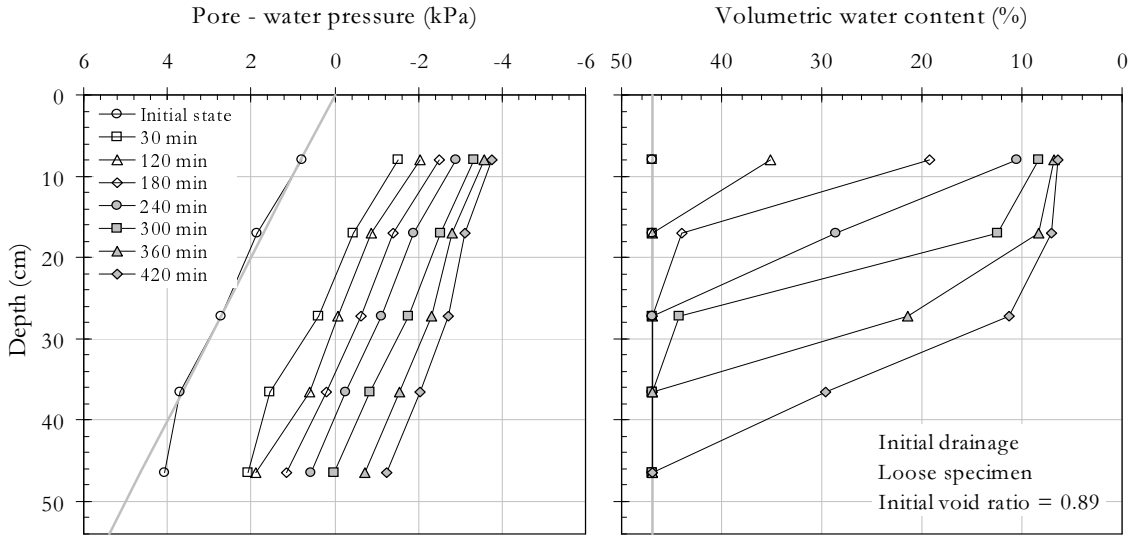

Figure 6.13: Pore-water pressure and volumetric water content profiles for initial drainage process (loose specimen)

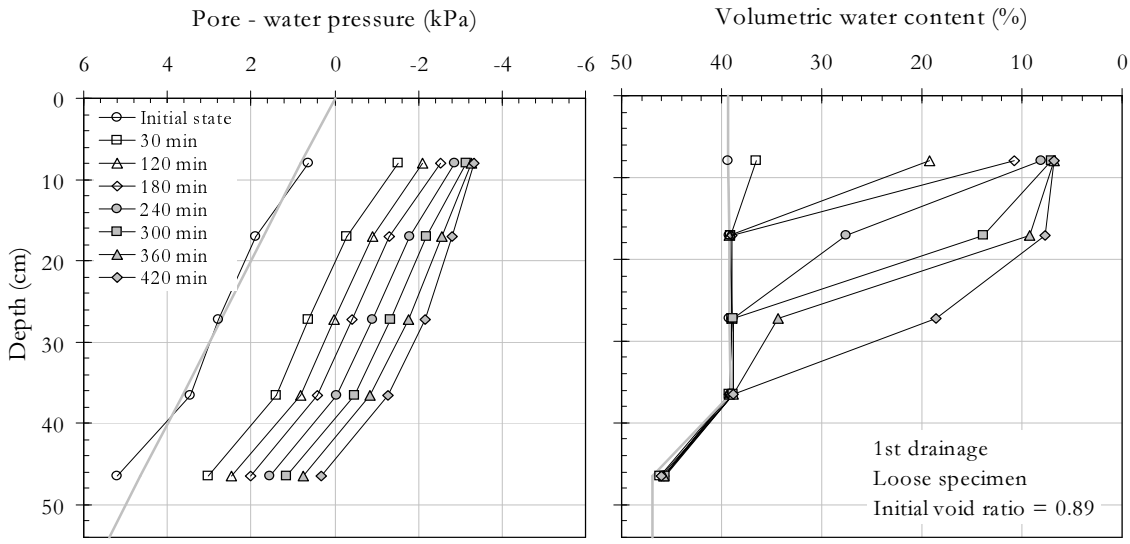

Figure 6.14: Pore-water pressure and volumetric water content profiles for 1^{st} drainage process (loose specimen)

6.4 Volumetric Behavior

For determination of the mechanical behavior of unsaturated Hostun sand stress-strain relationships derived from one dimensional compression rebound tests and collapse tests were investigated. The results are give in the section below.

6.4.1 Stress-Strain Relationship

Experimental results from one dimensional compression and rebound tests are presented in Fig. 6.15 for loose specimens and in Fig. 6.16 for dense specimens. Volumetric strain versus applied vertical net stress as well as void ratio versus applied vertical net stress results are given in the diagrams. For sands the following typical observations in the stress-strain curve are made (Lambe & Whitman 1969):

- *Observation during loading path:*

  As can be seen in the stress strain diagrams in Figs. 6.15 and 6.16 the sand becomes stiffer with increasing vertical stress. As the stress increases within the soil sample loose arrays collapse followed by denser arrays. Each movement results in a stiffer packed specimen and thus decreasing void ratio. With increasing stress the stress-strain curvature becomes concave to the strain axis resulting from fracturing of individual sand particles. Whereas sliding between particles occurs at all stress levels, fracturing and crushing becomes increasingly important with increase in vertical stress.

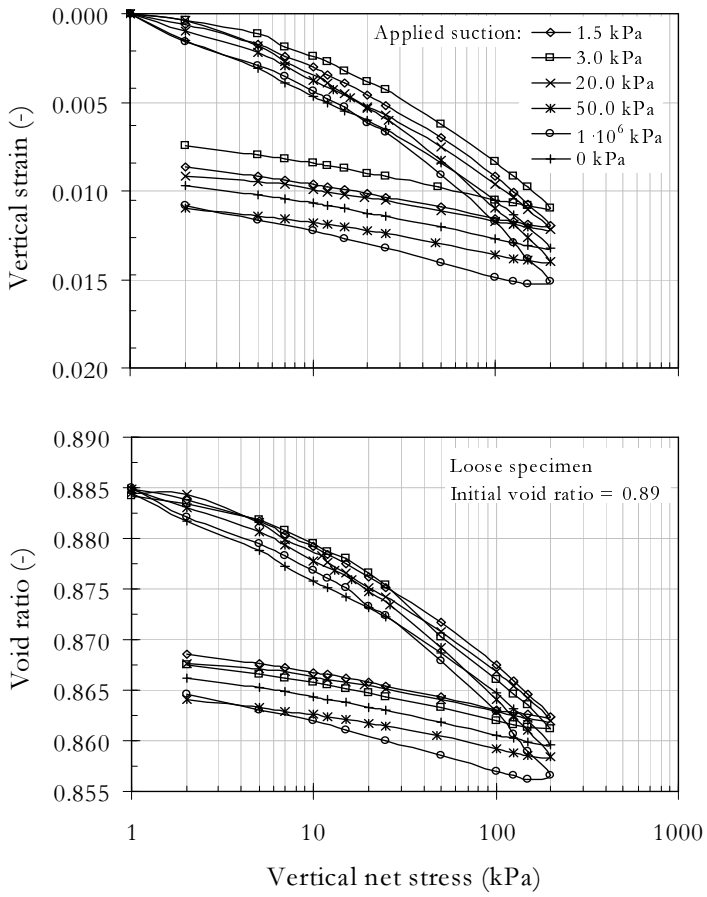

Figure 6.15: Experimental results of one dimensional compression rebound test for constant suction condition (loose specimen)

- *Observation during unloading path:*

  The unloading path shows that the initial strain is not reached again. The strain from sliding between particles or fracturing is an irreversible process. Some reverse sliding during unloading is observed. This is due elastic energy within few particles.

A comparison between the experimental results of the loose specimen and the dense specimen in Fig. 6.15 and Fig. 6.16 shows that as anticipated the stiffness for dense specimens is higher then for loose specimens. The difference in void ration during loading path is larger for the loose specimens with approximately $\Delta e = 0.025$ than for the dense specimens with approximately $\Delta e = 0.015$, which indicates a higher stiffness for the dense one. From the test results for both loose and dense specimens it is observed, that the change in void ratio for the specimens with applied suctions up to $\psi = 20$ kPa is smaller than for the dry as well as saturated ($S = 1$) specimens. The results of the test with applied suction $\psi = 50$ kPa are close

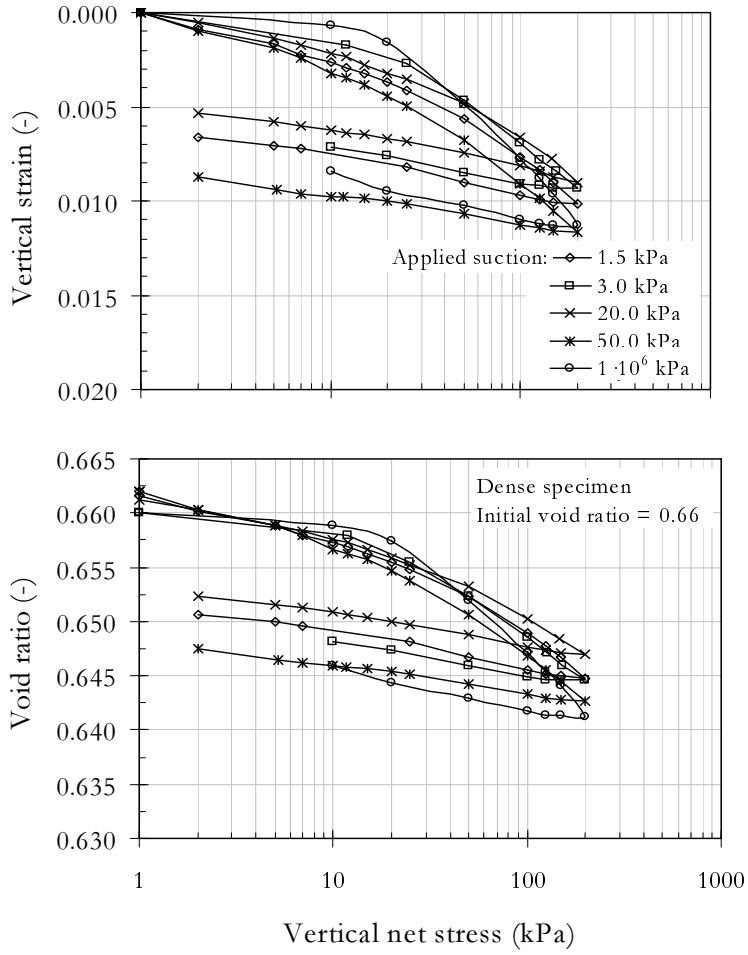

Figure 6.16: Experimental results of one dimensional compression rebound test for constant suction condition (dense specimen)

to the results performed under saturated condition, because the corresponding volumetric water content or saturation is close to zero under this condition (see for instance experimental result of soil-water characteristic curve for loose an dense specimen in Fig. 6.2 during drainage process). From the observations it can be concluded that with increasing suction the stiffness is increasing but after reaching an certain suction value the stiffness is decreasing again. Comparing the unloading path of all tests one can state, that there is a similar behavior for all the specimens. The curves are almost parallel.

6.4.2 Collapse Behavior

Results of oedometer tests for estimation of collapse potential are presented in Fig. 6.17 for Method 1 (left) and Method 2 (right) for loose Hostun sand samples. Volumetric strain versus

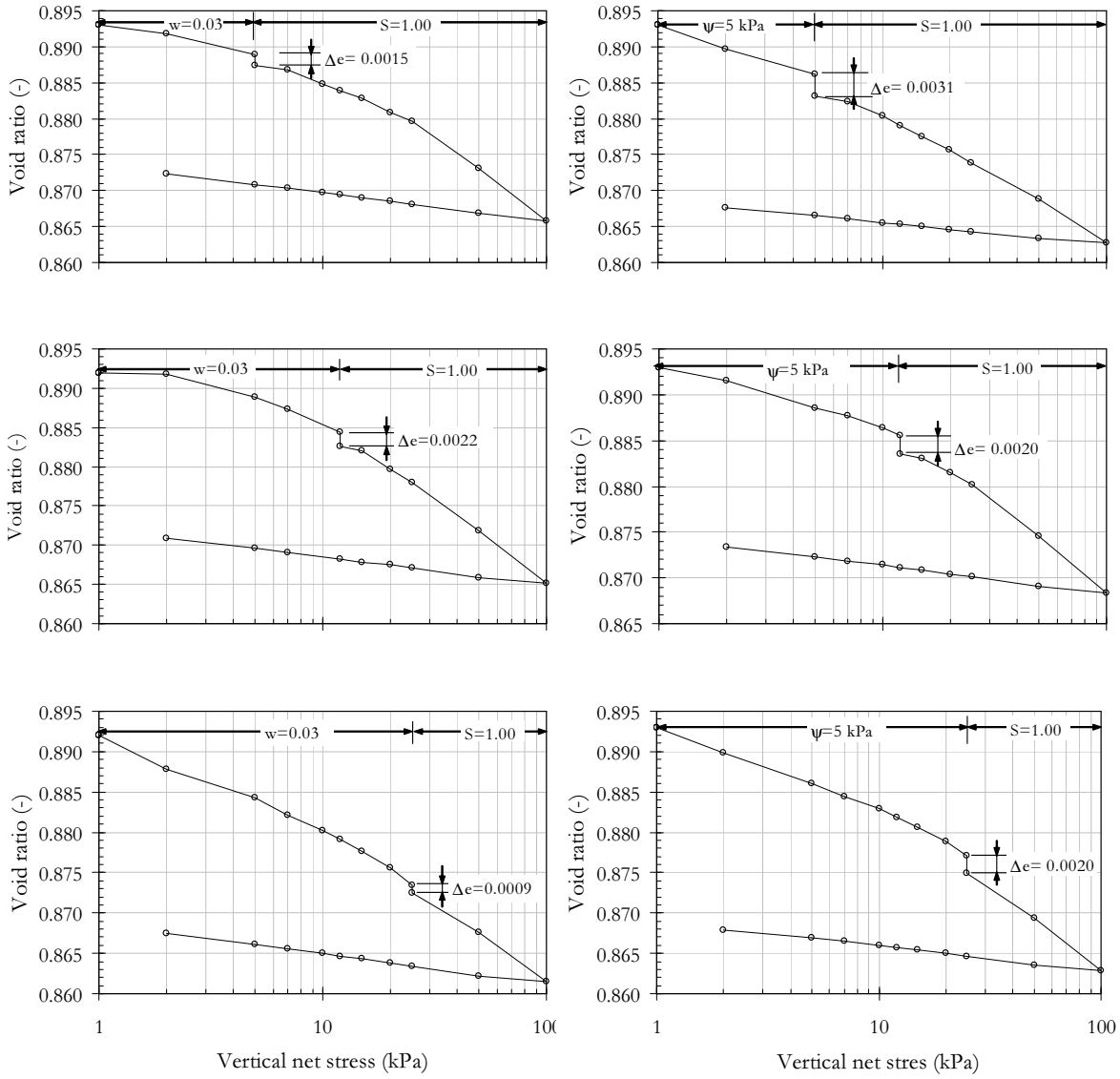

Figure 6.17: Experimental results of collapse potential for loose specimen - Method 1 (left) and Method 2 (right)

applied vertical net stress as well as void ratio versus applied vertical net stress results are presented. The overall behavior is, that the collapse potential of Hostun Sand seems to be small, when saturation process is carried out at vertical net stress $\sigma = 5, 12$ and 25 kPa. Results from Method 1 show differences in void ratio of $\Delta e = 0.0015$ for saturation at $\sigma = 5$ kPa, $\Delta e = 0.0022$ for saturation at $\sigma = 12$ kPa and difference in void ratio of $\Delta e = 0.0009$ for saturation at $\sigma = 25$ kPa. Results from Method 2 show differences in void ratio of $\Delta e = 0.0031$ for saturation at $\sigma = 5$ kPa, $\Delta e = 0.0020$ for saturation at $\sigma = 12$ kPa and difference in void

ratio of $\Delta e = 0.0020$ for saturation at $\sigma = 25$ kPa. Regarding the stiffness behavior before and after the saturation process it seems, that before saturated condition in the specimen the stiffness is higher. But calculations of compression index and stiffness modulus are required for proper conclusions. Results of the compression index and stiffness modulus are presented later in Chapter 7.

6.5 Summary

This chapter presents the results derived from the experiments performed. The experimental results from the column testing devices (i.e. volumetric water content and pore-water pressure versus time results and suction-water content results), the modified pressure plate apparatus (i.e. cumulative water outflow/inflow data, changes in void ratio and soil-water characteristic curves) as well as the controlled-suction oedometer cell (i.e. strain versus vertical net stress, void ratio versus vertical net stress) are presented and discussed.

The investigations on Hostun sand performed in the modified pressure plate apparatus and in the sand column testing devices I an II show, that the void ratio as well as the loading path direction (i.e. drainage or imbibition path) influence its hydraulic behavior. Derived soil-water characteristic curves established from steady state approach and transient state approach show quantitative similar behavior. The influence of net stress on the hydraulic behavior of unsaturated sand is found to be negligible. All cells enable to measure directly the soil-water characteristic curve. The unsaturated hydraulic conductivity can be directly determined using pore-water pressure and volumetric water content profiles measured during sand column testing devices I experiments.

The investigations carried out in the controlled-suction oedometer cell show, that not only the void ration but also the suction influences the stiffness behavior of unsaturated Hostun sand. The collapse potential was found to be small.

Chapter 7

Analysis and Interpretation of the Experimental Results

7.1 General

Based on the experimental results the hydro-mechancial behavior of unsaturated Hostun sand is analyzed and interpreted. Both the hydraulic functions, soil-water characteristic curve as well as unsaturated hydraulic conductivity and the influence of suction on the volumetric mechanical behavior is analyzed and interpreted.

In the present study experimental soil-water characteristic curve results are best fitted using empirical and physical models proposed in literature. For prediction of the model parameters suction-water content results are best fitted using residual analysis. Due to hysteresis behavior during drainage and imbibition, that also results in fitting scanning curves (e.g. scanning imbibition curves measured in sand column testing device I experiments), it is a laborious procedure, when using models that do not consider hysteresis. Therefore a method is introduced and implemented in Chapter 8 for an appropriate model that considers scanning imbibition curves.

Attention is also paid to the volumetric mechanical behavior that includes the influence of suction on the compression index and the stiffness modulus respectively and the collapse potential. An equation that considers suction, when calculation the stiffness modulus is proposed. Further it is investigated if the applied suction influences the soils history in case of preconsolidation pressure.

7.2 Soil-Water Characteristic Curve

The empirical equations (Eq. 2.9 to 2.11) introduced in Chapter 2 were used for determination of the soil-water characteristic curve. Following the statistical assessment described below in detail, best fit between experimental results (observed values) and the soil-water characteristic curve model (predicted values) was estimated.

Soil-water characteristic curves were predicted for several void ratios (loose and dense condition), different flow paths (drainage, imbibition and scanning paths) and also under different flow conditions (steady state and transient state condition). Taking these conditions into account the results are compared in the following sections. The curves derived from best fitting procedure are used for the comparison.

7.2.1 Residual Analysis

Soil-water characteristic curve is used in numerical simulation and for indirect estimation of unsaturated hydraulic conductivity, the relationship between volumetric water content and suction $\theta(\psi)$ or also quite often saturation and suction $S(\psi)$ is required. In the case of the indirect method for determining the unsaturated hydraulic conductivity function, the soil-water characteristic curve is used as basis for these calculations. Therefore it is important that the soil-water characteristic curve is accurately fitted. The curve fit is sensitive at points such as the air-entry value, the water-entry value as well as the residual water content and the residual suction.

It was mentioned before, that for solving the non-linear least-square regression problem the Levenberg-Marquardt algorithm (see Eq. 3.3) is used. Further statistical techniques as plots of predicted versus observed values and residual versus observed values were used for validation of the models. The observed values correspond to the experimental data (i.e. measured volumetric water content) and the predicted values correspond to the calculated data (i.e. calculated volumetric water content). From statistical point of view good set of parameters is found, when the results in the plot of predicted versus observed values are close to the bisection line $f(x) = x$. Indicating that the predicted value is similar to the observed value. If the points are located above the bisection line the observed values are underestimated by the predicted values and if the points are located beneath the bisection line the observed values are overestimated by the predicted values. The plot of residual (difference between observed and predicted value) and observed values should be randomly distributed above and below the line of $f(x) = 0$. Then the errors are randomly distributed over the measurement range. The coefficient of regression determination R^2 was also determined. A coefficient of $R^2 = 1$ means that the observed values are equal to predicted values and the error is equal to zero. Thus if R^2 is converging to 1 a good fit is found.

Exemplary results from the statistical analysis given in Fig. 7.1 as well as 7.2 show observed values (left) and the residuals (right) plotted versus predicted values derived from drainage as well as imbibition experiment carried out in the modified pressure plate apparatus for the loose specimens. The coefficient of regression determination R^2 is also given in the diagrams. Results are given in order of using the equation by Brooks and Corey (Eq. 2.9), van Genuchten with the assumption m is a non-flexible parameter $m = 1 - 1/n$ (Eq. 2.10a), van Genuchten with flexible parameter m (Eq. 2.10b) and Fredlund and Xing (Eq. 2.11).

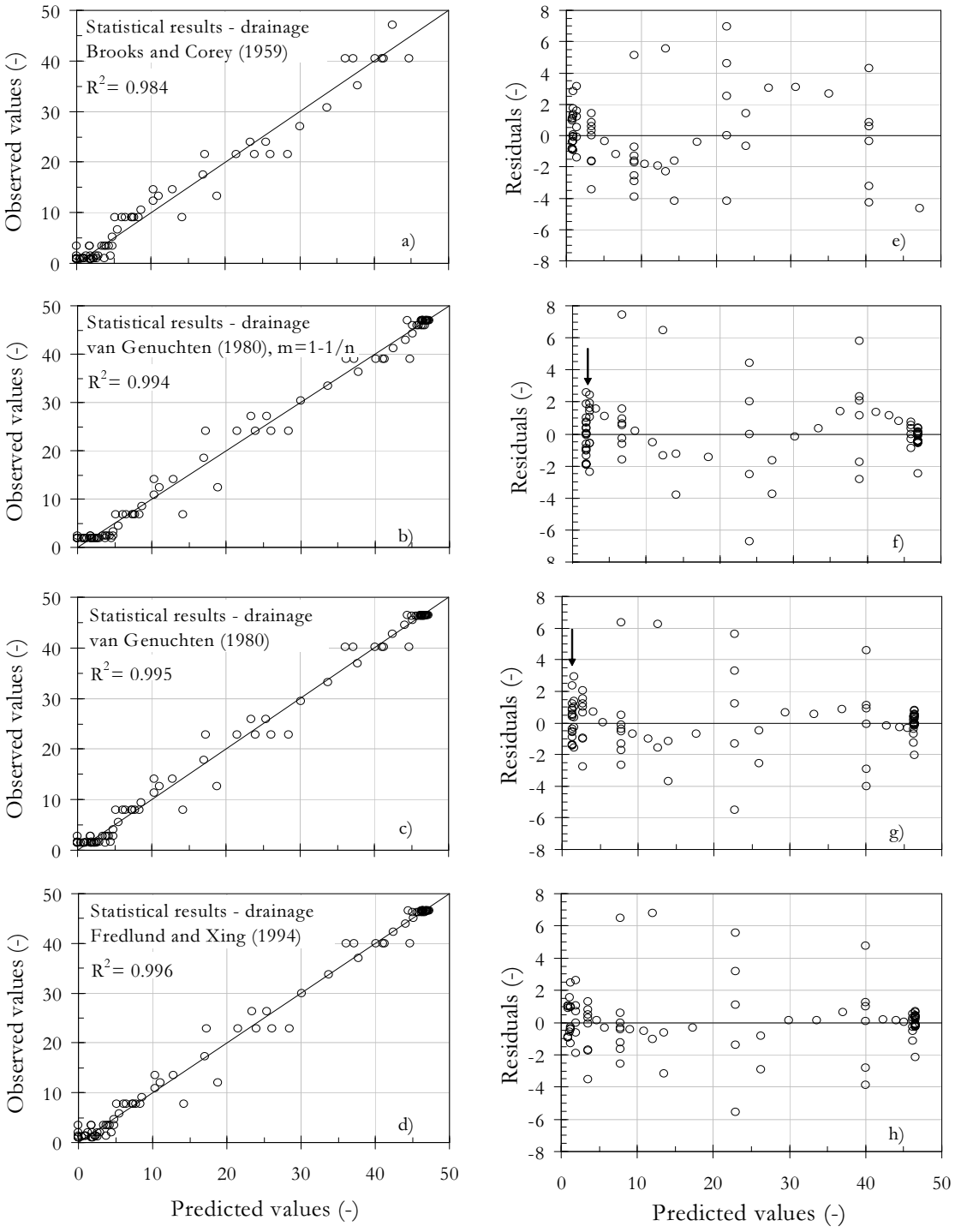

Figure 7.1: Statistical assessment of best fit results using several suction-water content models for drainage process from modified pressure plate apparatus (loose specimens, steady state test)

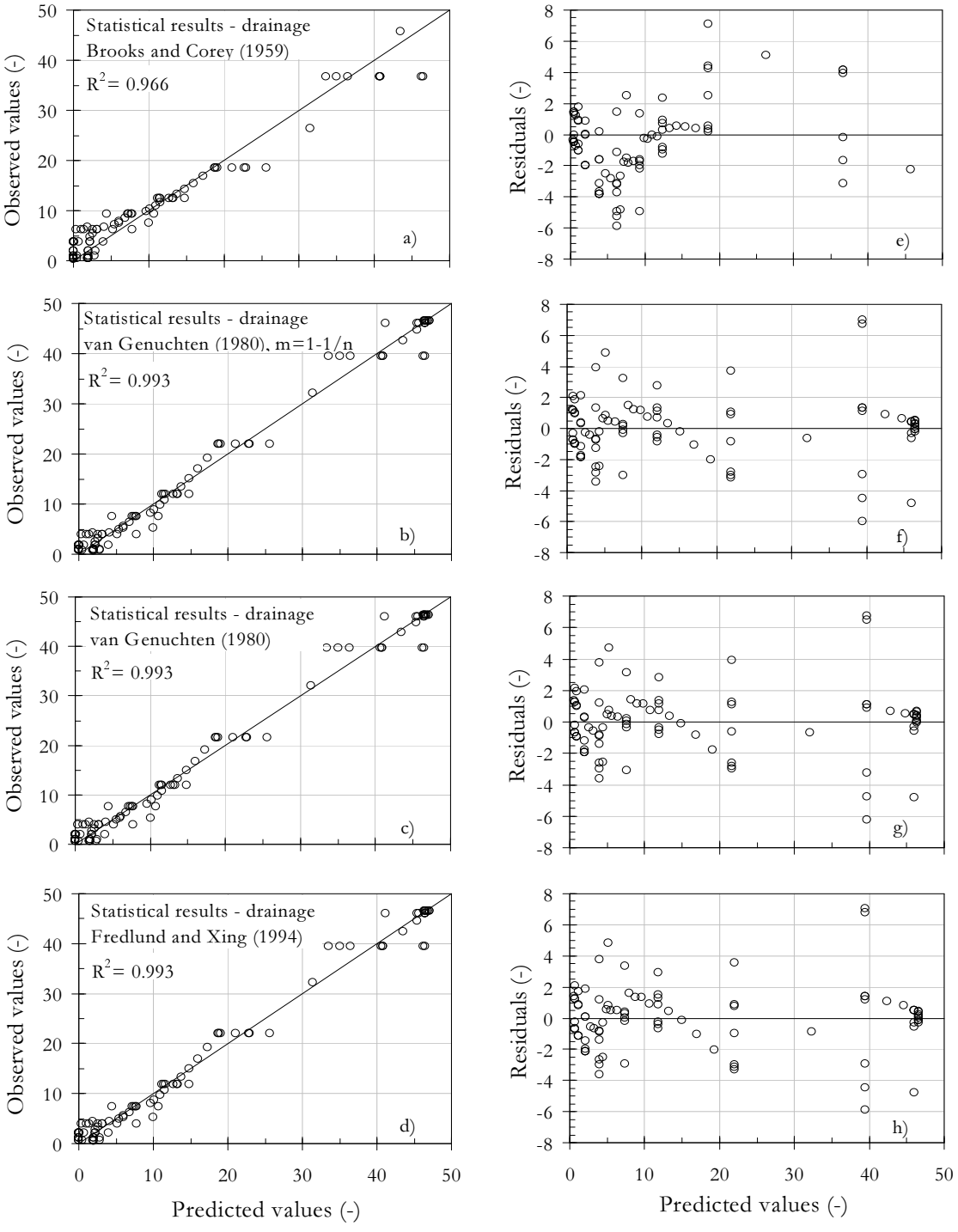

Figure 7.2: Statistical assessment of best fit results using several suction-water content models for imbibition process from modified pressure plate apparatus (loose specimens, steady state test)

In Fig. 7.1 a) to d) the overall impression is that the points are close to the bisection line in the diagrams of observed and predicted values. As closer the points to the bisection line $f(x) = x$ in the diagrams of observed versus predicted values as better the result of the curve fit. Using Brooks and Corey's (1964) power-law relationship saturated volumetric water contents are not considered in the best-fit procedure and statistical analysis. This equation is not valid in the saturated zone and is only applicable for suctions larger than air-entry value ($\psi > \psi_{aev}$), that corresponds to volumetric water contents smaller than saturated volumetric water content ($\theta < \theta_s$). Due to sudden increase in volumetric water content after reaching the air-entry value up to the residual water content, points are concentrated mainly at low values (see Fig 7.1 a) to d)) as well as high values (see Fig 7.1 b) to d)) that corresponds to volumetric water contents in the residual zone and respectively to saturated volumetric water contents. For low volumetric water contents good agreement between observed and predicted values was found for all model functions. At larger volumetric water contents between $\theta = 7\%$ to 20% for the most results the observed values are overestimated by the predicted values when using Brooks and Corey's (1964) model function and van Genuchten's (1980) model including $m = 1 - 1/n$. Except two points that are far underestimated by all model functions. Best agreement in the range of $\theta = 7\%$ to 20% was found for van Genuchten's (1980) and Fredlund and Xing's (1994) model. Using Brooks and Corey's (1964) equation for volumetric water content between $\theta = 20\%$ to 46 the most experimental values are underestimated by the predicted values. Even the points are closer to the bisection line in Fig 7.1 this trend can be observed also when using van Genuchten's (1980) equation considering $m = 1 - 1/n$. In this range best agreement between observed and predicted values was found for van Genuchtens (1980) as well as Fredlund and Xing's (1994) model function. At all the results are closest to the bisection line using Fredlund and Xing's (1994) model, which means that the observed values are similar to predicted values. This is also expressed by the coefficient of regression determination $R^2 = 0.996$. The plot of residuals versus predicted values should be randomly distributed above and below the line of $f(x) = 0$. The diagrams are given in Fig. 7.1 e) to h) respectively. The diagrams in Fig. 7.1 e) to h) show that for low volumetric water contents $\theta = 0\%$ to $\theta = 10\%$ the points are best scattered, when using Brooks and Corey's (1964) and Fredlund and Xing's (1994) model for fitting procedure. Mainly when using both van Genuchten's (1980) equations vertical orientation of points was found in the residual zone. In the range of $\theta = 10\%$ to $\theta = 46\%$ the results are randomly distributed.

Results derived from statistical analysis of fitting procedure from imbibition data (see Fig 7.2) show that observed and predicted values are in good agreement for fitting procedure using both van Genuchten's (1980) and Fredlund and Xing's (1994) model functions. This is also reflected in the coefficient of regression determination $R^2 = 0.993$. Results are randomly distributed in the plot of residual versus predicted values for all model functions. But for volumetric water contents $\theta = 20\%$ to 46% most points are located above the line of $f(x) = 0$ when using Brooks and Corey's (1964) function. This is also reflected in the underestima-

tion of the observed values in the plot of observed versus predicted values and in the lower coefficient of regression determination $R^2 = 0.966$.

All best fit results are given in Fig 7.3 for the loose specimens. Volumetric water content versus suction $\theta(\psi)$ and saturation versus suction $S(\psi)$ are shown. The best fitted curve derived from Brooks and Corey's (1964) function shows differences between the fit and experimental data in the region of the air-entry value (drainage process), in the residual zone (drainage process and imbibition process) and in the saturated zone (drainage process). However, the best fitted curve was derived by Fredlund and Xing's (1994) equation. Good agreement in the sensitive zones as air-entry value, residual zones, water-entry value was found. Thus Fredlund and Xing's (1994) equation is used for further best fit procedure and also for further analysis of unsaturated hydraulic conductivity (indirect method, statistical model). Best fit results derived from residual analysis from all the experimental data are summarized in Appendix B in Figs. B.1 to B.10. The soil-water characteristic curves are plotted as volumetric water content versus suction as well as saturation versus suction. For further interpretation and analysis of the results the best fitted of soil-water characteristic curves are used.

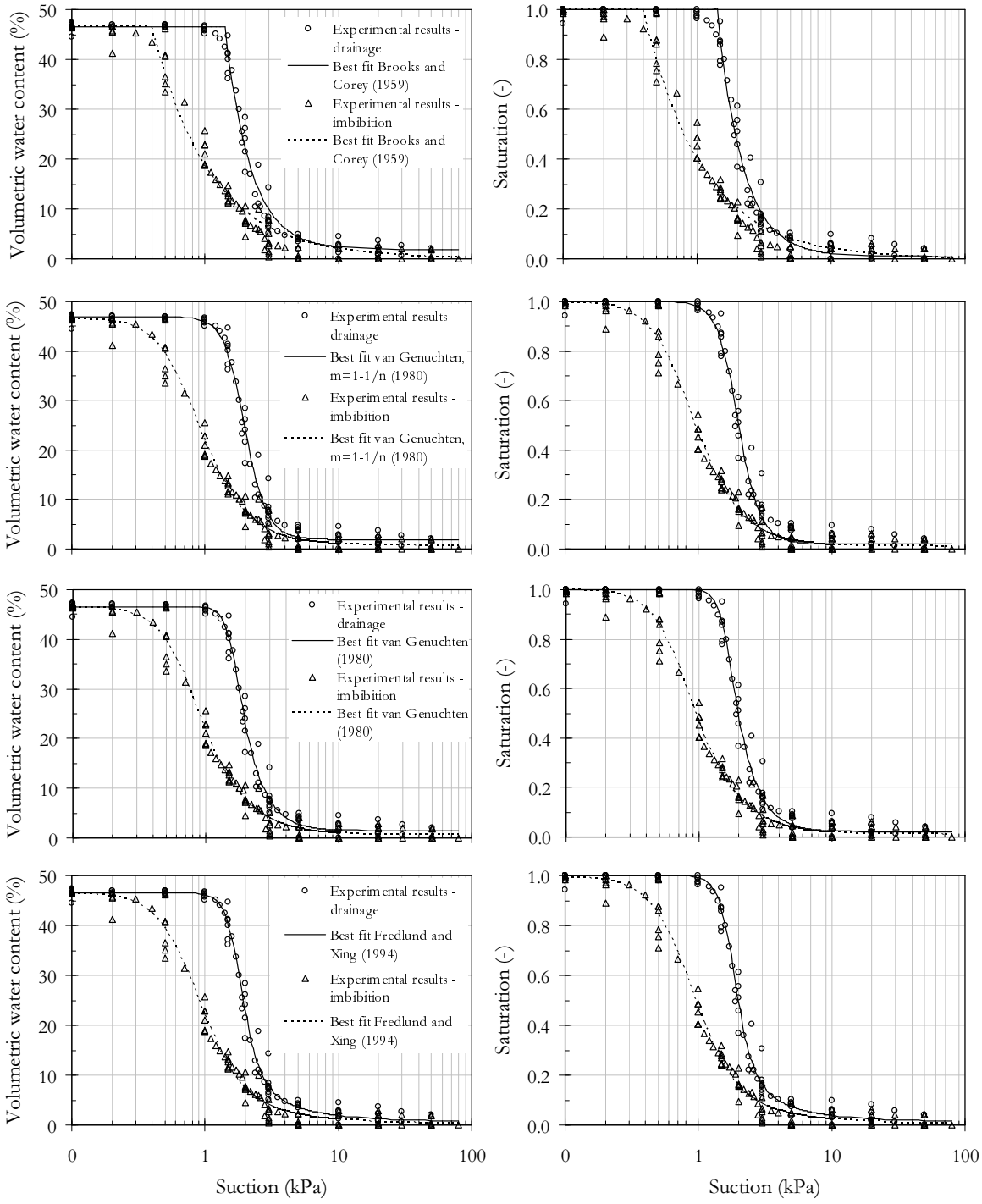

Figure 7.3: Comparison between experimental results and best fitted relations derived from several suction-water content models for drainage and imbibition process from modified pressure plate apparatus (loose specimens, steady state test)

7.2.2 Steady State Test Results

For interpretation and comparison of the results typical soil-water characteristic curve parameters as the air-entry value, the saturated volumetric water content and the residual volumetric water content with the corresponding residual suction were estimated. According to Fredlund and Xing (1994) these parameters were graphically determined.

For the soil-water characteristic curve determined in the modified pressure plate apparatus (see also Fig B.1 and B.2 for loose and dense specimen in Appendix B) an air-entry value of approximately $\psi_{aev} = 1.4$ kPa was found for the loose specimen. This value is smaller then that for the dense specimen which is about $\psi_{aev} = 1.9$ kPa. After reaching the air-entry value the water content decreases along a narrow range of suction for both sand specimens. The transition zone is between $\psi_{aev} = 1.4$ kPa to $\psi_r = 2.8$ kPa ($\theta_r = 5\%$) for the loose specimen and between $\psi_{aev} = 1.9$ kPa to $\psi_r = 3.3$ kPa ($\theta_r = 2\%$) for the dense specimen. The residual zone starts at a relatively low suction value for the drainage cycle for the dense specimens and the loose specimens. Along the imbibition path there is no significant change in water content measured in a range from approximately 50.0 kPa to 3.0 kPa. The transition zone for loose specimen starts at a water-entry value $\psi_{wev} = 2.8$ kPa and for the dense specimen at a water-entry value $\psi_{wev} = 3.3$ kPa. For the loose specimen the transition zone extends up to 0.27 kPa and up to 0.5 kPa for the dense specimen. The saturated zone falls in a relatively narrow range for both dense and loose specimens.

The experimental results of the steady state column tests I and best fitted curves are shown for loose and dense specimens in Fig. B.3 and B.4. The specimens are initially water saturated ($\theta_{s,loose} = 46\%$, $\theta_{s,dense} = 40\%$). After imbibition process both specimen do not reach complete saturation due to occlusion of air in the specimens voids. The saturated volumetric water content after imbibition process is $\theta_s' = 39\%$ for the loose specimen and $\theta_s' = 37\%$ for the dense specimen. While the loose specimen starts to drain approximately at an air-entry value $\psi_{aev} = 1.2$ kPa the dense specimen starts to drain at $\psi_{aev} = 1.9$ kPa (saturated zone). The residual suction is equal to $\psi_r = 2.8$ kPa with a corresponding residual volumetric water content $\theta_r = 4\%$ for the loose and $\psi_r = 3.2$ kPa and $\theta_r = 6\%$ for the dense specimen. In a narrow range of suction the volumetric water content is decreasing beginning from the air-entry value to the residual suction (transition zone). The residual zone starts at low suction value of $\psi_r = 2.8$, $\theta_r = 4\%$ for the loose and $\psi_r = 3.2$, $\theta_r = 6\%$ for the dense specimens. Influenced by occluded air after imbibition process apparent saturated volumetric water content of $\theta_s' = 39\%$ for loose and $\theta_s' = 37\%$ for dense specimen were achieved.

Influence of void ratio

Loose and dense soil-water characteristic curves are compared in Fig 7.4, that includes the main drainage (here the initial drainage curve is equal to the main drainage curve because after imbibition process fully saturated specimen was derived again) and imbibition loop

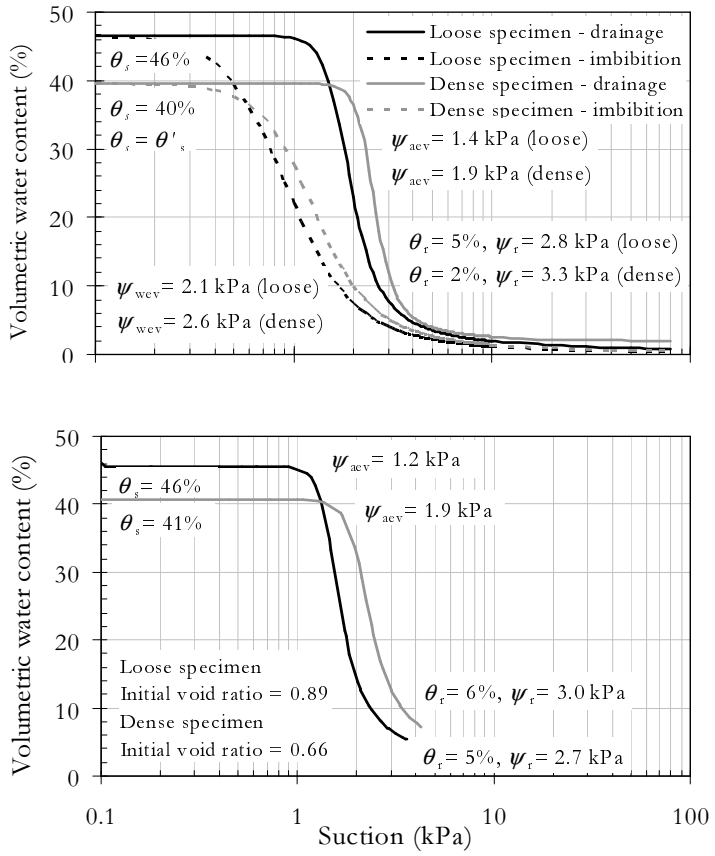

Figure 7.4: Influence of void ratio on the shape of the soil-water characteristic curve (steady state tests)

derived from modified pressure plate apparatus and the initial drainage curve derived from sand column test I. As can be observed from the curves the void ratio is influencing the shape of both, the drainage and the imbibition curve. The saturated volumetric water content of the loose specimens is larger then for the dense specimens ($\theta_{s,loose} > \theta_{s,dense}$). Here the larger voids of the loose specimen retain larger amount of water. Overall behavior is that with decreasing void ratio the soil-water characteristic curve is shifting to slightly higher suction values. This leads to higher air-entry value, residual suction as well as residual volumetric water content during drainage path and also higher water-entry value during imbibition path. Due to the smaller voids in the dense specimen the water is retained up to higher suction values ($\psi_{aev,dense} > \psi_{aev,loose}$) when draining the saturated specimen. However, this is also causing higher residual volumetric water contents ($\theta_{r,dense} > \theta_{r,loose}$) for the dense specimens. When wetting the specimen the smaller voids of the dense specimens do absorb water at slightly higher suction values than loose specimens ($\psi_{wev,dense} > \psi_{wev,loose}$). The saturated volumetric water content θ_s is reached first for the dense specimen.

Influence of loading path direction

Influence of loading path direction, i.e. main drainage and imbibition process was investigated in the modified pressure plate apparatus and in sand column test I, where the imbibition results are scanning imbibition curves. These results are given in Fig. 7.5. The main imbibition and drainage curves show significant influence of loading path on the shape of the suction-water content curves. Draining and imbibition processes of the specimen show non-unique behavior. For a suction value the corresponding volumetric water content (degree of saturation, water content) during imbibition process is smaller than during drainage process. The curves are characterized by the phenomena of hysteresis. The scanning imbibition curves are located between the main drainage and imbibition loop.

Whereas after imbibition procedure an initially saturated specimen was reached again for the tests performed in the modified pressure plate apparatus, in the sand column test I an initially saturated specimen was not reached ($\theta'_{s,loose} = 39\%, \theta'_{s,dense} = 37\%$). The results are characterized by occluded air.

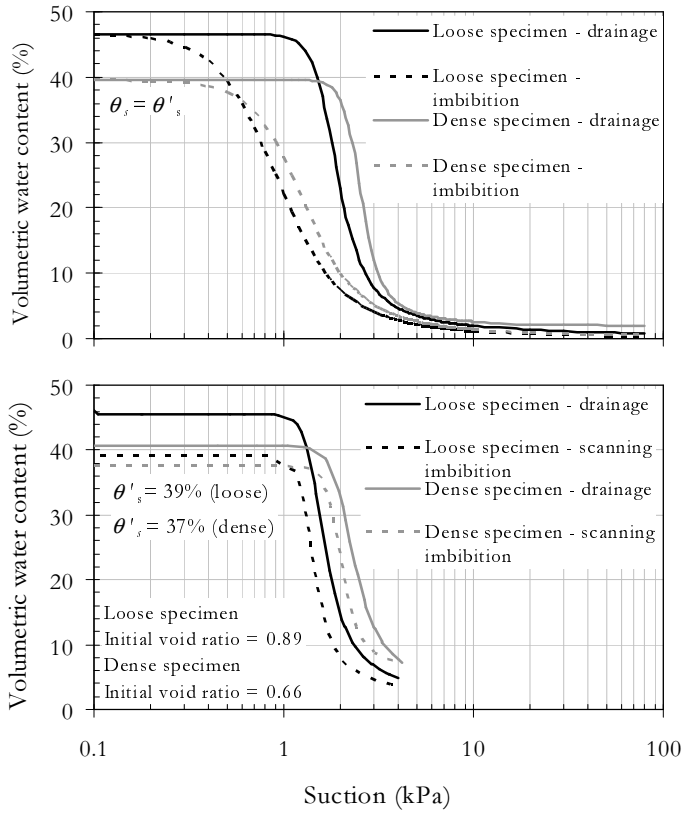

Figure 7.5: Influence of loading path direction (drainage, imbibition process) on the shape of the soil-water characteristic curve (steady state tests)

Influence of net stress

In contrast to cohesive soils the influence of net stress on the shape of the soil-water characteristic curve is small for Hostun sand as can be seen in Fig. 6.4. Changes in void ratio are negligible small during the whole experimental procedure. After saturation process and after application of net stress main changes in void ratio take place. While wetting the sand specimen with water small changes in settlements were measured and thus no significant changes in void ratio were observed.

7.2.3 Transient State Test Results

The experimental results of sand column tests I and the best curve fits respectively are given in in Appendix B in Figs. B.5 to B.8 for loose and dense specimens. Soil-water characteristic curves $\theta(\psi)$ and $S(\psi)$ are presented for the tests performed under transient state condition with a flow rate of 30 ml/min as well as 100 ml/min. The saturated volumetric water content is $\theta_s = 46\%$ for the loose specimen and $\theta_s = 39\%$ for the dense specimen under initially saturated condition. Caused by the occluded air after first imbibition process the saturated volumetric water content reduces to $\theta'_s = 39\%$ for the loose specimen and $\theta'_s = 35\%$ for the dense specimen. For the experimental results of the transient state test an air-entry value of approximately $\psi_{aev} = 1.6$ kPa was found for the loose specimen and $\psi_{aev} = 2.1$ kPa for the dense specimen. Up to the air-entry value the soil-water characteristic curve is located in the saturated zone. After reaching the air-entry value, the water content decreases rapidly for both sand specimens and reaches the transition zone. The transition zone is between $\psi_{aev} = 1.6$ kPa to $\psi_r = 2.7$ kPa ($\theta_r = 5\%$) for the loose specimen and between $\psi_{aev} = 2.1$ kPa to $\psi_r = 3.0$ kPa ($\theta_r = 6\%$) for the dense specimen. The residual zone starts at a relatively low suction value in the drainage cycle for both sand specimens.

In Fig. B.9 and B.10 the experimental results and the curve fits of the transient state tests performed in the column testing device II are shown. A saturated volumetric water content of $\theta_s = 47\%$ was measured for the loose specimen and $\theta_s = 41\%$ for the dense one. The volumetric water content is not changing till reaching the air-entry value, that is $\psi_{aev} = 1.7$ kPa for the loose specimen and $\psi_{aev} = 1.9$ kPa for the dense specimen (saturated zone). When passing the air-entry value the volumetric water content is rapidly decreasing and the soil reaches unsaturated condition. The transition zone extends from the air-entry value up to residual suction and the residual volumetric water content of $\psi_r = 3.6$ and $\theta_r = 6\%$ for the loose specimen and $\psi_r = 3.8$ and $\theta_r = 8\%$ for the dense specimen. Similar to all derived results the residual zone begins at low suction value.

Influence of void ratio

Soil-water characteristic curves derived for dense and loose specimen from transient state tests are presented in Fig. 7.6. Similar to the steady state tests a decrease in void ratio causes a shift of the soil-water characteristic curve to larger suction values (i.e. $\psi_{aev,dense} > \psi_{aev,loose}$, $\theta_{r,dense} > \theta_{r,loose}$).

Influence of loading path direction

Similar to the steady state tests the drainage and imbibition curves derived from transient state test are not unique (see also Fig 7.7). The imbibition curves measured in different depths at different conditions on the main drainage curve are found to be scanning imbibition curves. For the loose and the dense specimens the imbibition scanning curves measured in the upper part of the sand specimen start at a higher suction value than the imbibition scanning curves measured in the lower part of the sand specimen. These curves are located within the main drainage-imbibition hysteresis.

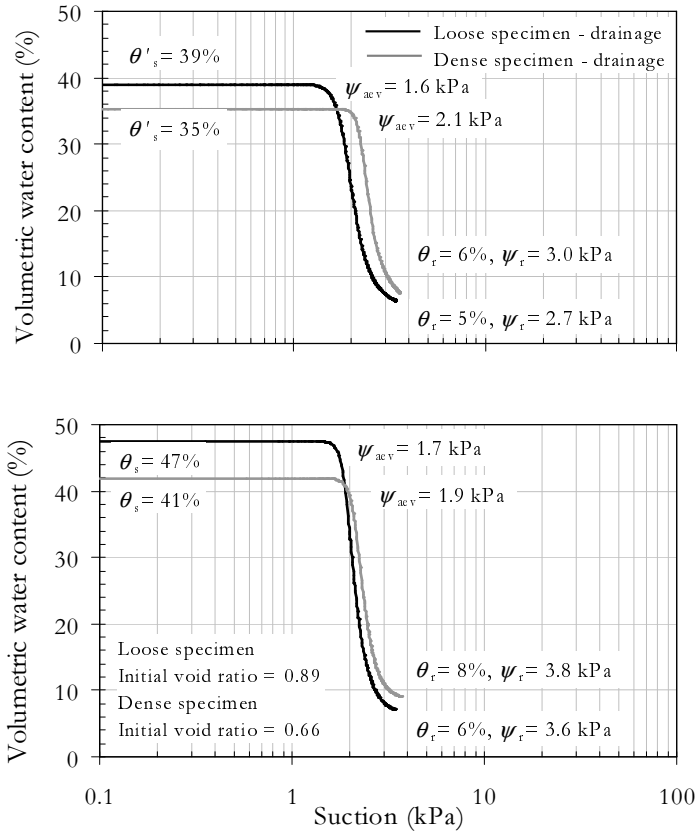

Figure 7.6: Influence of void ratio on the shape of the soil-water characteristic curve (transient state tests)

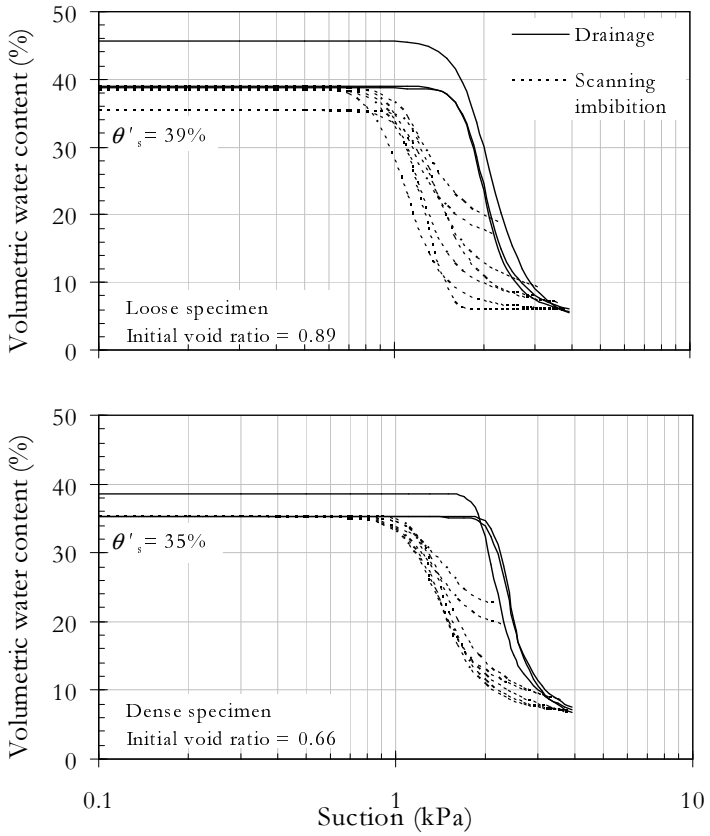

Figure 7.7: Influence of loading path direction (drainage, imbibition process) on the shape of the soil-water characteristic curve (transient state tests)

Due to occluded air bubbles the initial saturated volumetric water content is not achieved after subsequent imbibition process. The occurrence of occluded air in the sand column tests I (transient state test) shows differences ranging from $\theta_s = 46\%$ to $\theta'_s = 39\%$ for loose specimen and from $\theta_s = 39\%$ to $\theta'_s = 35\%$ for dense specimen. However, also the tests performed in the same testing device (sand column test I) but under steady state condition give similar results (see Fig. 7.5). The dense specimens show the phenomenon of occluded air to have a minor effect because the pores of the dense specimens are smaller and therefore the volume of occluded air appears to be smaller than for the loose specimens.

The phenomena of occluded air bubbles was not found to be significant for the results observed from the modified pressure plate apparatus (see also Fig. 7.5). The occurrence of occluded air in the modified pressure plate apparatus tests (steady state tests) has less effect than in the sand column tests I (transient state and steady state tests). The modified pressure plate apparatus tests were performed in a small scale apparatus and the sand column tests I were performed in large scale column. It appears that the size of the equipment influences the relative effect of occluded air.

Influence of flow condition

The drainage curves derived from transient state tests, that were performed under several flow conditions are shown in Fig. 7.8. For better view the plots are not given in logarithm form. Even a slow flow rate of 30 ml/min, a fast flow rate of 100 ml/min and air pressure $u_a = 3.5$ kPa were induced to the sand specimen no significant change or shift of the soil-water characteristic curve for both the loose and dense specimen was observed. It seems that the soil-water characteristic curve parameters (the parameter of the saturated volumetric water content is not taken into account due to presence of occluded air) are similar for drainage curves performed with a flow rate $\approx$ 30 ml/min, with a flow rate $\approx$ 100 ml/min and under applied air pressure $u_a = 3.5$ kPa. The so called dynamic effect was not found to be significant for Hostun sand.

Imbibition curves were also performed under several flow conditions (30 ml/min and 100 ml/min), but can not be compared due to different initial condition when starting the imbibition process.

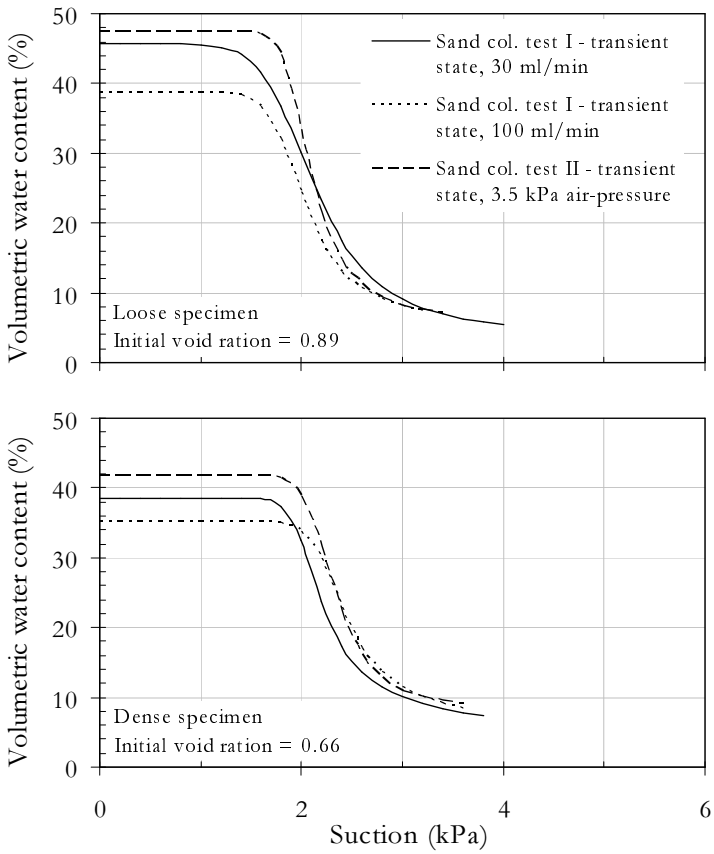

Figure 7.8: Influence of flow condition on the shape of the soil-water characteristic curve

7.2.4 Comparison of Steady State and Transient State Results

For investigation of the influence of flow condition on the shape of the soil-water characteristic curve, steady state tests were performed in the modified pressure plate apparatus and also in the sand column testing device I. Transient state tests were performed in sand column test I, where 2 different flow rates were applied to the sand specimen and in sand column test II, where air pressure was applied to the top of the sand specimen. Steady state as well as transient state drainage curves results are shown in Fig. 7.9. Neither for the loose specimens nor for the dense specimens significant influence of flow condition on the shape of the soil-water characteristic curve was observed. Soil-water characteristic curve parameters derived from all experiments are summarized in Tab. 7.1 for loose and dense specimens. Values as the air-entry value or the residual suction are in the same range for each the loose as well as dense specimens. Thus the dynamic effect is not influencing the shape of the soil-water characteristic curve for the investigated material. The drainage soil-water characteristic curve

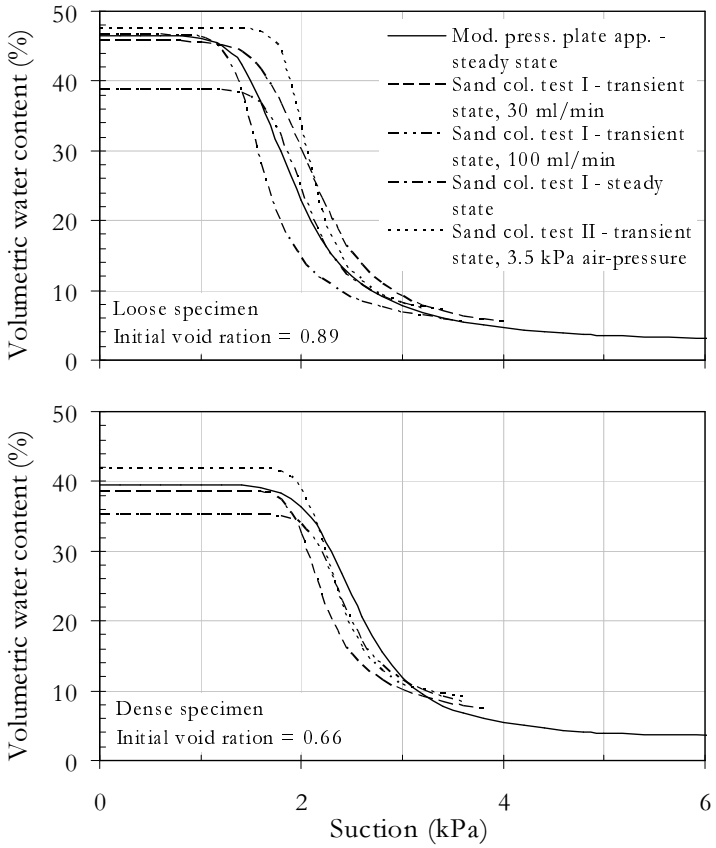

Figure 7.9: Influence of flow condition (steady state, transient state flow) on the shape of the soil-water characteristic curve

Table 7.1: Soil-water characteristic curve parameters

Cell	Test method	θ_s (%)	ψ_{aev} (kPa)	θ_r (%)	ψ_r (kPa)	ψ_{wev} (kPa)	$\theta_s^{'}$ (%)
	Loose specimen						
MPPA	Steady state	46	1.4	5	2.8	2.1	46
SCI	Steady state	46	1.2	5	2.7	-	39
SCI	Transient state	46	1.6	5	2.7	-	39
SCII	Transient state	47	1.7	6	3.6	-	-
	Dense specimen						
MPPA	Steady state	40	1.9	2	3.3	2.6	40
SCI	Steady state	40	1.9	6	3.0	-	37
SCI	Transient state	39	2.1	6	3.0	-	35
SCII	Transient state	41	1.9	8	3.8	-	-

parameters determined under steady-state condition are close to the results from the transient state tests. Slight differences may be due to measurement errors.

7.3 Hysteresis

As introduced in Chapter 2 a number of model equations have been proposed for the soil-water characteristic curve. When dealing with unsaturated soils, it is essential to take the phenomena of hysteresis into account. Because for a certain suction value the volumetric water content (water content or saturation) during drainage is not equal to the water content during imbibition. Thus involving non-unique unsaturated hydraulic conductivity, stiffness or shear strength for a certain suction value among drainage and imbibition path.

In the following several hysteresis models are used for determination of soil-water characteristic curve. Advantages and disadvantages are discussed. Finally in Chapter 8 a newly developed soil-water characteristic curve model is introduced, that accounts for hysteresis in soil-water characteristic curve and scanning curves.

7.3.1 Hysteretic Soil-Water Characteristic Curve Model by Zou (2003, 2004)

Hysteresis model by Zou (2003, 2004) was used for fitting experimental saturation-suction results including one scanning drainage and imbibition loop derived from modified pressure plate apparatus for a loose specimen (see Fig. 6.3). The model proposed by Zou defines the relationship between saturation and suction (see Equations in Appendix A). The best fit of the experimental results is given in Fig. 7.10, where the experimental as well as calculated results are plotted. Due to the complexity of the model the best fit was found by using an inverse

analysis, where experimental and calculated results were compared with an optimization routine (VARO^{2}PT) developed by Zimmerer & Lobers (2005). In a first step the parameters are set by conventional means followed by a first simulation. Based on the estimated parameter set the difference between experimental and calculated results are determined. Then the objective function of the optimization routine is modified until the difference between the experimental and calculated results is minimized, which indicates the best fit (Zimmerer & Schanz 2006).

Good agreement between the experimental and the theoretically calculated results was found for the scanning drainage and scanning imbibition curves within the drainage-imbibition loop. During imbibition process the experimental results are close to the calculated results. Poor fit was found for the drainage curve, where nearly all experimental results are significantly underestimated by the model. Only at low and high suction values the calculated values converge to the experimental results. Particularly in the zone of the air-entry value, the unsaturated zone and the zone of residual suction the experimental results are underestimated. The calculated results are not in good agreement to the experimental result. It seems the model does not take into account the suction value, where water enters the pores and thus the pores start to drain.

Nevertheless the advantage of the model is, that with soil mechanical and geometrical parameters only, it enables the estimation of the hysteretic soil-water characteristic curve based on physical understanding. Disadvantages of the proposed model are the large number of parameters in the model, that are used for the estimation. Among parameters as maximum as well as minimum void ratio, $e_{min,max}$, or the surface tension of the capillary water, T, at all a set of additional 7 parameters has to be optimized for the determination of the relation

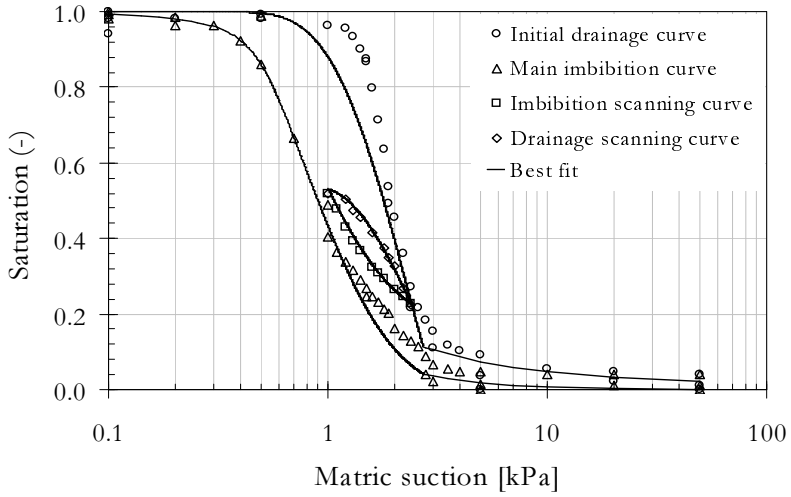

Figure 7.10: Experimental results of drainage and imbibition curve for loose specimen including best fit derived from Zou's model (2003, 2004)

between saturations and suction. These parameters are difficult to measure or they are not measurable at all (e.g. form parameter, ξ, material parameter, ζ, frustum number, η_{f0}).

7.3.2 Hysteretic Soil-Water Characteristic Curve Model by Feng & Fredlund (1999), Pham (2003)

Experimental results of water content and suction values from loose Hostun sand specimen carried out in the modified pressure plate apparatus were used for curve fit with Feng and Fredlund's (1999) model including the modifications proposed by Pham et al. (2003) (see Eqs. 2.13 to 2.15). Experimental results and calculated results are presented in Fig. 7.11 and the parameters derived from residual analysis are given in Tab. 7.2. The model fits the drainage curve well in the saturated zone and unsaturated zone, but differences between calculation and experimental results can be observed in the residual zone. The imbibition curve shows, that the calculated results are steeper than the experimental results. In the lower part of the water content-suction relationship the experimental results are underestimated and in the upper part the experimental results are overestimated by the calculated results.

Advantage of the model is, that the main drainage curve and only two measurements along the main imbibition curve are necessary to predict the entire range of the main drainage-imbibition loop. But using only two measurements points from the imbibition curve gives not the best agreement for Hostun sand between measured and calculated results. Scanning curves are not considered in the model.

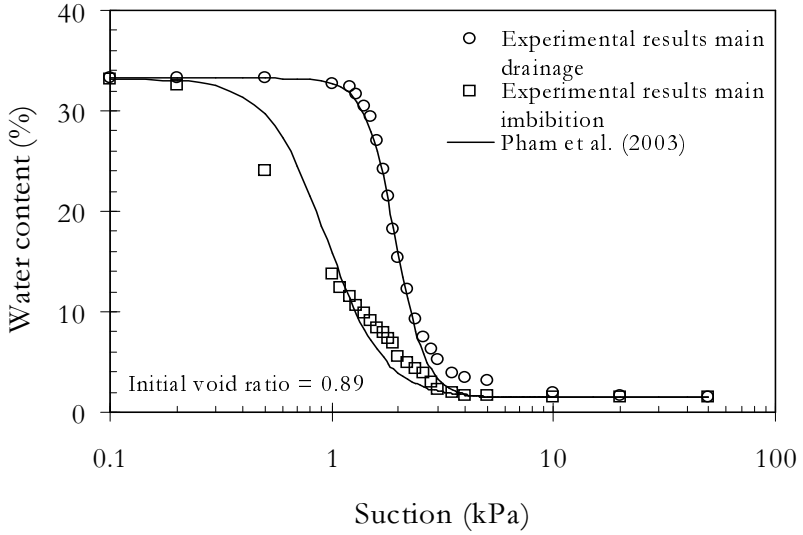

Figure 7.11: Experimental results of drainage and imbibition curve for loose specimen including best fit derived from Pham's model (2003)

Table 7.2: Constitutive parameters calibrated using the SWCC model by Pham et al. (2003)

Parameter	
$w_u(\%)$	33.22
$c(\%)$	1.24
b_d/b_w	64.57/0.83
d_d/d_w	6.29/3.27

7.4 Unsaturated Hydraulic Conductivity

For indirect calculation of unsaturated hydraulic conductivity statistical models (Eq. 2.20 to 2.22) introduced in Chapter 2 were used. As explained in detail in Chapter 2 the saturated conductivity, a best fitted soil-water characteristic curve (in this case the best fit from Fredlund & Xings (1994) model) as well as a statistical model are needed for indirect determination. Direct the unsaturated hydraulic conductivity was derived from tensiometer and TDR sensor measurements observed in the transient state sand column test I. However, the comparison of the measured soil-water characteristic curves showed, that significant influences to their shape is related to density and also flow path, but not to the flow condition (steady state test, transient state test). Therefore exemplary drainage and imbibition results derived from steady state modified pressure plate apparatus and transient state sand column tests I were used for calculation of unsaturated hydraulic conductivity. Whereas the results from the modified pressure plate apparatus were used for indirect method (statistical model) only, the measurements observed from the sand column test I were used additionally for direct method (instantaneous profile method).

Figure 7.12 gives the results of the unsaturated hydraulic conductivity functions for loose and dense sand specimens derived from modified pressure plate apparatus. In the saturated zone the hydraulic conductivity is only decreasing slightly till reaching the air-entry value. After reaching the air-entry value (the point where air starts to enter the largest pores), the unsaturated hydraulic conductivity decreases rapidly because the amount of water is dramatically decreasing due to the large and uniform pores of the Hostun sand. With increasing suction the flow path where water can flow becomes more tortuous and as a result the unsaturated hydraulic conductivity decreases. When reaching the residual zone where discontinuous water phase is present only as a thin layer on the sand grains, the unsaturated hydraulic conductivity tends to extremely low values and the remaining pore water is transported through vapor phase. Similar to the drainage path, along the imbibition path no relevant change in the unsaturated hydraulic conductivity could be observed in the residual zone. After reaching the water-entry value (the point where water starts to enter the smallest pores of the sand sample) during imbibition path, the unsaturated hydraulic conductivity increases along a narrow

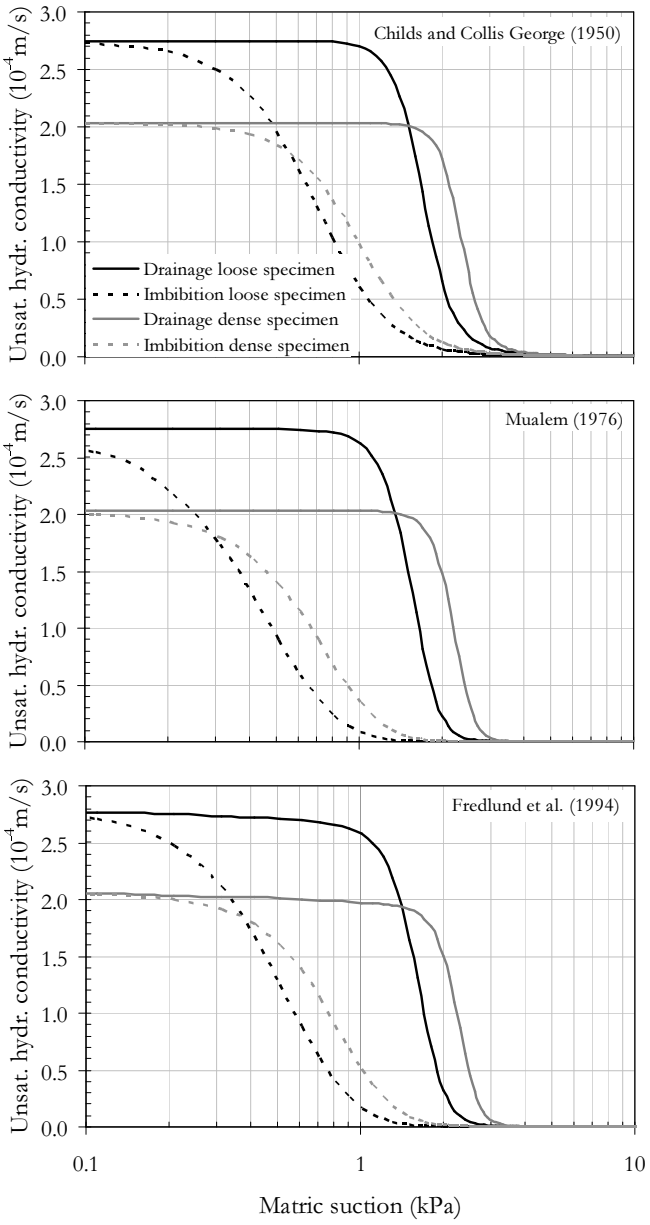

Figure 7.12: Unsaturated hydraulic conductivity from modified pressure plate apparatus (steady state test) determined by using statistical models (loose and dense specimen)

range of suctions up to the saturated zone. Drainage and imbibition hydraulic conductivity curves show the phenomenon of hysteresis.

The unsaturated hydraulic conductivity function was first estimated indirectly by using the best-fitted soil-water characteristic curve and the statistical models from sand column tests I. Figure 7.13 shows the results from the loose specimen and the dense specimen. Similar to the results achieved from modified pressure plate apparatus for both specimens the

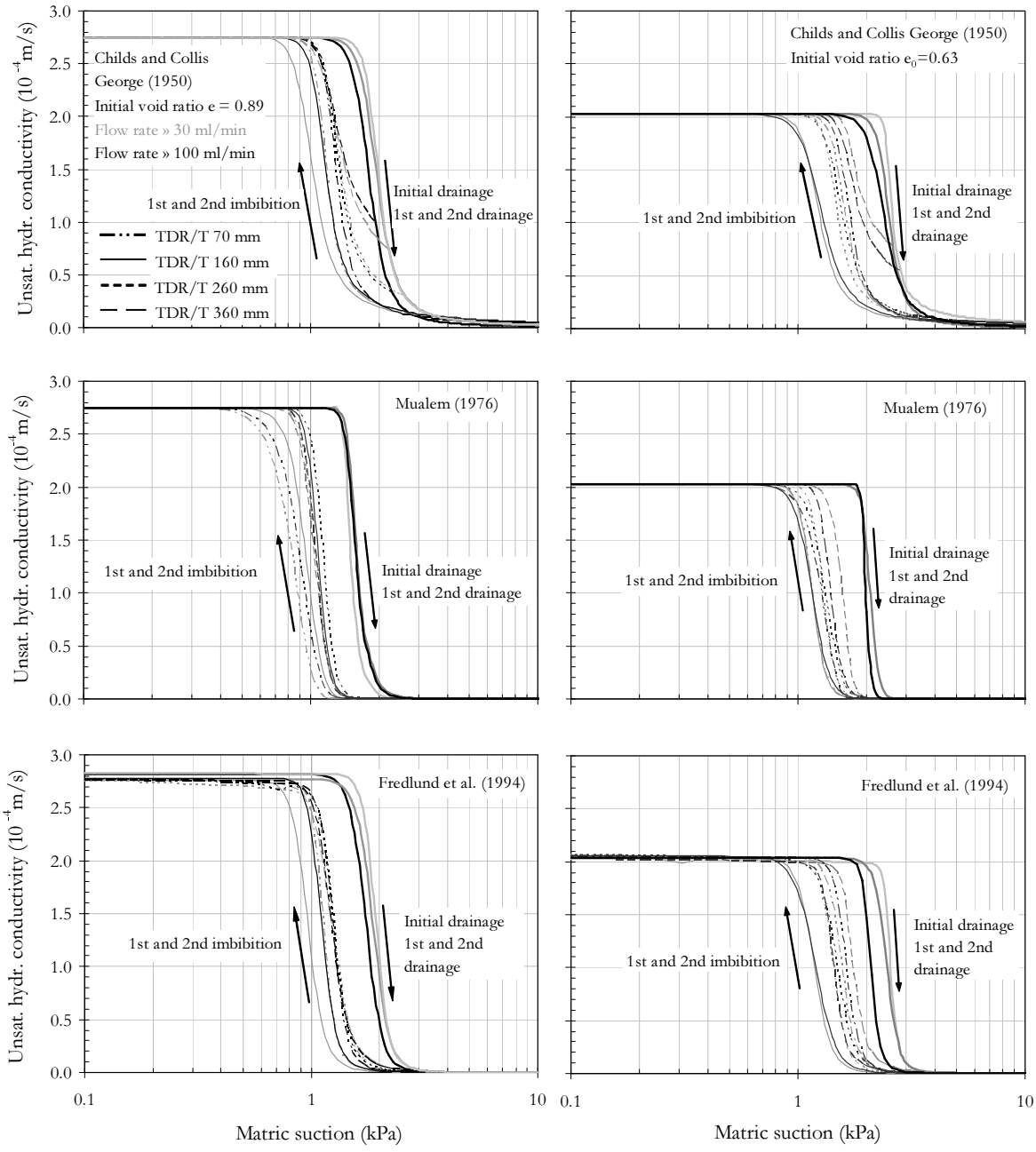

Figure 7.13: Unsaturated hydraulic conductivity from sand column test I (transient state test) determined by using statistical models (loose and dense specimen)

hydraulic conductivity is not changing in the saturated zone. When reaching the air-entry value the unsaturated hydraulic conductivity decreases drastically. In the residual zone, the unsaturated hydraulic conductivity approaches a zero value. No significant changes in the unsaturated hydraulic conductivity were observed in the residual zone along the drainage as well

as imbibition path. The imbibition curves start with an unsaturated hydraulic conductivity close to a zero value. With a decrease in the suction, the unsaturated hydraulic conductivity increases. The unsaturated hydraulic conductivity function increases first for the layers at the bottom of the (loose and dense) sand specimens where the voids are faster filled with water. In comparison to statistical models by Mualem (1976) and Fredlund et al. (1994), the scanning imbibition hydraulic conductivity curves derived using Childs and Collis George (1953) model begin at significant larger hydraulic conductivity values.

In a second analysis (i.e. the instantaneous profile method) the profiles of hydraulic head gradient and water content are used to calculate the unsaturated hydraulic conductivity function directly for the drainage process. Figure 7.14 shows the unsaturated hydraulic conductivity for loose and dense specimens ($1st$ drainage curve with a flow rate of 30 ml/min and $2nd$ drainage curve with a flow rate of 100 ml/min) calculated from both the instantaneous profile method (i.e. direct method) and the statistical models (i.e. indirect method). The instantaneous profile method is assuming that the water phase is continuous. The method is applicable in the saturated zone and in the unsaturated zone where water transport occurs in the wetting phase. The instantaneous profile method should not be applied in the residual zone, where water is believed to be exclusively transported in the vapor phase (non continuous water phase). The instantaneous profile method for the loose specimens shows unsaturated hydraulic conductivities in a range of approximately 0.3×10^{-4} to 0.007×10^{-4} m/s for a suction of 1.6 to 2.0 kPa respectively. For the dense specimen the hydraulic conductivities are in the range of approximately 0.4×10^{-4} to 0.005×10^{-4} m/s for suctions ranging from 1.7 to 2.2 kPa respectively. Similar to the results calculated when using the indirect method, the unsaturated hydraulic conductivity is decreasing rapidly along a narrow range of suctions. Results derived using statistical model by Mualem (1976) and Fredlund et al. (1994) are close to the results derived from direct method.

Unsaturated hydraulic conductivity functions resulting from modified pressure plate apparatus (steady state tests) and sand column I (transient state tests) are compared in Fig. 7.15 for loose specimen and in Fig. 7.16 for dense specimen. The results are given for the indirect as well as for the direct approach. The soil-water characteristic curve is strongly related to the unsaturated hydraulic conductivity function and therefore their behavior is similar (including the effect of hysteresis). The unsaturated hydraulic conductivity functions are close to each other during the drainage path. The unsaturated hydraulic conductivity functions along the scanning pathes are located within the main drainage and imbibition loop. This behavior is consistent with drainage and imbibition soil-water characteristic curves.

The following observations are made with regard to the effect of void ratio on the unsaturated hydraulic conductivity function. For low suction values the hydraulic conductivity for the loose specimen is higher due to the larger cross-sectional area available for water flow. When reaching the air-entry value, the unsaturated hydraulic conductivity for the loose specimen becomes less than the one for the dense specimen. The larger pores of the loose specimen

easily desaturate in this range whereas the smaller pores of the dense specimen are still available to conduct water. With an increase in suction, the unsaturated hydraulic conductivity decreases rapidly along a narrow range of suctions which is reflected in the interconnected and uniform pores. During the imbibition process the unsaturated hydraulic conductivity

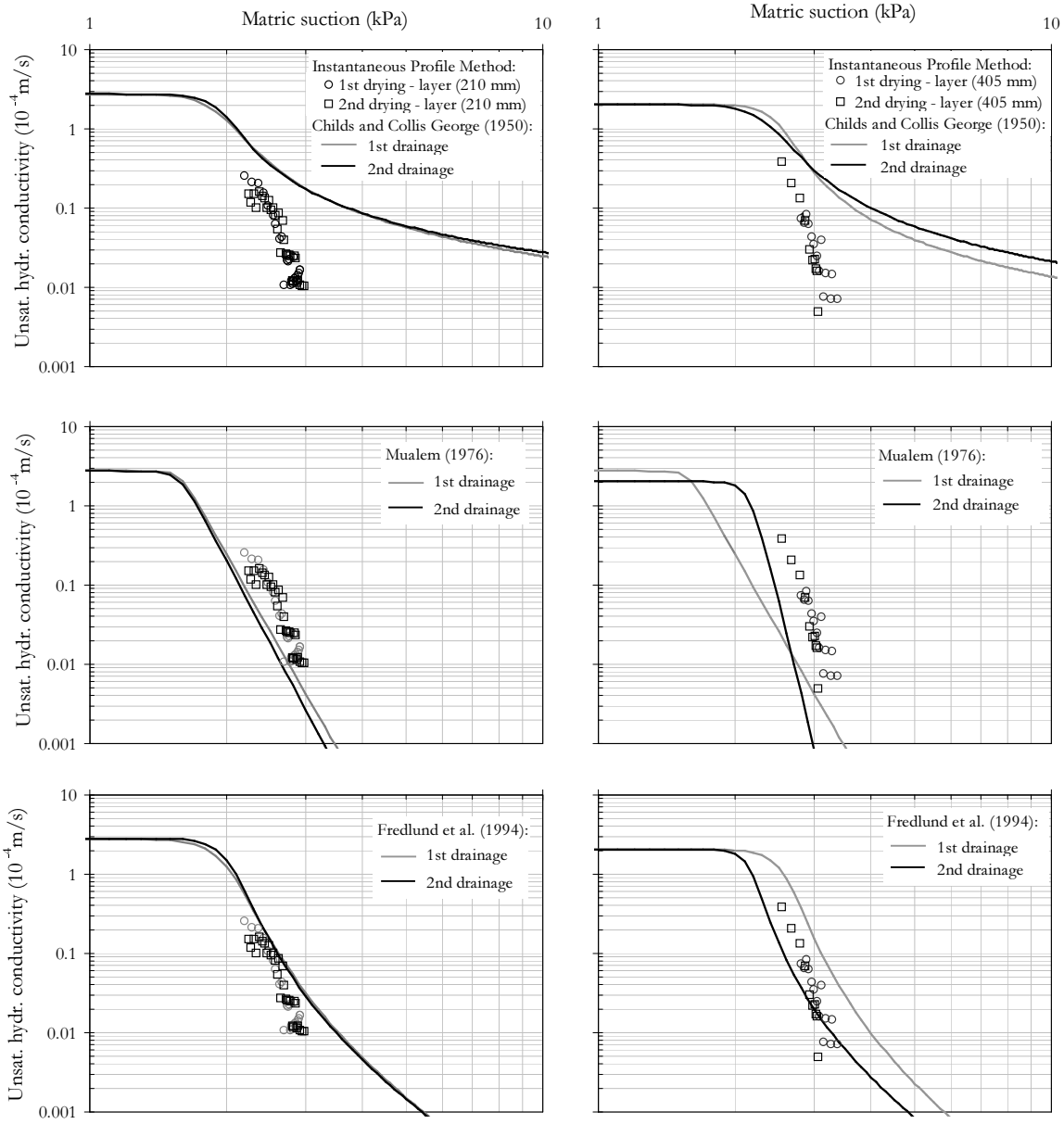

Figure 7.14: Comparison of the unsaturated hydraulic conductivity resulting from 1^{st} drainage curve (flow rate 30ml/min) and 2^{nd} drainage curve (flow rate 100ml/min) from sand column test I (transient state test) derived from statistical models and instantaneous profile method (loose specimen)

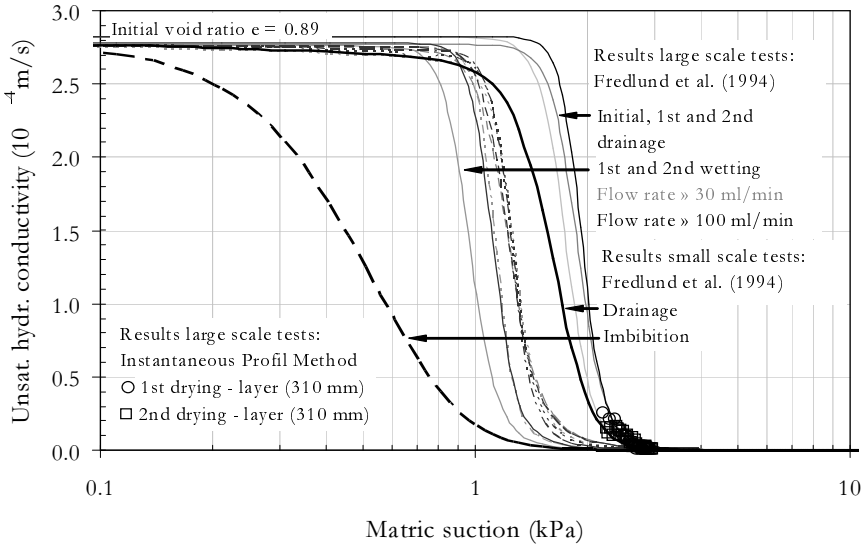

Figure 7.15: Comparison of unsaturated hydraulic conductivity curves resulting from modified pressure plate apparatus (steady state test) and sand column test I (loose specimen, transient state test)

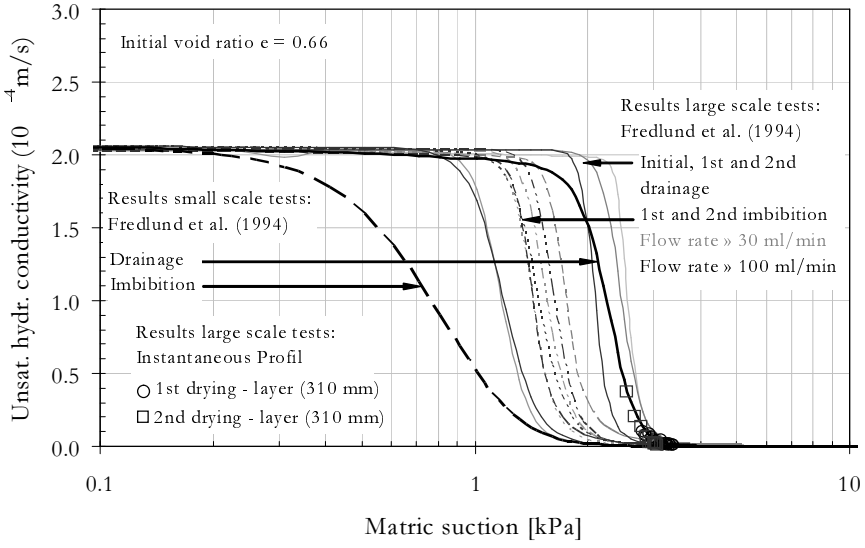

Figure 7.16: Comparison of unsaturated hydraulic conductivity curves resulting from modified pressure plate apparatus (steady state test) and sand column test I (dense specimen, transient state test)

first increases for the dense specimen. The smaller voids more easily absorb the water. Again the unsaturated hydraulic conductivity function for the dense specimen is located above the

one for the loose specimen. When saturated condition is reached, the unsaturated hydraulic conductivity for the loose specimen becomes larger.

Exemplary main drainage and imbibition curves derived from steady state tests in modified pressure plate apparatus for unsaturated hydraulic conductivity are plotted versus volumetric water content $k(\theta)$ in Fig. 7.17. Even at saturated conditions (S=1, S=0) the hydraulic conductivity is equal, the results show slight hysteresis between the drainage and the imbibition curve. This could be due to the fact, that during drainage curve water is different distributed in the pores than during imbibition curve. Differences may also occur from the best fitted soil-water characteristic curve and the applied statistical model (see also different shape of unsaturated hydraulic conductivity functions derived using several statistical model given in Fig.7.14).

The results of unsaturated hydraulic conductivity function for both loose and dense specimens achieved from modified pressure plate apparatus (steady state test) and also sand column tests I (transient state test) show significant hysteresis behavior during drainage and imbibition process. The derived unsaturated hydraulic conductivity functions from sand column tests I (transient state tests) for the drainage procedure are in good agreement with the results derived from the modified pressure plate apparatus (steady state test). As expected the unsaturated hydraulic conductivity functions for drainage path from both steady state and transient state test results and the unsaturated hydraulic conductivity functions for imbibition path from steady state tests enclose the imbibition scanning curves from the transient

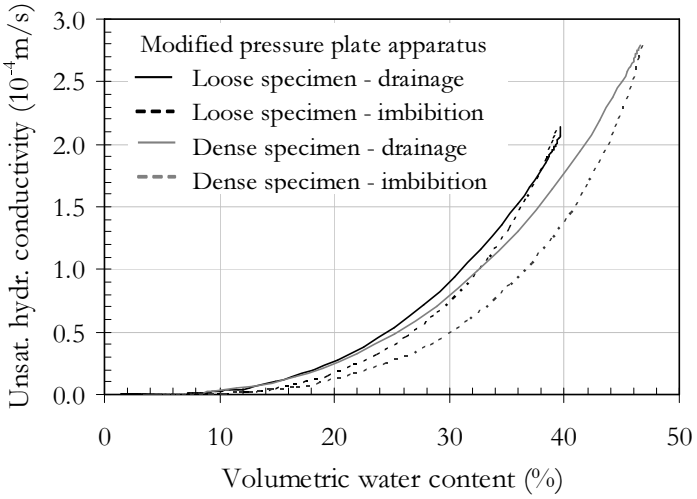

Figure 7.17: Unsaturated hydraulic conductivity versus volumetric water content resulting from modified pressure plate apparatus (loose and dense specimen, steady state test)

state tests. In the unsaturated hydraulic conductivity versus volumetric water content curve slight hysteresis was found for loose and dense specimens in the intermediate range.

7.5 Volumetric Behavior

To investigate the influence of suction on mechanical behavior of Hostun sand the stiffness modulus, the compression as well as swelling index, the collapse potential and the preconsolidation pressure are determined from the experimental results.

7.5.1 Stiffness Modulus, Compression and Swelling Index

Test results from one dimensional compression rebound tests were presented in Figs. 6.15 and 6.16, where the applied vertical net stress is plotted versus volumetric strain and void ratio for loose and dense specimen. 3D plots of the oedometer results for loose and dense sand specimen are added in this section in Fig. 7.18. As already mentioned in Chapter 6 from Figs. 6.15, 6.16 and Fig. 7.18 one can see that as anticipated the stiffness for dense specimen is higher then for loose specimen.

The stiffness increases with matric suction from $\psi = 1.5$ kPa, 3.0 kPa and 20.0 kPa for the tests carried out for dense specimen. Lowest stiffness results from the test with a matric suction of $\psi = 50.0$ kPa, for the dry and the saturated specimen. Similarly to the dense specimens for the loose one the lowest stiffness was calculated for the specimen with matric suction $\psi = 50.0$ kPa, for the dry and the saturated specimen. With increase in matric suction from $\psi = 1.5$ kPa to 20.0 kPa the stiffness is slightly increasing. Comparison of the results from the unloading path of all tests one can state that, there is a similar behavior for all the specimens.

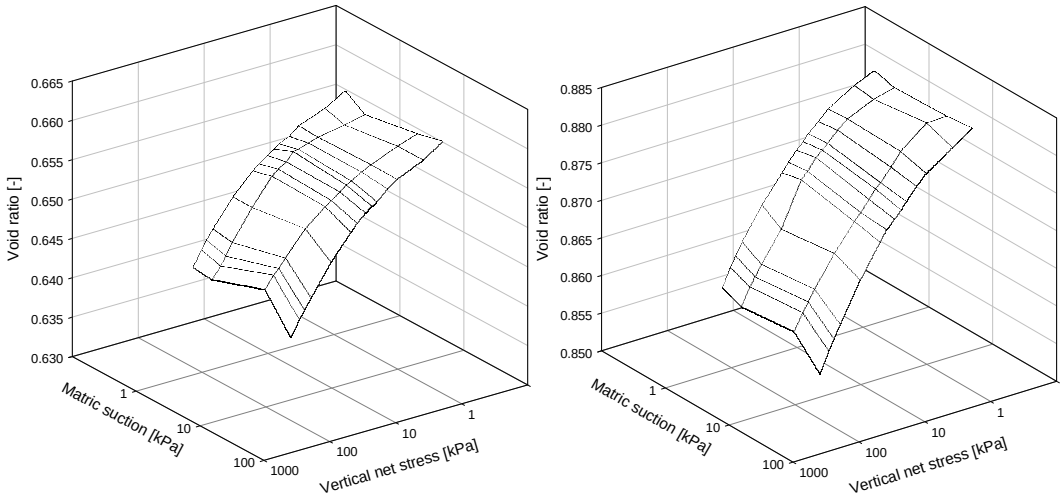

Figure 7.18: 3D plots of oedometer test results for dense (left) and loose (right) specimen

Table 7.3: Results for stiffness modulus in MPa for dense and loose specimen

Condition of specimen	S=1.0 (-)	$\psi = 1.5$ kPa	$\psi = 3.0$ kPa	$\psi = 20.0$ kPa	$\psi = 50.0$ kPa	dry (-)
loose						
E_{oed}, $\sigma = 100$	23.4	25.8	24.7	25.7	23.9	15.1
E_{oed}, $\sigma = 12$	4.9	7.0	6.5	7.1	5.2	6.8
E_{ur}, $\sigma = 100$	124.4	158.1	149.0	130.2	145.5	102.9
E_{ur}, $\sigma = 12$	13.6	15.1	14.2	15.9	16.7	7.6
dense						
E_{oed}, $\sigma = 100$	24.4	30.5	29.3	36.1	28.1	21.5
E_{oed}, $\sigma = 12$	6.0	6.5	7.9	7.6	5.4	10.4
E_{ur}, $\sigma = 100$	150.0	131.3	255.5	141.4	168.2	174.0
E_{ur}, $\sigma = 12$	9.5	13.6	9.7	14.8	15.1	8.3

To investigate in detail the influence of suction on the stiffness behavior of sand the compression index C_c and the swelling index C_s were estimated. The results are given in Fig 7.19. The compression index decreases first for suction less then about 20 kPa, that is equal to an increase in stiffness, and increases again for higher suction values, that is equal to a decrease in stiffness. As expected compression index of the dense specimen is less then the compression index of the loose one, which indicates a higher stiffness. No significant influence of the suction on the swelling index can be observed.

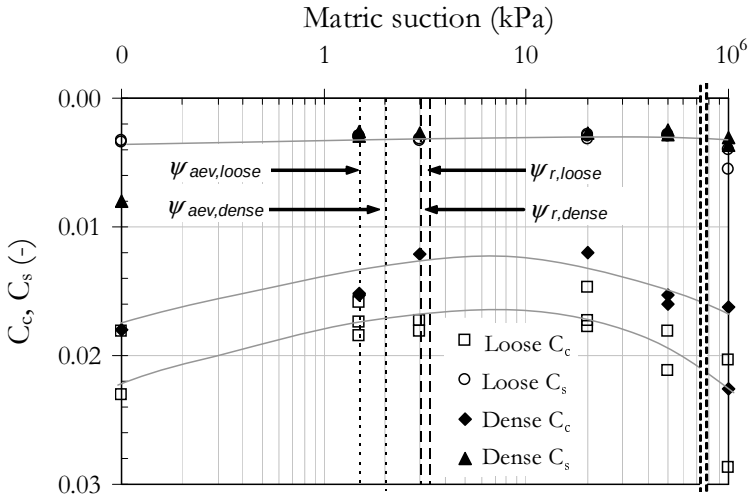

Figure 7.19: Compression and swelling index versus suction

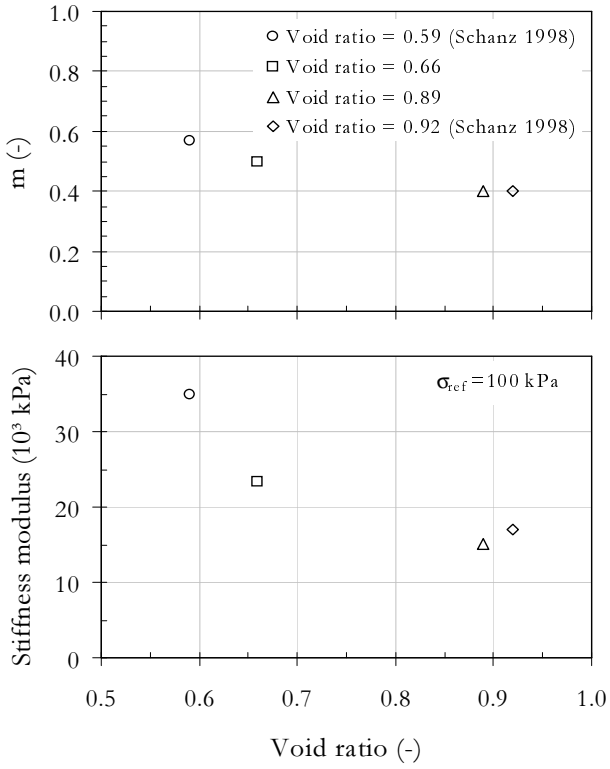

Figure 7.20: Calculated parameter $\hat{m}$ and stiffness modulus for dry specimens with different void ratios

The results of the stiffness moduli, that were derived from the experimental results are given in Tab. 7.3. This table summarizes stress dependent stiffness moduli, that were estimated for a low vertical net stress (σ = 12 kPa) as well as a high vertical net stress (σ = 100 kPa) to see the development of this value. For all calculations a reference stress of σ_{ref} = 100 kPa was used. For the stiffness modulus E_{oed} an increase with increasing suction (up to 20 kPa) is observed for σ = 12 kPa and σ = 100 kPa. With further increase in suction the stiffness modulus is decreasing again. For the parameter $\hat{m}$, values between $\hat{m}$ = 0.62 to 0.81 for dense and $\hat{m}$ = 0.58 to 0.76 for loose specimens were derived during loading path. For the un-/reloading path constant $\hat{m}$ = 0.97 for dense specimen and $\hat{m}$ = 0.93 for loose specimen was calculated. In Fig. 7.20 parameters $\hat{m}$ calculated from oedometer test results are given for dry specimens and compared to results derived by Schanz (1998) for Hostun sand. According to $\hat{m}$ the author found stiffness moduli of E_{oed} = 17.000 kPa (loose specimen) and E_{oed} = 35.000 kPa (dense specimen) for vertical net stress σ_{ref} = 100 kPa. As can be seen in Fig. 7.20 the results of parameter $\hat{m}$ and the stiffness modulus from the present study fit well to the results given in literature.

For description of one dimensional unloading and reloading test results of cohesive soils the stress dependent stiffness is calculated by using the following equation, that also was proposed by Schanz (1998). This equation is similar to Eq. 2.24:

$$E_{ur} = E_{ur}^{ref} \left(\frac{\sigma + c \cdot \cot \phi}{\sigma_{ref} + c \cdot \cot \phi} \right)^{\hat{m}} \tag{7.1}$$

where: E_{ur} is the stress dependent stiffness modulus for un-/reloading path, E_{ur}^{ref} is the normalized stiffness modulus, σ_{ref} is the reference stress, σ the vertical net stress and $\hat{m}$ a parameter. In this equation additionally the cohesion c and the influence of the friction angle ϕ are considered. In the present investigation it is suggested to replace in Eq. 7.1 the cohesion by the suction value ψ to take into account its influence on the stiffness behavior of unsaturated sand. The equation for determination of stress dependent stiffness modulus for initial loading E_{oed} becomes to:

$$E_{oed} = E_{oed}^{ref} \left(\frac{\sigma + \psi \cdot \cot \phi}{\sigma_{ref} + \psi \cdot \cot \phi} \right)^{\hat{m}} \tag{7.2}$$

where: ψ is the suction in the investigated sand. Experimental results performed under constant suction and appropriate results using Eq. 7.2 are given in Fig. 7.21 for loose as well

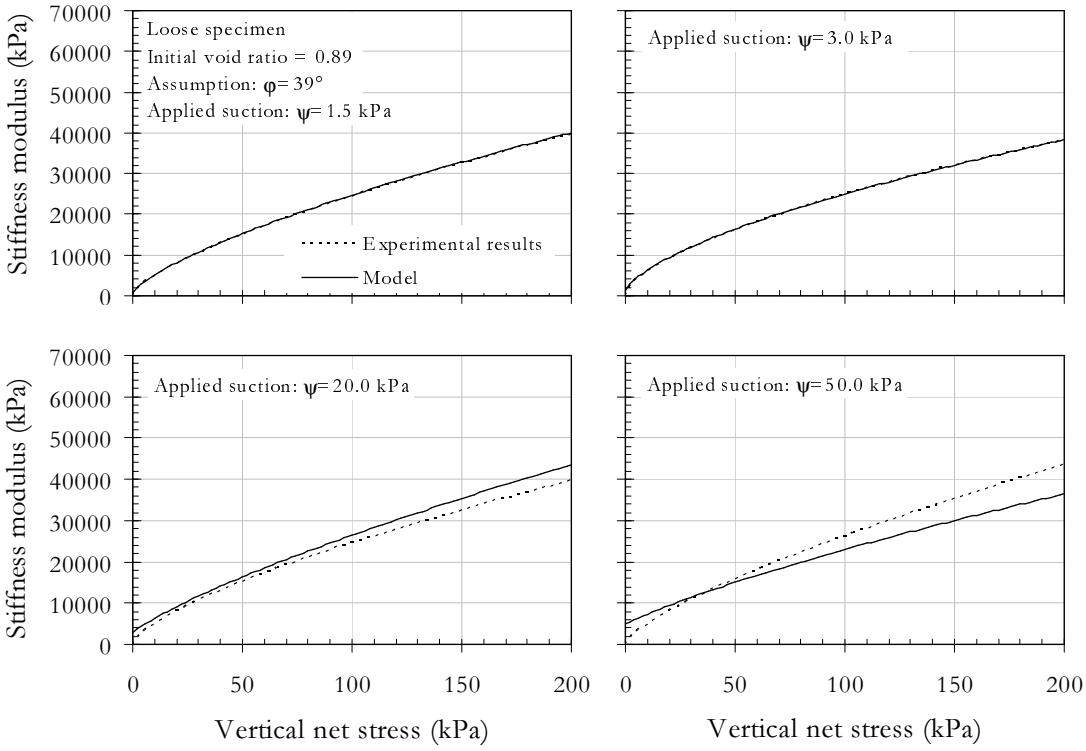

Figure 7.21: Comparison of experimental results and predicted results (loose specimen)

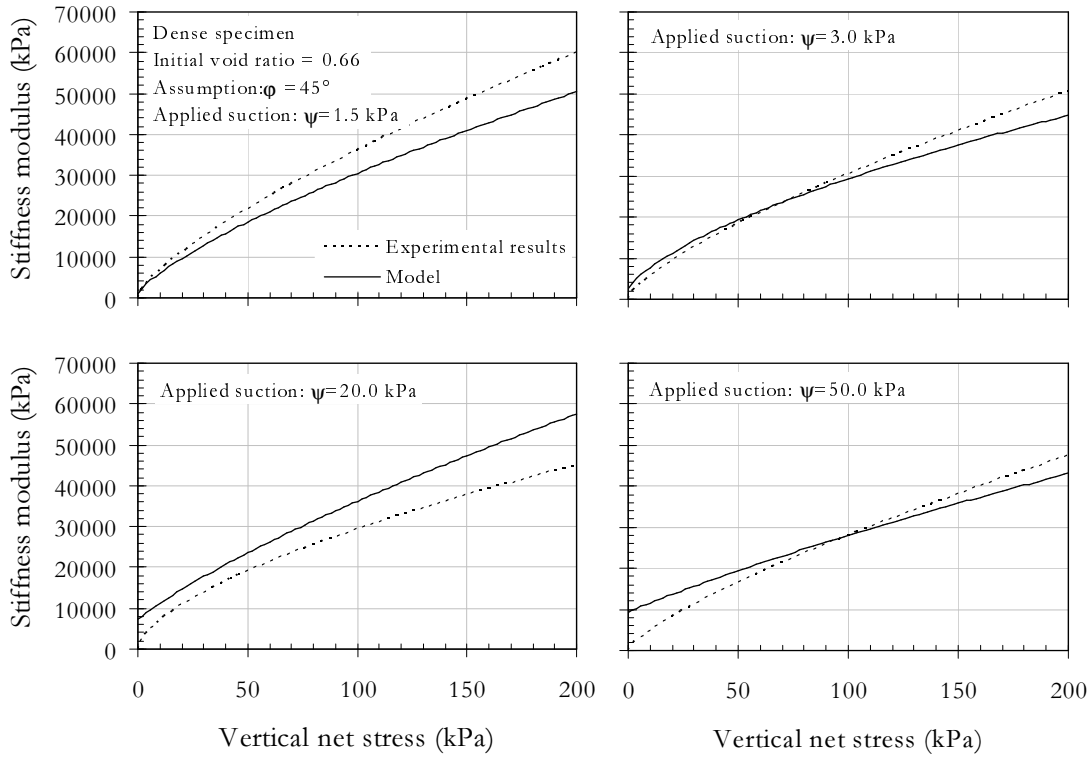

Figure 7.22: Comparison of experimental results and predicted results (dense specimen)

as in Fig. 7.22 for dense Hostun sand specimens. From the comparison can be concluded that the simple approach of replacing the cohesion c with the suction ψ leads to good results. It seems the model fits good to the experimental results for the loose specimen, but not so good for the dense specimen. The fit was found to be not so good for the specimens with high applied suction values (here $\psi = 50$ kPa).

7.5.2 Collapse Potential

Results of oedometer tests for estimation of collapse potential are presented for loose samples in Fig. 7.23 for Method 1 (results for Method 2 are given in Fig. C.1 in Appendix C). All diagrams show, that the collapse potential of Hostun Sand is very small. Results from Method 1 show differences in void ratio of $\Delta e = 0.0031$ for saturation at $\sigma = 5$ kPa, $\Delta e = 0.0020$ for saturation at $\sigma = 12$ kPa and difference in void ratio of $\Delta e = 0.0020$ for saturation at $\sigma = 25$ kPa. Results from Method 2 show differences in void ratio of $\Delta e = 0.0015$ for saturation at $\sigma = 5$ kPa, $\Delta e = 0.0022$ for saturation at $\sigma = 12$ kPa and difference in void ratio of $\Delta e = 0.0009$ for saturation at $\sigma = 25$ kPa. Using Eq. 2.26 collapse potentials between 0.08% and 0.17% were calculated that is negligible small. Reason for that are the equal grains (it

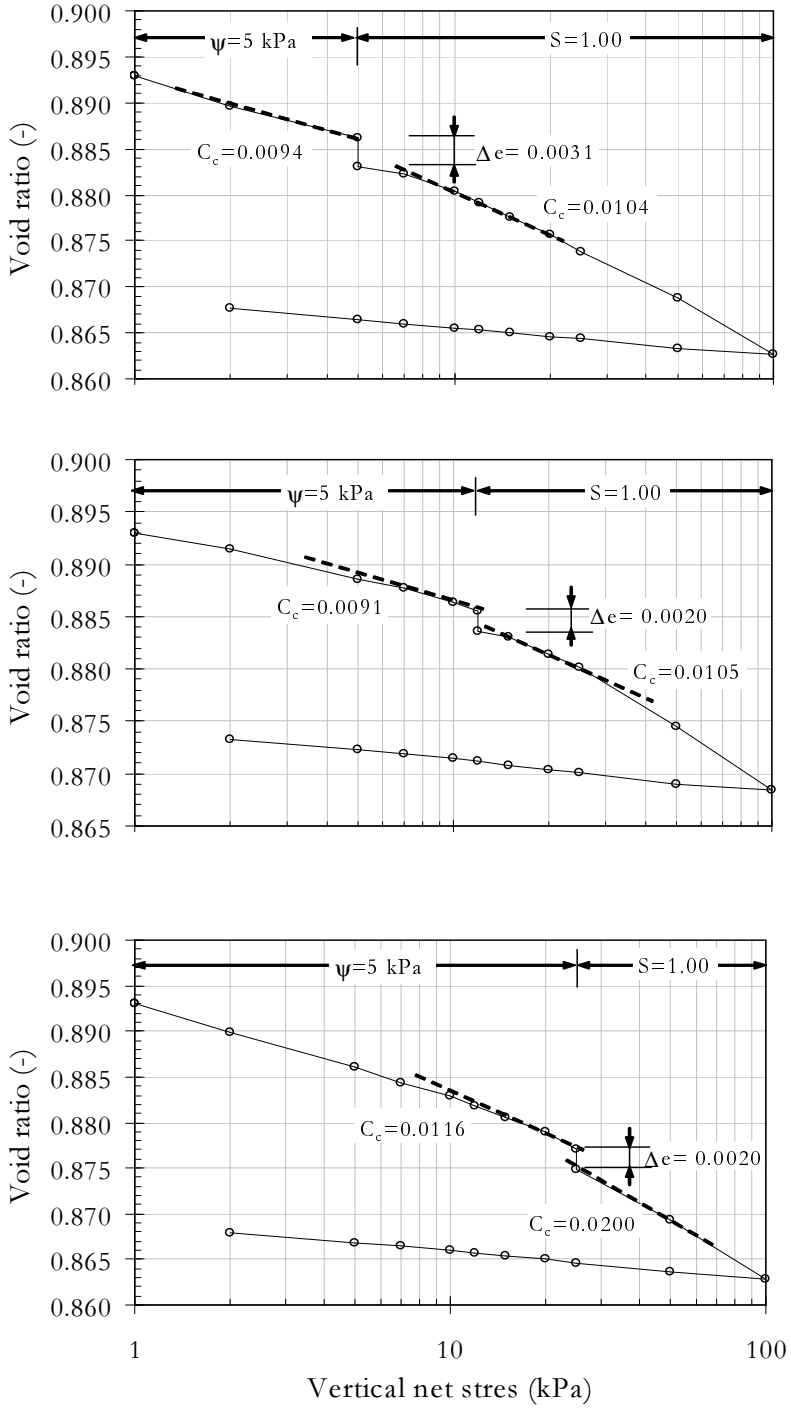

Figure 7.23: Experimental results of collapse potential test including results of compression index- Method 1 (loose specimen)

is a poorly graded sand) of the Hostun sand, where only few smaller particles tend to fill the existing pores of the soil.

Comparing the compression index for loading path before and after saturation one can find that stiffness of the sand decreases with saturation process (see also Schanz et al. 2002). The compression index is with $C_c = 0.0074$ to 0.0131 for the first loading path ($\psi = 5.0$ kPa, $w = 0.03$ respectively) smaller in comparison with $C_c = 0.0104$ to 0.0200 for the second loading path ($S = 1.00$) and indicates a higher stiffness for the unsaturated specimen (see Fig. 7.23 and in Appendix C in Fig. C.1 as well as Tab. 7.4 and 7.5). Also the stiffness moduli were calculated for these results using Eq. 2.24. The stiffness was determined for the results before saturation process as well as after saturation process at vertical net stress $\sigma = 5, 12$ and 25 kPa using a reference stress $\sigma_{ref} = 100$ kPa. The results are compared in Tab. 7.4 and 7.5. For all results and for both method it is shown, that the stiffness is larger before saturating the sand specimen. At unsaturated condition the stiffness is higher. This conclusion is consistent with the outcome of the one-dimensional compression tests analyzed in the previous section.

7.5.3 Influence of Stress History on Mechanical Behavior

The influence of stress history (i.e. in this study the applied suction) was graphically estimated using the methods proposed by Casagrande (1936) and Janbu (1969). In general the shape of the curves do not show an influence of stress history. Although it was tried to determine an influence of suction on the stress history. These results are given in Fig. 7.24 (left), where the

Table 7.4: Results for stiffness modulus in MPa for loose specimen collapse potential tests - Method 1

	$\sigma = 5$ $\psi = 5$ kPa	$\sigma = 5$ $S = 1$	$\sigma = 12$ $\psi = 5$ kPa	$\sigma = 12$ $S = 1$	$\sigma = 25$ $\psi = 5$ kPa	$\sigma = 25$ $S = 1$
E_{oed}	1.09	1.01	–	–	–	–
E_{oed}	–	–	4.5	4.3	–	–
E_{oed}	–	–	–	–	6.2	4.8

Table 7.5: Results for stiffness modulus in MPa for loose specimen collapse potential tests - Method 2

	$\sigma = 5$ $w = 0.03$	$\sigma = 5$ $S = 1$	$\sigma = 12$ $w = 0.03$	$\sigma = 12$ $S = 1$	$\sigma = 25$ $w = 0.03$	$\sigma = 25$ $S = 1$
E_{oed}	2.6	1.7	–	–	–	–
E_{oed}	–	–	4.3	3.8	–	–
E_{oed}	–	–	–	–	5.2	4.9

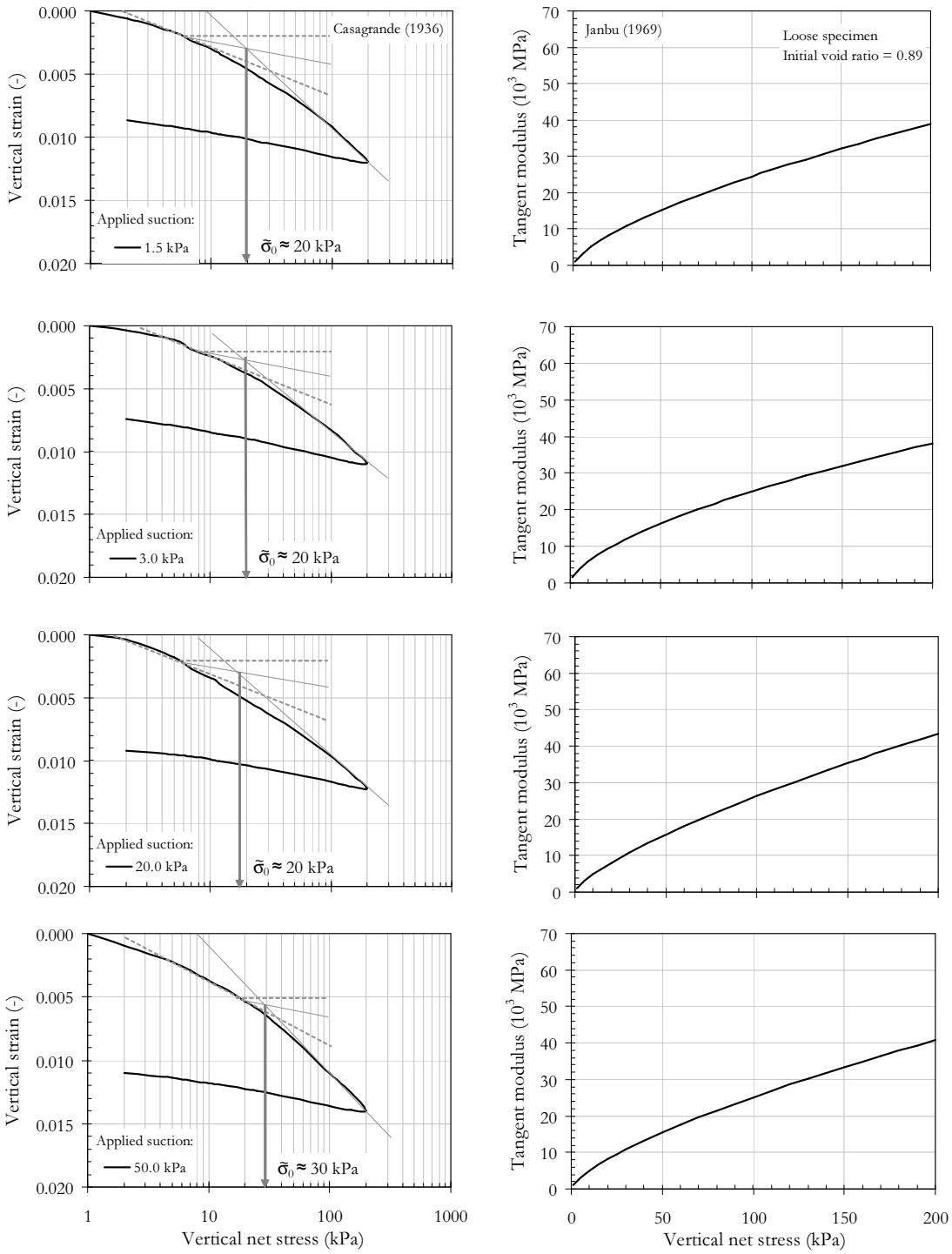

Figure 7.24: Prediction of yield stress using Casagrande's (left) and Janbu's (right) method (loose specimen)

Table 7.6: Yield stress for loose and dense specimen derived from Casagrande (1936)

	$\psi = 1.5$ kPa	$\psi = 3.0$ kPa	$\psi = 20.0$ kPa	$\psi = 50.0$ kPa
Loose	20 kPa	20 kPa	20 kPa	30 kPa
Dense	30 kPa	30 kPa	30 kPa	30 kPa

compression curves of loose specimen under applied constant suction are given. It was assumed to find an influence of the applied suction on the compression behavior (assumption: $\psi = \tilde{\sigma}_0$). But yield stress of approximately $\tilde{\sigma}_0 = 20$ kPa for loose and approximately $\tilde{\sigma}_0 = 30$ kPa for dense was found, which indicates that the applied suctions from $\psi = 1.5$ to $\psi = 50$ kPa do not influence the compression behavior (see also summary in Tab. 7.6). There is also the possibility to use Janbu's method (1969), where the tangent modulus M is plotted versus the vertical stress σ. A drop in the shape of the curve identifies an influence of stress history on the mechanical behavior of the soil. As can be seen in Fig 7.24 (right) no drop and thus no breakdown in the structural resistance occurs. Also for the dense specimen it was observed, that applied suction does not influences the stress history. Results of the dense specimen are shown in Fig. D.1 in Appendix D.

7.6 Summary

Based on the experimental results given in Chapter 6 relationship between suction and volumetric water content or saturation during initial drainage, main drainage and imbibition and scanning drainage and imbibition were derived using models proposed by several authors. The curve fit parameters are determined. The suction-water content models fit the experimental data well for drainage or imbibition process. But when using models dealing with hysteresis and also scanning drainage/ imbibition phenomena the experimental results are not in good agreement with the calculated results for several zones along the suction-water content curve. Also some models use to much parameters to identify this relationship or are rather complex in their application to experimental results. The interpretation of the results shows that the void ration and the loading path direction influence the shape of the soil-water characteristic curve. With decreasing void ratio the curves are shifting to higher range of suction values. Depending on the loading path direction for a certain suction value the water content is larger (drainage) or less (imbibition). This phenomenon is known as hysteresis. There are no significant differences found between curves carried out under steady state and transient state flow condition.

Several statistical models in combination with the soil-water characteristic curve are used for prediction of unsaturated hydraulic conductivity function. The results from direct deter-

mination of unsaturated hydraulic conductivity are close to the results estimated by Mualem (1976) and Fredlund et al. (1994).

The relations between vertical net stress and void ratio as well as vertical strain and void ratio are analyzed using the concept of stress dependent stiffness. Stiffness modulus is calculated and the results show an increase of stiffness with increasing suction. After reaching an optimum value an decrease of stiffness during loading occurs. When unloading the specimen the stiffness is similar for the tests performed under several constant suction value. It can be concluded, that the stiffness of Hostun sand is influenced by the matric suction and the water content (volumetric water content, saturation) respectively during loading procedure. The collapse potential for loose specimen at several net stresses was found to be small. The suction induced to the sand specimen does not act as preconsolidation pressure.

Chapter 8

New SWCC Model for Sand including Scanning Curves

8.1 General

As a result of the present analysis 2D models for the soil-water characteristic curve are proposed (Stoimenova et al. 2003*b*, 2005, 2006). The first model describes only the drainage process in the investigated sand. The second model incorporates the hysteretic nature of the relationship between volumetric water content θ and suction ψ including scanning imbibition curves. The models are based on non-linear least squares estimation of the data derived from experiments. Basic knowledge and theory for process modeling was given in Chapter 3.

For model building the available data of the transient state column tests I are used (drainage and imbibition results). The data contain measurements of the volumetric water content θ and the suction ψ at five different levels within the sand column. In this case, the suction ψ and the initial imbibition suction s_0 are used to obtain better estimates of soil properties, such as soil-water characteristic curve. Incorporating this available information about the suction-water content relation, a model is constructed that can be applied for prediction of the volumetric water content (saturation, gravimetric water content) for any position along the column. The uncertainty related to different measurement errors of TDR's is combined and used for estimating a global prediction error. The estimated error of the model is valid in entire interval of suction-values and for arbitrary depth level. The variable s_0 represents the suction measured in the corresponding depth and gives the initial suction distribution before each of the hydraulic loading test phases (imbibition process). Due to this the proposed 2D regression models acquire the advantage that they: i) can be applied for prediction of θ for any position along the column and thus any suction in the soil ii) give the functional form for the scanning curves. The experimental results are an effort to access based on statistical analysis the hysteretic form of the soil-water characteristic curve and to model scanning curves applying 2D statistical model.

8.2 Soil-Water Characteristic Curve Model

Following the steps of model building given in detail in Chapter 3 a soil-water characteristic curve model, that considers imbibition scanning curves is built.

Based on the experimental results (several drainage processes) derived in the transient state column tests I the model is constructed. To provide a single model for all drainage processes, observed experimental data from initial drainage, 1^{st} drainage and 2^{nd} drainage process from loose specimen (all results derived from dense specimen are given in Appendix E in Figs E.1 to E.9) are considered. The experimental results were already presented in Chapter 6 but are once more given in Fig 8.1, where the volumetric water content is plotted versus suction. Whereas usually the axis of suction is plotted in logarithmic form here the non-logarithmic form is used, to observe the true shape of the suction-water content curves measured in the several depths along the column. From the experimental procedure it is known, that the sensor pair in the upper part (TDR/T 450) of the column remains throughout the whole experiment in the saturated zone. Thus these measurements are excluded from the model building. It is also important to repeat, that no significant influence of applied flow rate was observed and hence a dynamic effect does not be taken into account when choosing an appropriate model.

When selecting a model a plot of the experimental data, process knowledge and process assumptions about the process are used for its suggestion. Plots of the soil-water characteristic curve are given in Fig. 8.1 for Hostun sand. As already mentioned before the main features of the suction water content relationship are the saturated volumetric water content, the air-entry value as well as the residual suction. Following the shape of the curves it is assumed that the volumetric water content is equal to the saturated volumetric water content before reaching the air-entry value. When passing this point the volumetric water content is decreasing (less steep for clay and most steep for sand). After the residual suction the curve is slanted. The curve show that a non-linear function is needed for the prediction. It is suggested that an exponential function might be appropriate for a model function.

In Fig. 8.2 (see Fig. E.2 in Appendix E results of transformation derived from dense data) exemplary results of transformation procedure are given for initial drainage, 1^{st} drainage as well as 2^{nd} drainage results for loose specimen derived from the transient sand column test I (see Fig. 8.1). Based on these plots it is decided to fit the model with double logarithm in the response variable $\ln\ln(\theta)$ and with logarithm in the predictor variable $\ln(\psi)$, that give the best linear transformation:

$$\ln\ln(\theta) = \beta_0 + \beta_1 \ln\ln(\psi) \tag{8.1}$$

where: θ is the volumetric water content, ψ is the suction as well as β_0 and β_1 are parameters. The linear model given in Eq. 8.1 is proposed to relate the volumetric water content to the suction. Because drainage and imbibition processes are similar in shape, it is assumed that

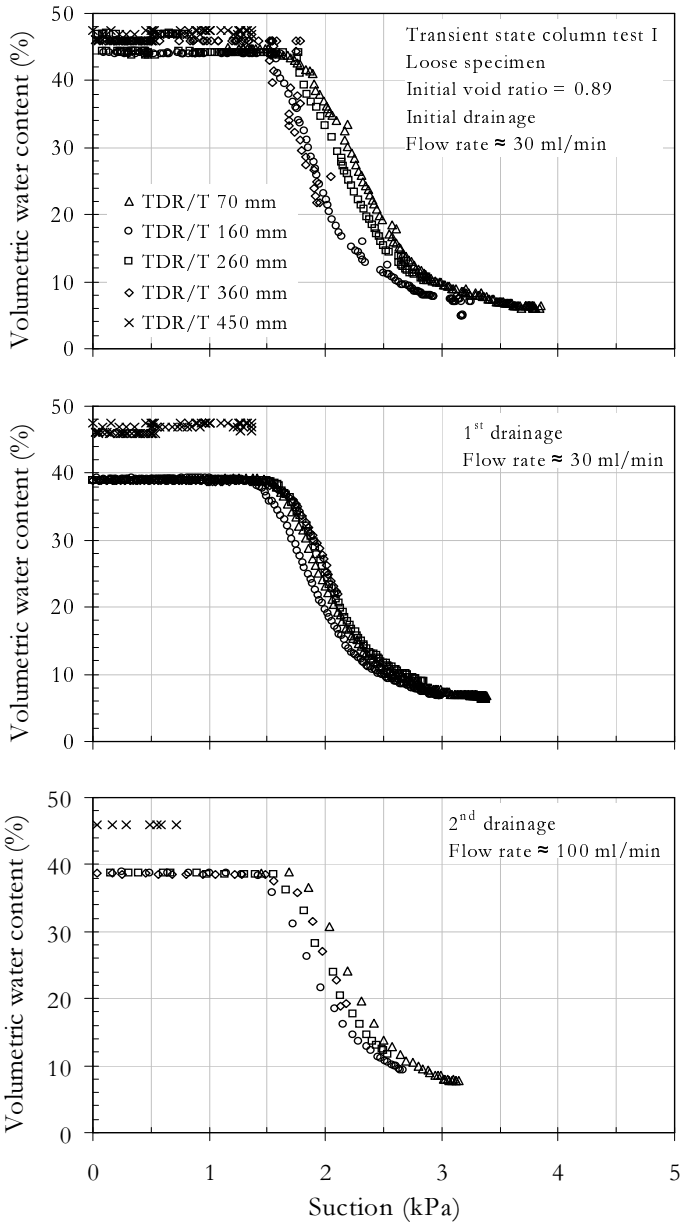

Figure 8.1: Experimental data (initial drainage, 1^{st} drainage, 2^{nd} drainage) from drainage transient state column tests used for model building (loose specimen)

this equation also can be used for fitting of imbibition suction-water content relation. Based on the appropriate transformation found in the previous step finally the corresponding non-linear model is proposed:

$$\theta(\psi) = \beta_0 + \beta_3 \exp(-\frac{\psi^{\beta_1}}{\beta_2}) \tag{8.2}$$

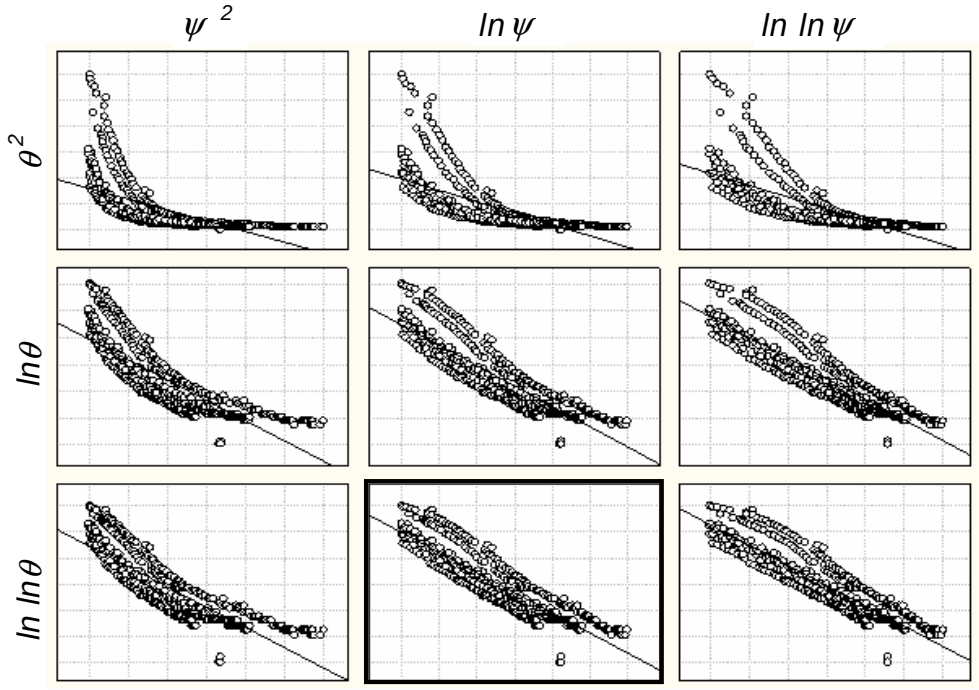

Figure 8.2: Results from data transformation using experimental results (initial drainage, 1^{st} drainage, 2^{nd} drainage) from drainage transient state column tests (loose specimen)

where: the parameter β_0 is the maximum volumetric water content, that is commonly the saturated volumetric water content θ_s and β_3 is related to the minimum volumetric water content, that is commonly the residual volumetric water content θ_r with $\theta_r = \beta_0 + \beta_3$ and β_1, β_2 are parameters. The new soil-water characteristic curve model was tested on experimental results measured in several depth in the transient sand column test (drainage process). The outcomes of the curve fits using the proposed model are given in Fig. 8.3 for loose specimen (see also Fig. E.3 in Appendix E for curve fits of experimental results from dense specimen). The

Table 8.1: Constitutive parameters for the new SWCC model (calibrated against drainage data)

Experimental results	β_0	β_1	β_2	β_3	R^2
Loose specimen, drainage process					
TDR/T 70 mm	39.00	−6.57	0.0146	−33.118	0.999
TDR/T 160 mm	38.66	−5.69	0.0316	−33.106	0.999
Dense specimen, drainage process					
TDR/T 260 mm	36.72	−8.07	0.0015	−28.592	0.999
TDR/T 360 mm	34.21	−9.32	0.0003	−23.621	0.992

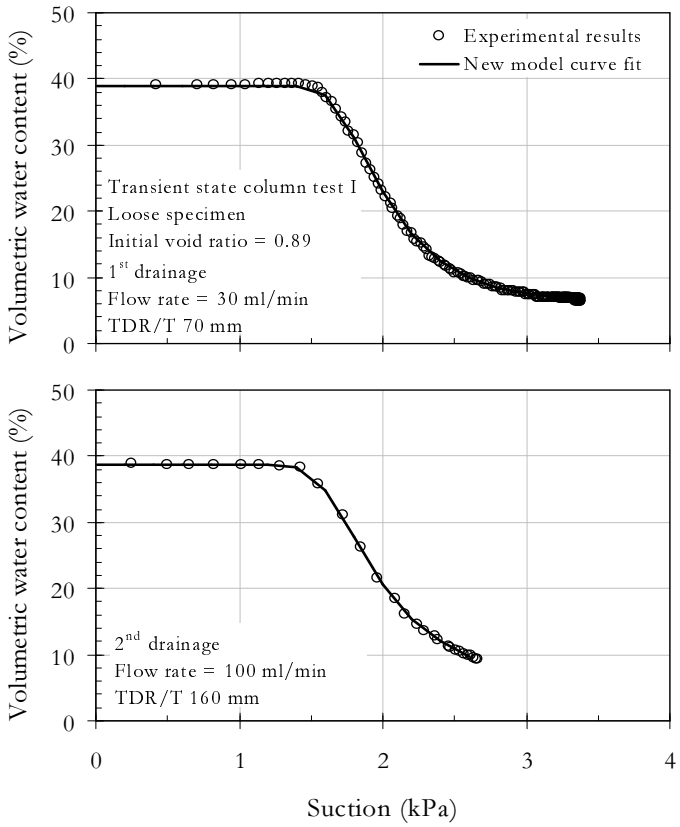

Figure 8.3: Experimental drainage results from several depth and new SWCC model best fit (loose specimen, transient state sand column test)

corresponding parameters and the linear regression coefficient R^2 are given in Tab. 8.1. From the first view it seems that the proposed model fits the experimental results well. However, later on the model validation procedure is used wether or not the model is suitable to fit the suction-water content data.

Now it is tried to extend the proposed model in this way, that it also could be used for scanning imbibition curve fit. It is focused on a model that describes with a single set of parameters several scanning imbibition curves. The fact that the suction-volumetric water content profiles of θ versus ψ (respectively the profiles of saturation S versus suction ψ) vary with depth, that leads to different initial imbibition suction s_0, confirms that any functional description of the process will need to include the variable s_0. Further insight into the appropriate function to use can be obtained by separately modeling each cross-section of the experimental data using the proposed model and then relating the individual models to one another. Examining plots of the estimated parameters versus s_0 roughly indicates how the suction measurement should be incorporated into the model of the data. Regression curves to the cross-sections data for the 1^{st} imbibition as well as the 2^{nd} imbibition process at several

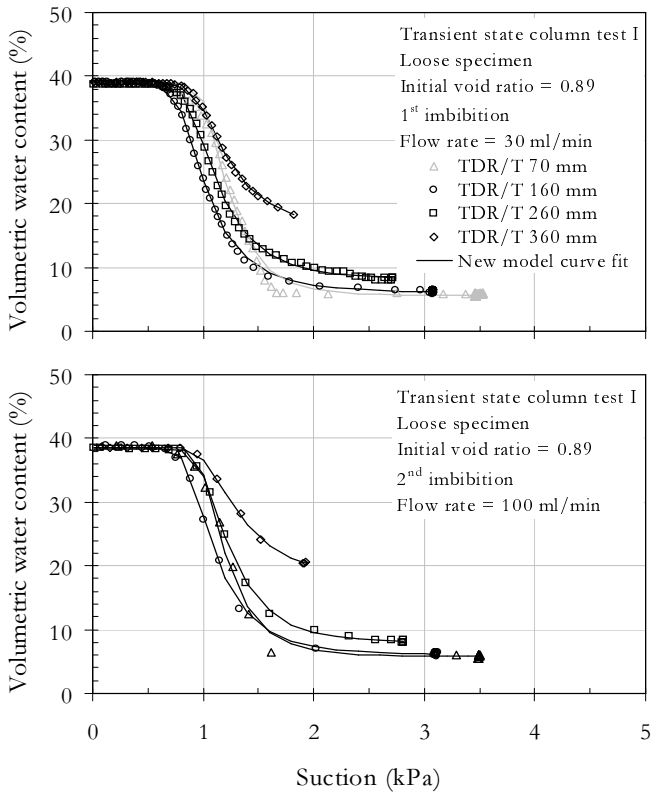

Figure 8.4: Experimental imbibition results (1^{st} imbibition, 2^{nd} imbibition) and new SWCC model best fit (loose specimen, transient state sand column test)

depth are given in Fig. 8.4 for loose specimen (see also Fig. E.4 in Appenidx). The tensiometer and TDR sensor measurements observed for loose specimen during 1^{st} imbibition in a depth of 70 mm (TDR/T70 mm) were excluded from the examination, because they show untypical behavior (measurements are therefore given in grey color in Fig. 8.4). The individual exponential fits to each cross-section of the data reveal the influence of initial imbibition suction s_0. An exemplary comparison of the parameters is given in Tab. 8.2 for the 2^{nd} imbibition process of the loose specimen. It is shown that three of the estimated parameters are not sufficiently different for different depth:

- Parameter β_0 that is equal to the saturated volumetric water content and that should be equal under saturated condition in each depth. The saturated volumetric water content is approximately $\theta_s = 38.5\%$ that is similar to β_0.

- Parameter β_1 that influences the slope of the curve and is in all depth approximately $\beta_1 = -5$.

Table 8.2: Constitutive parameters for the new SWCC model (calibrated against imbibition data)

Experimental results	β_0	β_1	β_2	β_3	s_0
Loose specimen, 2^{nd} imbibition process					
TDR/T 70 mm	38.86	−5.91	0.50	−33.12	3.49
TDR/T 160 mm	38.56	−4.63	0.92	−32.62	3.11
TDR/T 260 mm	38.28	−5.05	0.50	−30.42	2.81
TDR/T 360 mm	38.55	−4.37	0.42	−20.92	1.92

- Parameter β_2 that also influences the slope of the curve and is in all depth approximately $\beta_2 = 0.5$.

An influence according to the initial imbibition suction s_0 was found for the scaling parameter β_3 that influences the minimum volumetric water content θ_{min}. With increasing initial imbibition suction s_0 the parameter β_3 is decreasing. Further, it is now tried to replace β_3 with a term expression depending on s_0, which incorporates the variation of this parameter for different layers. Simple linear term of s_0 instead a constant β_3 showed the best fit over the trial models. The resulting hysteresis model is:

$$\theta(\psi) = \beta_0 + (\beta_3^1 + \beta_3^2 \cdot s_0)\, \exp(-\frac{\psi^{\beta_1}}{\beta_2}) \tag{8.3}$$

where: s_0 is the initial imbibition suction measurement that has been recorded using tensiometer sensor. Results of the proposed hysteresis model curve fit for both the 1^{st} and 2^{nd} imbibition process are show in Fig. 8.5 for the loose specimen (and in Fig. E.5 for curve fit of dense specimen in Appendix E). In the 3D plots the initial imbibition suction s_0 is introduced as 3rd dimension on the z-axis. Similar to the curve fit results from the drainage process the calculated results seem to be in good agreement to the experimental results for loose specimen (1^{st} imbibition and 2^{nd} imbibition process). The identified parameters and the coefficient of linear regression R^2 are summarized in Tab. 8.3. For drainage as well as imbibition curve fitting procedure the Levenberg-Marquardt algorithm was used, that is an improvement of the classical Gauss-Newton method for solving non-linear least-square regression problems.

The plots given in Figs. 8.6 to 8.9 derived from regression analysis of loose specimen are used to appreciate wether or not the model fits the experimental data well (see also the results derived from regression analysis of dense specimen in Figs E.6 to E.9 in Appendix E). Both statistical techniques, coefficient of regression determination and residual analysis were used to validate the model and to see the adequacy of different aspects of the model. The statistical results from model validation are shown in Figs. 8.6 and 8.7 for the model fit of several drainage suction-water content measurements for loose specimens. The model validation results of the statistical analysis derived from the 1^{st} as well as 2^{nd} imbibition

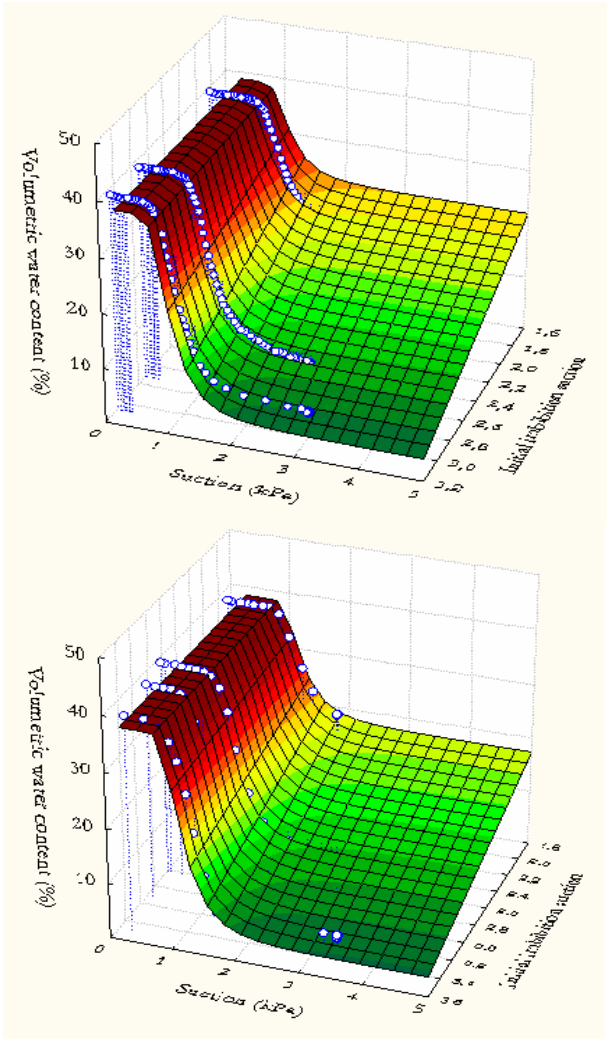

Figure 8.5: Experimental imbibition results (1^{st} imbibition, 2^{nd} imbibition) and new hysteresis SWCC model best fit (loose specimen, transient state sand column test)

Table 8.3: Constitutive parameters for the new hysteresis SWCC model (calibrated)

Experimental results	b_0	b_1	b_2	b_{31}	b_{32}	R^2
Loose specimen						
1^{st} imbibition	38.87	−4.69	1.04	0.90	−11.14	0.997
2^{nd} imbibition	38.11	−4.96	0.60	−7.16	−7.67	0.992
Dense specimen						
1^{st} imbibition	35.21	−4.63	0.28	−3.98	−6.59	0.998
2^{nd} imbibition	35.12	−3.99	0.27	−8.09	−5.49	0.998

processes are shown in Figs. 8.8 and 8.9 for loose specimen. These figures depict the outcome from the residual analysis for the three test phases used in building the 2D models. The plots of observed versus residual values, observed versus predicted values are shown as well as the normal probability plots and histograms.

- *Plots of residual versus predicted variables and observed versus predicted variables:*

  Plots of residual versus predicted variables and observed versus predicted variables are given in Fig. 8.6 and 8.7 for drainage process (appropriate results from dense specimen are given in Figs. E.6 and E.7 in Appendix E). The points in the plots of the observed versus predicted values are close to the bisection line that indicates a small error in observed and predicted values. The plots of the residuals versus predicted values do not exhibit any systematic structure and thus indicate that the model fits the experimental data well. Even the points are crowded in the saturated zone and residual zone the range of residuals looks essentially constant across the levels of the predicted values. Additionally it is stated here, that some discrepancies can be observed in Fig. E.7 (see

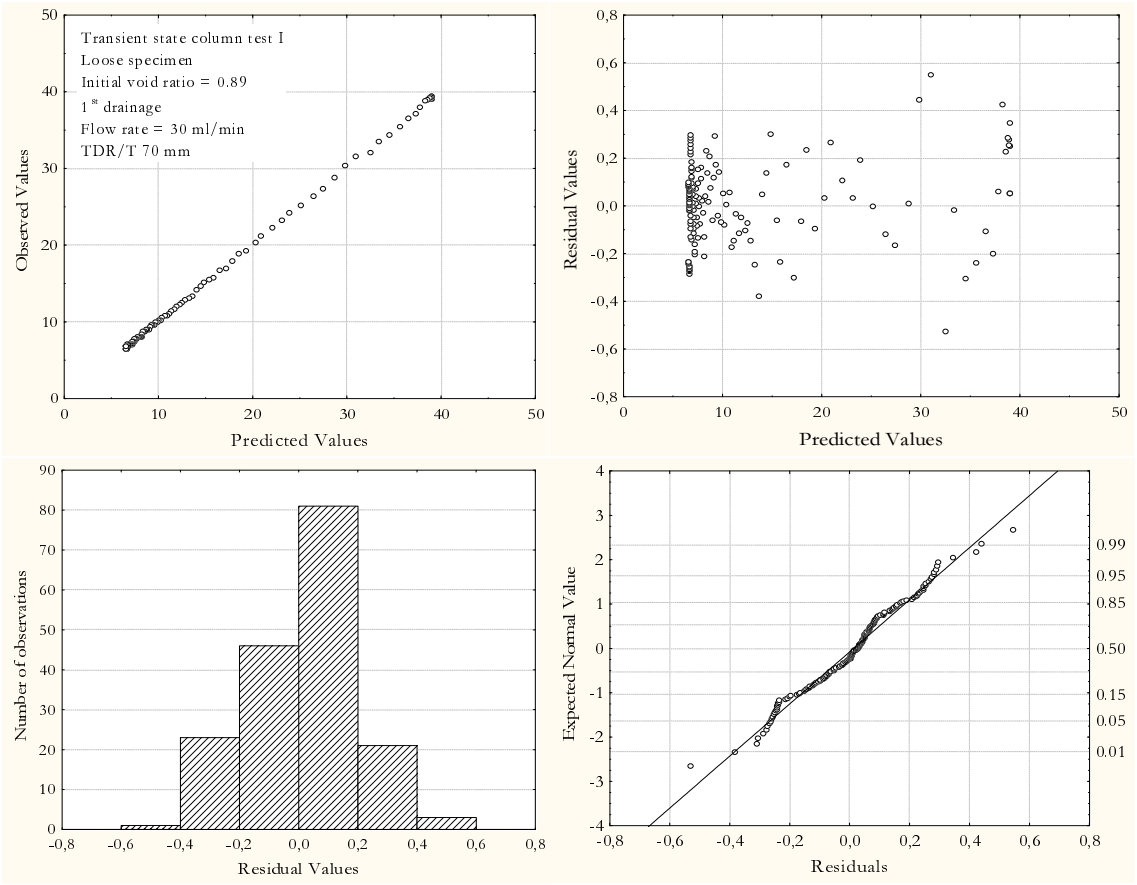

Figure 8.6: Model validation results from 1^{st} drainage process (loose specimen, TDR/T70 mm)

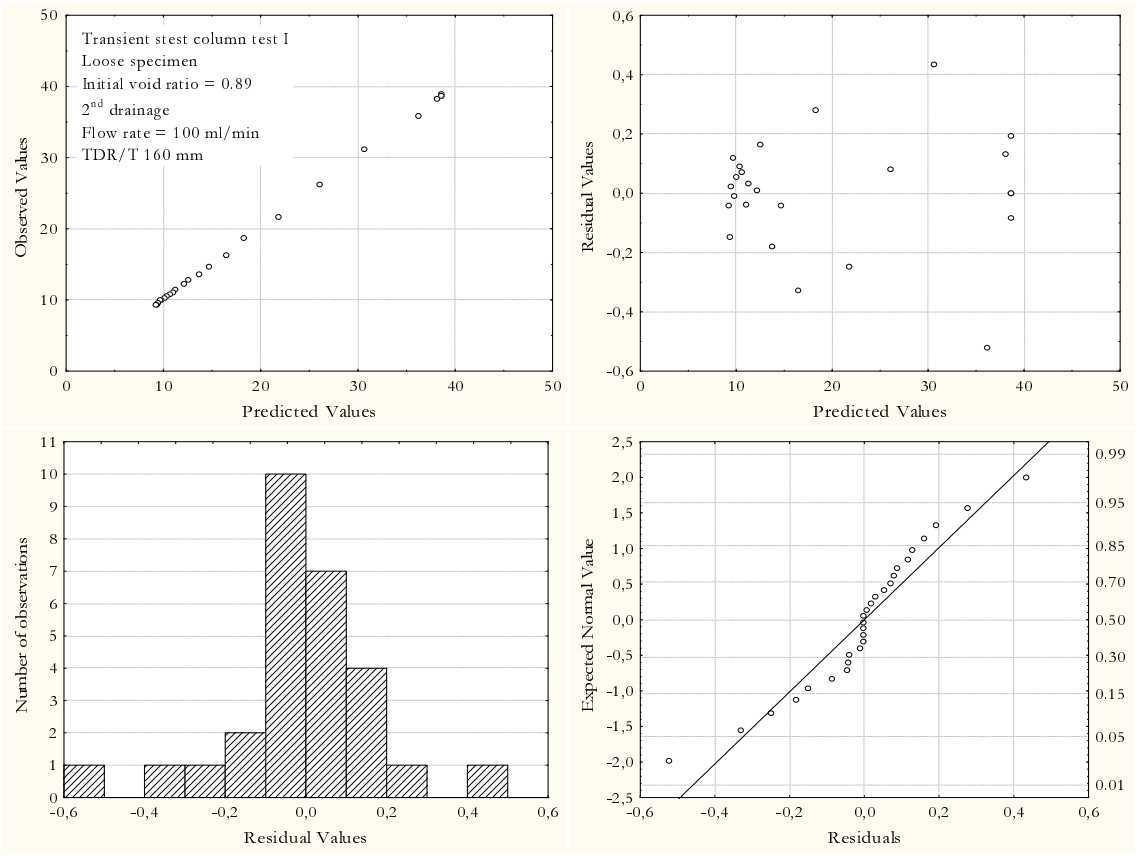

Figure 8.7: Model validation results from 2^{nd} drainage process (loose specimen, TDR/T160 mm)

Appendix E) for dense specimen during drainage process that is attributed to the minor set of data, where only few results are available in the unsaturated zone ($\theta < 34\%$) and most data are available in the saturated zone ($\theta = 34\%$).

Plots of residual versus predicted variables and observed versus predicted variables are given in Fig. 8.8 and 8.9 for imbibition process of loose specimen (and respectively in Appendix E in Figs. E.8 and E.9 for dense specimen). The plots of the observed versus predicted values from imbibition curve show slight variations between measured and calculated values. Nevertheless the points are linear related. The scatterplots of the residual versus predicted values are randomly distributed in Fig. 8.9. Non-randomness is observed in Fig. 8.8. Similar to the results derived from drainage curve fit the points are crowded in the saturated zone and in the residual zone, where most measurements were achieved while withdrawing and injecting water.

- *Normal probability plot:*

The normal probability plots in Figs. 8.6 and 8.9 from both, drainage and imbibition process, show that it is reasonable to assume that the random errors of the process are

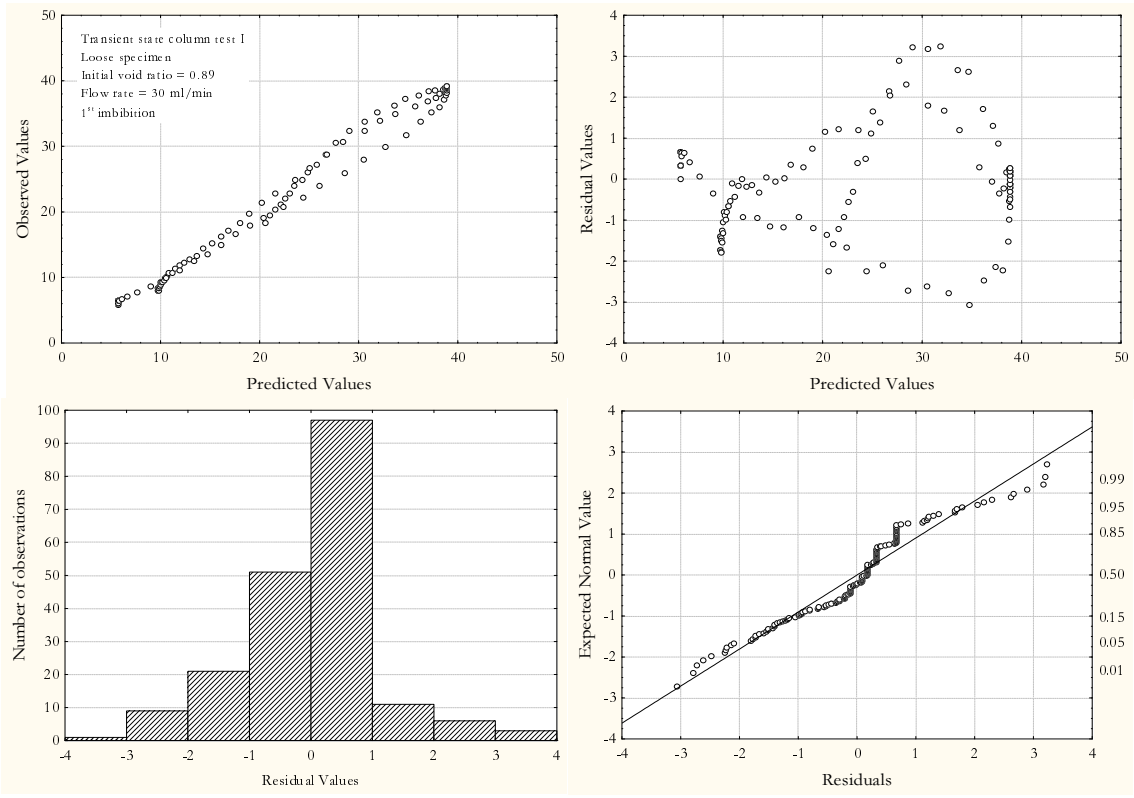

Figure 8.8: Model validation results from 1^{st} imbibition process (loose specimen)

drawn from approximately normal distributions (see also Figs E.6 and E.9 Appendix E). Also if the plots show that the relationship is not perfectly deterministic a strong linear behavior between the residuals and the theoretical values from the standard normal distribution is given. Since non of the points in these plots deviate much from the linear relationship it is reasonable to conclude that there are no outliers in the experimental results.

- *Histogram:*

  The histograms in Figs. 8.6 to 8.9 (and Figs. E.6 to E.9 Appendix E) are bell-shaped for drainage and imbibition process and confirm the conclusions from the normal probability plot. Only the histogram in Fig. E.7 (see Appendix E), where few set of experimental data are available does not give a good normal distribution (see also plot of residual versus predicted values).

- *Coefficient of non-linear regression R^2:*

  The values of non-linear regression R^2 are very close to 1 ($R^2 = 0.99$, see also Tab. 8.1) for the drainage process. The non-linear regression coefficient for imbibition process is also close to 1 with a value of $R^2 = 0.99$ (see Tab. 8.3).

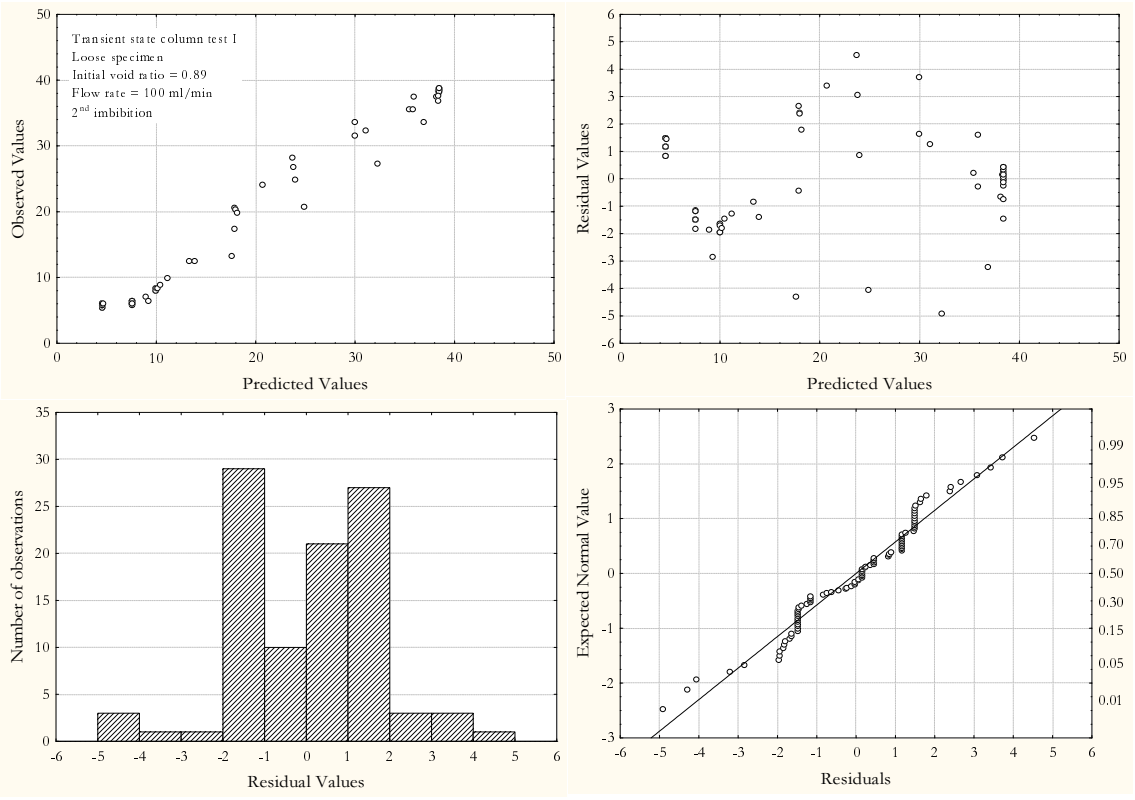

Figure 8.9: Model validation results from 2^{nd} imbibition process (loose specimen)

Both, residual analysis and coefficient of regression determination give enough support to use the proposed model equation for predicting drainage volumetric water content θ with sufficient small error. For the imbibition process the residual analysis also gives enough support to use the proposed model equation for predicting hysteresis imbibition suction-water content relation. The non-linear regression coefficient underlines this conclusion.

For validation of the proposed models experimental data derived in the modified pressure plate apparatus were also fitted. Experimental results of main drainage and main imbibition curve, where Eq. 8.2 was used for prediction are presented in Fig. 8.10. The predicted curve fits the experimental data very well. This can be stated for the saturated zone, unsaturated zone as well as transition zone. The fits of the drainage and imbibition curves for the loose and dense specimen each reach a coefficient of regression $R^2 > 0.99$. Experimental results of scanning imbibition curves including results of the main imbibition curve were best fitted using the proposed model (Eq. 8.3) for fitting scanning imbibition curves. The derived best fit and the corresponding experimental results are presented in Fig. 8.11. The calculated results and the observed results are in good agreement even a single model, that is a simple application, was used for fitting several imbibition curves. Regression coefficient of $R^2 = 0.993$ for the loose and $R^2 = 0.992$ for the dense experimental results was achieved. Differences between experimental and predicted results were observed for the scanning imbibition curves

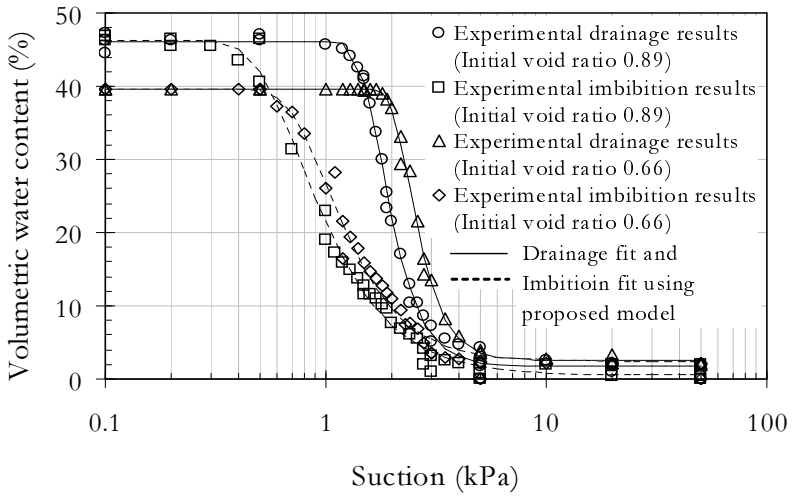

Figure 8.10: Model validation results from main drainage and main imbibition curve derived from steady state tests in the modified pressure plate apparatus (loose and dense specimen)

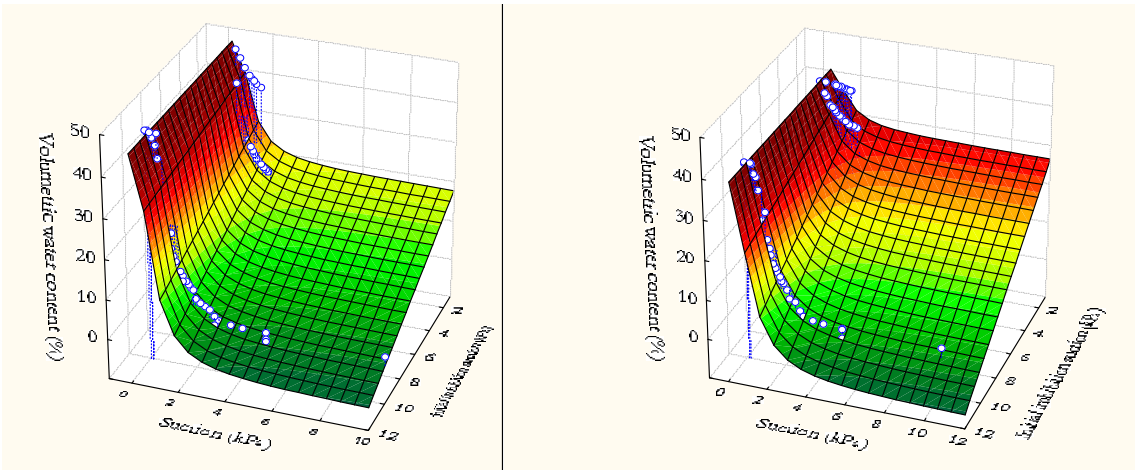

Figure 8.11: Model validation results from scanning imbibition curves derived from steady state tests in the modified pressure plate apparatus (loose specimen-left, dense specimen-right)

in upper part of the soil-water characteristic curve. Modifications of the proposed model may be necessary, using the above described procedure.

8.3 Summary

Following a well understood statistical method (process modeling) new soil-water characteristic curve models were proposed for drainage and imbibition process. The procedure was introduced in detail in Chapter 3 and easily could be applied in this chapter for any suction-volumetric water content (saturation, gravimetric water content) measurements derived from

sand column tests I. In this way the obtained soil-water characteristic curve models allow to better assess the measurement error and also provide functional form for the scanning curves. Two models were derived: i) Model 1 (see Eq. 8.2) that can be used for drainage or imbibition process and ii) Model 2 (see Eq. 8.3), that is an extension and incorporates hysteresis behavior (scanning curves). Extended regression analysis and validation support the usage of the new soil-water characteristic curve models for the investigated sand.

Chapter 9

Numerical Simulation of Column Test by FEM

9.1 General

The investigation presented in the following chapter shows numerical simulations. Boundary value problem is solved and compared to the experimental results. Numerical investigation of drainage as well as imbibition processes of experiments carried out in the sand column I under transient state condition are performed.

Two approaches are discussed, that are carried out using suction-water content parameters directly derived from transient state test (sand column test I) and from steady state test (modified pressure plate apparatus), that is classical method for prediction of suction-water content parameters used for numerical investigation. The aim is to find reliable predictions on unsaturated flow including the phenomena of hysteresis and entrapped air, which are found to be significant for the experiments performed in the sand column test I. Therefore following requirements to the numerical simulation are necessary:

- Simulation including hysteresis behavior.
- Simulation including scanning behavior.
- Simulation considering the phenomena of entrapped air.

The numerical simulations in this work are carried out with the multi-phase flow module of the numerical simulator MUFTE-UG (Multiphase Flow Transport and Energy model-Unstructured Grids). The balance equations for the two phases are solved fully coupled using on a node-centered Finite-Volume discretization in space, the BOX-scheme (Bastian et al. 1997, Helmig 1997, Huber & Helmig 1999). A backward-difference Euler scheme is applied for the time discretization. The resulting non-linear system of equations is solved with a quasi Newton-Raphson scheme, where the linear system of equations is handled with a BiCGStab (stabilized biconjugate gradient) scheme utilizing a V-multi-grid cycle as pre- and post-smoother.

9.2 Model used for Numerical Investigation

Based on the suction-water content model developed by Parker & Lenhard (1987) numerical investigation are carried out. The model is an empirical scaling hysteresis approach that can produce a realistic representation of scanning curves and hysteresis loops. For prediction of main drainage and main imbibition curve Parker & Lenhard (1987) used the suction-water content model by van Genuchten (1980). Their concept introduces an *apparent* saturation in order to account for the effect of residual trapped non-wetting phase saturation. Thus they distinguish between the effective and the apparent wetting phase saturation. The effective saturation $\bar{S}_w$ is considered as the mobile part of the phase. The apparent saturation $\bar{\bar{S}}_w$ is the sum of the effective saturation $\bar{S}_w$ and the trapped effective saturation $\bar{S}_{nt}$ of the non-wetting phase (see Fig. 9.1). If there is non-wetting phase entrapment ($\bar{S}_{nr(i)}$), the soil-water characteristic curve for drainage and imbibition do not form closed loops. The formation of closed loops is possible by substitution of the effective by the apparent saturation (Fig. 9.1), that also accounts for fluid entrapment. Consequently, hysteresis is formed by scaling the apparent saturation. For example, saturation at point ζ that lies on an imbibition scanning curve (see Fig. 9.1, right) can be scaled as follows:

$$\bar{\bar{S}}_w(\zeta) = \frac{\bar{\bar{S}}_7 - \bar{\bar{S}}_6}{\bar{\bar{S}}_5 - \bar{\bar{S}}_6} \cdot (\bar{\bar{S}}_4 - \bar{\bar{S}}_3) + \bar{\bar{S}}_3. \tag{9.1}$$

For simulation of flow in unsaturated porous media and considering hysteresis effect in these simulations the model by Parker & Lenhard (1987) was implemented into MUFTE-UG by Sheta (1999) and Papafotiou (2008).

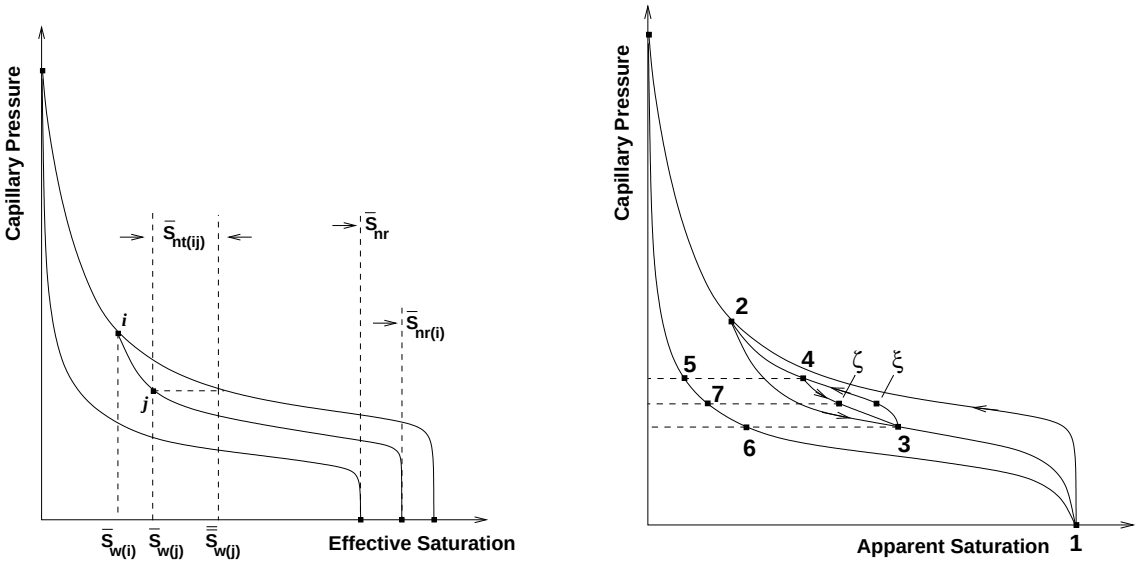

Figure 9.1: Hysteresis and phase entrapment properties of the soil-water characteristic curve

9.3 Setup of Numerical Simulations

For the numerical simulation, a regular rectangular FE mesh is used. The spacing of the grid is 5 mm along the z-axis (direction of gravity). The width of the finite elements on the x-axis is chosen such that the bottom area of the discretized model domain corresponds to the bottom area of the cylindrical sand column described in the previous section. In the numerical simulation, although the problem is one-dimensional, the model domain has a depth of 1.0 m. Thus, the width of the domain in the numerical model is chosen to be 0.073062 m (see Fig. 9.2). A timestep of 4 s is chosen.

The initial and boundary conditions in the numerical simulation correspond to those of the experiment. The primary variables are the water pressure u_w and the air saturation S_n. The specimen is initially saturated and thus the effective saturation of water in the model domain is equal to 1.0. A hydrostatic distribution is given for the water pressure. At the top boundary, a Dirichlet boundary condition is applied for the water and the air phase. This boundary condition defines directly a water pressure value equal to -3400 Pa at the top of the column. This water pressure is equal to the maximum value of matric suction measured during the sand column test I experiment. In combination with the Dirichlet boundary value 1.0 for the air saturation, the definition of phase pressure difference ($\psi = u_a - u_w$) delivers that the pressure of air at the top boundary is equal to zero (atmospheric condition). The applied Dirichlet boundary condition at the top of the numerical model does not avoid water to flow through this boundary and therefore might introduce an error in the mass balance. To prevent any mass of water from leaving the domain through the top boundary, the wetting phase relative permeability at the finite elements of the upper layer is explicitly set to zero.

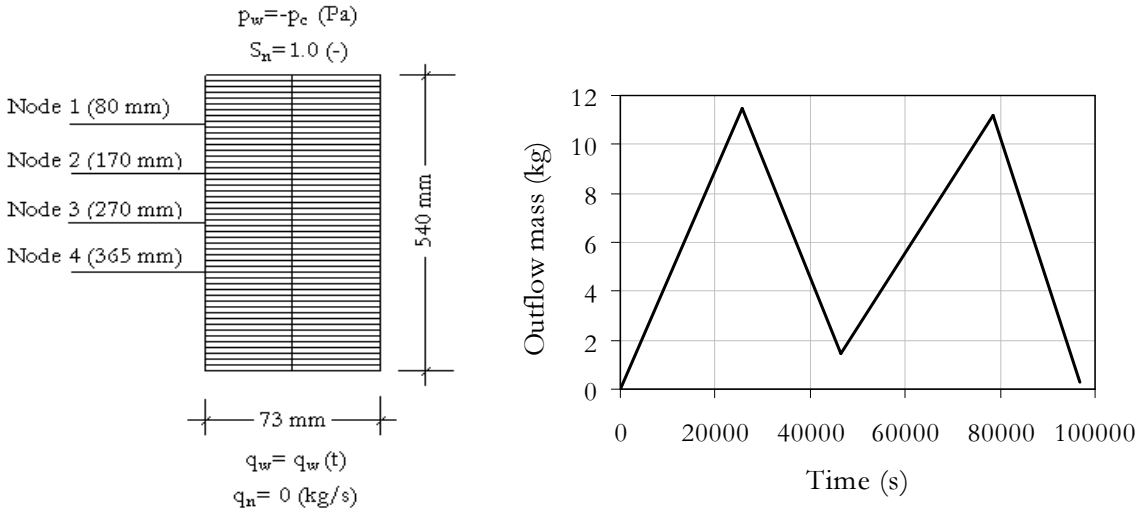

Figure 9.2: Domain and boundary conditions (left) and water outflow and inflow (right) in the numerical simulation

Table 9.1: Input parameters for the soil-water characteristic

Van Genuchten parameter	S_{wr}	S_{nr}	α	n
Transient state test - drainage	0.13	0.005	0.0005	8.0
Transient state test - imbibition	0.13	0.18	0.001	6.5
Steady state test - drainage	0.05	0.01	0.00055	6.0
Steady state test - imbibition	0.02	0.01	0.0015	2.8

In the experiment and also in the numerical simulations air is not allowed to reach the bottom of the sand column and of the model domain respectively. At the bottom of the numerical model, a Neumann no-flow boundary condition is assigned to air, that ensures that no mass of air flows through the bottom. For the water phase, also a Neumann boundary condition is applied. In this case, the amount of water flux in or out of the model domain is a predefined function of time as presented in Chapter 5. The fixed flux of water phase introduced by the Neumann boundary condition implies that at a certain time a certain mass of water has entered the model domain. For instance, during imbibition the total mass of water in the domain does not depend on the hysteresis model, or even on whether hysteresis is taken into account at all, but only on the value of water influx at the bottom boundary. The same is true for the hydraulic properties of the sand that are used as input in the numerical simulation. Permeability, porosity and soil-water characteristic curve do not relate to the amount of water mass in the domain, but strongly influence how this mass distributes in it. The water mass outflow and inflow is shown in Fig. 9.2.

Two different sets of parameters for the hysteretic soil-water characteristic curve were identified that are given in Table 9.1. First the hysteretic soil-water characteristic curve is determined directly from the sand column test results during the transient state test. An additional hysteretic soil-water characteristic curve is determined based on the results from classical steady state experiment.

9.4 Comparison of Simulation Results and Experimental Results

Experimental pore-water pressure and volumetric water content versus time results and numerical pore-water pressure and volumetric water content versus time results as well as experimental and numerical soil-water characteristic curves are compared.

- *Comparison using soil-water characteristic curve from transient state test:*

  In the first numerical simulation, the soil-water characteristic curve parameters are used as input parameters directly measured by the TDR sensors and tensiometer sensors. Simulation results are compared to the experimental results in terms of saturation versus

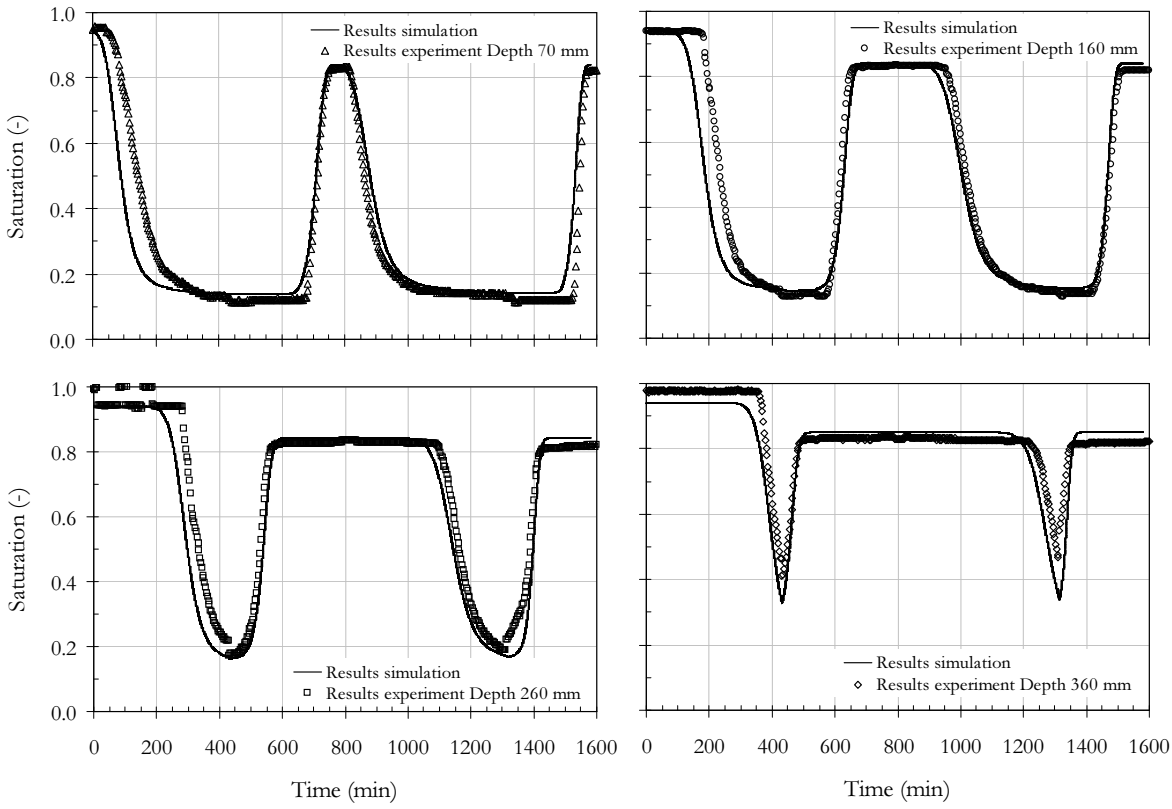

Figure 9.3: Comparison of pore-water pressure measurements and simulation including hysteresis model from Parker and Lenhard (1987) - transient state test

time as well as pressure versus time measurements at several depths in the column. The simulation results including the hysteresis concept from Parker and Lenhard that considers also entrapped air compared to the experimental results are given in Fig. 9.3 and 9.4. The comparison between the predicted and measured saturation and pressure is illustrated for four measurement depths. The results for the measurement point near the bottom of the column are not presented as saturated conditions are maintained there in both the experiment and the numerical simulation. As the comparison of the results shows, the numerical simulation provides a good prediction of the experiment both in terms of saturation and pressure. For the entire sequence of drainage and imbibition events, the numerical simulation predicts the starting values of saturation and pressure for each event (that strongly relate to the amount of trapped air) as well as to variation of pressure and saturation in time. This can also be illustrated by plotting the resulting soil-water characteristic curves from the experiment and the simulation (see Fig 9.5). The simulation uses a rather simple scaling hysteresis concept and therefore achieved a good prediction of the entire flow behavior in the transient state test.

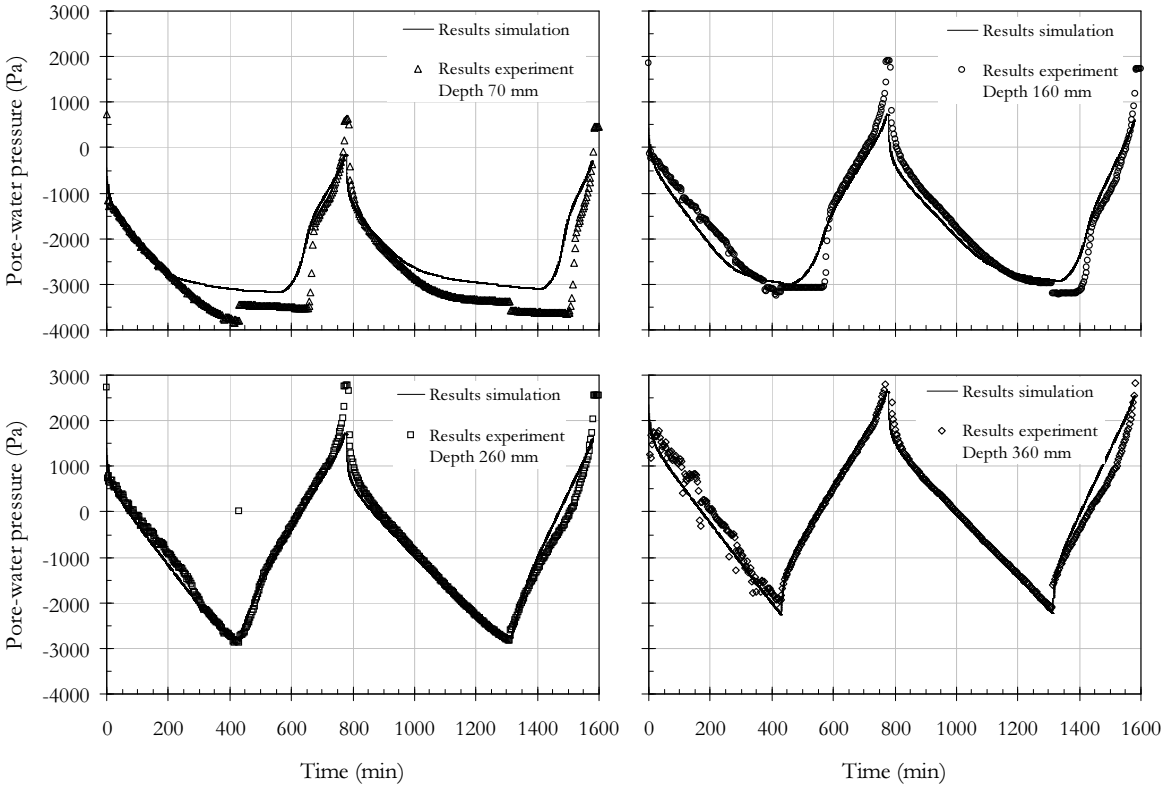

Figure 9.4: Comparison of saturation versus time measurements and simulation including hysteresis model from Parker and Lenhard (1987) - transient state test

- *Comparison using soil-water characteristic curve from steady-state experiment:*

  Due to missing information on either saturation or pressure measurements it is quite common to use suction-water content parameter set from separately performed tests. The simulations presented above show that if the soil-water characteristic curve that is directly measured in the transient state test is used combined with the numerical implementation of the Parker and Lenhard hysteresis concept, a good agreement between measured and predicted pressure versus time and saturation versus time relationships is obtained. However, the traditional approach is to measure the drainage and imbibition suction-water content curves in separate steady-state test (here modified pressure plate apparatus) and then use this information as input for numerical simulation in order to obtain predictions on hysteretic unsaturated flow. The classical approach is applied here and the results are given in Fig. 9.6 and 9.7. While during the transient state tests air trapping for imbibition process was measured, during steady state test no air trapping for imbibition process is observed. Therefore it is expected that the soil-water characteristic curve from the steady-state experiment will not provide a good prediction. As assumed the simulation results show no proper agreement with respect to the entrapped

air saturations (see Fig. 9.8). The obtained water saturation values are significantly overestimated by the simulation for saturation $Sw > 0.8$ in the first imbibition, second drainage and also second imbibition cycle. Although the pressure versus time results show good agreement between obtained and simulated results, strong deviations were observed in the residual zone. This is directly related to the ending saturations on the suction-water content curve measured during steady-state experiment.

The resulting soil-water characteristic curve demonstrates strong hysteresis and air trapping effects. Numerical simulations of the transient state test are carried out using the two-phase flow module of the MUFTE-UG simulator. The simulation and experimental results are compared in terms of saturation versus time as well as pressure versus time for the entire sequence of alternating drainage and imbibition conditions. The comparison shows the necessity of the inclusion of a hysteresis concept in the numerical simulator, especially related to the effect of air trapping and the formation of residual air saturations during imbibition.

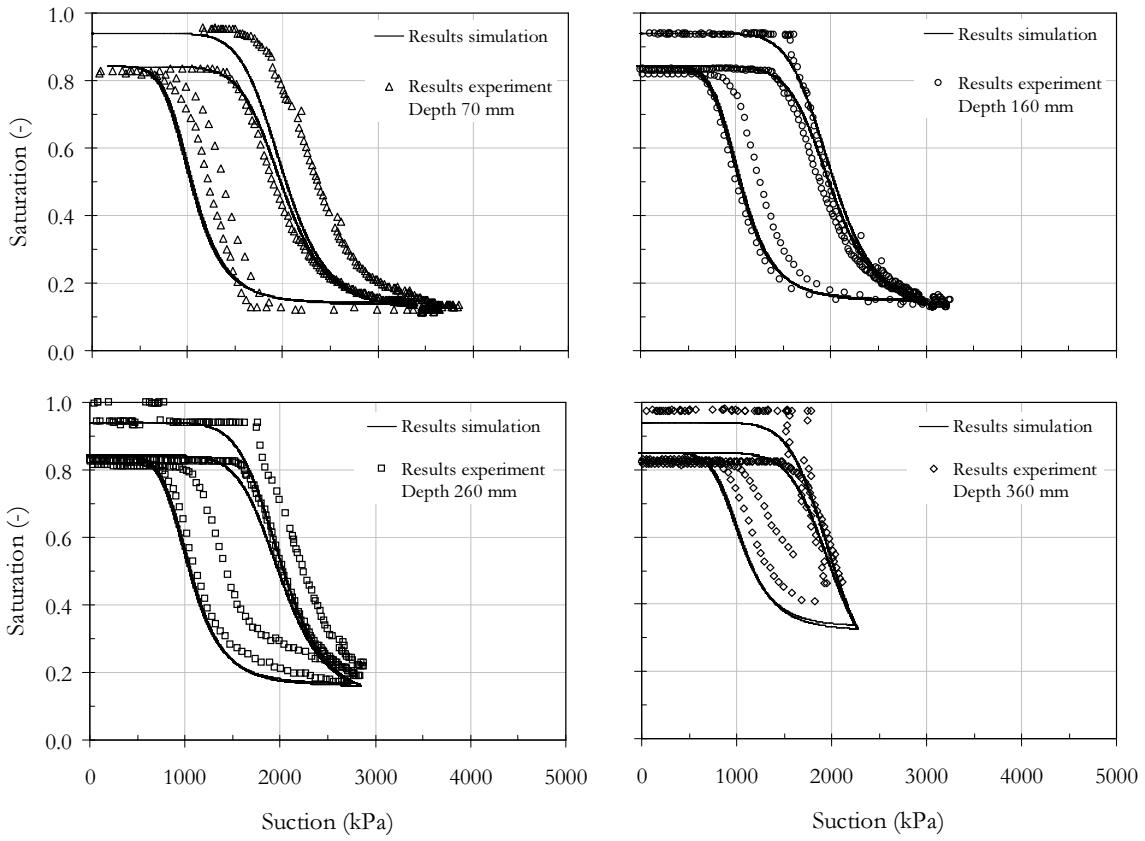

Figure 9.5: Comparison of suction-water content measurements and simulation including hysteresis model from Parker and Lenhard (1987) - transient state test

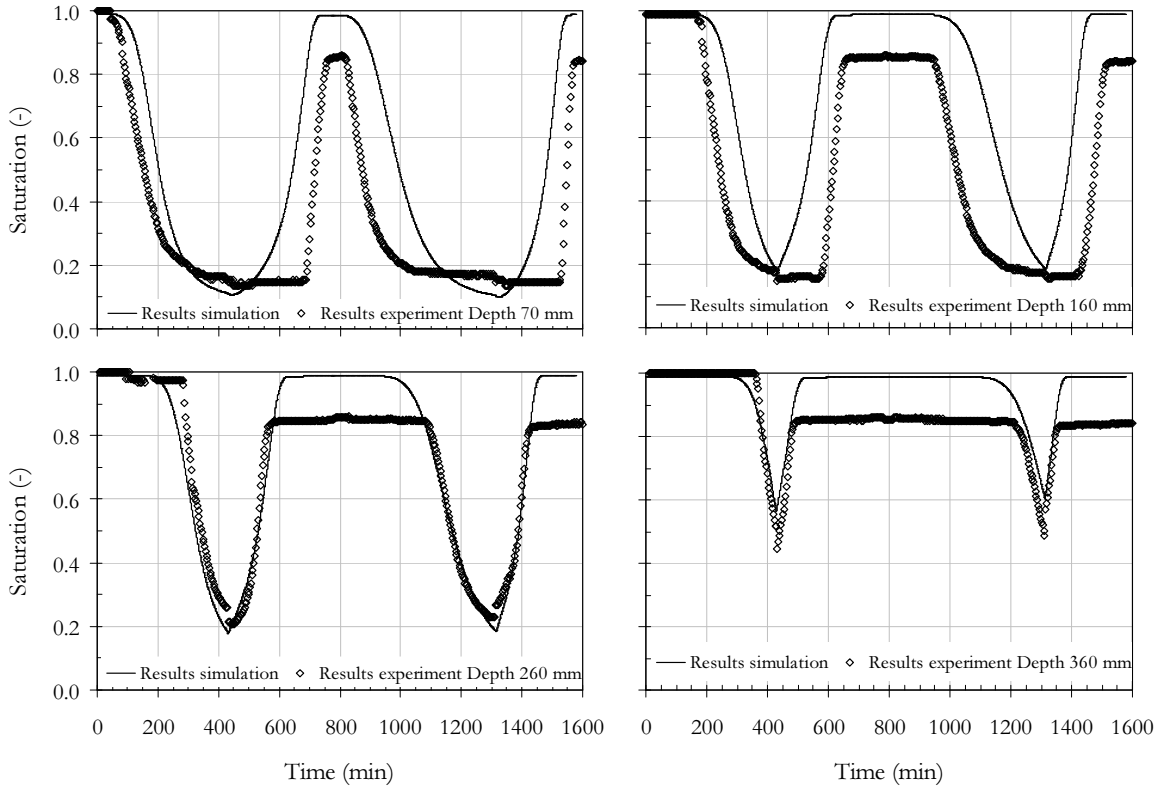

Figure 9.6: Comparison of pore-water pressure measurements and simulation including hysteresis model from Parker and Lenhard (1987) - steady state test

In general, it can be stated that a good prediction of the flow process in the transient state test has been obtained with a conceptually simple scaling approach for hysteresis.

In a further investigation an additional soil-water characteristic curve is determined from steady state experiment on Hostun sand specimens and consequently used for a numerical simulation. This is a common procedure in applications involving unsaturated flow. However, the suction-water content curve determined with this approach demonstrates absence of air residual saturation in imbibition, in contrast to the transient state test where a strong trapping effect is observed. The numerical simulation carried out here incorporates the Parker and Lenhard (1987) hysteresis, however cannot predict correctly the flow process in the transient state experiment due to the inappropriate input soil-water characteristic curve.

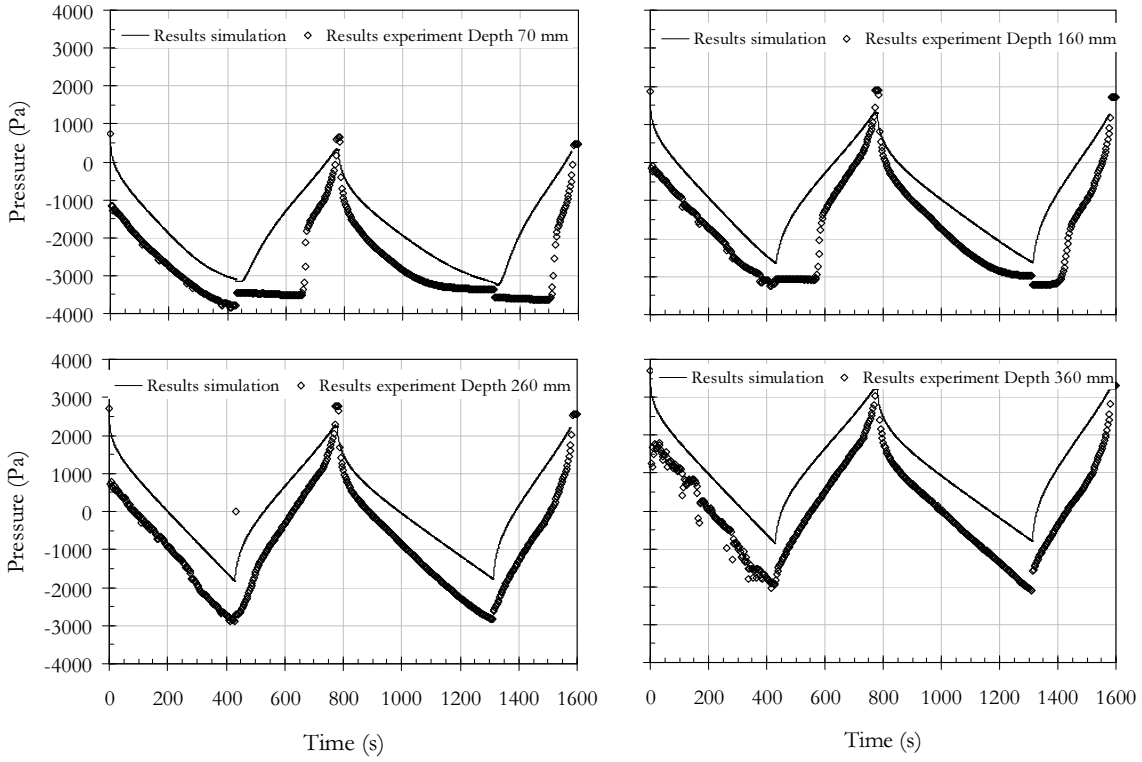

Figure 9.7: Comparison of saturation versus time measurements and simulation including hysteresis model from Parker and Lenhard (1987) - steady state test

9.5 Summary

Concluding, this work shows how modeling and experimental work can optimally be combined in order to gain reliable predictions of hysteretic unsaturated flow. From the modeling point of view, it is demonstrated that the implementation of a simple scaling approach for hysteresis can provide a good prediction of hysteretic unsaturated flow including phase trapping effects. However, this needs to be combined with reliable information of the input suction-water content parameters that is commonly measured in the laboratory. It is shown that this is possible by using direct saturation and pressure measurements on the column. If such data were not available, the traditional approach that determines the soil-water characteristic curve with separate steady state outflow/inflow would provide false information on the amount of air trapping and, consequently, a misleading prediction by means of numerical simulations.

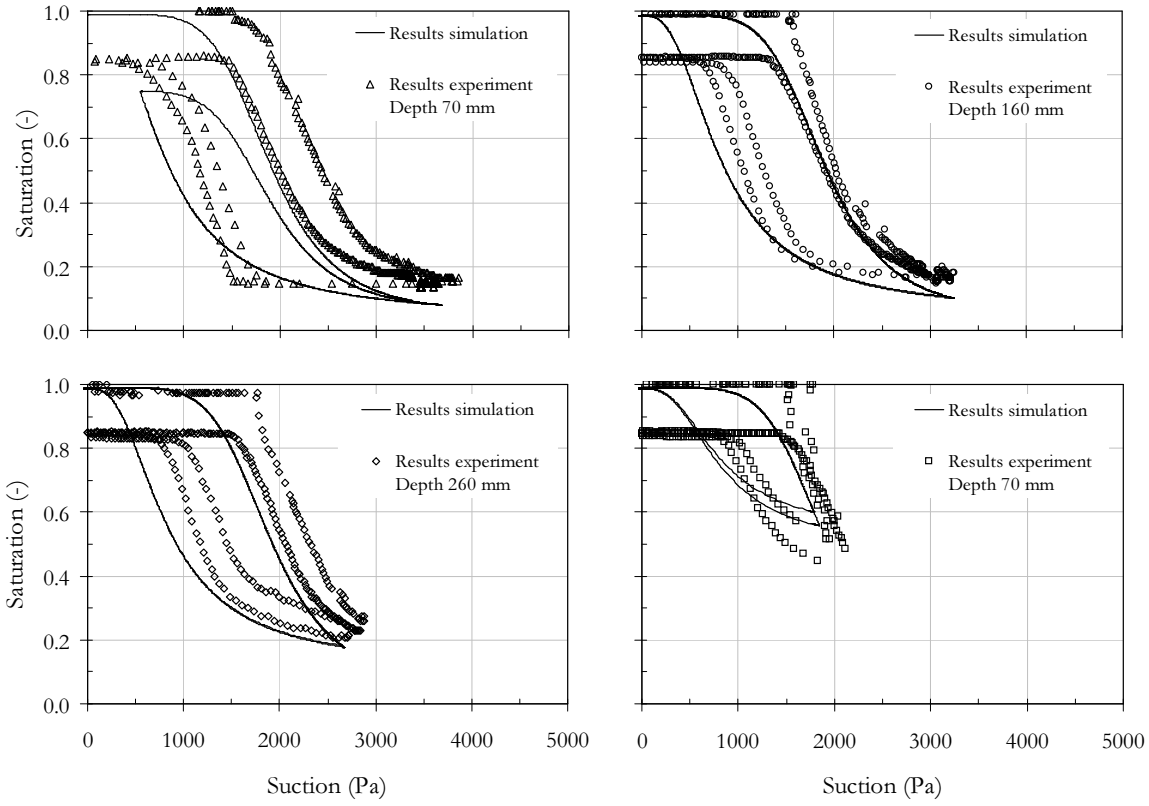

Figure 9.8: Comparison of suction-water content measurements and simulation including hysteresis model from Parker and Lenhard (1987) - steady state test

Chapter 10

Bearing Capacity of a Strip Footing on Unsaturated Hostun Sand

10.1 General

Most of the shallow foundations are typically located above the groundwater table that requires an understanding of bearing capacity and settlement behavior of soils under unsaturated conditions. The influence of soil suction is however not addressed in conventional design of foundations and a framework for interpreting these results is not available. The foundations are conventionally designed assuming saturated conditions for the soil. To investigate the influence of suction on the bearing capacity, a series of model footing tests was carried out to determine the ultimate bearing capacity of the Hostun sand respectively under both unsaturated ($\psi = 2, 3$ and 4 kPa) and saturated ($S = 0$ as well as $S = 1$) conditions. A box was specially designed to load model continuous (i.e. strip) footings under plane strain condition. The experimental results show that ultimate bearing capacity increases up to a certain suction value and then decreases with an increase in the suction value.

Further the soil-water characteristic curve as well as saturated shear strength parameter are used to predict unsaturated bearing capacity. Therefore the model proposed by Vanapalli & Mohamed (2007) is used.

The bearing capacity is the key parameter required when designing foundations. The bearing capacity theory on saturated soil has been investigated in the last century by many researchers. Prandtl (1921) was one of the first author, who studied the behavior of a strip footing. The author loaded the strip footing until it penetrated into the soil. Prandtl (1921) introduced the ultimate bearing capacity q_u of a soil, that is the stress applied for reaching failure in the tested soil. Bearing capacity analysis was developed by Terzaghi (1943), Meyerhof (1951), Vesic (1973), Bolton (1986). Based on the assumption, that a soil is either in fluid saturated condition or dry condition several researchers as for instance Prandtl (1921), Terzaghi (1943), Meyerhof (1951) proposed approaches for the estimation of the bearing capacity.

The solution given by Terzaghi (1943) is accepted since decades:

$$q_u = N_c c' + N_q q + 0.5 B N_\gamma \gamma \tag{10.1}$$

where: q_u is the ultimate bearing capacity, N_c, N_q as well as N_γ are bearing capacity factors providing the contribution of cohesion in the soil, the surcharge and unit weight, c' is the cohesion, q is the overburden pressure, γ is the weight of the soil and B is the width of the footing. Bearing capacity factors based on different assumptions were proposed by several researchers (Terzaghi 1943, Meyerhof 1951, Gussmann 1986, Kumbhojkar 1993, Zhu et al. 2001).

However, foundation designs are complex and due to presence of suction in the soil (i.e. most foundations are located above the groundwater table) an understanding of the soil behavior that comprises the role of suction is required. Only view researchers performed experimental investigations on the influence of suction on the bearing capacity. Broms (1963) found an influence of suction on the bearing capacity of flexible pavements, Oloo et al. (1997) carried out the influence of suction of unpaved roads and presented a procedure for the determination of the bearing capacity in pavement systems. Plate load tests were conducted by Steensen-Bach et al. (1987), Costa et al. (2003), Rojas et al. (2007) on unsaturated sand, lateritic soils and lean clay. Their field tests showed increasing bearing capacity with increase in suction. Bearing capacity tests of a square model surface footing were carried out by Mohamed & Vanapalli (2006), Vanapalli & Mohamed (2007) on an unsaturated coarse grained soil. The authors found the bearing capacity derived from unsaturated specimen 5 to 7 times higher than the bearing capacity from saturated specimen.

Since several experimental studies show non-linear behavior of unsaturated shear strength (Gan et al. 1988, Escario & Juca 1989, Vanapalli & Mohamed 2007), Vanapalli et al. (1996) extended the linear unsaturated shear strength theory proposed by Fredlund et al. (1978). The authors proposed an non-linear equation for prediction of unsaturated shear strength using the soil-water characteristic curve in combination with the saturated shear strength:

$$\tau = [c' + (\sigma_n - u_a)\tan\phi] + (u_a - u_w)(S^\kappa \tan\phi) \tag{10.2}$$

where: c and ϕ are the cohesion and friction angle of saturated soil for a particular net stress σ_n, $(u_a - u_w)$ is the difference between pore-air pressure and pore-water pressure, that is the matric suction, S is the saturation and κ is a fitting parameter. The matric suction and the saturation are derived from the soil-water characteristic curve. The first part includes the parameters of saturated shear strength and the second part includes shear strength due to matric suction. Using the term, that describes the non-linear behavior of the unsaturated shear strength $((u_a - u_w)S^\kappa \tan\phi)$ following equation was proposed to predict the bearing capacity of unsaturated soil (Vanapalli & Mohamed 2007):

$$q_u = [c' + (u_a - u_w)S^\alpha \tan\phi] \cdot N_c \xi_c + 0.5 B N_\gamma \gamma \xi_\gamma \tag{10.3}$$

where: α is a parameter similar to κ in Eq. 10.2, ξ_c is a shape factor due to cohesion and ξ_γ is a shape factor due to unit weight. Before reaching the air-entry value the contribution of the suction to the bearing capacity is linear. This is considered by the following equation given by (Vanapalli & Mohamed 2007):

$$q_u = [c' + (u_a - u_w)_{aev}(1 - S^\alpha)\tan\phi + (u_a - u_w)_{avr} S^\alpha \tan\phi] \cdot N_c \xi_c + 0.5 B N_\gamma \gamma \xi_\gamma \quad (10.4)$$

where: $(u_a - u_w)_{aev}$ is equal to the air-entry value and $(u_a - u_w)_{avr}$ is the average suction measured in the stress bulb below the foundation. In Eqs. 10.3 and 10.4 the influence of overburden pressure is set to zero because unsaturated bearing capacity was tested on surface footings. Following factors were proposed by Vesic (1973) to account for the different shape of footings:

$$\xi_c = 1 + \frac{N_q}{N_c} \cdot \frac{B}{L} \quad (10.5)$$

$$\xi_\gamma = 1 - 0.4 \cdot \frac{B}{L} \quad (10.6)$$

where: B is the width and L the length of the foundation.

When investigating bearing capacity 2 main failure mechanisms are available. Gussmann's (1986) study shows typical failure patterns below strip foundation with rough and smooth surfaces respectively (see Fig. 10.1 and 10.2). The failure pattern with a rough footing is different from a smooth footing. A rough footing typically offers more resistance in comparison to a smooth footing. The ultimate bearing capacity for rough footing is twice the value in comparison to a smooth footing (Gussmann 1986). Therefore the bearing capacity q_u derived in Eq. 10.4 (this equation is based on Eq. 10.1, that considers failure mechanism as given in Fig. 10.1) is reduced to $q_u/2$, when estimating the bearing capacity for smooth footings.

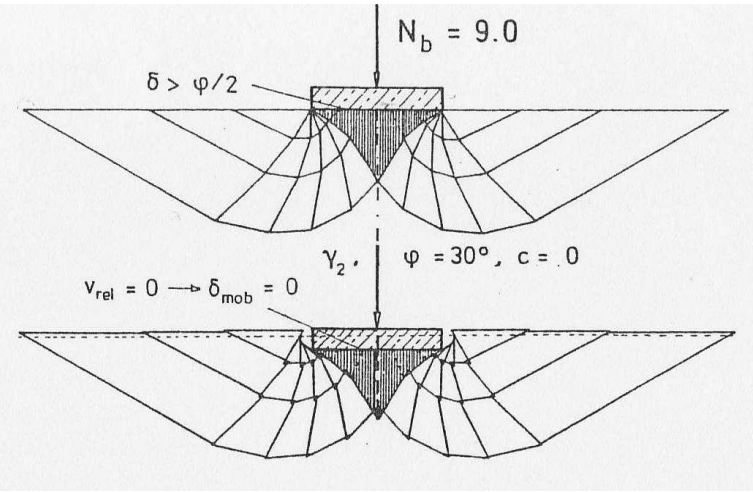

Figure 10.1: Mechanism of failure below rough footing (Gussmann 1986, reprint with permission from P. Gussmann)

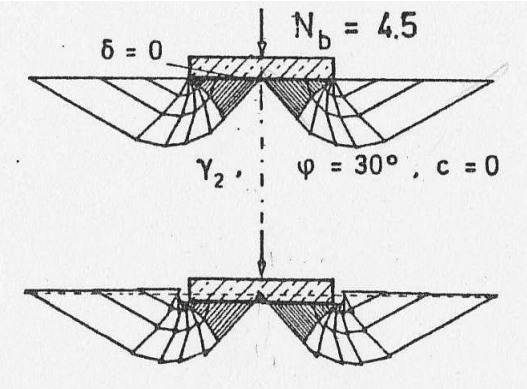

Figure 10.2: Mechanism of failure below smooth footing (Gussmann 1986, reprint with permission from P. Gussmann)

10.2 Bearing Capacity Equipment

Bearing capacity of a surface model footing was measured in a box specially designed for this study. In Fig. 10.3 the bearing capacity equipment is shown. For determination of bearing capacity of model footing a box 1000 mm in length, 500 mm in height and 500 mm in width was designed. The box consists of an outer frame made of wood and an inner tank. The outer frame serves as a stiffener to prevent lateral bending or deformations that may occur when loading the model footing in the tank. The tank was constructed using 9 mm thick plates made of plexiglas. The tank has 4 openings (2 at each side), that are used for application of water to the box. During the testing procedure the openings are connected to

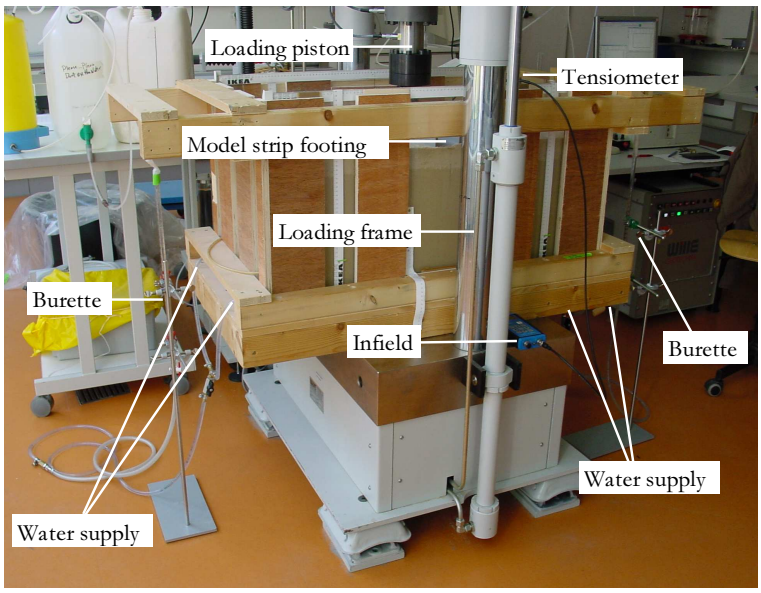

Figure 10.3: Bearing capacity equipment

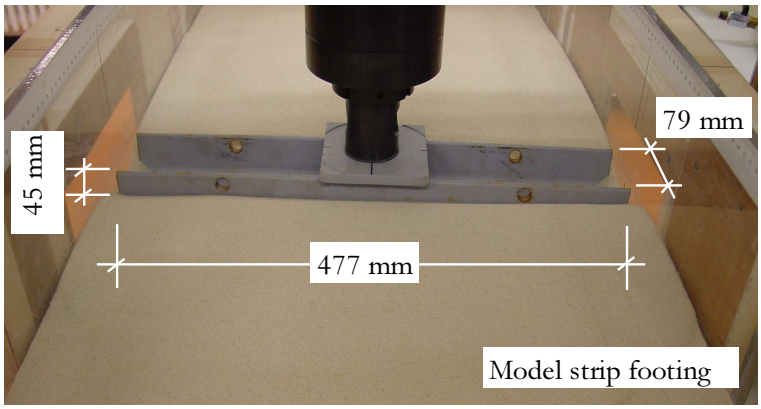

Figure 10.4: Model strip footing

2 burettes (1 at each side), that are used to apply suction to the specimen by hanging water column technique. Bearing capacity tests are performed using a model footing 477 mm in length, 79 mm in width and 45 mm in height, that is a strip footing. The strip footing is made of steel and is shown in Fig. 10.4. The friction angle was determined for plane strain loading conditions using a double wall cell (Schanz & Alabdullah 2007, Alabdullah & Schanz 2009). The measured friction angle was equal to $\phi = 46.9°$. The calculations using Rankine's analysis shows that the failure zones extends to a length approximately equal to 500 mm and the maximum depth to 100 mm. The box was designed such that the box dimensions are greater than the calculated values of the failure zone (i.e. 1000 mm in length, 500 mm in width and 500 mm in height). The failure mechanism is given in Fig. 10.5. Additionally the box may be equipped also with tensiometer sensors in several depth for measuring pore-water pressure. The bearing capacity equipment is placed in a loading frame. Using the loading frame the bearing capacity was measured by loading the surface footing in the saturated specimens as well as unsaturated specimens. During the test the loading system is measuring settlements and the applied load. The accuracy of settlement readings is 0.001 mm and the

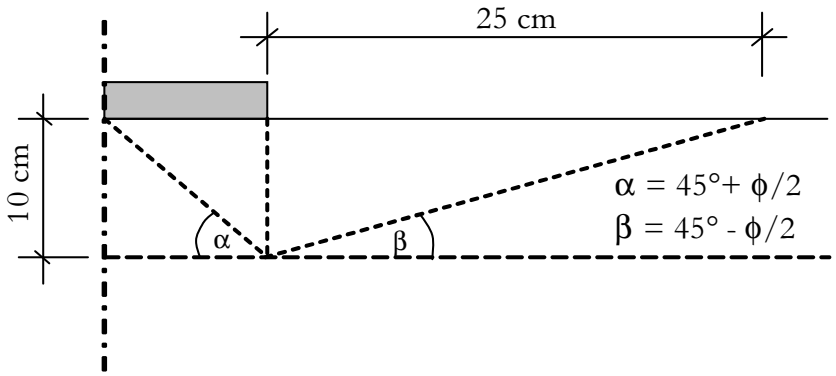

Figure 10.5: Failure below strip footing following Rankine

accuracy of the applied load is 0.05%. A maximum load of 40 kN can be applied when using the loading system. When tensiometer sensor measurements were carried out during testing procedure adequate data logging system was used to compute pore-water pressure.

10.3 Experimental Program

Bearing capacity tests include the loading of a strip footing model, that is placed on the surface of the saturated sand specimen (i.e. either fluid or air saturated) as well as the unsaturated sand specimen ($\psi = 2, 3$ and 4 kPa). The footing was loaded at a constant rate of 0.002 mm/s. Also during loading procedure the footing is not fixed to vertical deformations (i.e. horizontal deformations occur). In a depth of 50 mm the pore-water pressure (i.e. matric suction) was measured using tensiometer sensor when bearing capacity of unsaturated specimen was investigated.

The dry specimen with a height of about 36 cm was prepared by uniformly pluviating oven dry sand with a funnel (500 ml capacity) into the bearing capacity box in several layers. After each layer the specimen was compacted using a 2 kg hand compactor. The water saturated and unsaturated specimen with a height of about 36 cm were prepared by uniformly pluviating oven dry sand with a funnel (500 ml capacity) into the bearing capacity box filled with deaired water. The box was filled with water successively using a water tank, that was connected at one side to the water supply during specimen preparation. The deaired water was stepwise injected into the box from the tank. During the specimen preparation the water level was always kept above the sand specimen to avoid occlusion of air. Similar to the preparation of the dense specimen in the sand column device I the falling height of the sand specimen was approximately 30 cm. To reach unsaturated condition, a matric suction was then induced to the initially fluid saturated specimen by using hanging water column technique. Therefore the connection to the water tank was replaced by a connection to a burette. For preparation of an unsaturated specimen the height of water in both burettes (one at the right hand and one on the left hand side) was set $200, 300$ and 400 mm below the surface of the sand specimen. The bearing capacity tests were performed on specimen with a void ration $e = 0.70$. Denser specimen was not achieved during specimen preparation. When the bearing capacity was tested on the unsaturated specimen pore-water pressure was measured in the vicinity of the expected stress bulb near the model footing using tensiometer.

10.4 Experimental Results

Fig. 10.6 shows the failure pattern observed for the present study undertaken with a smooth footing. The failure pattern is consistent with Gussmann's study showing a smooth surface footing. Some horizontal deformation and sliding occurs (also because the footing is not vertically fixed during loading) along with vertical deformations when a footing has a smooth

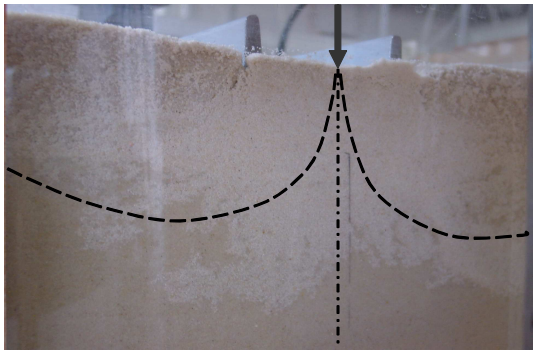

Figure 10.6: Mechanism of failure below footing

surface during the loading of the footing. Experimental results derived from the bearing capacity tests on water and air saturated as well as unsaturated specimen are presented in Fig. 10.7, where the load is plotted versus settlements and the stress is plotted versus

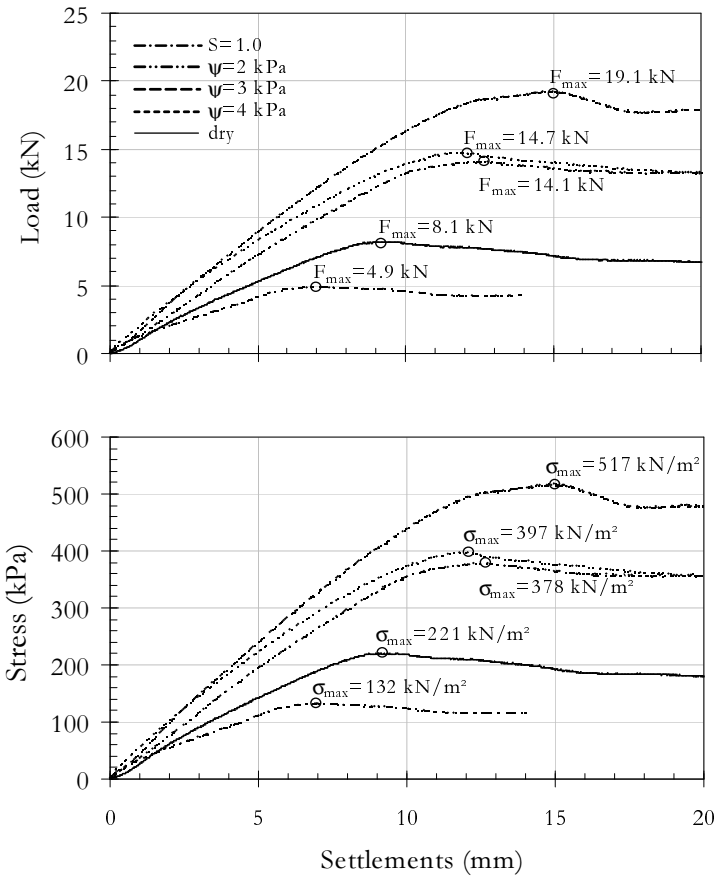

Figure 10.7: Experimental results of bearing capacity tests

settlements. With increasing settlement the load and also the stress are linearly increasing. With larger settlements this behavior becomes non-linear until reaching maximum value (i.e. ultimate bearing capacity), where the soil fails. After the failure the settlements are further increasing but the load and the stress are decreasing. From the results clearly can be seen, that the unsaturated specimens have a higher bearing capacity than the saturated specimens. While the maximum load reached for the unsaturated specimen is $F_{max} = 19$ kN, that refers to a stress of $\sigma_{max} = q_u = 517\ kN/m^2$, the maximum load of the air saturated (S=0) specimen is $F_{max} = 4.9$ kN, that corresponds to a stress of $\sigma_{max} = q_u = 132\ kN/m^2$. The maximum value of the applied load and the stress is reached for the unsaturated specimen for larger settlement value. The results show that the suction and thus the water content in a sand is strongly influencing the behavior of the bearing capacity of strip footings. The bearing capacity of the sand tested under unsaturated condition was found to be approximately 2.5 to 4 times higher then for the saturated specimen. The bearing capacity is increasing with increase in suction and then after reaching an maximum value decreasing.

10.5 Prediction of Bearing Capacity

Following the proposal given by Vanapalli & Mohamed (2007) the bearing capacity is estimated using Eq. 10.3 and compared to the experimental data. Therefore the drainage soil-water characteristic curve derived from the modified pressure plate apparatus for dense specimen, the bearing capacity factors derived by Terzaghi and the shape factors derived from Eqs. 10.5 and 10.6, a friction angle of $\phi = 46.9°$ as well as an air-entry value of $\psi_{aev} = 1.9$ kPa were used, the average suction is equal to the suction observed by the tensiometer. The parameter κ is set to 1. This equation takes the same form as Terzaghi's equation shown in Eq. 10.1 without the surcharge contribution if $(u_a - u_w)$ value is set to zero. The contribution of surcharge is not necessary in the present study as the model footing was loaded placing them directly on the sand surface. Important parameters used for the prediction are also given in Tab. 10.1. In Fig. 10.8 the experimental results in comparison to the predicted results are shown. The prediction shows an increase of the bearing capacity with increasing suction, that is consistent with the experimental results. Overall observation is that the predicted values follow the trend of the experimental results. Whereas after reaching the air-entry value (transition zone) the experimental results of bearing capacity are still increasing the predicted values are already decreasing. The experimental results are underestimated by the predicted results. In the residual zone a decrease of bearing capacity was observed by

Table 10.1: Parameters used for prediction of bearing capacity

Parameter	ψ_{aev}	ϕ	N_c	N_γ	ξ_c	ξ_γ
	1.9 kPa	46.9°	223	407	1	0.93

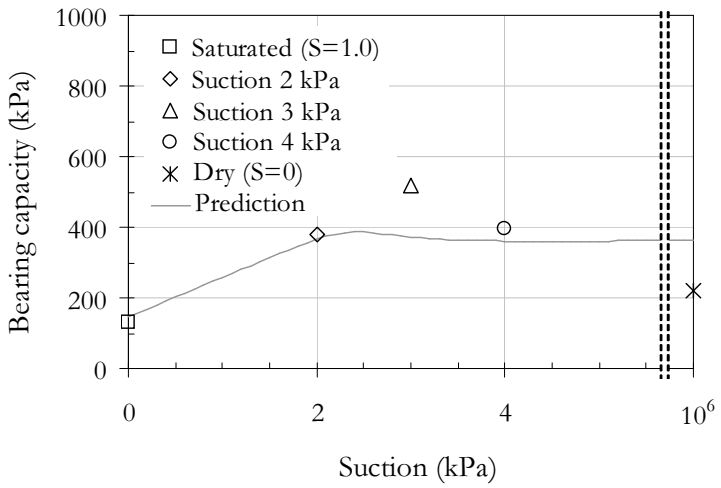

Figure 10.8: Comparison of experimental and predicted results of bearing capacity

the measurements. Predicted values are only slightly decreasing, which is not consistent with theory. In theory mechanical behavior of saturated soils is equal. The experimental results are overestimated by the predicted results. Further investigation on bearing capacity of strip footings on unsaturated soils and the development as well as validation of an equation for predicting unsaturated soils bearing capacity is needed.

10.6 Summary

Bearing capacity of a surface model footing was carried out on saturated as well as unsaturated sand in a fundament box. According to Gussmann (1986) failure mechanism of smooth footing was found below the footing. The results show, that the bearing capacity is improved when dealing with unsaturated sand. Similar to the influence of suction on the stiffness of Hostun sand, the bearing capacity is increasing first with increasing suction and is than after reaching an optimum decreasing with further increase in suction. At all the bearing capacity was found to be 2.5 to 4 times higher then for the saturated specimen.

The approach suggested by Vanapalli & Mohamed (2007) was successfully applied to the derived experimental results. Further experimental investigation of bearing capacity on unsaturated Hostun sand is necessary in the residual zone to validate and modify the approach given by Vanapalli & Mohamed (2007). The difference between measured and predicted results in the residual zone has to be reduced. Also the predictions of bearing capacity of water and air saturated specimen are not in the same range when using the model by Vanapalli & Mohamed (2007). Theoretically water and air saturated specimen show similar mechanical behavior.

Chapter 11

Summary and Outlook

11.1 General

In the following chapter the main results of the present study are summarized. Advantages and disadvantages of the testing devices and equipment used for investigation of unsaturated sand are given in detail. The results derived from these devices and equipments are hydro-mechancial properties of unsaturated Hostun sand, which are also concluded. The influence of several conditions (e.g. initial condition) on the unsaturated hydro-mechancial is given.

Unsaturated hydraulic behavior was investigated in sand column testing device I, that was simulated using MUFTE-UG. Two sets of parameters were used: i) a parameter set directly estimated from the transient state sand column test I and ii) a parameter set derived from conventional test (steady state results from modified pressure plate apparatus). The main outcomes are given below.

In case of a typical engineering problem, i.e. bearing capacity, the importance of consideration of suction in a soil was shown in the present investigation. As important key relation for prediction of unsaturated bearing capacity the soil-water characteristic curve is required. Results from experiments carried out and the predictions are concluded.

Finally future work for further investigation on hydro-mechancial behavior of unsaturated sand is proposed. This includes experimental investigations as well as theoretical investigations on numerical simulations and development and improvement of models for describing hydraulic and mechanical unsaturated soils behavior (soil-water characteristic curve model, model for prediction of unsaturated stiffness, model for prediction of unsaturated bearing capacity).

11.2 Testing Devices and Equipment

A newly developed modified pressure plate apparatus and two column testing devices (sand column testing device I, sand column testing device II), which were additionally equipped with sensors for measuring water content and pore-water pressure, are introduced in the present

study and used to perform a series of imbibition and drainage tests on Hostun sand. The hydraulic behavior of unsaturated Hostun sand was examined in these cells. In the following advantages and disadvantages of the cells are summarized that were found when performing experiments on unsaturated sand.

The following advantages (+) and disadvantages (-) were found when using the *Modified Pressure Plate Apparatus* :

+ Only a small specimen needs to be prepared. The distribution of void ratio and suction along the height of the specimen can be assumed to be homogeneous.

+ The application of small suction values along with small suction steps enables a precise estimation of the shape of the soil-water characteristic curve and the parameters near the air-entry value, residual suction, residual volumetric water content and water-entry value. This is an important requirement when using the best-fit procedure on an equation.

+ The drainage curve, imbibition curve as well as scanning drainage and imbibition curves can be measured. Predefined suction values can be applied.

+ The application of vertical net stress enables the investigation of mechanical loading on an unsaturated soil.

+ Measurements of changes in volume during drainage and imbibition processes can be carried out.

+ The apparatus is relatively inexpensive, small and user-friendly.

+ The 1 bar ceramic disk can be replaced with a 5 bar ceramic disk to investigate silty soils or conventional disk made of porous stone.

- Only steady-state tests can be performed.

- The testing procedure is time consuming.

- A permanent observation of water outflow and inflow is necessary in order to find equilibrium conditions.

Following advantages and disadvantages were found when using the *Sand Column Testing Device I* :

+ Transient state tests as well as steady state tests can be performed under various flow rates. The influence of flow rate on the hydraulic behavior of unsaturated sand can be determined using the attached pump.

+ The drainage curve, imbibition curve as well as scanning drainage and imbibition curves can be measured.

+ The procedure is not time consuming.

+ Volumetric water content measurements $\theta(t)$ and suctions measurements $\psi(t)$ can be used to directly determine hydraulic functions (suction-water content relation, unsaturated hydraulic conductivity).

- Expensive equipment is required (i.e., TDR sensors, tensiometers, 2 computers for computing results).

- Careful calibration of the sensors is necessary.

- Preparation of the specimen is time consuming and a large mass of material to be tested is needed.

- The specimen must be a disturbed specimen.

Following advantages and disadvantages were found when using the *Sand Column Testing Device II* :

+ Drainage transient state tests can be performed under various flow rates. The influence of flow rate on the hydraulic behavior of unsaturated sand can be determined using the attached air-pressure system.

+ Measurements of changes in volume can be performed.

+ The procedure is not time consuming.

+ Volumetric water content measurements $\theta(t)$ and suctions measurements $\psi(t)$ can be used to directly determine hydraulic functions.

- Expensive equipment is required (i.e., TDR sensors, tensiometers, 2 computers for computing results).

- Careful calibration of the sensors is necessary.

- It is not useful to carry out steady state tests in the sand column testing device II, due to the size of specimen. The testing procedure would be very time consuming.

- The specimen is a disturbed specimen.

Even it is a time consuming procedure for prediction of soil-water characteristic curve including initial drainage, main drainage and imbibition curve as well as scanning curves the modified pressure plate apparatus was found to be the favorite equipment. Due to possibility of application of small suction increments the equipment enables precise determination of the shape of the soil-water characteristic curve during drainage and imbibition. For investigation of influence of flow condition to the shape of the soil-water characteristic curve sand column

testing devices I and II should be used. These equipments provide volumetric-water content and pore-water pressure versus time measurements and thus give information of the flow of water in the specimen. The information is useful, when numerical simulations are carried out. Whereas sand column testing device II requires stepwise the application of suction to the specimen, sand column testing device I uses the attached pump for changing the suction in the specimen.

11.3 Hydro-Mechanical Behavior

Soil-water characteristic curve measurements were performed for loose and dense specimen under variable loading paths (i.e. drainage and imbibition path). It was found that the shape of the soil-water characteristic curve was related to the void ratio of the specimen and to the hydraulic loading path direction, namely whether it is a drainage or a imbibition path. Experiments carried out using steady state and transient state methodologies show quantitatively similar behavior for the soil-water characteristic curve and the hydraulic conductivity function. The following conclusions can be drawn from the present study:

- *Influence of void ratio:*

  The soil-water characteristic curve of Hostun Sand shows that desaturation takes place over a narrow range of relatively low suction values. Desaturation is reflected in a rapid decrease in the unsaturated hydraulic conductivity function. Experimental results on the dense specimens show a higher retention and higher absorption of water due to smaller voids compared to loose samples. Therefore with increasing void ratio the air-entry value, the residual volumetric water content, the corresponding residual suction as well as the water-entry value also increases. The saturated volumetric water content decreases with increasing void ratio.

- *Influence of loading path direction:*

  The effect of hysteresis was quantified for loose and dense specimen along the main drainage and imbibition curves. Several scanning imbibition as well as scanning drainage curves were found between the main drainage and imbibition loop. Whereas the results derived from sand column testing devices I show the effect of occluded air (entrapped air), the results derived from the modified pressure plate apparatus do not show this phenomenon.

- *Influence of flow condition:*

  The transient state tests were performed in sand column testing device I and II with different flow rates. There was no significant influence of the rate of suction applied on the soil-water characteristic curves. The results derived under transient state condition

are similar to the results derived under steady state conditions. No significant dynamic effect was found.

- *Influence of net stress:*

  No significant influence from the applied net stress on the shape of the soil-water characteristic curve was found.

Childs and Collis George (1950), Mualem´s (1976) and Fredlund and Xing's (1994) model were applied for further calculations of the unsaturated hydraulic conductivity. The experimental results from the transient state tests, where volumetric water content and suction are measured, were used to calculate the unsaturated hydraulic conductivity using the instantaneous profile method. This results are conform with those calculated indirectly by using statistical model from Fredlund et al. (1994).

In the present work the experimental results were used to introduce a method for model building, that is based on statistical assessment. As a result, a new soil-water characteristic curve model was introduced, which accounts for scanning imbibition processes. The model is simple in use and it was found that the observed values are conform to the predicted values. Statistical techniques, i.e. graphical and numerical methods, support to use of the developed model. Advantages and disadvantages of the proposed suction-water content model are:

+ The single model is a simple application and thus is simple in its usage.

+ The model is based on detailed statistical analysis.

+ Only 4 parameters ($\beta_1, \beta_2, \beta_{31}, \beta_{32}$) have to be determined. Parameter β_0 is related to the saturated water content and β_3 is related to the residual water content.

- The proposed scanning model can not be used for scanning drainage curves.

The proposed soil-water characteristic curve model was successfully applied to the experimental results derived in the present investigation. Slight modifications may be necessary, when using different type of sandy soils. To further upgrade of the new model, the consideration of scanning drainage processes has to be included.

The mechanical behavior of unsaturated Hostun sand was investigated in one-dimensional compression and rebound tests. The experimental investigation showed, that the compression index and thus the stiffness modulus are clearly influenced by suction during loading. With increase in matric suction the compression index decreases and vice versa the stiffness increases. After reaching an optimum value the compression index increases, that means the stiffness modulus decreases again. The mechanical behavior under dry condition ($S = 0$) is similar to the mechanical behavior under saturated condition ($S = 1$). No influence of suction on the mechanical behavior during unloading path was found. Collapse potential was studied

for specimens under loose condition. Two different methods of sample preparation related to variation of initial conditions are described. It was found that the collapse potential is very small for the stress paths analyzed. Investigations on preconsolidation pressure lead to the conclusion, that no influence of suction on the soil history was observed.

To underline the importance of unsaturated soil behavior, bearing capacity of surface model footing was carried out for saturated and unsaturated specimens. A meaningful influence of suction was found to the bearing capacity of strip foundation. The bearing capacity significantly improved for unsaturated specimen. The bearing capacity of the unsaturated sand specimen was found to be approximately 2.5 to 4 times higher than for the saturated specimen ($S = 0$ and $S = 1$). Similar to the influence of suction on the stiffness behavior of sand, the bearing capacity increases with increasing suction and again decreases when reaching dry condition. Using the equation proposed by Vanapalli & Mohamed (2007) bearing capacity was predicted. Measured and predicted values are in good agreement, but further experimental and theoretical investigations are necessary.

Calculations of unsaturated bearing capacity as well as unsaturated hydraulic conductivity showed, that the soil-water characteristic curve is an important tool when dealing with unsaturated soil behavior. It is the basic relation used for prediction of unsaturated hydromechancial behavior.

11.4 Numerical Simulation using MUFTE-UG

A transient state test was conducted on loose Hostun sand specimen in the column testing device I for several alternating drainage and imbibition events. TDR and tensiometer sensors are used to measure saturation and pore-water pressure at different depths over the time.

The derived soil-water characteristic curves demonstrate significant hysteresis and air trapping effects. Numerical simulations of the transient state test are carried out using the two-phase flow module of the MUFTE-UG simulator. The simulations incorporate information on the soil-water characteristic curve determined directly on the column. The scaling hysteresis concept from Parker & Lenhard (1987) was used, that accounts for entrapped non-wetting phase saturation.

The simulation and experimental results were compared in terms of saturation versus time as well as pore-water pressure versus time for the entire sequence of alternating drainage and imbibition conditions. The comparison showed the necessity of the inclusion of a hysteresis concept in the numerical simulator, especially related to the effect of air trapping and the formation of residual air saturations during imbibition. Using the hysteresis concept from Parker & Lenhard (1987), only small deviations in the predicted and measured suction-water content curves for the second imbibition have been observed. Despite this limitation, it can be stated that a positive prediction of the flow process in the transient state test has been obtained with a conceptually simple scaling approach for hysteresis.

In a further investigation an additional soil-water characteristic curve was determined from the steady state experiment on Hostun sand specimens and consequently used for a numerical simulation. This is a common procedure in applications involving unsaturated flow. However, the soil-water characteristic curve determined with this approach demonstrates absence of air residual saturation in imbibition, in contrast to the transient state test where a strong trapping effect was observed. The numerical simulation carried out here incorporates the Parker and Lenhard hysteresis. However, the simulation cannot correctly predict the flow process in the transient state experiment due to the inappropriate input suction-water content curve.

It is demonstrated that the implementation of a simple scaling approach for hysteresis can provide a good prediction of hysteretic unsaturated flow including phase trapping effects. However, this needs to be combined with reliable information of the input soil-water characteristic curve parameters that is commonly measured in the laboratory. It is shown that this is possible by using direct saturation and pressure measurements from the sand column test I. The investigation showed that a single pair of TDR and tensiometer sensors in combination with the implemented scaling concept for hysteresis provides good prediction of the flow in the entire 0.54 m high porous medium column, for all drainage and imbibition events. If TDR and tensiometer data were not available, the traditional steady state method would be used for the determination of the suction water content relationship. Although the specimens used in the steady state outflow/ inflow experiments correspond to the same spatial scale as the TDR-T pairs, they provide different information on the amount of air trapping and consequently a misleading prediction of flow in the transient state test. This observation suggests that the amount of phase trapping strongly depends on the methodology used and the time scales linked to it. When predicting hysteretic flow by means of numerical simulations, it is therefore necessary to use hysteretic suction-water content curves that are determined under conditions (i.e. fast or slow imbibition) similar to those of the application they are purposed for.

11.5 Future Work

Due to the reason that the majority of civil engineering problems are related to unsaturated soils, there is a strong motivation to understand their hydro-mechancial behavior and the impact of suction vice versa water content on the stress-strain, shear strength and flow behavior. To support the investigations carried out in the present study and to complete the present study following tests are proposed to carry out:

- Performance of triaxial tests for investigation of the influence of suction on the shear strength.

- Performance of biaxial tests for investigation of the influence of suction on shear strength.

- Direct determination of unsaturated hydraulic conductivity.

- Continuation of bearing capacity tests for several suction values.

Further development and enhancement of the new-suction water content model, that includes the incorporation of scanning drainage process into the model is needed. The numerical simulation of the sand column tests I using the new suction-water content model, which has to be implemented into an appropriate software is future work. Present results also can be used to develop a hydro-mechancial model for description of unsaturated sand behavior.

In a next step numerical simulation of the bearing capacity tests conducted on unsaturated sand specimen have to be carried out. Classical bearing capacity equation has to be extended or the equation by Vanapalli & Mohamed (2007) has to be modified, so that the effect of suction can be considered. Depending on the suction in the soil the shear strength increases and decreases respectively due to capillary forces. The shear strength caused by a certain suction value has to be implemented into the bearing capacity equation. The aim for further investigations is to use KEM method to include the shear strength component caused by suction.

Appendix A

Details Zou's Model (2003, 2004)

During a main imbibition process of a soil, first all the contact regions are at the same time filled with water from the position angle $\alpha = 0$ to $\alpha = \alpha_{max}$ (Fig. 2.22(a)). For $\alpha = \alpha_{max}$ some adjacent capillary menisci contact with each other, and some frustum-shaped pores are formed. Then, all the frustum-shaped pores are at the same time filled with water from $y = 0$ to $y = r_s$ gradually (Fig. 2.22(b)). During a main drainage process of a soil, first a part of the frustum-shaped pores begins to drain gradually from $y = r_s$ to $y = 0$. Then another part begins to drain and one after another. Subsequently the contact regions begin to drain from $\alpha = \alpha_{max}$ to $\alpha = 0$, and a part of frustum-shaped pores with the number $\mu \cdot n_{f0}$ (where μ is a percentage) is just drained during the drainage process of the contact regions. If in a soil all the contact regions have been filled with water to $\alpha = \alpha_{max}$ and all the frustum-shaped pores have been filled with water to $y = y_1 < r_s$ during a previous main imbibition process, and now the soil begins to dry, then the drainage process is called as secondary drainage process. Similar to the main drainage process, during the secondary drainage process, first a part of the frustum-shaped pores that have been filled with water to $y = y_1$ previously begins to drain gradually. Then another part begins to drain and one after another. Subsequently the contact regions begin to drain from $\alpha = \alpha_{max}$ to $\alpha = 0$, and a part of frustum-shaped pores with the number $\mu \cdot n_{f0}$ is also just drained during the drainage process of the contact regions. If in a soil only a part of the frustum-shaped pores has been drained to $y = y_2 < r_s$ during a previous main drainage process, the other parts are still filled with water to $y = r_s$, and now the soil begins to be wetted again, then the imbibition process is called secondary imbibition process. During the secondary imbibition process only the part of the frustum-shaped pores that have been drained to $y = y_2$ previously are at the same time wetted again.

The volume $V_{w1}(\alpha)$ of the pore water in a contact region between two tangent particles (spheres) with the same radius r_s, depending on α, can be expressed approximately as:

$$\frac{V_{w1}(\alpha)}{r_s^3} = 2\pi\,(1 - \cos\alpha)\left[sin^2(\alpha) - \frac{(1 - \cos\alpha)(2 + \cos\alpha)}{3}\right] \tag{A.1}$$

The average pore volume V_{v0} per particle in a soil with pore ratio e, in proportion to r_s^3, can be written as:

$$\frac{V_v}{r_s^3} = \frac{4\pi \cdot e}{3} \tag{A.2}$$

When the contact regions in a soil are wetted or dried to a position angle α, according to the so-called capillary law (Fredlund & Rahardjo 1993*b*) the dimensionless suction $\sigma_u(\alpha)$ in pore water, in relation to α can be expressed as follows:

$$\sigma_u(\alpha) = \frac{(u_a - u_w) \cdot r_s}{T_s} = \frac{(2 - \sin\alpha - 2\cos\alpha) \cdot \cos\alpha}{1 - \sin\alpha(1 - \cos\alpha) - \cos\alpha(2 - \cos\alpha)} \tag{A.3}$$

where u_a and u_w are air and water pressure respectively, T_s is the so-called surface tension of capillary water (e.g. $T_s = 72.75mN/m$ for the temperature $T = 20C^\circ$).

In Zou (2003), Zou (2004) it was proposed that the form of the ideal symmetrical frustum-shaped pores can be described using a function y relating to the radius r (Fig. 2.22(b)) as following:

$$\frac{y}{r_s} = a - \frac{b}{r^2/r_s^2 - c} \quad (0 \le y \le r_s) \tag{A.4}$$

where a, b and c are three constants that can be determined according to geometrical and physical boundary conditions using following equations:

$$a\,(a-1)\left(\ln\frac{a}{a-1} - \frac{1}{a}\right)\left[\rho((\alpha_{max}) + \xi)^2 - \varrho^2(\alpha_{max})\right] \tag{A.5}$$

$$= \frac{4e}{3n_{f0}} - \frac{n_c \cdot V_{w1}(\alpha_{max})}{2\pi \cdot n_{f0} \cdot r_s^3} - \rho^2(\alpha_{max})$$

$$b = a\,(a-1)\left[\left(\rho(\alpha_{max}) + \xi\right)^2\right) - \rho^2(\alpha_{max})\right] \tag{A.6}$$

and

$$c = \rho^2(\alpha_{max}) - \frac{b}{a} \tag{A.7}$$

where $\rho(\alpha_{max}) = (1 - \cos\alpha_{max})/\cos\alpha_{max}$ and ξ is a form parameter which describes the form of the symmetrical frustum-shaped pores.

When a symmetrical frustum-shaped pore is filled with water up to y, from Eq. A.4 and by integration the volume $V_{w1}(y)$ of the pore water in the symmetrical frustum-shaped pore can be written as:

$$\frac{V_{w1}(y)}{r_s^3} = \pi\left(c\frac{y}{r_s} + b \cdot \ln\frac{a}{a - y/r_s}\right) \quad (0 \le y \le r_s) \tag{A.8}$$

The total volume $V_w(y, \alpha)$ of pore water per particle during the main imbibition and drainage processes as well as during the secondary imbibition and drainage processes, depending on y and/or α, can be written as:

$$\frac{V_w(y,\alpha)}{r_s^3} = n_f(y)\frac{V_{w1}(y)}{r_s^3} + n_{fi}(y,\alpha)\frac{V_{w1}(y_i)}{r_s^3} + n_c\frac{V_{w1}(\alpha)}{2r_s^3} \tag{A.9}$$

Table A.1: Overview of equations for determination of several parameters of Zou's model (2004)

processes	y_i	$n_f(y)$	$n_{fi}(y,\alpha)$	α
main imbibition				
contact regions	-	0	0	$0 \sim \alpha_{max}$
frustum-shaped pores	$y_0 = r_s$	n_{f0}	0	α_{max}
main drainage				
frustum-shaped pores	$y_0 = r_s$	$n_{f0}(1-\mu)(1-y/r_s)$	$n_{f0}[\mu + (1-\mu)y/r_s]$	α_{max}
contact regions	$y_0 = r_s$	0	$\mu \cdot n_{f0} \cdot \alpha/\alpha_{max}$	$0 \sim \alpha_{max}$
secondary drainage				
frustum-shaped pores	y_1	$n_{f0}(1-\mu)(1-y/y_1)$	$n_{f0}[\mu + (1-\mu)y/y_1]$	α_{max}
contact regions	y_1	0	$\mu \cdot n_{f0} \cdot \alpha/\alpha_{max}$	$0 \sim \alpha_{max}$
secondary imbibition				
frustum-shaped pores	y_2	$n_{f0}(1-\mu)(1-y_2/r_s)$	$n_{f0}[\mu + (1-\mu)y_2/r_s]$	α_{max}

$$(0 \le y \le r_s; 0 \le \alpha \le \alpha_{max}, i = 0, 1, 2)$$

where $n_f(y)$ is the average number of the frustum-shaped pores that are wetting or draining per particle, $n_{fi}(y,\alpha)$ is the average number of the frustum-shaped pores that are filled with water to $y = y_i$ (where y_i is the maximal filling height). $n_f(y)$, $n_{fi}(y)$, y_i and the position angle α in Eq. A.9 can be determined corresponding to Table A.1 for different imbibition and drainage processes.

The degree of saturation $S_r(y,\alpha)$, depending on y and/or α , can estimated using the following equation:

$$S_r(y,\alpha) = S_{r0}\frac{V_w(y,\alpha)}{V_v} \tag{A.10}$$

where S_{r0} is the degree of saturation for suction $(u_a - u_w) \approx 0$.

To determine the suction in pore water during wetting and draining the frustum-shaped pores, in Zou (Zou 2003, 2004) it is assumed that the contact angle $\beta(y)$ (Fig. 2.22(b)) as function of y can be described using the following equation:

$$\beta(y) = \sqrt{\frac{B}{A - \frac{y}{r_s}} + C} \tag{A.11}$$

The three constants A, B and C can be determined according to physical boundary conditions using following equations:

$$A = \zeta, \quad B = \zeta(\zeta - 1)\left(\frac{\pi^2}{4} - \beta_0^2\right), \quad C = \zeta \cdot \beta_0^2 - (\zeta - 1)\frac{\pi^2}{4} \tag{A.12}$$

where

$$\beta_0 = \arccos\left[\frac{1 - \sin\alpha_{max}/2 - \cos\alpha_{max}(1 - \cos\alpha_{max})}{1 - \sin\alpha_{max}(1 - \cos\alpha_{max}) - \cos\alpha_{max}(2 - \cos\alpha_{max})}\right] \tag{A.13}$$

and $\zeta > 1$ is a meniscus parameter which describes the physical properties of soil particle surfaces.

According to the so-called capillary law (Fredlund & Rahardjo 1993*b*), the dimensionless suction $\sigma_u(y)$ in pore water during wetting and draining the frustum-shaped pores, depending on r and β and so that on y, can be expressed as:

$$\sigma_u(y) = \frac{(u_a - u_w) \cdot r_s}{T_s} = \frac{2\cos\beta}{r/r_s} = \frac{2\cos\cdot\left(\frac{B}{A-y/r_s} + C\right)^{0.5}}{\left(\frac{b}{a-y/r_s} + c\right)^{0.5}} \tag{A.14}$$

Now using equations Eq. A.10 and Eq. A.3 the relationship between degree of saturation $Sr(\alpha)$ and suction $\sigma_u(\alpha)$ during wetting and draining the contact regions for $0 < \alpha \leq \alpha_{max}$ can be calculated, and using equations Eq. A.10 and Eq. A.14 the relationship between $S_r(y)$ and $\sigma_u(y)$ during wetting and draining the frustum-shaped pores for $0 < y \leq r_s$ can be also estimated.

Appendix B

Soil-Water Characteristic Curve - Experimental Results and Best Fits

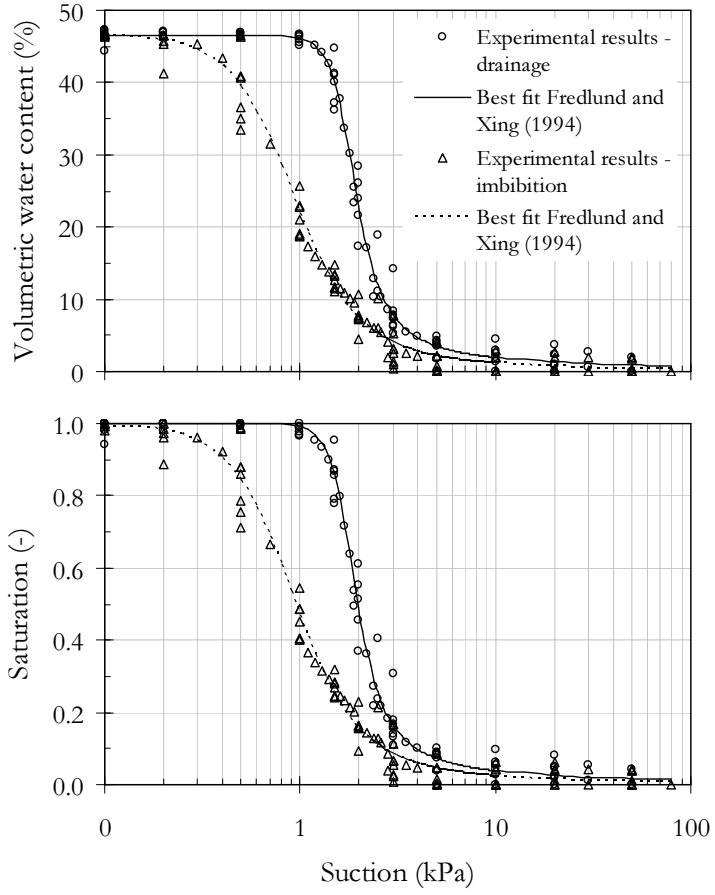

Figure B.1: Experimental results and best fit (Fredlund and Xing 1994) for drainage and imbibition process from modified pressure plate apparatus (loose specimen, steady state test)

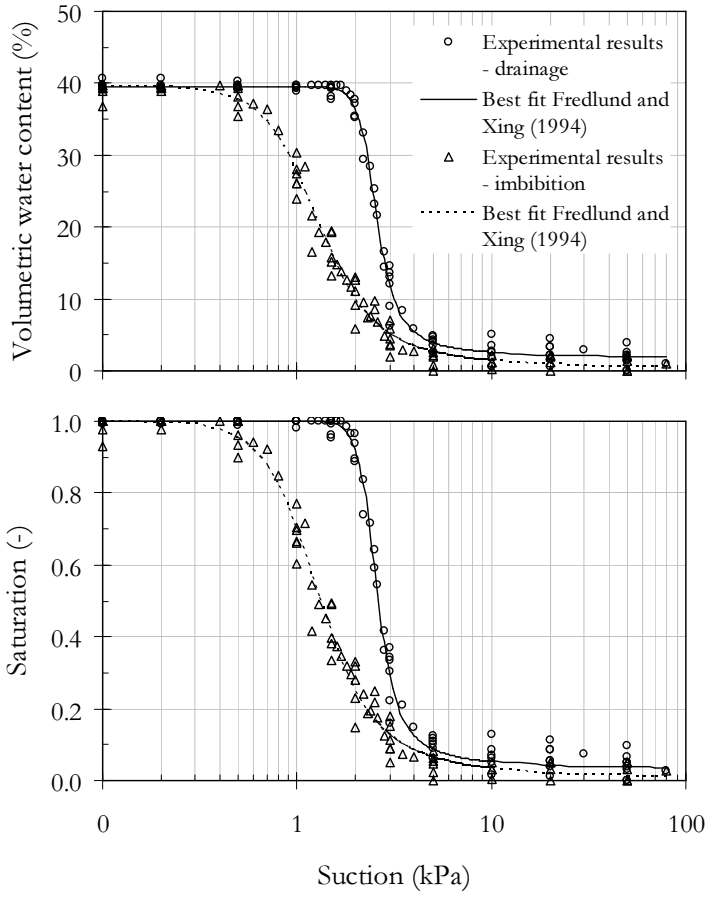

Figure B.2: Experimental results and best fit (Fredlund and Xing 1994) for drainage and imbibition process from modified pressure plate apparatus (dense specimen, steady state test)

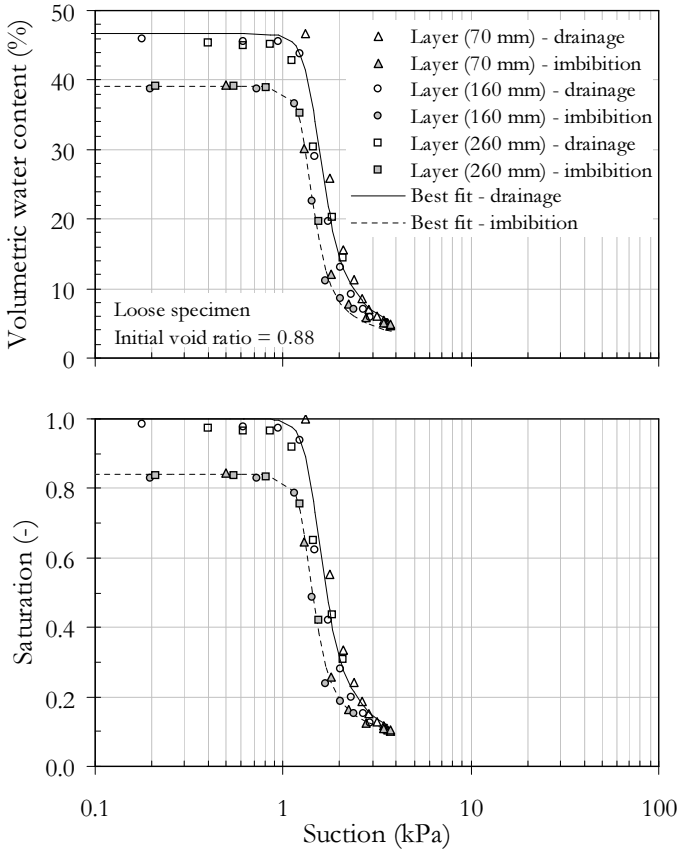

Figure B.3: Experimental results and best fit (Fredlund and Xing 1994) for drainage and imbibition process from sand column test II (loose specimen, steady state test)

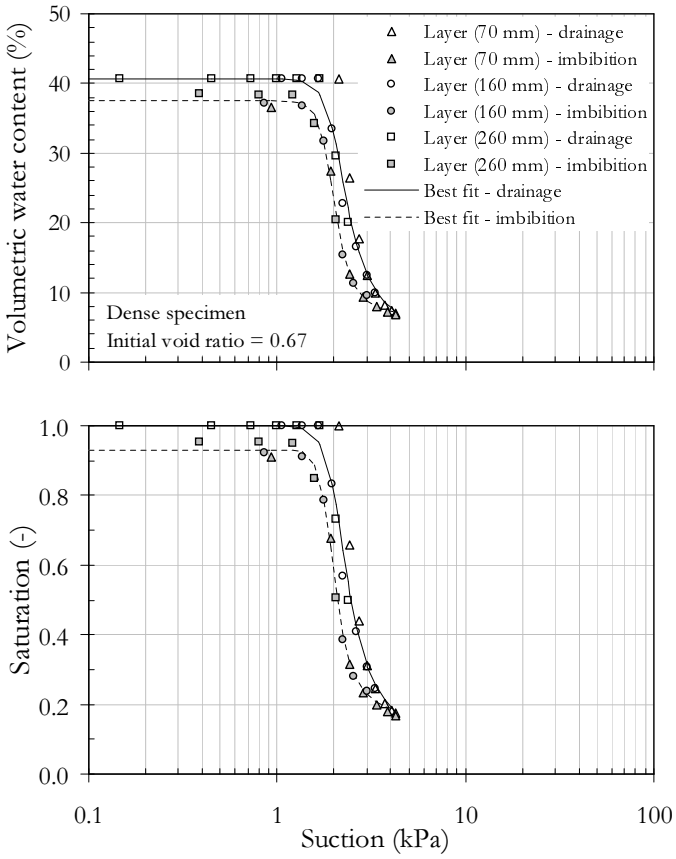

Figure B.4: Experimental results and best fit (Fredlund and Xing 1994) for drainage and imbibition process from sand column test II (dense specimen, steady state test)

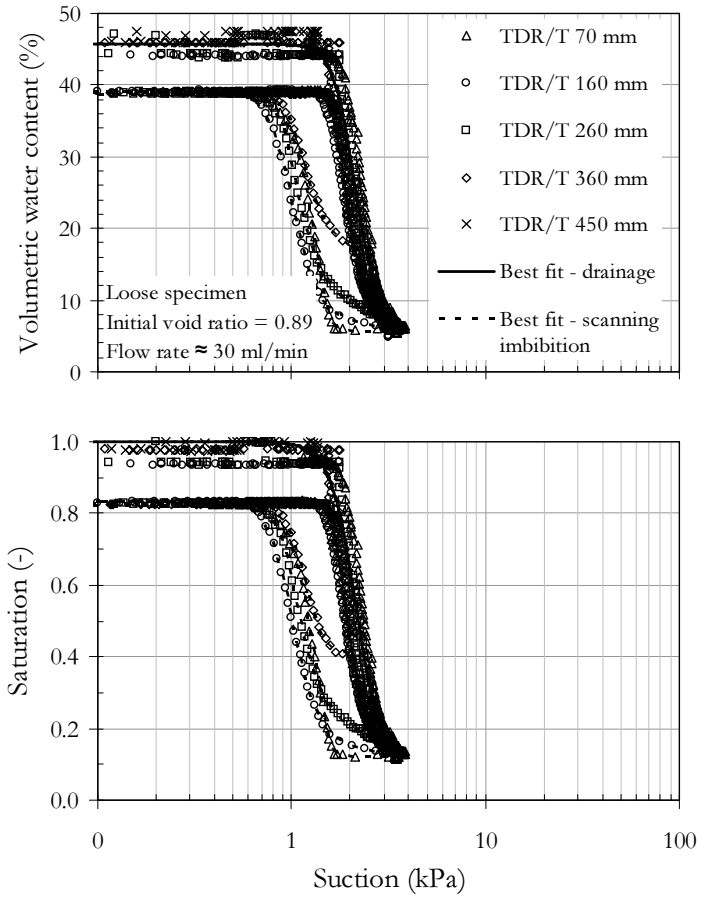

Figure B.5: Experimental results and best fit (Fredlund and Xing 1994) for drainage and imbibition process from sand column test I (loose specimen, transient state test - 100 ml/min)

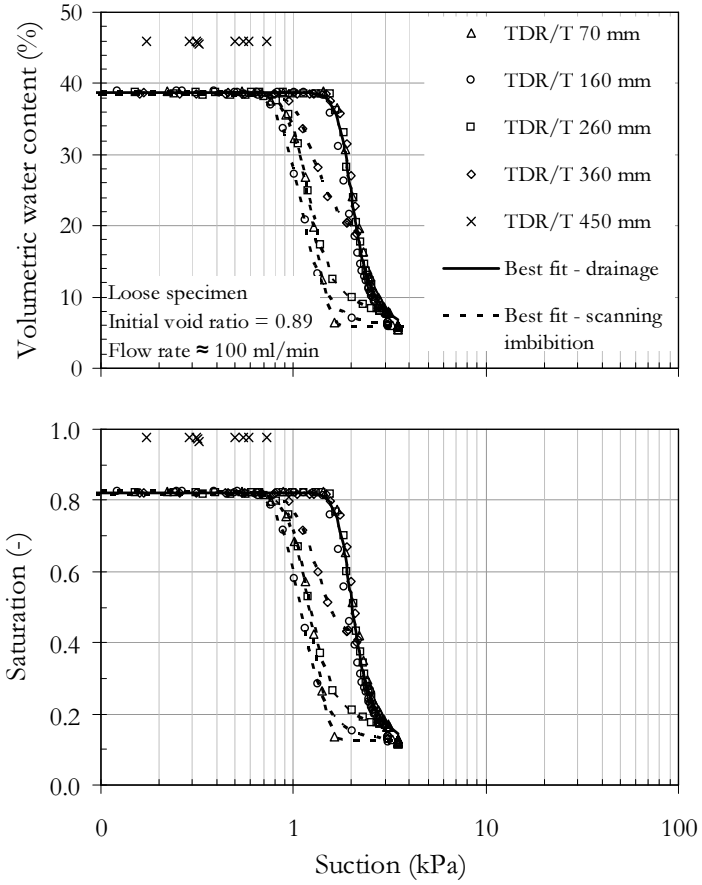

Figure B.6: Experimental results and best fit (Fredlund and Xing 1994) for drainage and imbibition process from sand column test I (loose specimen, transient state test - 30 ml/min)

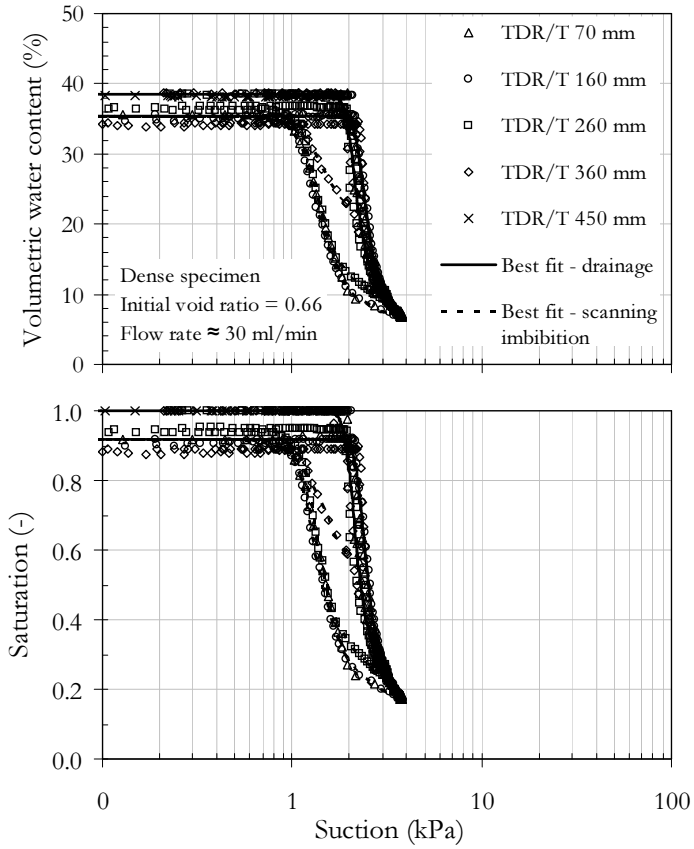

Figure B.7: Experimental results and best fit (Fredlund and Xing 1994) for drainage and imbibition process from sand column test I (dense specimen, transient state test - 30 ml/min)

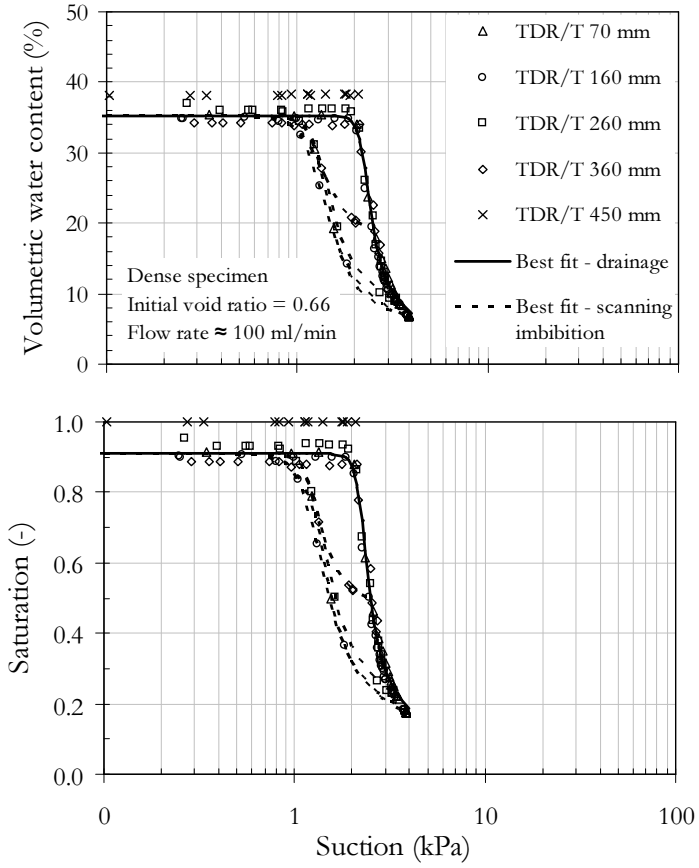

Figure B.8: Experimental results and best fit (Fredlund and Xing 1994) for drainage and imbibition process from sand column test I (dense specimen, transient state test - 100 ml/min)

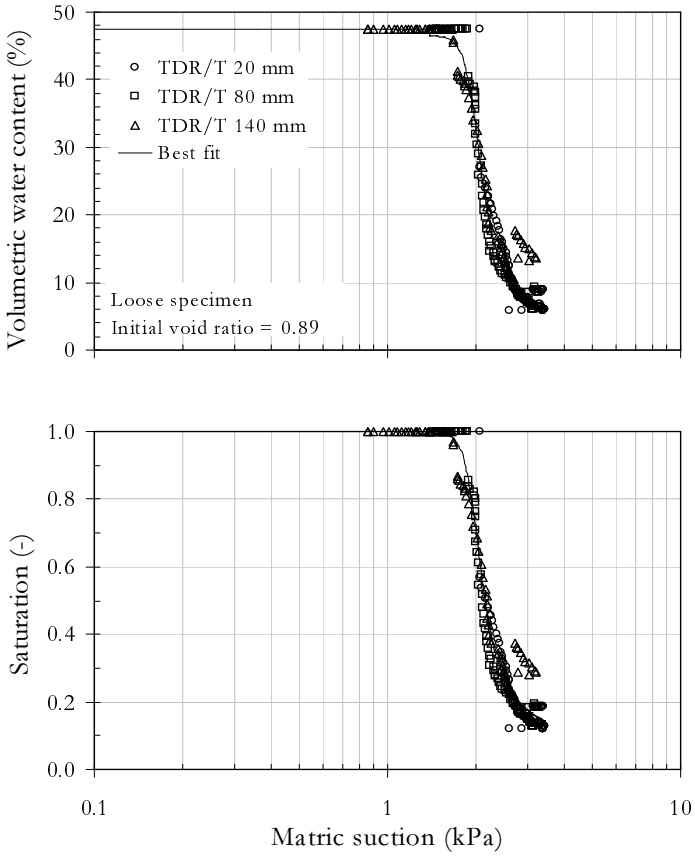

Figure B.9: Experimental results and best fit (Fredlund and Xing 1994) for drainage process from sand column test II (loose specimen, transient state test)

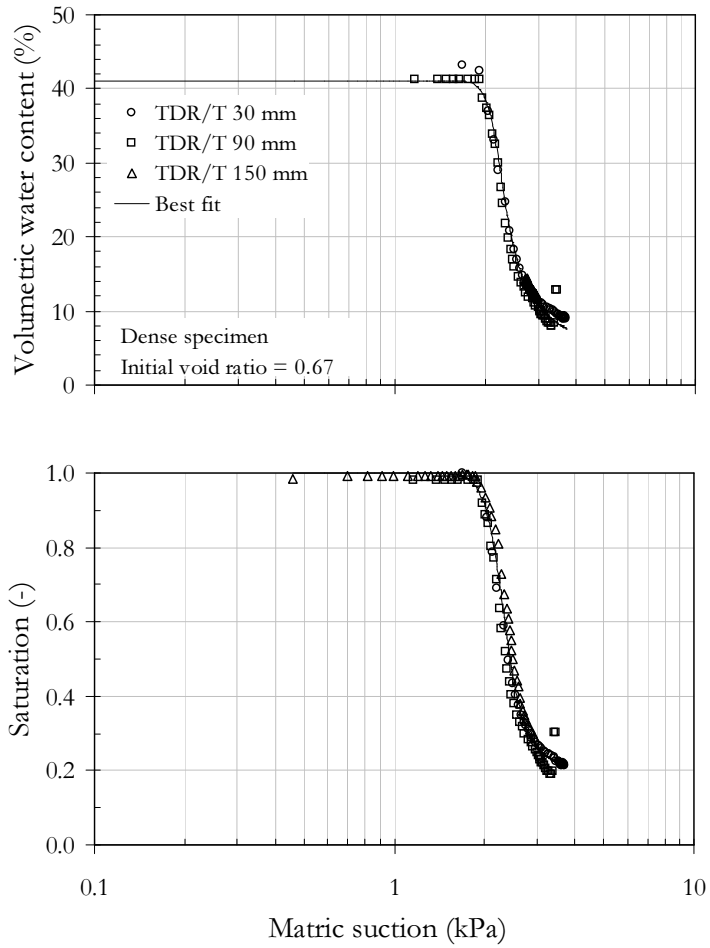

Figure B.10: Experimental results and best fit (Fredlund and Xing 1994) for drainage process from sand column test II (dense specimen, transient state test)

Appendix C

Collapse Potential of Partially Saturated Sand

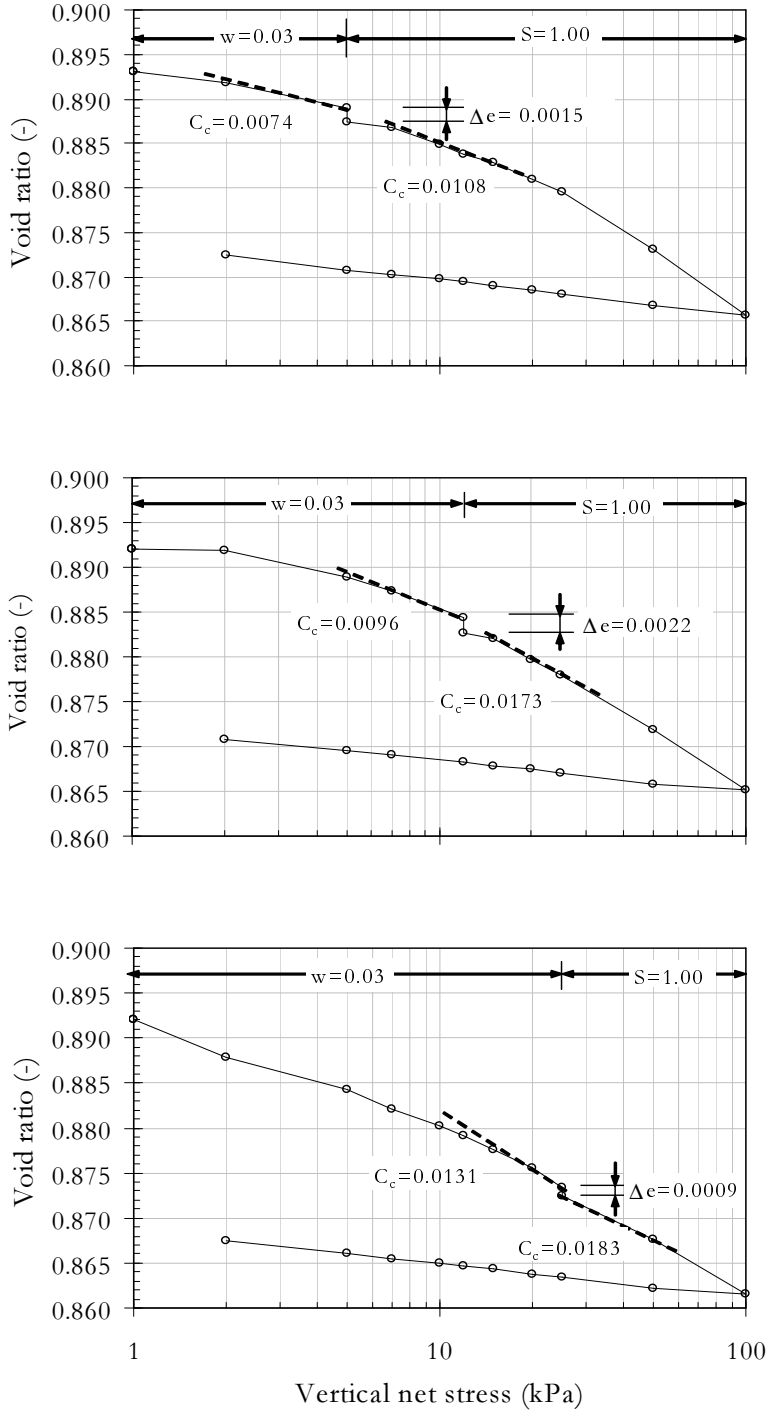

Figure C.1: Experimental results of collapse potential test including results of compression index- Method 2 (loose specimen)

Appendix D

Preconsolidation Pressure of Partially Saturated Sand

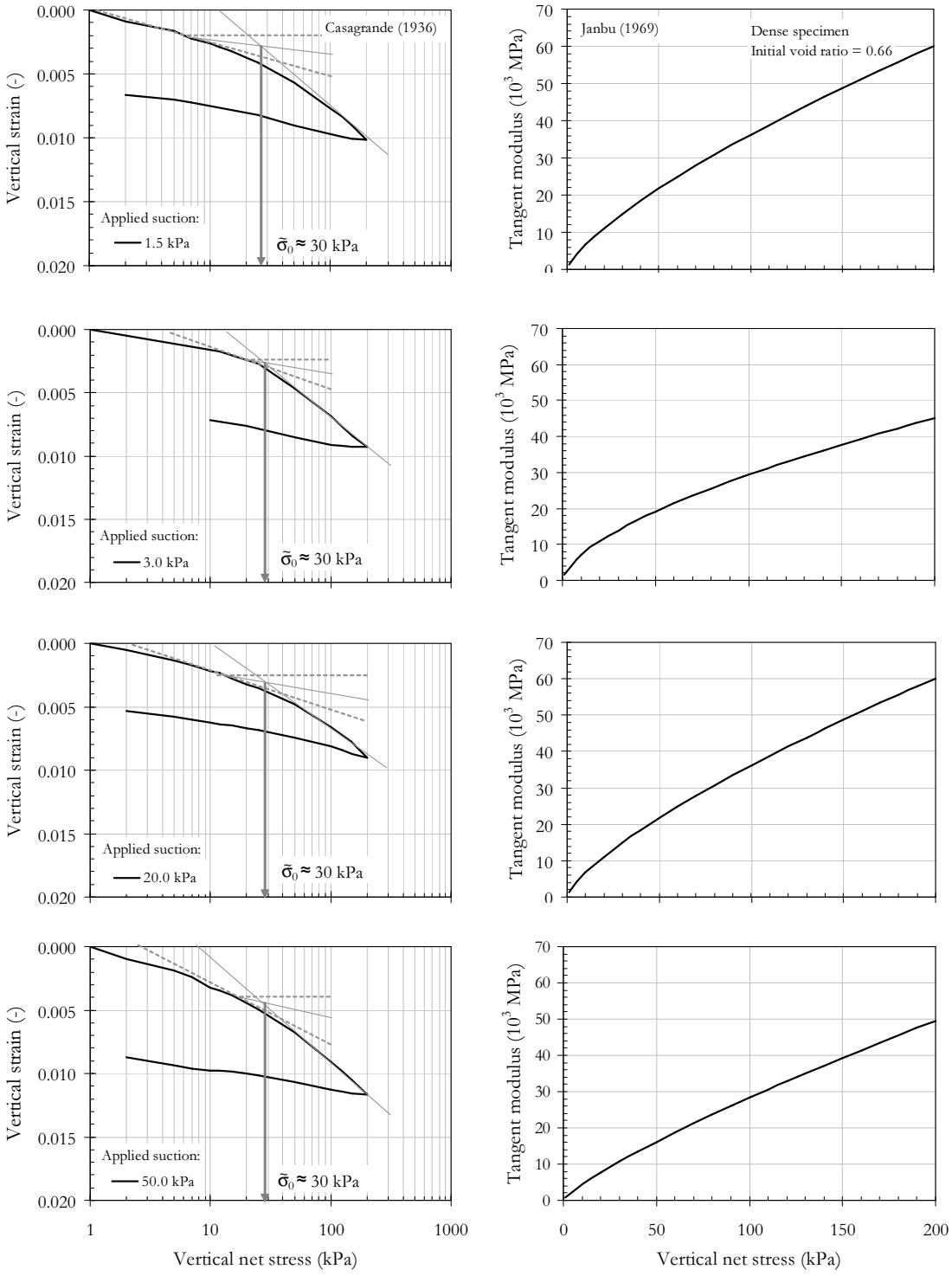

Figure D.1: Prediction of yield stress using Casagrande's (left) and Janbu's (right) method (dense specimen)

Appendix E

New SWCC Model - Development, Validation, Application

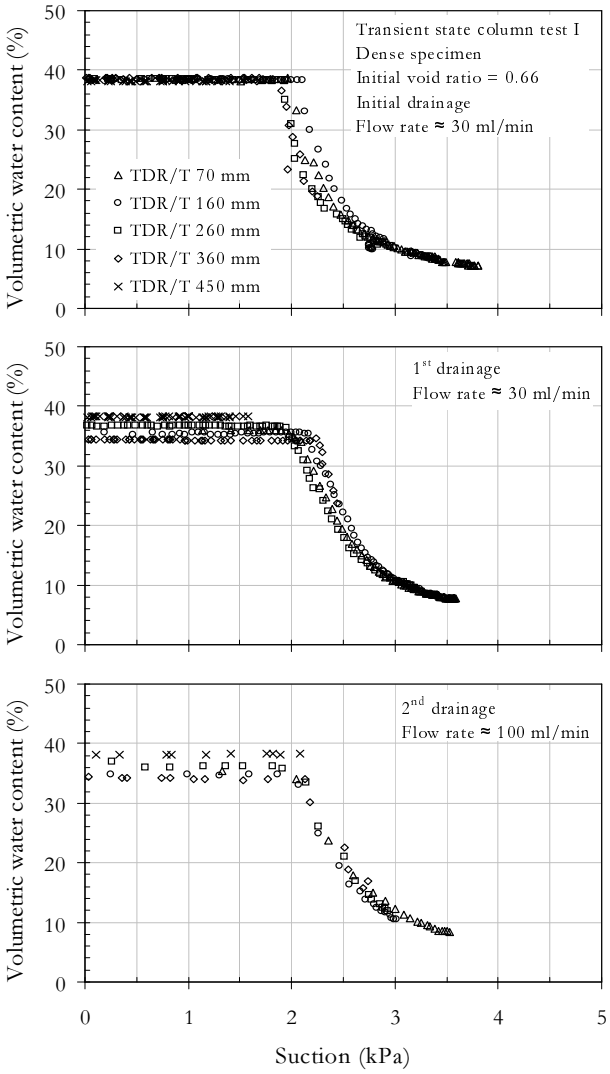

Figure E.1: Experimental data (initial drainage, 1^{st} drainage, 2^{nd} drainage) from drainage transient state column tests used for model building (dense specimen)

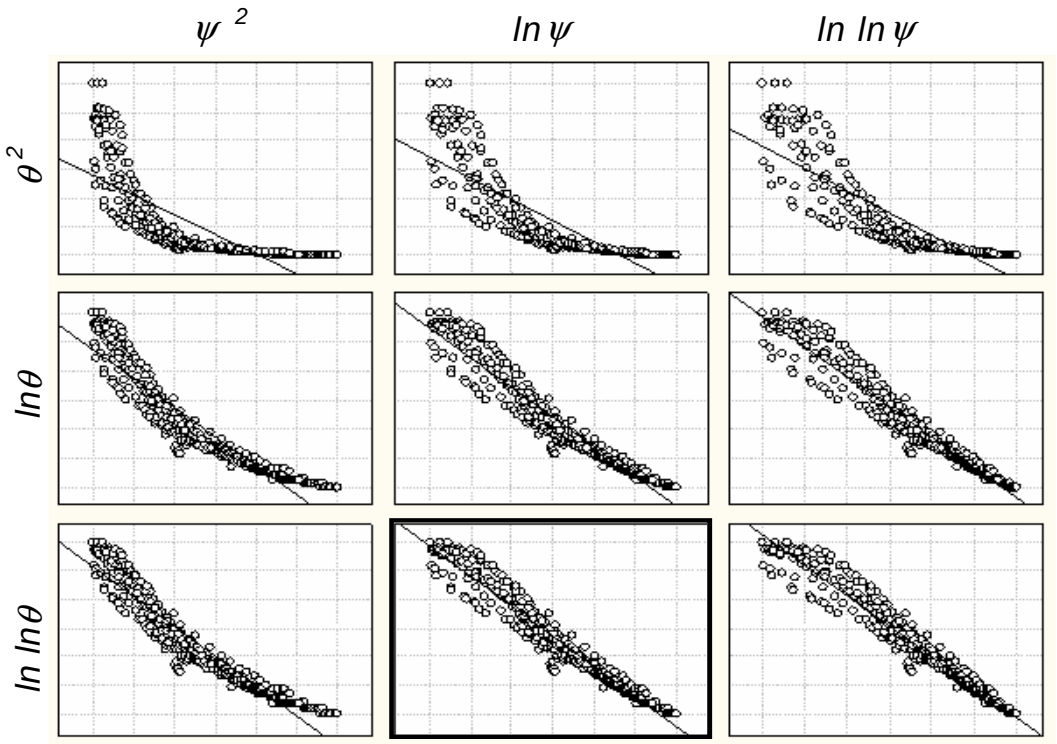

Figure E.2: Results from data transformation using experimental results (initial drainage, 1^{st} drainage, 2^{nd} drainage) from drainage transient state column tests (dense specimen)

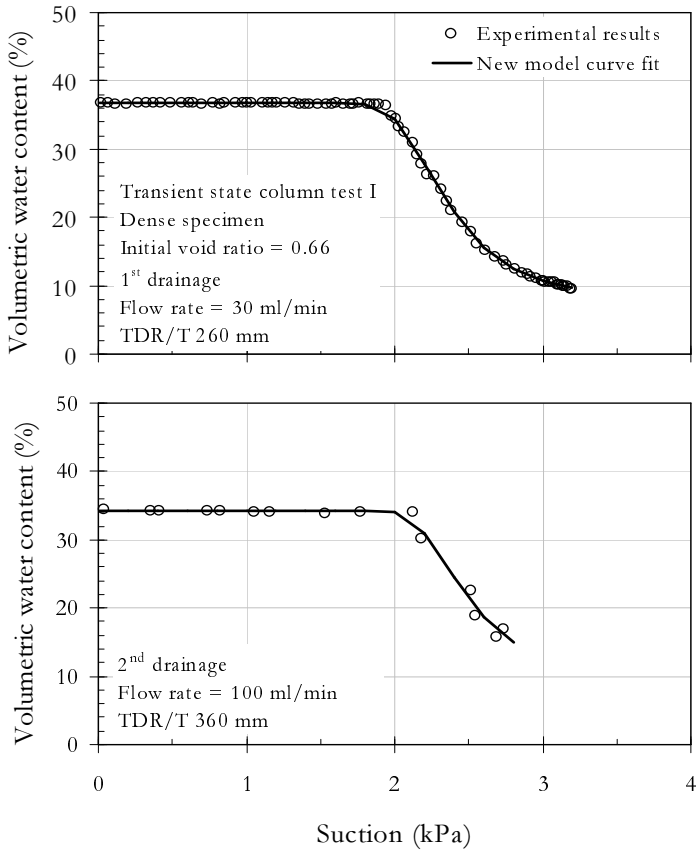

Figure E.3: Experimental drainage results from several depth from transient state sand column test and achieved curve fit from the proposed model (loose specimen)

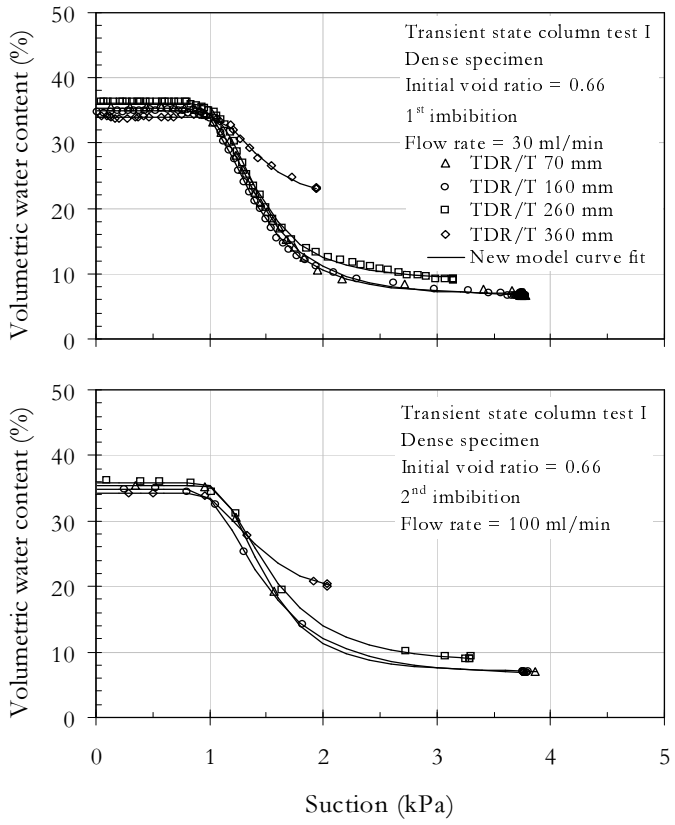

Figure E.4: Experimental drainage results from several depth from transient state sand column test and achieved curve fit from the proposed model (dense specimen)

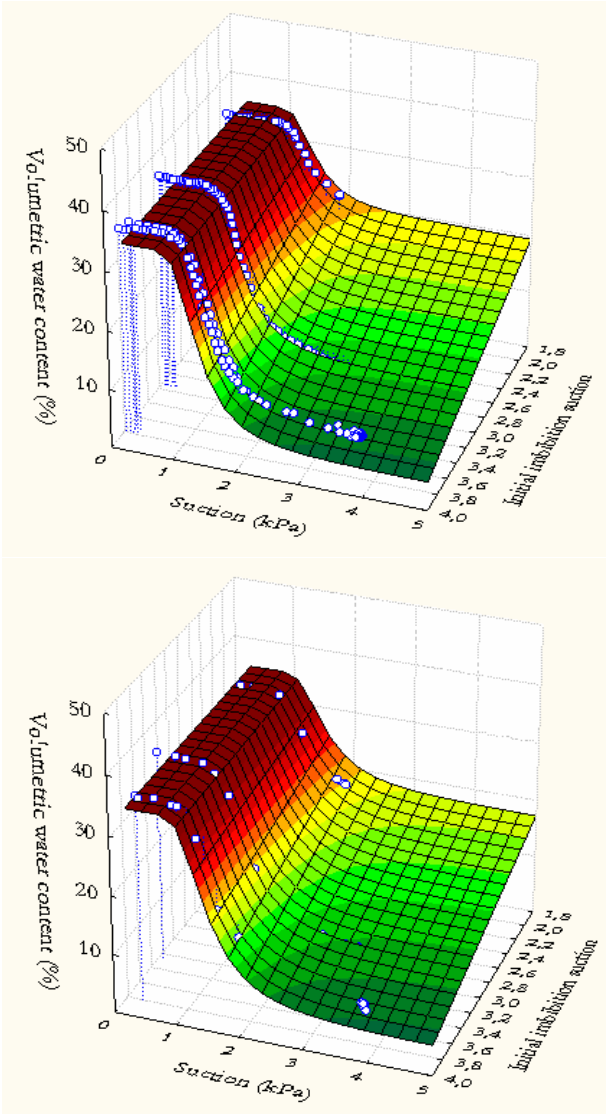

Figure E.5: Experimental imbibition results (1^{st} imbibition, 2^{nd} imbibition) from transient state sand column test and achieved curve fit from the proposed imbibition hysteresis model (dense specimen)

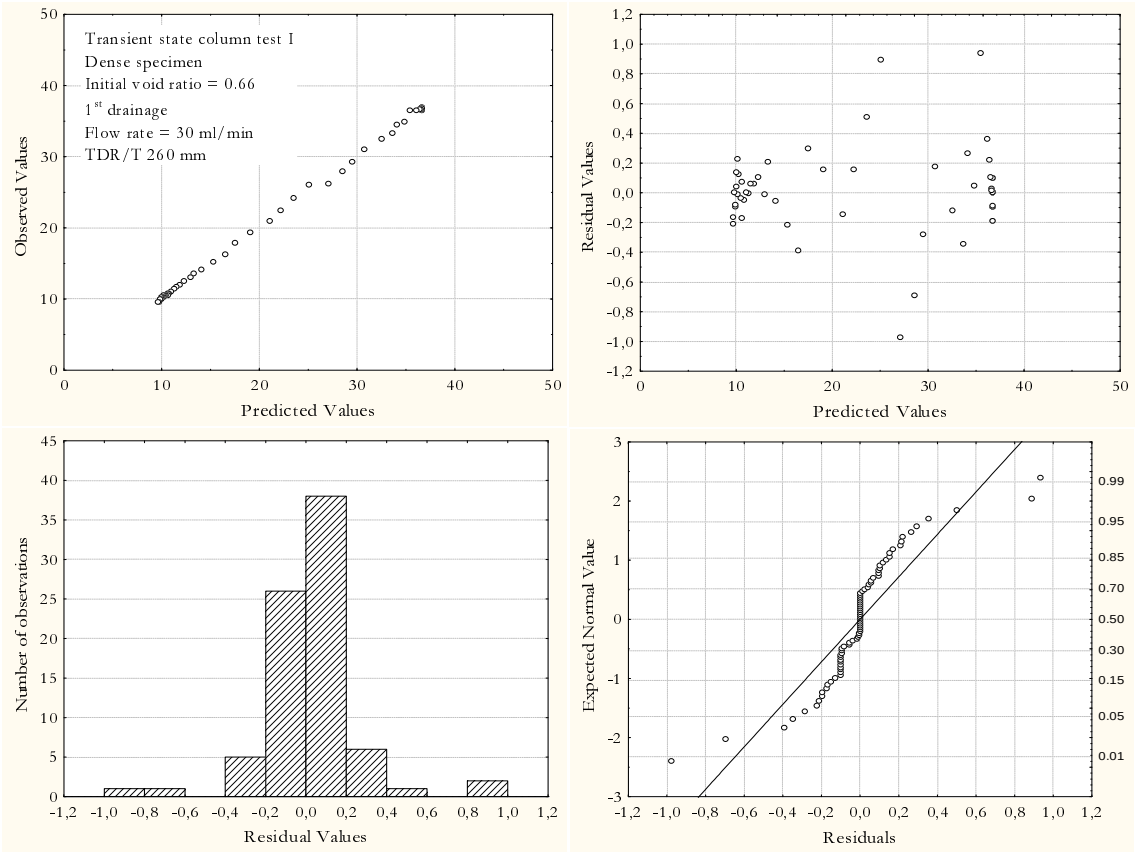

Figure E.6: Model validation results from 1^{st} drainage process (dense specimen, TDR/T260 mm)

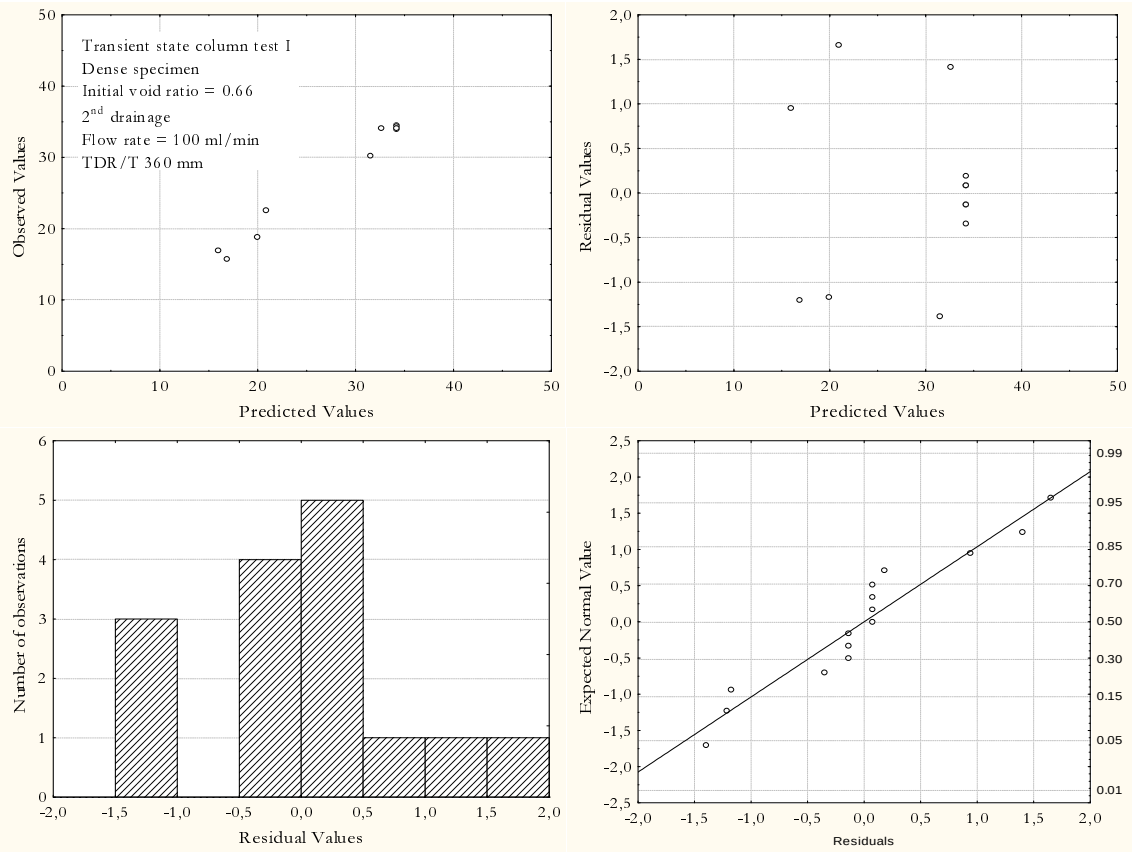

Figure E.7: Model validation results from 2^{nd} drainage process (dense specimen, TDR/T360 mm)

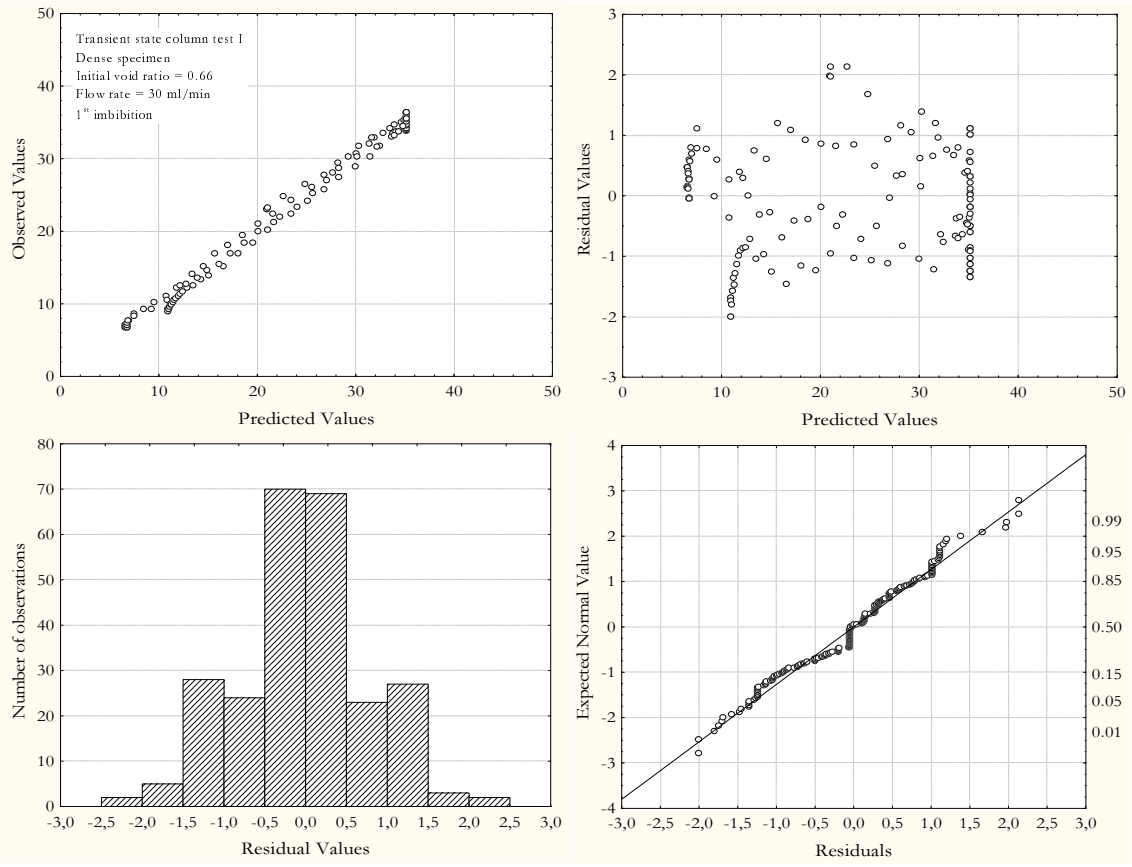

Figure E.8: Model validation results from 1^{st} imbibition process (dense specimen)

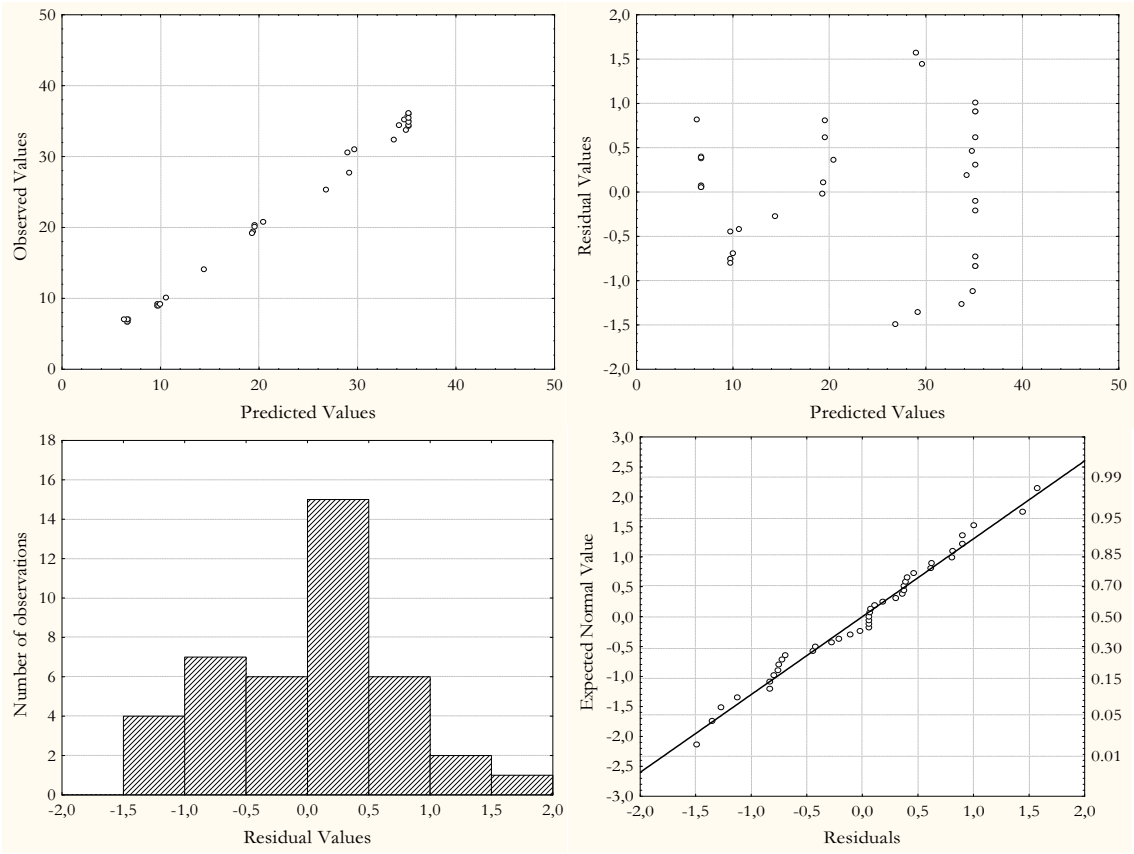

Figure E.9: Model validation results from 2^{nd} imbibition process (dense specimen)

Bibliography

Agus, S. S. (2005), An experimental study on hydro-mechanical characteristics of compacted Bentonite-Sand mixtures, PhD thesis, Bauhaus-Universität Weimar.

Agus, S. S., Leong, E. C. & Schanz, T. (2003), 'Assessment of statistical models for indirect determination of permeability functions from soil-water characteristic curves', *Géotechnique* **53**, 279–282.

Ahuja, L. R. & El-Swaify, S. A. (1976), 'Determining both water characteristics and hydraulic conductivity of a soil core at high water contents from a transient flow experiment', *Soil Science* **121**(4), 198–204.

Aitchison, G. D. (1961), Relationship of moisture and effective stress function in unsaturated soils, *in* 'Pore Pressure and Suction in Soils', London, Butterworth, pp. 47–52.

Al-Khafaf, S. & Hanks, R. J. (1974), 'Evaluation of the filter paper method for estimating soil water potential', *Soil Science* **117**(4), 194–199.

Alabdullah, J. & Schanz, T. (2009), Shear strength of unsaturated sand under plain strain conditions, *in* '4th Asia-Pacific Conference on Unsaturated Soils', Newcastle, Australia.

Alosnso, E. E., Gens, A. & Hight, D. W. (1987), Special problem soils - general report, *in* '9th European Conference on Soil Mechanics and Foundation Engineering', Dublin, Irland, pp. 1087–1146.

Ankeny, M. D., Ahmed, M., Kaspar, T. C. & Horton, R. (1991), 'Simple field method for determining unsaturated hydraulic conductivity', *Soil Science Society of American Journal* **55**, 467–469.

Arya, L. M. & Paris, J. F. (1981), 'A physico-empirical model to predict the soil moisture-characteristic from particle size distribution and bulk density data', *Soil Science Society of America Journal* **45**, 1023–1030.

ASTM (Standard D2434), 'Test method for permeability of granular soils (constant head)', *Annual Book of ASTM Standards* **04.08**.

Aubertin, M., Mbonimpa, M., Bussiere, B. & Chapius, R. P. (2003), 'A model to predict the water retention curve from basic geotechnical properties', *Canadian Geotechnical Journal* **40**(6), 1104–1122.

Averjanov, S. F. (1950), About permeability of subsurface soils in case of incomplete saturation, *in* 'The Theory of Ground Water Movement', Vol. 7 of *English Collection*, Princeton Univ. Press, Princeton, NJ, pp. 19–21.

Barden, L., Gown, A. M. & Collins, K. (1973), 'The collapse mechanism in partially saturated soil', *Engineering Geology* **7**(1), 49–60.

Barden, L. & Pavlakis, L. (1971), 'Air and water permeability of compacted unsaturated cohesive soil', *Journal of Soil Science* **22**(3), 302–317.

Bastian, P., Birken, K., Johannsen, K., Lang, S., Eckstein, K., Neuss, N., Reichert, H. R. & Wieners, C. (1997), 'UG - A flexible software toolbox for solving partial differential equations', *Computing and Visualization in Science* **1**, 27–40.

Bear, J. (1972), *Dynamics of fluids in porous media*, American Elsevier Publishing Company, Inc., New York.

Bear, J. & Verruijt, A. (1987), *Modeling groundwater flow and pollution*, D. Reidel Publ. Co., Dordrecht, The Netherlands.

Benson, C. & Gribb, M. (1997), Measuring unsaturated hydraulic conductivity in the laboratory and field, *in* S. Houston & D. G. Fredlund, eds, 'Unsaturated Soil Engineering Practice', number 68, ASCE, New York, NY, pp. 113–168.

Benson, C. H. & Bosscher, P. J. (1999), Time-domain reflectometry TDR in geotechnics: A review, *in* W. A. Marr & C. E. Fairhurst, eds, 'Nondestructive and Automated testing for Soil and Rock Properties', STP 1350, ASTM, pp. 113–135.

Biarez, J., Fleureau, J. M., Indarto, S. T. & Zerhouni, M. I. (1989), Influence of water negative pore pressure on the flow of granular materials in silos, *in* Biarez & Gourvès, eds, 'Powders and Grains', Balkema, Rotterdam, The Netherlands, pp. 385–392.

Biot, M. A. (1941), 'General theory for three-dimensional consolidation', *Journal of Applied Physics* **12**(2), 155–164.

Bishop, A. W. (1959), 'The principle of effective stress', *Teknisk Ukeblad I Samarbeide Med Teknikk* **106**(39), 859–863.

Bishop, A. W. (1960), The measurement of pore pressure in the triaxial test, *in* 'Pore Pressure and Suction in Soils', London, Butterworth, pp. 38–46.

Bishop, A. W., Alphan, I., Blight, G. E. & Donald, I. B. (1960), Factors controlling the shear strength of partly saturated cohesive soils, *in* 'Research Conf. on Shear Strength of Cohesive Soils', ASCE, Univ. of Colorado, Boulder, Colo., pp. 503–532.

Bishop, A. W. & Blight, G. E. (1963), 'Some aspects of effective stress in saturated and unsaturated soils', *Géotechnique* **13**(3), 177–197.

Bishop, A. W. & Donald, I. B. (1961), The experimental study of partially saturated soil in the triaxial apparatus, *in* 'Proc. 5th Int. Conf. Soil Mech.', Paris, pp. 13–22.

Bitterlich, S., Durner, W. & Knabner, P. (2004), 'Inverse estimation of the unsaturated soil hydraulic properties from column outflow experiments using free-form parameterizations', *Vadose Zone Journal* **3**, 971–981.

Blight, G. E. (1961), Strength and consolidation characteristics of compacted soils, PhD thesis, University of London.

Blight, G. E. (1965), A study of effective stresses for volume change, *in* G. D. Aitchison, ed., 'Moisture Equilibria and Moisture Changes in Soils Beneath Covered Areas', Australia, Butterworths, pp. 259–269.

Bolton, M. D. (1986), 'The strength and dilatancy of sands', *Geotechnique* **36**(1), 65–78.

Broms, B. B. (1963), 'The effect of degree of saturation on the bearing capacity of flexible pavements', *Highway Research Record* **71**, 1–14.

Brooks, R. H. & Corey, A. T. (1964), Hydraulic properties of porous medium, Hydrology Paper No. 3, Civil Engineering Department, Colorado State Univ., Fort Collins. Colorado.

Buckingham, E. (1907), Studies on the movement of soil moisture, Technical Report 38, Bur. of Soils Bull., U. S. Dept. of Agric. Washington, D. C.

Burdine, N. T. (1953), 'Relative permeability calculations from pore size distribution data', *Journal of Petroleum Technology* **198**, 71–78.

Burland, J. B. (1965), Some aspects of the mechanical behavior partly saturated soils, *in* G. D. Aitchison, ed., 'Moisture Equilibria and Moisture Changes in the Soils Beneath Covered Areas', Australia, Butterworth, pp. 270–278.

Cabral, A. R., Burnotte, F. & Lefebvre, G. (1999), 'Application of tdr technology to water content monitoring of capillary barriers made of pulp and paper residues', *Geotechnical Testing Journal* **22**, 39–43.

Campbell, G. S. (1974), 'A simple method for determining unsaturated conductivity from moisture retention data', *Soil Science* **117**(6), 311–314.

Campbell, J. D. (1973), Pore pressures and volume changes in unsaturated soils, PhD thesis, University of Illinois at Urbana-Champaign, Urbana-Champaign, Ill.

Carrera, J. & Neumann, S. P. (1986), 'Estimation of aquifer parameters under transient and staedy state conditions: 2. uniqueness, stability, and solution algoritms', *Water Resources Research* **22**(2), 211–227.

Casagrande, A. (1930), 'The structure of clay and its importance in foundation engineering', *Journal of the Boston Society of Civil Engineers* **19**(4), 168–209.

Casagrande, A. (1936), The determination of the preconsolidation load and its practical significance, *in* '1st Int. Conf. Soil Mech. Found. Eng.', Cambridge Mass., p. 60.

Cassel, D. K. & Klute, A. (1986), Water potential: tensiometry, *in* A. Klute, ed., 'Methods of Soil analysis. Part 1. Physical and mineralogical methods', American Society of Agronomy (ASA) and Soil Science Society of America (SSSA), Madison, WI, U.S.A., pp. 563–596.

Chapius, R. P., Masse, I., Madinier, B. & Aubertin, M. (2007), 'A drainage column test for determining unsaturated properties of coarse materials', *Geotechnical Testing Journal* **30**, 83–88.

Chatzis, I. & Dullien, F. (1983), 'Dynamic immiscible displacement mechanisms in pore doublets: theory versus experiment', *Journal of Colloid and Interface Science* **91**, 199–222.

Childs, E. C. & Collis-George, G. N. (1950), The permeability of porous materials, *in* 'Proceedings of The Royal Society, 210 A', London, U.K., pp. 392–405.

Clothier, B., Scotter, D. & Green, A. (1983), 'Diffusivity and one-dimensional absorption experiments', *Soil Science Society of America Journal* **47**, 641–644.

Coleman, J. D. (1962), 'Stress/ strain relations for partly saturated soils', *Géotechnique* **12**(4), 348–350.

Collis-George, M. & Rosenthal, M. J. (1966), 'Proposed outflow method for the determination of the hydraulic conductivity of', *Australian Journal of Soil Research* **4**, 165–180.

Corey, A. T. (1954), 'The interrelation between gas and oil relative permeabilities', *Producer's Monthly* **19**(1), 7–10.

Corey, A. T. (1957), 'Measurement of water and air permeability in unsaturated soil', *Soil Science Society of America Journal* **21**, 7–10.

Costa, Y. D., Cintra, J. C. & Zornberg, J. G. (2003), 'Influence of matric suction on the results of plate load tests perfromed on a lateritic soil deposit', *Geotechnical Testing Journal* **26**(2), 219–227.

Cox, D. W. (1978), Volume change of compacted clay fill, *in* 'Clay Fills', Inst. of Civ. Engrs., London, England, pp. 79–87.

Croney, D. & Coleman, J. D. (1954), 'Soil structure in relation to soil suction (pf)', *Journal of Soil Science* **5**(1), 75–84.

Croney, D., Coleman, J. D. & Black, W. P. M. (1958), Studies of the movement and distribution of water in soil in relation to highway design and performance, Highway Research Board, Washington, D. C., pp. 226–252.

Cui, Y. J. & Delage, P. (1996), 'Yielding and plastic behavior of an unsaturated compacted silt', *Géotechnique* **46**(2), 291–311.

Dam, J. C., Stricker, J. N. M. & Dro, P. (1992), 'Inverse method for determing soil hydraulic functions from one-step outflow experiments', *Soil Science Society of America Journal* **56**, 1042–1050.

Dam, J. C., Stricker, J. N. M. & Dro, P. (1994), 'Inverse method to determine soil hydraulic functions from multistep outflow experiments', *Soil Science Society of America Journal* **58**, 647–652.

Dane, J. H. & Klute, A. (1977), 'Salt effects on hydraulic properties of a swelling soil', *Soil Science Society of America Journal* **41**, 1043–1049.

Dane, J. H. & Topp, G. C. (2002), *Methods of Soil Analysis*, SSSA Book Series No.5, Soil Science of America, Madison, WI, chapter Part 4, Physical Methods.

Dane, J. H. & Wierenga, P. J. (1975), 'Effect of hysteresis on the prediction of infiltration, redistribution and drainage of water in layered soil', *Journal of Hydrology* **25**, 229–242.

Daniel, D. (1982), 'Measurement of hydraulic conductivity of unsaturated soils with thermocouple psychrometers', *Soil Science Society of America Journal* **46**(6), 1125–1129.

Daniel, D. E. (1983), 'Permeability test for unsaturated soil', *Geotechnical Testing Journal* **6**(2), 81–86.

Dasberg, S. & Hopmans, J. (1992), 'Improved calibration of time domain calibration for uniformly and nonuniformly wetted sandy and clayay loam silt', *Soil Science Society of America Journal* **49**, 1341–1345.

Datcheva, M. & Schanz, T. (2003), 'Anisotropic bounding surface plasticity with rotational hardening for unsaturated frictional materials', *Journal de Physique IV* **105**, 305–312.

Davidson, J. M., Nielsen, D. R. & Biggar, J. W. (1966), 'The dependence of soil water uptake and release upon the applied pressure increment', *Soil Science Society of America Journal* **30**, 298–303.

Davis, J. L. & Annan, A. P. (2002), Ground penetrating radar to measure soil water content, *in* J. H. Dane & G. C. Topp, eds, 'Methods of Soil Analysis. Part 4: Physical Methods', SSSA Book Series No. 5, Soil Science Society of America, Madison, WI, pp. 446–463.

Davis, J. L. & Chudobiak, W. J. (1975), 'In situ meter for mesuring relative permittivity of soils', *Geological Survey of Canada Paper* **75-1A**, 75–79.

Dean, T. J., Bell, J. P. & Bary, A. J. B. (1987), 'Soil moisture measurement by an improved capacitance technique. Part 1. Sensor design and performance', *Journal of Hydrology* **93**, 67–78.

Delage, P. (2002), Experimental unsaturated soil mechanics, *in* J. F. T. Jucá, T. M. P. de Campos & F. A. M. Marinho, eds, '3rd International Conferencre on Unsaturated Soils', Balkema, Recife, Brazil.

Desrues, J., Chambon, R., Mokni, M. & Mazerolle, F. (1996), 'Void ratio evaluation inside shear bands in triaxial sand specimens studued by computer tomography', *Géotechnique* **46**(3), 529–546.

Desrues, J. & Viggiani, G. (2004), 'Strain localization in sand: an overview of the experimental results obtained in grenoble using stereophotogrammetry', *International Journal for Numerical and Analytical Methods in Geomechanics* **28**(4), 279–321.

Dewitz, K.-D. (1996), 'Baustoffanalyse mittels computer-tomografie', *Bautenschutz und Bausanierung* **7**, 26–29.

Donald, I. B. (1956), Shear strength measurements in unsaturated non-cohesive soils with negative pore pressures, *in* 'Proc. 2nd Australia-New Zealand Conf. Soil Mech. Found. Eng.', Christchurch, New Zealand, pp. 200–205.

Duliu, O. G. (1999), 'Computer axial tomography in geosciences: An overview', *Earth-Science Reviews* **48**(4), 265–281.

Durner, W. (1991), 'Vorhersage der hydraulischen Leitfähigkeit strukturierter Böden', *Bayreuther Bodenkundliche Berichte 20* pp. 1–180.

Durner, W., Schultze, B. & Zurmühl, T. (1999), State-of-the-art in inverse modeling of inflow/outflow experiments, *in* M. T. van Genuchten, F. J. Leij & L. Wu, eds, 'Proc. Int. Workshop on Characterization and Measurement of the Hydraulic Properties of Unsaturated Porous Media', University of California, Riverside, CA., pp. 661–681.

Eching, S. O. & Hopmans, J. W. (1993), 'Optimization of hydraulic functions from transient outflow and soil water pressure data', *Soil Science Society of America Journal* **57**, 1167–1175.

Eching, S. O., Hopmans, J. W. & Wendroth, O. (1994), 'Unsaturated hydraulic conductivity from transient multistep and soil water pressure data', *Soil Science Society of America Journal* **58**, 687–695.

Edlefsen, N. E. & Anderson, A. B. C. (1943), 'Thermodynamics of soil moisture', *Hilgardia* **15**, 31–298.

Elrick, D., Reynolds, W., Baumgartner, N., Tan, A. & Bradshaw, K. (1987), In situ measurements of hydraulic properties of soils using guelph permeameter and guelph infiltrometer, *in* 'Proceedings, 3rd International Workshop on Land Drainage', Dept. of Agric. Eng., Ohio State Univ., Columbus, OH.

Enderby, J. A. (1955), 'The domain model of hysteresis: 1 independent domains', *Transaction of Faraday Society* **51**, 835–848.

Escario, V. & Juca, J. (1989), Strength and deformation of partly saturated soils, *in* '12th International Conference on Soil Mechancis and Foundation Engineering', Rio de Janeiro, Vol.3, pp. 43–46.

Escario, V. & Saez, J. (1973), Measurement of the properties of swelling and collapsing soils under controlled suction, *in* '3rd International Conference on Expansive Soils', Haifa, pp. 195–200.

Everett, D. H. (1955), 'A general approach to hysteresis: 4. An alternative formulation of the domain model', *Transaction of Faraday Society* **51**, 1551–1557.

Everett, D. H. (1967), 'Adsorption hysteresis', *The Solid Gas Interface* **2**, 1055–1113.

Everett, D. H. & Smith, F. W. (1954), 'A general approach to hysteresis: 2. Development of the domain theory', *Transaction of Faraday Society* **50**, 187–197.

Everett, D. H. & Whitton, W. I. (1952), 'A general approach to hysteresis: 1', *Transaction of Faraday Society* **48**, 749–752.

Farrell, D. A. & Larson, W. E. (1972), 'Modeling the pore structure of porous media', *Water Resources Research* **8**(3), 699–706.

Fawcett, R. G. & Collis-George, N. (1967), 'A filter-paper method for determining the moisture characteristics of soil', *Australian Journal of Experimental Agriculture and Animal Husbandry* **7**, 162–167.

Feng, M. & Fredlund, D. G. (1999), Hysteresis influence associated with thermal conductivity sensor measurements, *in* 'Theory to the Practice of Unsaturated Soil Mechanics in Association with the 52nd Canadian Geotechnical Conference and the Unsaturated Soil Group', Regina, Sask., pp. 14:2:14–14:2:20.

Ferré, P. A. & Topp, G. C. (2002), Time domain reflectometry, *in* J. H. Dane & G. C. Topp, eds, 'Methods of soil analysis. Part 4: Physical Methods', SSSA Book Series No. 5, Soil Science Society of America, Madison, WI, pp. 434–446.

Finn, W. D. L., Pickering, D. J. & Bransby, P. L. (1971), 'Sand liquifaction in triaxial and simple shear tests', *Journal of the Soil Mechanics and Foundations Division* **97**, 639–659.

Flavigny, E., Desrues, J. & Palayer, B. (1990), 'Note technique: Le sable d'hostun rf', *Revue Française de Géotechnique* **53**, 67–70.

Fredlund, D. G. (1973), 'Second canadian geotechnical colloqium: Appropriate concepts and technology for unsaturated soils', *Canadian Geotechnical Journal* **16**(1), 121–139.

Fredlund, D. G. (2002), Use of the soil-water characteristic curvein the implementation of unsaturated soil mechanics, *in* '3rd Int. Conf. on Unsaturated Soils, UNSAT 2002', Balkema, Recife, Brazil, pp. 887–902.

Fredlund, D. G. & Morgenstern, N. R. (1977), 'Stress state variables for unsaturated soils', *Journal of the Geotechnical Engineering Division* **5**(103), 447–466.

Fredlund, D. G., Morgenstern, N. R. & Widger, R. A. (1978), 'The shear strength of unsaturated soils', *Canadian Geotechnical Journal* **15**, 313–321.

Fredlund, D. G. & Rahardjo, H. (1993*a*), The role of unsaturated soil behavior in geotechnical practice, *in* '11th Southeast Asian Geotechnical Conference', Singapore, pp. 37–49.

Fredlund, D. G. & Rahardjo, H. (1993*b*), *Soil mechanics for unsaturated soils*, John Wiley and Sons, New York.

Fredlund, D. G., Rahardjo, H., Leong, E. C. & Ng, C. W. W. N. (2001), Suggestions and recommendation for the interpretation of soil-water characteristic curves, *in* K. K. Ho & K. S. Li, eds, '14th Southeast Asian Geotechnical Conference', Hongkong, pp. 1–6.

Fredlund, D. G. & Xing, A. (1994), 'Equations for soil-water characteristic curve', *Canadian Geotechnical Journal* **31**, 521–532.

Fredlund, D. G., Xing, A., Fredlund, M. D. & Barbour, S. L. (1996*a*), 'The relationship of the unsaturated soil shear strength to the soil-water characteristic curve', *Canadian Geotechnical Journal* **33**, 440–448.

Fredlund, D. G., Xing, A., Fredlund, M. D. & Barbour, S. L. (1996*b*), 'The relationship of the unsaturated soil shear strength to the soil-water characteristic curve', *Canadian Geotechnical Journal* **33**, 440–448.

Fredlund, D. G., Xing, A. & Huang, S. (1994), 'Predicting the permeability function for unsaturated soils using the soil-water characteristic curve', *Canadian Geotechnical Journal* **31**, 533–546.

Fredlund, M. D., Fredlund, D. G. & Wilson, G. W. (1997), Prediction of the soil-water characteristic curve from grain-size distribution and volume-mass properties, *in* 'Proceedings of the 3rd Brazilian Symposium on Unsaturated Soils, Vol. 1', Rio de Janeiro, pp. 13–23.

Fredlund, M. D., Fredlund, D. G. & Wilson, G. W. (2000), 'An equation to represent grain-size distribution', *Canadian Geotechnical Journal* **37**, 817–827.

Frost, J. D. & Park, J.-Y. (2003), 'A critical assessment of the moist tamping technique', *Geotechnical Testing Journal* **26**(1), 1–13.

Fujimaki, H. & Inoue, M. (2003), 'Reevaluation of the multistep outflow method for determining unsaturated hydraulic conductivity', *Vadose Zone Journal* **2**, 409—415.

Fung, Y. C. (1977), *A first course in continuum mechanics*, 2nd edn, Englewood Cliffs, NJ: Princton-Hall.

Gan, J. K. M., Fredlund, D. G. & Rahardjo, H. (1988), 'Determination of the shear strength parameters of an unsaturated soil using the direct shear test', *Canadian Geotechnical Journal* **25**, 500–510.

Gardner, C. M. K., Robinson, D., Blyth, K. & Cooper, D. (2001), Soil water content, *in* K. A. Smith & C. E. Mullins, eds, 'Soil and environmental analysis: Physical Methods', Marcel Dekker, New York, NY, pp. 1–64.

Gardner, W. (1956), 'Calculation of capillary conductivity from pressure plate outflow data', *Soil Science Society of America Journal* **20**, 317–320.

Gardner, W. R. (1958), 'Some staedy state solutions of the unsaturated moisture flow equation with application to evaporation from a water table', *Soil Science* **85**, 228–232.

Gee, G., Campbell, M., Campbell, G. & Campbell, J. (1992), 'Rapid measurement of low soil potentials using a water activity meter', *Soil Science Society of America Journal* **56**, 1068–1070.

Gennaro, V. D., Canou, J., Dupla, J. C. & Benahmed, N. (2004), 'Influence of loading path on the undrained behavior of a medium sand', *Canadian Geotechnical Journal* **41**, 166–180.

Gens, A. & Alonso, E. E. (1992), 'A framework for the behaviour of unsaturated expansive clay', *Canadian Geotechnical Journal* **29**, 1013–1032.

Gilbert, P. A. & Marcuson, W. F. (1988), 'Density variation in specimens subjected to cyclic and monotonic loading', *Journal of Geotechnical Engineering Division* **114**(1), 1–20.

Grozic, J. L. H., Kunne, T. & Pande, S. (2003), 'An oedometer test study on the preconsolidation stress of galciomarine clays', *Canadian Geotechnical Journal* **40**, 857–872.

Guan, Y. & Fredlund, D. G. (1997), 'Use of the tensile strength of water for the direct measurement of high soil suction', *Canadian Geotechnical Journal* **34**, 604–614.

Gussmann, P. (1986), Die Methode der kinematischen Elemente, Mitteilung 25, Institut für Geotechnik, Universität Stuttgart.

Haines, W. B. (1930), 'The hysteresis effect in capillary properties and the modes of moisture distribution associated therewith', *Journal of Agriculture Science* **20**, 96–105.

Hamilton, J. M., Daniel, D. E. & Olson, R. E. (1979), Measurement of hydraulic conductivity of partially saturated soils, *in* T. F. Zimmie & C. O. Riggs, eds, 'Permeability and Groundwater Contaminant Transport', ASTM, STP 746, pp. 182–196.

Hamilton, J. M., Daniel, D. E. & Olson, R. E. (1981), Measurement of hydraulic conductivity of partially saturated soils, *in* T. F. Zimmie & C. O. Riggs, eds, 'Permeability and Groundwater Contaminant Transport', ASTM, STP 746-EB, pp. 182–196.

Hammad, W. I. (1991), Modélisation non linéaire et étude experiméntale des bandes de cisaillement dans les sable, PhD thesis, Institut de Mécanique de Grenoble.

Hanks, R. J. (1969), 'A numerical method for estimating infiltration, redistribution, draiange, and evaporation of water from soil', *Water Resources Research* **5**, 1064–1069.

Hassanizadeh, S. M., Celia, M. A. & Dahle, H. K. (2002), 'Dynamic effect in the capillary pressure-saturation relationship and its impacts on unsaturated flow', *Vadose Zone Journal* **1**, 38–57.

Hassanizadeh, S. M. & Gray, W. G. (1990), 'Mechanics and thermodynamics of multiphase flow in porous media including interphase boundaries', *Advances in Water Resources* **13**, 169–186.

Hassanizadeh, S. M. & Gray, W. G. (1993), 'Thermodynamic basis of capillary pressure in porous media', *Water Resources Research* **29**, 3389–3405.

Haverkamp, R. & Parlange, J.-Y. (1986), 'Predicting the water retention curve from particle size distribution: 1. Sandy soils without organic matter', *Soil Science* **142**, 325–339.

Helmig, R. (1997), *Multiphase flow and transport processes in the subsurface - a contribution to the modeling of hydrosystems*, Berlin: Springer-Verlag.

Herkelrath, W., Hamburg, S. & Murphy, F. (1991), 'Automatic realtime monitoring of soil moisture in a remote field area with time domain reflectometry', *Water Resources Research* **27**, 857–864.

Hilf, J. W. (1956), An ivestigation of pore-water pressure in compacted cohesive soils, Tech. memo. 654, U.S. Dept. of the Interior, Beureau of Reclamation, Design and Const. Div., Denver.

Hillel, D. & Gardner, W. (1970), 'Measurement of unsaturated conductivity and diffusivity by infiltration through an impeding layer', *Soil Science* **109**(3), 149–153.

Hillel, D., Krentos, V. D. & Stylianou, Y. (1972), 'Procedure and test of an internal drainage method for measuring soil hydraulic characteristics in-situ', *Soil Science* **114**, 295–400.

Hogarth, W. L., Hopmans, J., Parlange, J.-Y. & Haverkamp, R. (1988), 'Application of a simple soil-water hysteresis model', *Journal of Hydrology* **98**, 21–29.

Houston, S. L., Houston, W. N. & Wagner, A. (1994), 'Laboratory filter paper suction measurements', *Geotechnical Testing Journal* **17**(2), 185–194.

Huang, S., Barbour, S. L. & Fredlund, D. G. (1998), 'Development and verification of a coefficient of permeability function for a deformable unsaturated soil', *Canadian Geotechnical Journal* **35**, 411–425.

Huang, S., Fredlund, D. G. & Barbour, S. L. (1998), 'Measurement of the coefficient of permeability for a deformable unsaturated soil using a triaxial permeameter', *Canadian Geotechnical Journal* **35**, 426–432.

Huber, R. & Helmig, R. (1999), 'Multiphase flow in heterogeneuos porous media: A classical finite element method versus an implicit pressure-explicit saturation based mixed finite element-finite volume approach', *International Journal for Numerical Methods in Fluids* **29**, 899–920.

Huisman, J. A., Hubbard, S. S., Redmond, J. D. & Annan, A. P. (2003), 'Measuring soil water content with ground penetrating radar: A review', *Vadose Zone Journal* **2**, 476–491.

Irmay, S., ed. (1954), *On the hydraulic conductivity of unsaturated soils*, Trans. Am. Geophysics Union 35.

Iwata, S., Tabuchi, T. & Warkentin, B. P. (1995), *Soil-Water Interactions: Mechanisms and Applications*, 2nd edn, New York.

Iyer, B. (1990), Pore water extraction: comparison of saturation extract and high-pressure squeezing, *in* K. B. Hoddinott & R. B. Lamb, eds, 'Physo-chemical aspects of soil and related materials', American Society for Testing and Materials, Philadelphia, pp. 159–170.

Jackson, R. D. (1964), 'Water vapor diffusion in relatively dry soil, i: Theoretical consideration and sorption experiments', *Soil Science Society of America Journal* **28**, 172–175.

Janbu, N. (1969), The resistance concept applied to deformation of soils, *in* '7th International Soil Mechanics and Foundation Engineering Conference', A. A. Balkema, Rotterdam, Boston, Mexico City, pp. 191–196.

Jang, D. J. (1997), Quantification of sand structure and its evolution during shearing using image analysis, PhD thesis, Georgia Institute of Technology, Atlanta.

Jang, D. J., Frost, J. D. & Park, J. Y. (1999), 'Preparation of epoxy imgregnated sand coupons for image analysis', *Geotechnical Testing Journal* **22**(2), 147–158.

Jaynes, D. B. (1984), 'Comparison of soil-water hysteresis models', *Journal of Hydrology* **75**, 287–299.

Jennings, J. E. (1961), A revised effective stress law for use in the prediction of the behavior of unsaturated soils, *in* 'Pore Pressure and Suction in Soils', London, Butterworth, pp. 26–30.

Jennings, J. E. & Burland, J. B. (1962), 'Limitations to the use of effective stresses in partly saturated soils', *Géotechnique* **2**(12), 125–144.

Johnston, L. N. (1942), 'Water permeable jacketed thermal radiators as indicators of field capacity and permanent wilting percentage in soils', *Soil Science* **54**, 123–126.

Kassiff, G. & Shalom, A. B. (1971), 'Experimental relationship between swell pressure and suction', *Géotechnique* **21**, 245–255.

Kelleners, T. J., Soppe, R. W. O., Robinson, D. A., Schaap, M. G., Ayars, J. & Skaggs, T. H. (2004), 'Calibration of capacitance probe sensors using electric circuit theory', *Soil Science Society of America Journal* **68**, 430–439.

Klute, A. (1965), Laboratory measurement of hydraulic conductivity of unsaturated soils, *in* C. A. Black, ed., 'Methods of soil ananlysis', American Society of Agronomy (ASA), Madison, WI, U.S.A., pp. 253–261.

Klute, A. (1972), 'The determination of the hydraulic condcutivity and diffusivity of unsaturated soils', *Soil Science* **113**(4), 264–276.

Klute, A. (1986), Water retention: laboratory methods, *in* A. Klute, ed., 'Methods of Soil analysis. Part 1. Physical and mineralogical methods', American Society of Agronomy (ASA) and Soil Science Society of America (SSSA), Madison, WI, U.S.A., pp. 635–662.

Klute, A. & Dirksen, C. (1986*a*), Hydraulic conductivity and diffusivity: laboratory methods, *in* A. Klute, ed., 'Methods of Soil analysis. Part 1. Physical and mineralogical methods', American Society of Agronomy (ASA) and Soil Science Society of America (SSSA), Madison, WI, U.S.A., pp. 687–734.

Klute, A. & Dirksen, C. (1986*b*), Hydraulic conductivity and diffusivity: Laboratory methods, *in* A. Klute, ed., 'Methods of Soil analysis. Part 1. Physical and mineralogical methods', American Society of Agronomy (ASA) and Soil Science Society of America (SSSA), Madison, WI, U.S.A., pp. 687–734.

Klute, A., Whisler, F. D. & Scott, E. J. (1964), 'Soil water diffusivity and hysteresis data from radial flow pressure cells', *Soil Science Society of America Journal* **28**, 160–164.

Kool, J. B., Parker, J. C. & van Genuchten, M. T. (1985*a*), 'Determining soil hydraulic properties from one-step outflow experiments by parameter estimation: I. Theory and numerical studies', *Soil Science Society of America Journal* **49**, 1348–1354.

Kool, J. B., Parker, J. C. & van Genuchten, M. T. (1985*b*), 'Determining soil hydraulic properties from one-step outflow experiments by parameter estimation: II. Experimental studies', *Soil Science Society of America Journal* **49**, 1354–1359.

Kovacs, G. (1981), *Seepage hydraulics*, Elsevier Science Publisher, Amsterdam.

Krahn, J. & Fredlund, D. G. (1972), 'On total, matric and osmotic suction', *Soil Science* **114**(5), 339–348.

Kumbhojkar, A. S. (1993), 'Numerical evaluation of Terzaghi's N (gamma)', *Journal of Geotechnical Engineering* **119**(3), 598–607.

Kunze, R. J., Uehara, G. & Graham, K. (1968), 'Factors important in the calculation of hydraulic conductivity', *Soil Science Society of America Journal* **32**, 760–765.

Ladd, R. S. (1974), 'Specimen preparation and liquefaction of sands', *Journal of Geotechnical Engineering Division, ASCE* **100**(10), 118–184.

Ladd, R. S. (1978), 'Preparing test specimens using undercompaction', *Geotechnical Testing Journal* **1**(1), 16–23.

Lambe, T. W. & Whitman, R. V. (1969), *Soil mechanics*, New York, Wiley.

Lawton, E. C., Fragaszy, R. J. & Hardcastle, J. H. (1989), 'Collapse of compacted clayey sand', *Journal of Geotechnical Engineering* **115**(9), 1252–1267.

Lawton, E. C., Fragaszy, R. J. & Hardcastle, J. H. (1991), 'Stress ratio effects on collapse of compacted clayey sand', *Jounral of Geotechnical Engineering* **117**(5), 714–730.

Lawton, E. C., Fragaszy, R. J. & Hetherington, M. D. (1991), Significance and control of wetting-induced collapse in compacted soils, Technical Report 91-01, University of Utah, Salt Lake City, Utah.

Lawton, E. C., Fragaszy, R. J. & Hetherington, M. D. (1992), 'Review of wetting-induced collapse in compacted soil', *Journal of Geotechnical Engineering* **118**(9), 1376–1394.

Ledieu, J., de Ridder, P., de Clerck, P. & Dautreband, S. (1986), 'A method of measuring soil moisture by time-domain reflectometry', *Journal of Hydrology* **88**, 319–328.

Leong, E. C., He, L. & Rahardjo, H. (2002), 'Factors affecting the filter paper method for total and matric suction measurements', *Geotechnical Testing Journal* **25**(3), 321–332.

Leong, E. C. & Rahardjo, H. (1997*a*), 'Permeability for unsaturated soils', *Journal of Geotechnical and Geoenvironmental Engineering* **123**(12), 1118–1126.

Leong, E. C. & Rahardjo, H. (1997*b*), 'Review of soil-water characteristic curve equations', *Journal of Geotechnical and Geoenvironmental Engineering* **123**(12), 1106–1117.

Leong, E.-C., Tripathy, S. & Rahardjo, H. (2003), 'Total suction measurement of unsaturated soils with a device using the chilled-mirror dew-point technique', *Géotechnique* **53**(2), 173–182.

Liakopoulos, A. C. (1964), Transient flow through unsaturated porous media, PhD thesis, University of Berkley, California.

Lins, Y., Agus, S. S., Tripathy, S. & Schanz, T. (2002), Determination of unsaturated coefficient of permeability for sand, *in* T. Schanz, ed., '4. Workshop Weimar - Teilgesättigte Böden', Bauhaus-Universität Weimar, pp. 93–99.

Lins, Y. & Schanz, T. (2005), Determination of hydro-mechanical properties of sand, *in* T. Schanz, ed., 'Unsaturated Soils: Experimental Studies, Vol. I', Springer Proceedings in Physics 93, Springer-Verlag, Berlin Heidelberg, pp. 15–32.

Lins, Y., Zou, Y. & Schanz, T. (2007), Physical modeling of SWCC for granular materials, *in* T. Schanz, ed., 'Theoretical and Numerical Unsaturated Soil Mechanics', Springer Proceedings in Physics 113, Springer-Verlag, Berlin Heidelberg, pp. 61–74.

Logsdon, S. & Jaynes, D. (1993), 'Methodology for determining hydraulic conductivity with tension infiltrometers', *Soil Science Society of America Journal* **57**, 1426–1431.

Look, B. & Reeves, I. (1992), 'The application of time domain reflectometry in geotechnical instrumentation', *Geotechnical Testing Journal* **13**(3), 277–283.

Lu, N. & Likos, W. (2004), *Unsaturated soil mechanics*, John Wiley and Sons, Inc., Hoboken, New Jersey.

Mahler, F. M. & Diene, A. A. (2007), Tensiometer development for high suction analysis in laboratory lysimeters, *in* T. Schanz, ed., 'Experimental Unsaturated Soil Mechanics', Springer Proceedings in Physics 112, Springer-Verlag, Berlin Heidelberg, pp. 103–115.

Malicki, M., Plagge, R., Renger, M. & Walczak, R. (1992), 'Application of time domain reflectometry (TDR) soil moisture miniprobe for the determination of unsaturated soil water characteristics from undisturbed soil cores', *Irrigation Science* **13**(2), 65–72.

Malicki, M., Plagge, R. & Roth, C. H. (1996), 'Improving the calibration of dielectric TDR soil moisture determination taking into account the solid soil', *European Journal of Soil Science* **47**, 357–366.

Manthey, S. (2006), Two phase flow processes with dynamic effects in porous media - parameter estimation and simulation, PhD thesis, Institut für Wasserbau, Universität Stuttgart.

Marshall, T. J. (1958), 'A relation between permeability and size distribution of pores', *Journal of Soil Science* **9**(1), 1–8.

Meerdink, J. S., Benson, C. H. & Khire, M. V. (1996), 'Unsaturated hydraulic conductivity of two compacted barrier soils', *Journal of Geotechnical Engineering* **7**(122), 565–576.

Meyerhof, G. G. (1951), 'The ultimate bearing capacity of foundations', *Géotechnique* **2**, 301–332.

Miller, E. & Miller, R. (1988), 'Physical theory for capillary flow phenomena', *Transport in porous media* **3**, 324–332.

Millington, R. J. & Quirk, J. P. (1961), 'Permeability of porous solids', *Transaction of Faraday Society* **57**, 1200–1206.

Mitchell, J. K. (1993), *Fundamentals of Soil Behavior*, 2nd edn, John Wiley and Sons Inc., NY.

Miura, S. & Toki, S. (1982), 'A sample preparation method and its effect on static and cyclic deformation strength properties', *Soils and Foundations* **22**(1), 61–77.

Mohamed, F. M. O. & Vanapalli, S. K. (2006), Laboratory investigations for the measurement of the bearing capacity of an unsaturated coarse-grained soil, *in* '59th Canadian Geotechnical Conference', BC, Vancouver.

Mokni, M. & Desrue, J. (1999), 'Strain localisation measurements in undrained plane-strain biaxial tests on hostun rf sand', *Mechanics of cohesive-frictional materials* **4**, 419–441.

Mualem, Y. (1974), 'A conceptual model of hysteresis', *Water Resources Research* **10**, 514–520.

Mualem, Y. (1976), 'A new model for predicting the hydraulic conductivity of unsaturated porous media', *Water Resources Research* **12**, 593–622.

Mualem, Y. (1977), 'Extension of the similarity hypothesis used for modeling the soil water characteristic', *Water Resources Research* **13**, 773–780.

Mualem, Y. (1984*a*), 'A modified dependent domain theory of hysteresis', *Soil Science* **137**(5), 283–291.

Mualem, Y. (1984*b*), 'Prediction of the soil boundary wetting curve', *Soil Science* **137**(6), 379–390.

Mualem, Y. (1986), Hydraulic conductivity of unsaturated soils: prediction and formulas, *in* A. Klute, ed., 'Methods of Soil Analysis. Part 1: Physical and Mineralogical Methods', American Society of Agronomy (ASA) and Soil Science Society of America (SSSA), Madison, WI, U.S.A., pp. 799–823.

Mualem, Y. & Dagan, G. (1975), 'A dependent domain model of capillary hysteresis', *Water Resources Research* **11**, 452–460.

Mulilis, J. P., Chan, C. K. & Seed, H. B. (1975), The effects of method of sample preparation on the cyclic stress strain behavior of sands, Technical Report 75-18, EERC Report.

Mulilis, J. P., Seed, H. B., Chan, C. K., Mitchell, J. K. & Arulanandan, K. (1977), 'Effects of sample preparation on sand liquifaction', *Journal of the Geotechnical Engineering Division* **103**, 91–108.

Néel, L. (1942), 'Théories des lois d'aimantation de Lord Raileigh', *Cah. Phys.* **12**, 1–20.

Néel, L. (1943), 'Théories des lois d'aimantation de Lord Raileigh', *Cah. Phys.* **13**, 19–30.

Nielsen, D. R. & Biggar, J. W. (1961), 'Measuring capillary conductivity', *Soil Science* **92**, 192–193.

Nimmo, J. R. (1992), 'Semiempirical model of soil water hysteresis', *Soil Science Society of America Journal* **56**, 172–173.

Nimmo, J. R. & Akstin, K. C. (1988), 'Hydraulic conductivity of a saturated soil at low water content after compaction by various methods', *Soil Science Society of America Journal* **52**, 303–310.

Nimmo, J. R., Rubin, J. & Hammermeister, D. P. (1987), 'Unsaturated flow in a centrifugal field: Measurement of hydraulic conductivity and testing of darcy´s law', *Water Resources Research* **23**(1), 124–134.

Nützmann, G., Thiele, M., Maciejewski, S. & Joswig, K. (1998), 'Inverse modelling techniques for determining hydraulic properties of coarse-textured porous media by transient outflow method', *Advances in Water Resources* **22**, 273–284.

Oda, M., Koishikawa, I. & Higuehi, T. (1978), 'Experimental study of anisotropic shear strength of sand by plane strane test', *Soils and Foundations* **18**(1), 25–38.

Ohde, J. (1939), 'Zur theorie der druckverteilung im baugrund', *Bauingenieur* **20**, 93–99.

Oloo, S. Y., Fredlund, D. G. & Gan, J. K.-M. (1997), 'Bearing capacity of unpaved roads', *Canadian Geotechnical Journal* **34**, 398–407.

Overman, A. & West, H. (1972), 'Measurement of unsaturated hydraulic conductivity by the constant outflow method', *Transactions of the American Society of Agricultural Engineers* **15**(6), 1110–1111.

Papafotiou, A. (2008), Numerical Investigations of the Role of Hysteresis in Heterogeneous Two-Phase Flow Systems, PhD thesis, Institut für Wasserbau, Universität Stuttgart.

Parker, J. C. & Lenhard, R. J. (1987), 'A model for hysteretic constitutive relations governing multiphase flow: 1. Saturation pressure relations', *Water Resources Research* **23**(12), 2187–2196.

Parlange, J.-Y. (1976), 'Capillary hysteresis and the relationship between drying and wetting curves', *Water Resources Research* **12**, 224–228.

Pavlakis, G. & Barden, L. (1972), 'Hysteresis in the moisture characteristics of clay soil', *Journal of Soil Science* **23**, 350–361.

Peroni & Tarantino, A. (2005), Measurement of osmotic suction using squeezing method, *in* T. Schanz, ed., 'Unsaturated Soils: Experimental Studies, Vol. I', Springer Proceedings in Physics 93, Springer-Verlag, Berlin Heidelberg, pp. 159–168.

Perroux, K. M., Raats, P. A. C. & Smiles, D. E. (1982), 'Wetting moisture characteristic curves derived from constant-rate infiltration into thin samples', *Soil Science Society of America Journal* **46**, 231–234.

Pham, H. Q., Fredlund, D. G. & Barbour, S. L. (2003), 'A practical hysteresis model for the soil-water characteristic curve for soils with negligible volume change', *Géotechnique* **53**(2), 293–298.

Pham, H. Q., Fredlund, D. G. & Barbour, S. L. (2005), 'A study of hysteresis models for soil-water characteristic curves', *Canadian Geotechnical Journal* **42**(11), 1548–1568.

Pham, H. Q., Fredlund, D. G. & Padilla, J. M. (2004), Use of the gcts apparatus for the measurment of soil-characteristic curves, *in* '57th Canadian Geotechnical Conf.', Quebec, pp. 1–6.

Phene, C. J., Hoffman, G. J. & Rawlins, S. L. (1971), 'Measuring soil matric potential in situ by sensing heat dissipation with a porous body: Theory and sensor contruction', *Soil Science Society of America Journal* **35**, 27–32.

Philip, J. R. (1964), 'Similarity hypothesis for capillary hysteresis in porous materials', *Journal of Geophysical Research* **69**, 1553–1562.

Plagge, R., Häupl, P. & Renger, M. (1997), Transient effects on the hydraulic properties of porous media, *in* F. J. L. M. Th. Van Genuchten & L. Wu, eds, 'Proc. of the Int. Workshop on Characterization and Measurement of the Hydraulic Properties of Unsaturated Porous Media', University of California, Riverside, CA., pp. 905–912.

Poulovassilis, A. (1962), 'Hysteresis of pore water - An application of the concept of independent domains', *Soil Science* **92**, 405–412.

Poulovassilis, A. (1969), 'The effect of hysteresis of pore water on the hydraulic conductivity', *Journal of Soil Science* **20**(1), 52–56.

Poulovassilis, A. (1970), 'Hysteresis of pore water in granular porous bodies', *Soil Science* **109**(1), 5–12.

Poulovassilis, A. & El-Gharmy, W. M. (1978), 'The dependent domain theory applied to scanning curves of any order in hysteretic soil water relationship', *Journal of Soil Science* **126**, 1–8.

Prandtl, L. (1921), 'Eindringungsfestigkeit und Festigkeit von Schneiden', *Zeitschrift für Angewandte Mathematik und Mechanik* **1**(4), 15–20.

Rahardjo, H. & Fredlund, D. G. (2003), 'Ko-volume change charactersitics of an unsaturated soil with respect to various loading paths', *Canadian Geotechnical Journal* **26**(1), 1–11.

Rampino, C., Mancuso, C. & Vinale, F. (1999), 'Laboratory testing on an unsaturated soil: equipment, procedures, and first experimental results', *Canadian Geotechnical Journal* **36**, 1–12.

Rampino, C., Mancuso, C. & Vinale, F. (2000), 'Experimental behavior ang modelling of an unsaturated compacted soil', *Canadian Geotechnical Journal* **37**, 748–763.

Reeve, M. J., Smith, P. D. & Thomasson, A. J. (1973), 'The effect of density on water retention properties of field soils', *Journal of Soil Science* **24**(3), 355–367.

Reginato, R. J. & van Bavel, C. H. M. (1962), 'Pressure cell for soil cores', *Soil Science Society of America Journal* **26**, 1–3.

Rendulic, L. (1936), Relation between void ratio and effective principles stresses for a remoulded silty clay, *in* '1st Int. Conf. Soil Mech. Found. Eng.', Cambridge, MA, pp. 48–51.

Reynolds, W. & Elrick, D. (1991), 'Determination of hydraulic conductivity using a tension infiltrometer', *Soil Science Society of America Journal* **55**, 633–639.

Richards, L. A. (1928), 'The usefulness of capillary potential to soil moisture and plant investigators', *Journal of Agricultural Research* **37**, 719–742.

Richards, L. A. (1931), 'Capillary conduction of liquids thgrough porous medium', *Physics* **1**, 318–333.

Richards, L. A. (1941), 'A pressure-membrane extraction apparatus for soil solution', *Soil Science* **51**, 377–386.

Richards, L. A. (1947), 'Pressure-membrane apparatus - constrution and use', *Agricultural Engineering* **28**, 451–454.

Richards, L. A. & Weaver, L. R. (1944), 'Moisture retention by some irrigated soils related to soil moisture tension', *Journal of Agricultural Research* **69**, 215–235.

Richards, S. & Weeks, L. (1953), 'Capillary conductivity values from moisture yield and tension measurements on soil columns', *Soil Science Society of America Journal* **55**, 206–209.

Ridley, A. M. & Burland, J. B. (1993), 'A new instrument for the measurement of soil suction', *Géotechnique* **43**(2), 321–324.

Ridley, A. M. & Wray, W. K. (1996), Suction measurement: A review of current theory and practices, *in* E. E. Alonso & P. Delage, eds, '1st International Conference on Unsaturated Soils (UNSAT 95)', Balkema, Rotterdam, Paris, pp. 1293–1322.

Robinson, D. A., Gardner, C. M. K., Evans, J., Cooper, J. D., Hodnett, M. G. & Bell, J. P. (1998), 'The dielectric calibration of capacitance probes for soil hydrology using an oscillation frequency response mode', *Hydrology and Earth System Sciences* (2), 83–92.

Robinson, D. A., Jones, S. B., Wraith, J. M., Or, D. & Freidman, S. P. (2003), 'A review of advance s in dielctric and electrical conductivity measurements in soils using time domain reflectometry', *Vadose Zone Journal* **2**, 444–475.

Rogers, J. S. & Klute, A. (1971), 'The hydraulic conductivity-water content relationship during nonsteady flow through a sand column', *Soil Science Society of America Journal* **35**, 695–700.

Rojas, E. & Rojas, F. (2005), 'Modeling hysteresis of the soil-water characteristic curve', *Japanese Geotechnical Society* **45**(3), 135–145.

Rojas, J. C., Salinas, L. M. & Sejas, C. (2007), Plate-load tests on an unsaturated lean clay, *in* T. Schanz, ed., 'Experimental Unsaturated Soil Mechanics', Springer-Verlag, Berlin Heidelberg, pp. 445–451.

Romero, E. (1999), Characterisation and thermo-hydromechanical behaviour of unsaturated boom clay: an experimental studys, PhD thesis, Universitat Politècnica de Catalunya, Barcelona, Spain.

Rose, D. (1968), 'Water movement in porous materials. iii. evaporation of water from soil', *British Journal of Applied Physics* **2**(1), 1770–1791.

Roth, C. H., Malicki, M. A. & Plagge, R. (1992), 'Empirical evaluation of the relationships between soil dielectric constent and volumetric water content as the basis for calibrating soil moisture measurements by TDR', *Journal of Soil Science* **43**(1), 1–13.

Salter, P. L. & Williams, J. B. (1965), 'The influence of texture on the moisture characteristics of soils. Part 1: A critical comparison of techniques for determining the available water capacity and moisture characteristic curve of a soil', *Journal of Soil Science* **16**, 1–15.

Schanz, T. (1998), Zur Modellierung des mechanischen Verhaltens von Reibungsmaterialien, Mitteilung 45, Institut für Geotechnik, Universität Stuttgart.

Schanz, T. & Alabdullah, J. (2007), Testing unsaturated soil for plane strain condition: A new double wall biaxial device, *in* T. Schanz, ed., 'Experimental Unsaturated Soil Mechanics', Springer Proceedings in Physics 112, Springer-Verlag, Berlin Heidelberg, pp. 169–178.

Schanz, T., Lins, Y., Tripathy, S. & Agus, S. S. (2002), Model test for determination of permeability and collapse potential of a partially saturated sand, *in* J. P. Magnan, ed., 'Parametre de calcul geotéchnique', Presses de l'ENPC/LCPC, Paris, pp. 111–121.

Schanz, T., Mikulitsch, V. & Lins, Y. (2001), Untersuchungen an teilgesättigten, granularen Reibungsmaterialien, *in* T. Schanz, ed., '3. Workshop - Teilgesättigte Böden', Bauhaus-Universität Weimar, pp. 145–159.

Schanz, T. & Vermeer, P. A. (1996), 'Angles of friction and dilatancy of sand', *Géotechnique* **46**(1), 145–151.

Schultze, B., Ippisch, O., Huwe, B. & Durner, W. (1997), Dynamic nonequilibrium during unsaturated water flow, *in* M. T. V. Genuchten, F. J. Leij & L. Wu, eds, 'Proc. of the Int. Workshop on Characterization and Measurement of the Hydraulic Properties of Unsaturated Porous Media', University of California, Riverside, CA., pp. 877–892.

Scott, P. S., Farquhar, G. J. & Kouwen, N. (1983), Hysteretic effects on net infiltration, *in* 'Advances in infiltration', ASAE St. Joseph, MI, Publ. 11, pp. 163–170.

Selig, E. & Mansukhani, S. (1975), 'Relationship of soil moisture to dielectric property', *Journal of the Geotechnical Engineering Division* **107**(8), 755–770.

Shaw, B. & Baver, L. D. (1939), 'An electrothermal method for following moisture changes of the soil insitu', *Soil Science Society of America Journal* **4**, 78–83.

Sheta, H. (1999), Simulation von Mehrphasenvorgängen in porösen Medien unter Einbeziehung von Hysterese-Effekten, PhD thesis, Institut für Wasserbau, Universität Stuttgart.

Siddiqui, S. I. & Drnevich, V. P. (1995), A new method of measuring density and moisture content of soil using the technique of time domain reflectometry, Technical Report FHWA/IN/JTRP-95/9, Indiana Department of Transportation, Purdue University.

Sillers, W. S. (1997), The mathmetical representation of the soil-water characteristic curve, PhD thesis, University of Saskatchewan.

Sillers, W. S. & Fredlund, D. G. (2001), 'Statistical assessment of soil-water characteristic curve models for geotechnical engineering', *Canadian Geotechnical Journal* **38**, 1297–1313.

Singh, V. P. (1997), *Kinematic Wave Modelling in Water Resources: Environmental Hydrology*, Wiley, New York.

Skempton, A. W. (1961), Effective stress in soils, concrete and rocks, *in* 'Pore Pressure and Suction in Soils', London, Butterworth, pp. 4–16.

Spanner, D. C. (1951), 'The peltier effect and its use in the measurement of suction pressure', *Journal of Experimental Botany* **11**, 145 –168.

Stannard, D. I. (1992), 'Tensiometers - theory, construction and use', *Geotechnical Testing Journal* **15**(1), 48–58.

Staple, W. J. (1965), 'Moisture tension, diffusivity, and conductivity of a loam soil during wetting and drying', *Canadian Journal of Soil Science* **45**, 78–86.

Stauffer, F. (1977), Einfluss der kapillaren Zone auf instantionäre Drainagevorgänge, PhD thesis, ETH Zürich, Zürich, Switzerland.

Steensen-Bach, J. O., Foged, N. & Steenfelt, J. S. (1987), Capillary induced stresses - Fact or fiction?, *in* 'Nineth ECSMFE, Groundwater Effects in Geotechnical Engineering', Dublin, pp. 83–89.

Stoimenova, E., Datcheva, M. & Schanz, T. (2003*a*), 'Application of two-phase regression to geotechnical data', *Pliska Stud. Math. Bulgar.* **16**, 245–257.

Stoimenova, E., Datcheva, M. & Schanz, T. (2003*b*), Statistical modeling of the soil-water characteristic curve for geotechnical data, *in* '1st International Conference: Mathematics and Informatics for Industry', Thessaloniki, Greece, pp. 356–366.

Stoimenova, E., Datcheva, M. & Schanz, T. (2005), Statistical approach in soil-water characteristic curve modelling, *in* T. Schanz, ed., 'Unsaturated Soils: Numerical and Theoretical Approaches, Vol. II', Springer Proceedings in Physics 94, Springer-Verlag, Berlin Heidelberg, pp. 189–200.

Stoimenova, E., Lins, Y., Datcheva, M. & Schanz, T. (2006), Inverse modelling of soil hydraulic characteristic functions, *in* K. Gürlebeck & C. Könke, eds, '17th International Conference on the Application of Computer Science and Mathematics in Architecture and Civil Engineering', Weimar, Germany. http://euklid.bauing.uni-weimar.de/templates/papers/f105.pdf.

Suwansawat, S. (1997), Using time domain reflectometry for measuring water content in compacted clays, Master's thesis, University of Wisconsin-Madison.

Suwansawat, S. & Benson, C. H. (1999), 'Cell size for water content-dielectric constant calibratios for time domain reflectometry', *Geotechnical Testing Journal* **22**, 3–12.

Talsma, T. (1970), 'Hysteresis in two sands and an independent domain model', *Water Resources Research* **6**, 964–970.

Tarantino, A. & Mongiovi, L. (2002), 'Calibration of tensiometer for direct measurement of matric suction', *Géotechnique* **53**(1), 137–141.

Tarantino, A., Romero, E. & Cui, Y. J. (2008), 'Special issue on laboratory and field testing of unsaturated soils', *Geotechnical and Geological Engineering* **26**(6).

Terzaghi, K. (1943), *Theoretical soil mechanics*, Wiley, New York.

Toorman, A. F. & Wierenga, P. J. (1992), 'Parameter estimation of hydraulic properties from one-step outflow data', *Water Resources Research* **28**(11), 3021–3028.

Topp, G. C. (1969), 'Soil water hysteresis measured in a sandy loam compared with the hysteresis domain model', *Soil Science Society of America Journal* (33), 645–651.

Topp, G. C. (1971*a*), 'Soil water hysteresis on silt loam and clay loam soils', *Water Resources Research* **7**(4), 914–920.

Topp, G. C. (1971*b*), 'Soil-water hysteresis: The domain model theory extended to pore interaction conditions', *Soil Science Society of America Journal* **35**, 219–225.

Topp, G. C. (1987), The application of time-domain refelectometry (TDR) to soil water content measurment, *in* 'Int. Conf. on Measurment of Soil and Plant Water Status', Logan, Utah, pp. 85–93.

Topp, G. C., Davis, J. L. & Annan, A. P. (1980), 'Electromagnetic determination of soil water content: Measurements in coaxial transmission lines', *Water Resources Research* **16**(3), 574–582.

Topp, G. C., Klute, A. & Peters, D. B. (1967), 'Comparison of water content-pressure head data obtained by equilibrium, steady state and unsteady state methods', *Soil Science Society of America Journal* **31**, 312–314.

Topp, G. C. & Miller, E. E. (1966), 'Hysteresis moisture characteristics and hydraulic conductivities for glass-bead media', *Soil Science Society of America Journal* **30**, 156–162.

Topp, G. C. & Reynolds, W. D. (1998), 'Time domain reflectometry : A seminal technique for measuring mass and energy in soil', *Soil Tillage Reserach* **47**, 125–132.

Tripathy, S. & Schanz, T. (2003), Evaluation of two devices for measuring total suction of unsaturated soils, *in* 'Symposium on advances in Geotechnical Engineering', IIT Kanpur, India, pp. 172–182.

Vachaud, G., Vauclin, M. & Wakil, M. (1972), 'A study of the uniqueness of the soil moisture characteristic during desorption by vertical drainage', *Soil Science Society of America Journal* **36**, 531–532.

Vaid, Y. P. & Negussy, D. (1988), 'Preparation of reconstituted sand specimen', *Advanced Triaxial Testing of Soil and Rock* pp. 405–417.

van Dam, J. C., Stricker, J. N. M. & Droogers, P. (1990), From one-step to multi-step. determination of soil hydraulic functions by outflow experiments, Technical Report 7, Agricultural University Wageningen, Netherlands.

van Genuchten, M. T. (1980), 'A closed-form equation for predicting the hydraulic conductivity of unsaturated soils', *Soil Science Society of America Journal* **44**(5), 892–898.

van Grinsven, J., Dirksen, C. & Bouten, W. (1985), 'Evaluation of the hot air method for measuring soil water diffusivity', *Soil Science Society of America Journal* **49**, 1093–1099.

Vanapalli, S. K., Fredlund, D. G., Pufahl, D. E. & Clifton, A. W. (1996), 'Model for the prediction of shear strength with respect to soil solution', *Canadian Geotechnical Journal* **33**, 379–392.

Vanapalli, S. K. & Mohamed, F. M. O. (2007), Bearing capacity of model footings in unsaturated soils, *in* T. Schanz, ed., 'Experimental Unsaturated Soil Mechanics', Springer Proceedings in Physics 112, Springer-Verlag, Berlin Heidelberg, pp. 483–493.

Vanapalli, S. K., Nicotera, M. V. & Sharma, R. S. (2008), 'Axis translation and negative water column techniques for suction control', *Geotechnical and Geological Engineering* **26**(6), 645–660.

Vesic, A. S. (1973), 'Analysis of ultimate loads of shallow foundations', *Journal of the Soil Mechanics and Foundation Devision* (SM1), 45–73.

Viaene, P., Vereecken, H., Diels, J. & Feyen, J. (1994), 'A statistical analysis of six hysteresis models for the moisture retention characteristic', *Soil Science* **157**(6), 345–355.

von Soos, P. (2001), *Grundbautaschenbuch Teil1: Geotechnische Grundlagen*, 6. edn, Ernst und Sohn, chapter Eigenschaften von Boden und Fels - Ihre Ermittlung im Labor, pp. 117–201.

Wan, A. W. L. (1996), The use of thermocouple psychrometers to measure in situ suctions and water content in compacted clays, PhD thesis, University Manitoba.

Wana-Etyem, C. (1982), Static and dynamic water content pressure head relations of porous media, PhD thesis, Colorado State Univ., Ft. Collins, CO.

Wang, Z., Wu, L. & Wu, Q. J. (2000), 'Water-entry value as an alternative indicator of soil water-repellency and wettability', *Journal of Hydrology* **231–232**, 76–83.

Watson, K. (1966), 'An instantaneous profile method for determining the hydraulic conductivity of unsaturated porous media', *Water Resources Research* **4**(2), 709–715.

Watson, K. K. (1965), Non-continuous porous media flow, Technical Report 84, Water Res. Lab., Univ. of New South Wales, Manly Vale, N. S. W., Australia.

Weiler, K. W., Steenhuis, T. S., Boll, J. & Kung, K.-J. S. (1998), 'Comparison of ground penetrating radar and time domain reflectometry as soil water sensors', *Soil Science Society of America Journal* **62**, 1237–1239.

Wendroth, O., Ehlers, W., Hopmans, J., Kage, H., Halbertsma, J. & Wosten, J. (1993), 'Reevaluation of the evaporation method for determining hydraulic functions in unsaturated soils', *Soil Science Society of America Journal* **57**, 1436–1443.

Wildenschild, D. & Hopmans, J. (1997), Flow rate dependence of hydraulic properties of unsaturated porous media, *in* M. T. V. Genuchten, F. J. Leij & L. Wu, eds, 'Proc. of the Int. Workshop on Characterization and Measurement of the Hydraulic Properties of Unsaturated Porous Media', University of California, Riverside, CA, pp. 893–904.

Wildenschild, D., Hopmans, J. W. & Simunek, J. (2001), 'Flow rate dependence of soil hydraulic characteristics', *Soil Science Society of America Journal* **65**, 35–48.

Wildenschild, D., Jensen, K. H., Hollenbeck, K. J., Illangasekare, T. H., Znidarcic, D., Sonnenborg, T. & Butts, M. B. (1997), 'A two-stage procedure for determining unsaturated hydraulic characteristics using a syringe pump and outflow observations', *Soil Science Society of America Journal* **61**, 347–359.

Williams, P. J. (1982), *The surface of the Earth: An introduction to geotechnical science*, Longman Inc., New York.

Wind, G. (1966), Capillary conductivity data estimated by a simple method, *in* P. Ritjema & H. Wassnik, eds, 'Water in the unsaturated zone, Vol. 1, Proc. Wageningen Symp.', Intl. Assoc. of Scientific Hydrologists, UNESCO, Paris.

Wind, G. P. (1955), 'Field experiment concerning capillary rise of moisture in heavy clay soils', *Neth. J. Agric. Sci.* **3**, 60–69.

Yang, H., Rahardjo, H., Leong, E.-C. & Fredlund, D. G. (2004*a*), 'Factors affecting drying and wetting soil-water characteristic curves of sandy soils', *Canadian Geitechnical Journal* **41**, 908–920.

Yang, H., Rahardjo, H., Leong, E. & Fredlund, D. (2004*b*), 'A study of infiltration on three sand capillary barriers', *Canadian Geotechnical Journal* **41**, 629–643.

Yang, H., Rahardjo, H., Wibawa, B. & Leong, E.-C. (2004), 'A soil column apparatus for laboratory infiltration study', *Geotechnical Testing Journal* **27**(4), 347–355.

Youngs, E. G. (1964), 'An infiltration method of measuring the hydraulic conductivity of unsaturated porous media', *Soil Science* **97**, 307–311.

Yu, X. & Drnevich, V. P. (2004), 'Soil water content and dry density by time domain reflectometry', *Journal of Geotechnical and Geoenvironmental Engineering* **130**(9), 922–933.

Zachmann, D. W., Duchateau, P. C. & Klute, A. (1981), 'The calibration of the richards flow equation for a draining column by parameter identification', *Soil Science Society of America Journal* **45**, 1012–1015.

Zachmann, D. W., Duchateau, P. C. & Klute, A. (1982), 'Simultaneous approximation of water capacity and soil hydraulic conductivity by parameter estimation', *Soil Science* **134**, 157–163.

Zapata, C. E., Houston, W. N., Houston, S. L. & Walsh, K. D. (2000), Soil-water characteristic variability, *in* C. D. Shackelford, S. L. Houston & N.-Y. Chang, eds, 'Advances in

Unsaturated Geotechnics, Geotechnical Institut Special Publication No. 99', ASCE, Reston, Va., pp. 84–124.

Zhu, D. Y., Lee, C. F. & Jiang, H. D. (2001), 'A numerical study of the bearing capacity factor N (gamma)', *Canadian Geotechnical Journal* (38), 1090–1096.

Zimmerer, M. M. & Lobers, S. (2005), 'Varo^{2}pt-software for inverse analysis, varocon-software and engineering for geotechnical application weimar', www.varocon.com.

Zimmerer, M. M. & Schanz, T. (2006), Determination of soil parameters for modeling of deep excavations utilizing an inverse approach, *in* T. Triantafyllidis, ed., 'Numerical modelling of construction processes in geotechnical engineering for urban environment', Taylor and Francis Group, London, pp. 21–28.

Zou, Y. (2003), 'Ein physikalisches Modell der pF-Kurve für teilgesättigte grobkörnige Böden', *Bautechnik* **80**, 913–921.

Zou, Y. (2004), 'Ein physikalisches Modell der pF-Kurve für teilgesättigte grobkörnige Böden auf primäre Entwässerung und sekundäre Be- und Entwässerung', *Bautechnik* **81**, 371–378.

Zurmühl, T. & Durner, W. (1996), 'Modeling transient water and solute transport in a biporous soil', *Water Resources Research* **32**, 819–829.

Schriftenreihe des Lehrstuhls für Grundbau, Boden- und Felsmechanik der Ruhr-Universität Bochum

Herausgeber: H. L. Jessberger

1	(1979)	**Hans Ludwig Jessberger** Grundbau und Bodenmechanik an der Ruhr-Universität Bochum
2	(1978)	**Joachim Klein** Nichtlineares Kriechen von künstlich gefrorenem Emschermergel
3	(1979)	**Heinz-Joachim Gödecke** Die Dynamische Intensivverdichtung wenig wasserdurchlässiger Böden
4	(1979)	**Poul V. Lade** Three Dimensional Stress-Strain Behaviour and Modeling of Soils
5	(1979)	**Roland Pusch** Creep of soils
6	(1979)	**Norbert Diekmann** Zeitabhängiges, nichtlineares Spannungs-Verformungsverhalten von gefrorenem Schluff unter triaxialer Belastung
7	(1979)	**Rudolf Dörr** Zeitabhängiges Setzungsverhalten von Gründungen in Schnee, Firn und Eis der Antarktis am Beispiel der deutschen Georg-von-Neumayer- und Filchner- Station
8	(1984)	**Ulrich Güttler** Beurteilung des Steifigkeits- und Nachverdichtungsverhaltens von ungebundenen Mineralstoffen
9	(1976)	**Peter Jordan** Einfluss der Belastungsfrequenz und der partiellen Entwässerungsmöglichkeiten auf die Verflüssigung von Feinsand
10	(1986)	**Eugen Makowski** Modellierung der künstlichen Bodenvereisung im grundwasserdurchströmten Untergrund mit der Methode der finiten Elemente
11	(1986)	**Reinhard A. Beine** Verdichtungswirkung der Fallmasse auf Lastausbreitung in nichtbindigem Boden bei der Dynamischen Intensivverdichtung
12	(1986)	**Wolfgang Ebel** Einfluss des Spannungspfades auf das Spannungs-Verformungsverhalten von gefrorenem Schluff im Hinblick auf die Berechnung von Gefrierschächten
13	(1987)	**Uwe Stoffers** Berechnungen und Zentrifugen-Modellversuche zur Verformungsabhängigkeit der Ausbaubeanspruchung von Tunnelausbauten in Lockergestein
14	(1988)	**Gerhard Thiel** Steifigkeit und Dämpfung von wassergesättigtem Feinsand unter Erdbebenbelastung

15 (1991) **Mahmud Taher**
Tragverhalten von Pfahl-Platten-Gründungen im bindigen Baugrund, Berechnungsmodelle und Zentrifugen-Modellversuche

16 (1992) **Rainer Scherbeck**
Geotechnisches Verhalten mineralischer Deponieabdichtungsschichten bei ungleichförmiger Verformungswirkung

17 (1992) **Martin M. Bizialiele**
Torsional Cyclic Loading Response of a Single Pile in Sand

18 (1993) **Michael Kotthaus**
Zum Tragverhalten von horizontal belasteten Pfahlreihen aus langen Pfählen in Sand

19 (1993) **Ulrich Mann**
Stofftransport durch mineralische Deponieabdichtungen: Versuchsmethodik und Berechnungsverfahren

20 (1992) **Festschrift anlässlich des 60. Geburtstages von Prof. Dr.- Ing. H. L. Jessberger**
20 Jahre Grundbau und Bodenmechanik an der Ruhr-Universität Bochum

21 (1993) **Stephan Demmert**
Analyse des Emissionsverhaltens einer Kombinationsabdichtung im Rahmen der Risikobetrachtung von Abfalldeponien

22 (1994) **Diethard König**
Beanspruchung von Tunnel- und Schachtausbauten in kohäsionslosem Lockergestein unter Berücksichtigung der Verformung im Boden

23 (1995) **Thomas Neteler**
Bewertungsmodell für die nutzungsbezogene Auswahl von Verfahren zur Altlastensanierung

24 (1995) **Ralph Kockel**
Scherfestigkeit von Mischabfall im Hinblick auf die Standsicherheit von Deponien

25 (1996) **Jan Laue**
Zur Setzung von Flachfundamenten auf Sand unter wiederholten Lastereignissen

26 (1996) **Gunnar Heibrock**
Zur Rißbildung durch Austrocknung in mineralischen Abdichtungsschichten an der Basis von Deponien

27 (1996) **Thomas Siemer**
Zentrifugen-Modellversuche zur dynamischen Wechselwirkung zwischen Bauwerken und Baugrund infolge stoßartiger Belastung

28 (1996) **Viswanadham V. S. Bhamidipati**
Geosynthetic Reinforced Mineral Sealing Layers of Landfills

29 (1997) **Frank Trappmann**
Abschätzung von technischem Risiko und Energiebedarf bei Sanierungsmaßnahmen für Altlasten

30 (1997) **André Schürmann**
Zum Erddruck auf unverankerte flexible Verbauwände

31 (1997) **Jessberger, H. L. (Herausgeber)**
Environment Geotechnics, Report of ISSMGE Technical Committee TC 5 on Environmental Geotechnics

Herausgeber: Th. Triantafyllidis

32 (2000) **Triantafyllidis, Th. (Herausgeber)**
Workshop "Boden unter fast zyklischer Belastung: Erfahrung und Forschungsergebnisse" Bochum April 2000

33 (2002) **Christof Gehle**
Bruch- und Scherverhalten von Gesteinstrennflächen mit dazwischenliegenden Materialbrücken

34 (2003) **Andrzej Niemunis**
Extended hypoplastic models for soils

35 (2004) **Christiane Hof**
Über das Verpressankertragverhalten unter kalklösendem Kohlensäureangriff

36 (2004) **René Schäfer**
Einfluss der Herstellungsmethode auf das Verformungsverhalten von Schlitzwänden in weichen bindigen Böden

37 (2005) **Henning Wolf**
Zur Scherfugenbänderung granularer Materialien unter Extensionsbeanspruchung

38 (2005) **Torsten Wichtmann**
Explicit accumulation model for non-cohesive soils under cyclic loading

39 (2008) **Christoph M. Loreck**
Die Entwicklung des Frischbetondruckes bei der Herstellung von Schlitzwänden

40 (2008) **Igor Arsic**
Über die Bettung von Rohrleitungen in Flüssigböden

41 (2009) **Anna Arwanitaki**
Über das Kontaktverhalten zwischen einer Zweiphasenschlitzwand und nichtbindigen Böden

Herausgeber: T. Schanz

42 (2009) **Yvonne Lins**
Hydro-Mechanical Properties of Partially Saturated Sand

43 (2010) **Tom Schanz (Herausgeber)**
Geotechnische Herausforderungen beim Umbau des Emscher-Systems
Schriftenreihe zum RuhrGeo Tag 2010